Precision Calculations in Supersymmetric Models using Phenomenological Tools

Dissertation
zur
Erlangung des Doktorgrades (Dr. rer. nat.)
der
Mathematisch-Naturwissenschaftlichen Fakultät
der
Rheinischen Friedrich-Wilhelms-Universität Bonn

von
Kilian Nickel
aus
Remagen

Bonn, 21.07.2016

Dieser Forschungsbericht wurde als Dissertation von der Mathematisch-Naturwissenschaftlichen Fakultät der Universität Bonn angenommen und ist auf dem Hochschulschriftenserver der ULB Bonn `http://hss.ulb.uni-bonn.de/diss_online` elektronisch publiziert.

Abstract

We present a Higgs mass calculation at two-loop level based on the effective potential approach, which has been made available in the public computer codes `SARAH` and `SPheno`. The approach is based on generic formulae for the two-loop effective potential available from literature and can be applied to a large number of renormalisable supersymmetric models in a highly automated way. Three equivalent algorithms are presented, which are completely independent of one another. The code enables the study of the neutral Higgs boson masses at two loops in models beyond the MSSM with a similar precision as has been widely available in MSSM spectrum generators before the Higgs discovery in 2012. Details about the implementation, validation and limitations of the code are presented. This precision calculation is applied to four supersymmetric models, including the MSSM with large flavour violation, the MSSM with R-parity violation and the NMSSM, where we found throughout that the two-loop corrections give rise to significant contributions. An additional model, namely the MSSM extended by vectorlike quarks, is also studied. Here we do not focus only on the two-loop Higgs mass but also on the fine-tuning in the context of gauge mediated supersymmetry breaking. Finally, we present a collider study examining the production of exotic long-lived neutral particles at the LHC, assuming that these particles escape the detector. By applying analyses from the ATLAS and CMS collaborations that focus on a large missing transverse energy signature, we obtain upper cross section limits for arbitrary lifetimes. We found this method to be a complementary approach compared to traditional displaced vertex searches.

Acknowledgements

List of publications

The results of my PhD research are contained in the following publications, the contents of which are all part of this thesis, except (8) and (9).

1. M. D. Goodsell, K. Nickel, F. Staub, *Two-loop Higgs mass calculations in supersymmetric models beyond the MSSM with SARAH and SPheno*
   Published in **Eur.Phys.J. C75 (2015) no.1, 32**, arXiv:1411.0675 [hep-ph]

2. M. D. Goodsell, K. Nickel, F. Staub, *Two-loop corrections to the Higgs masses in the NMSSM*
   Published in **Phys.Rev. D91 (2015) 035021**, arXiv:1411.4665 [hep-ph]

3. H. K. Dreiner, K. Nickel, F. Staub, *On the two-loop corrections to the Higgs masses in trilinear R-parity violation*
   Published in **Phys.Lett. B742 (2015) 261-265**, arXiv:1411.3731 [hep-ph]

4. K. Nickel, F. Staub, *Precise determination of the Higgs mass in supersymmetric models with vectorlike tops and the impact on naturalness in minimal GMSB*
   Published in **JHEP 1507 (2015) 139**, arXiv:1505.06077 [hep-ph]

5. M. D. Goodsell, K. Nickel, F. Staub, *Generic two-loop Higgs mass calculation from a diagrammatic approach*
   Published in **Eur.Phys.J. C75 (2015) no.6, 290**, arXiv:1503.03098 [hep-ph]

6. M. D. Goodsell, K. Nickel, F. Staub, *The Higgs Mass in the MSSM at two-loop order beyond minimal flavour violation*
   Published in **Phys.Lett. B758 (2016), pp. 18-25**, arXiv:1511.01904 [hep-ph]

7. A. Belyaev, S. Moretti, K. Nickel, M. C. Thomas, I. Tomalin, *Hunting for neutral, long-lived exotica at the LHC using a missing transverse energy signature*
   Published in **JHEP 1603 (2016) 018**, arXiv:1512.02229 [hep-ph]

8. H. K. Dreiner, K. Nickel, F. Staub, $B_{s,d}^0 \to \mu\bar\mu$ and $B \to X_s\gamma$ in the R-parity violating MSSM
   Published in **Phys.Rev. D88 (2013) no.11, 115001**, arXiv:1309.1735 [hep-ph]

9. F. Staub, P. Athron, L. Basso, M. D. Goodsell, D. Harries, M. E. Krauss, K. Nickel, T. Opferkuch, L. Ubaldi, A. Vicente, *Precision tools and models to narrow in on the 750 GeV diphoton resonance*
   arXiv:1602.05581 [hep-ph]

Contents

Introduction

Modern particle physics is the study of the smallest building blocks of the world and the laws governing their interactions. The understanding of which particles are considered fundamental underwent many changes up to the current viewpoint of point-like quarks and leptons with forces transmitted between them by force carrier particles. From atomic distances of 10^{-9} m down to the size of a nucleus, 10^{-15} m = 1 fm, observations in the particle world change drastically and are enabled by powerful particle accelerators of increasing energy. The theoretical framework of high-energy physics is quantum field theory (QFT), the extension of quantum mechanics into relativistic space-time. An excitation of a field that propagates through space is called a particle.

One important ingredient of such theories in order to make meaningful predictions is that the force mediating particles obey an internal gauge symmetry. The field that describes the electromagnetic force transforms under a $U(1)$ gauge symmetry. The resulting field theory is quantum electrodynamics (QED), which is highly successful in predicting the properties of the electron (or μ/τ) and photon and their cross sections. The success of gauge theories motivated the incorporation of the other fundamental forces into gauged interactions. A milestone was the unification of the weak force and the electromagnetic force by Glashow, Weinberg and Salam (1968) [1–3]. Afterwards it was found that the strong nuclear force is described by the non-Abelian gauge group $SU(3)$ in a theory which is now known as Quantum Chromodynamics (QCD) [4–8].

The electroweak theory replaced the Fermi model of weak interactions (4-fermion vertex) and predicted two massive vector bosons as the force mediators. In 1983, the UA1 and UA2 collaborations at CERN discovered the new $W^{\pm}$ [9, 10] and Z [11, 12] bosons. Finally, the combination of QCD and the Glashow-Weinberg-Salam electroweak theory became known as the Standard Model of particle physics (SM). Its missing pieces were discovered over the years, like the top quark in 1995 by the CDF and DØ collaborations at Fermilab [13, 14].

In a theory with local gauge symmetry the gauge bosons need to be massless. Including mass terms explicitly breaks the symmetry, which results in unphysical divergent predictions for the scattering of heavy gauge bosons (unitarity violation). This problem was solved prior to all the mentioned particle discoveries by an ingenious trick based on spontaneous symmetry breaking of the gauge symmetry. A new scalar field was hypothesised which "condensates" while the universe cooled down. This means that it assumes a non-zero vacuum expectation value, similar to a ferromagnet which spontaneously experiences magnetisation during cool-down. In the new vacuum, fermions and gauge bosons obtain masses and the gauge symmetry is broken, but its

virtues persist. This phenomenon is called electroweak symmetry breaking (EWSB) and is incorporated into the SM as the famous Brout-Englert-Higgs mechanism [15–20], after its first postulation by Robert Brout and François Englert [19] in 1964 and shortly after by Peter Higgs [16, 17]. In EWSB the gauge group of the weak interaction, $SU(2)_L \times U(1)_Y$, is spontaneously broken to $U(1)_{\text{em}}$ with the side effect that three gauge bosons turn massive. The mechanism predicts another fundamental particle, the Higgs boson. Since its creation the Standard Model provided excellent predictions that agree with a large number of experimental measurements. But the foundation of the model needed to be confirmed by the direct discovery of the Higgs boson. Previous generations of colliders like the Tevatron at Fermilab and the LEP collider at CERN set out to find it, but despite great scientific achievements they did not have the energetic reach to give the proof. This was one of the main motivations to build the Large Hadron Collider (LHC) at CERN. The LHC pioneered a new energy frontier with proton-proton collisions at a centre-of-mass energy of $\sqrt{s} = 7\,\text{GeV}$ since its start-up in 2009. After the first upgrade to $8\,\text{TeV}$ and a longer maintenance pause starting 2013, the machine became operational again in early 2015 at the maximum CM energy of $13\,\text{TeV}$ (Run II). During the first run already, the discovery of the elusive boson was announced on the 4th of July 2012 by the ATLAS and CMS collaborations who reported a mass of $125\,\text{GeV}$ [21, 22]. This marks another milestone in particle physics and lead to the award of the Nobel Prize in Physics 2013 to Peter Higgs and François Englert (Robert Brout, co-author of Ref. [19], deceased before the nomination).

It is not clear whether the new boson is really the one as predicted by the Standard Model. Many extended theories predict a larger Higgs sector with several new bosons. After the discovery and with the start of Run II of the LHC, particle physics entered the era of precision Higgs physics. Signal and coupling strengths were scrutinised and the mass measurement precision increased to below 0.3% [23–25]. Any deviation from the SM properties can hint at new physics. For example, in 2015 both ATLAS and CMS experiments reported a slight excess in the decay $h \to \mu\tau$ [26, 27]. Such lepton flavour violation is highly suppressed in the SM. Excesses like this can turn out to be statistical fluctuations, but cause excitement and speculation in the scientific community.

Despite the success of the Standard Model, it cannot answer all experimental observations. It does not include gravity, which is mostly irrelevant in high-energy physics due to its weakness compared to the other three fundamental forces. The laws of gravity described by Einstein's theory of General Relativity (GR) accurately describe the large-scale structure of the universe, including stars, galaxies and other celestial bodies. The combination of both theories into a single theory of quantum gravity has been pursued by generations of physicists including Einstein himself. Although the Standard Model is internally consistent, the absence of gravity states that the model is incomplete. For processes at an energy scale of $M_P = 10^{19}\,\text{GeV}$, the Planck mass, quantum effects of gravity become relevant. This scale is related to the gravitational constant G,

$$M_P = \sqrt{\frac{\hbar c}{G}} \approx 1.22 \times 10^{19}\,\text{GeV}. \tag{1.1}$$

Unfortunately, this scale is so high that it exceeds by far any beam energy that can be reached by an accelerator based on earth. It is unlikely that the Standard Model is the ultimate theory and valid for all energies. Then, it has to be an effective theory in the low energy limit of some ultraviolet (UV) complete theory. At most at the Planck scale (preferably below) there must be new physics, which will be accompanied by new massive states. The Higgs mass is the weak spot

in the sense that the existence of new massive states at a scale as high as M_P poses a theoretical problem to the SM. Through quantum effects the Higgs mass is expected to be pushed to the same order of magnitude. Having such a large hierarchy between the Higgs mass and the Planck mass is considered unnatural and would imply a highly fine-tuned universe. This hierarchy problem [28–31] hints at the existence of some deeper mechanism which protects the Higgs mass from large scales.

Besides gravity, there are many other observations which motivate physics beyond the Standard Model. Important examples (which are briefly introduced in section 2.2) are dark matter [32–38], neutrino masses [39–41] and the baryon asymmetry of the universe [42–46]. All attempts to extend the theory of the Standard Model are referred to as Beyond the Standard Model physics (BSM). A popular idea to solve the hierarchy problem is supersymmetry (SUSY), which relates bosonic and fermionic particles. In the context of quantum field theory, the idea dates back to Refs. [47–49] [1] and was popularised in 1974 by Wess and Zumino [51]. The first realistic SUSY model was the Minimal Supersymmetric Standard Model (MSSM) [52, 53]. Until today SUSY has attracted significant attention and is subject of many works, including Refs. [30, 54–67].

The MSSM predicts many yet undiscovered superpartner particles ("sparticles") as well as an extended Higgs sector. Supersymmetry does not only prevent the hierarchy problem, but provides solutions to other problems like the aforementioned ones. By adding more particles and interactions to the MSSM or SM, a large amount of extended models have been constructed. To deal with this multitude of models in an efficient way, computer tools have been developed that can perform analytic calculations. The key to this are generic expressions, that hold for a model with arbitrary many particles and interactions.

Especially in supersymmetric models, the structure of a valid Lagrangian is much more restricted than in non-supersymmetric models. The necessary steps to construct it can be automatised by a computer. The software package `SARAH` [68–74], developed by Florian Staub, automatises many otherwise time-consuming analytic tasks that come with model building. In combination with other numerical tools, this software can be used to perform precision calculations of observables for a wide range of models. By comparing these observables to experimental measurements the validity of a model can be studied. In particular, the mass of the Higgs boson is a new precision observable, measured by the ATLAS and CMS collaborations to a high precision, which will possibly be improved by a future linear collider [75]. Supersymmetric models predict the Higgs mass by its internal parameters - it is not a free parameter itself, as it is in the Standard Model. Therefore, a precise prediction in SUSY models is desirable.

This thesis is structured as follows. In section 2.1 a short introduction to the SM is given. We also list the arguments for BSM physics and supersymmetry in section 2.2 and demonstrate the hierarchy problem. The MSSM is introduced in section 2.3 with emphasis on the Higgs potential. The main contribution of this thesis is the implementation of a two-loop Higgs mass calculation based on the effective potential approach in the model-independent framework of `SARAH`/`SPheno`. Chapter 3 explains how the approach is built upon existing results from literature and shows the necessary calculations. The practical details of the implementation are explained in chapter 4. With the new routines, two-loop effects can be studied in different models at a level that was not available before. We performed numerical studies of the two-loop Higgs mass effects in four supersymmetric models, which are presented in chapter 5.

Chapter 6 contains a collider study that is thematically set apart from the Higgs mass calculations. The study considers large E_T^{miss} signatures from long-lived exotic particles at the

---

[1] SUSY was considered even earlier in a different context as a relation between mesons and baryons [50].

LHC as a complementary approach to traditional displaced vertex searches. We explore the potential of this approach as a way to extend the existing cross section limits on the production of long-lived particles.

The thesis concludes in chapter 7 and highlights future developments in this field. The modular appendix contains additional information, definitions of the necessary loop functions and detailed results. In addition, we present the first derivatives of the effective potential contributions including massive gauge bosons in appendix B.3.2, which is a new result and will be useful for future calculations.

Theory

2.1 The Standard Model of particle physics

The Standard Model is a quantum field theory with local gauge invariance with respect to the gauge group

$$G_{\text{SM}} = SU(3)_C \times SU(2)_L \times U(1)_Y. \tag{2.1}$$

This group describes the strong interaction by $SU(3)_C$ ("colour") and the electroweak force by $SU(2)_L \times U(1)_Y$ ("left", "hypercharge"). Table 2.1 lists the field content of the SM and the representations underneath which these fields transform. The electroweak interaction has the peculiarity of treating left and right chiral fields on a different footing. In the SM, left handed fields are doublets under $SU(2)$ while right handed fields are singlets. Right-handed neutrino fields are absent from the SM. The fact that we observe massive fermions and vector bosons has to be represented by mass terms in the Lagrangian, i.e. terms quadratic in the fields. However,

name	spin s	symbol	generations	$SU(3)_C$	$SU(2)_L$	$U(1)_Y$
Higgs doublet	0	$H = \begin{pmatrix} H^+ \\ H^0 \end{pmatrix}$	1	**1**	**2**	$\frac{1}{2}$
Left-handed quark doublet	1/2	$Q = \begin{pmatrix} u_L \\ d_L \end{pmatrix}$	3	**3**	**2**	$\frac{1}{6}$
Right-handed up-quark	1/2	u_R	3	**3**	**1**	$\frac{2}{3}$
Right-handed down-quark	1/2	d_R	3	**3**	**1**	$-\frac{1}{3}$
Left-handed lepton doublet	1/2	$L = \begin{pmatrix} \nu_L \\ e_L \end{pmatrix}$	3	**1**	**2**	$-\frac{1}{2}$
Right-handed electron	1/2	e_R	3	**1**	**1**	-1
B boson	1	B_μ	-	adjoint of $U(1)_Y$
W bosons	1	W_μ^a	-	adjoint (**3**) of $SU(2)_L$
gluons	1	G_μ^a	-	adjoint (**8**) of $SU(3)_C$

Table 2.1: This table lists the fundamental fields of the Standard Model and the representations of the gauge group G_{SM} underneath which they transform.

Dirac mass terms such as $\bar{e}_L e_R$ do not respect gauge invariance. The rescue comes with the Higgs mechanism, which introduces a scalar H that is a doublet under $SU(2)_L$. It provides mass terms while preserving the advantages of gauge symmetry. This is achieved by Yukawa couplings between H and fermions, contained in $\mathcal{L}_{\text{Yukawa}}$,

$$\mathcal{L}_{\text{Yukawa}} = Y_u^{ij}\overline{Q}_i\widetilde{H}u_{Rj} + Y_d^{ij}\overline{Q}_i H d_{Rj} + Y_e^{ij}\overline{L}_i H e_{Rj} + \text{h.c.}, \tag{2.2}$$

with $\overline{L}_i = (\overline{\nu}_{Li}, \overline{e_{Li}})$ and $\overline{Q}_i = (\overline{u}_{Li}, \overline{d}_{Li})$.[1] The $SU(3)_C$-invariant contraction of $\mathbf{\overline{3}} \times \mathbf{3}$ is implicitly assumed, $\bar{q}^\alpha q^\beta \delta_{\alpha\beta}$. To form all necessary Yukawa couplings, a Higgs doublet $\widetilde{H}$ with opposite hypercharge $Y = -\frac{1}{2}$ is needed, which is constructed from a conjugated H,

$$\widetilde{H} \equiv i\sigma^2 H^* = \begin{pmatrix} 0 & 1 \\ -1 & 0 \end{pmatrix}\begin{pmatrix} (H^+)^* \\ (H^0)^* \end{pmatrix} = \begin{pmatrix} (H^0)^* \\ -(H^+)^* \end{pmatrix}. \tag{2.3}$$

To explain the Higgs mechanism and the generation of mass terms for vector bosons, consider the Higgs Lagrangian

$$\mathcal{L}_{\text{Higgs}} = (D^\mu H)^\dagger(D_\mu H) - V(H), \tag{2.4a}$$

$$V = \mu^2 H^\dagger H + \lambda(H^\dagger H)^2. \tag{2.4b}$$

The minimum of the scalar potential $V(H)$ defines the vacuum state of the theory. V only depends on $\phi \equiv |H|$, so the minimum is defined by

$$\frac{\partial V}{\partial \phi} = 2\phi\left(\mu^2 + 2\lambda\phi^2\right) = 0. \tag{2.5}$$

The solutions are either $\phi = 0$ or $\pm\sqrt{-\mu^2/(2\lambda)}$, which requires a negative μ^2. The case $\mu^2 > 0$ corresponds to an unbroken theory with a ground state $\langle H \rangle = 0$. The quartic parameter λ needs to be positive for the potential to be bounded from below. Having μ^2 negative is the important condition for symmetry breaking to occur, and it fixes the VEV $\langle |H| \rangle$ up to a complex phase. In the Mexican hat visualisation of V, all possible ground states are connected by a circle. Using gauge invariance, we can apply a gauge transformation such that the minimum is described by $\langle H^+ \rangle = 0$ for the charged Higgs component and $\langle H^0 \rangle = v/\sqrt{2}$ for the neutral component with a real v. A non-zero VEV for a charged field would imply an electrically charged vacuum state, which is unphysical. If a state $|\Phi\rangle$ is invariant under a group transformation $S|\Phi\rangle = \exp(i\alpha^a T^a)|\Phi\rangle$ with generators T^a, then $T^a|\Phi\rangle = 0$. The generators of $SU(2)$ are defined as $T^a \equiv \frac{1}{2}\sigma^a$ with the Pauli matrices σ^a. For the Abelian symmetry group $U(1)_Y$ the generator is just a complex number, $\exp(i\alpha Y)$, with a real number Y called hypercharge. The VEV of the Higgs doublet

$$\langle H \rangle = \begin{pmatrix} 0 \\ \frac{v}{\sqrt{2}} \end{pmatrix} \tag{2.6}$$

leads to $\sigma^i\langle H \rangle \neq 0$ and $Y\langle H \rangle \neq 0$. The generators σ^i and Y are said to be broken. But there exists a linear combination out of T^3 and Y,

$$Q \equiv T^3 + Y, \tag{2.7}$$

---

[1] The bar operator on Dirac spinors is defined as $\overline{\Psi} \equiv \Psi^\dagger\gamma^0$.

which fulfils $Q\langle H\rangle = 0$ and is thus unbroken. Q is the charge generator of the electromagnetic group $U(1)_{\text{em}}$. This demonstrates electroweak symmetry breaking (EWSB) through the VEV of the Higgs boson with the breaking pattern

$$SU(2)_L \otimes U(1)_Y \rightarrow U(1)_{\text{em}}. \tag{2.8}$$

For every broken generator, the Goldstone theorem [76, 77] predicts the emergence of massless Nambu-Goldstone bosons. In the SM they can be identified with the three real degrees of freedom in $H^\pm \equiv G^\pm$ and G^0. These fields can be set to zero by a local gauge transformation which we are free to apply. In this way, Goldstones bosons are completely decoupled and absent from any further calculation (unitary gauge). Explicitly, if $H(x)$ is expressed by real fields $\alpha^a(x), h(x)$ as

$$H(x) = U(x)\begin{pmatrix} 0 \\ (v+h(x))/\sqrt{2} \end{pmatrix}, \qquad U(x) \equiv \exp\left(\frac{i\alpha^a(x)\sigma^a}{2v}\right), \tag{2.9}$$

then going to the unitary gauge transforms all doublets $\Phi(x)$ of $SU(2)_L$ as $\Phi(x) \rightarrow U^{-1}(x)\Phi(x)$. Alternatively, we can parameterise the neutral Higgs component as

$$H^0(x) = \frac{1}{\sqrt{2}}\left(v + h(x) + iG^0(x)\right). \tag{2.10}$$

This allows to express eq. (2.4) as a function of $v, h(x), G^0(x)$. The covariant derivative of a field Φ is defined as

$$D_\mu\Phi = (\partial_\mu - \underbrace{ig_3 G^a_\mu \frac{\lambda^a}{2}}_{\text{only for } Q, u_R, d_R} - \underbrace{ig_2 W^a_\mu \frac{\sigma^a}{2}}_{\text{only for } H, L, Q} + ig_1 Y B_\mu)\Phi, \tag{2.11}$$

with the Gell-Mann matrices λ^a as the generators of $SU(3)$ and the Pauli matrices σ^a as the generators of $SU(2)$. [2] The first term of eq. (2.4a) gives

$$\mathcal{L}_{\text{Higgs}} = \cdots + \frac{1}{8}g_2^2 v^2 W^3_\mu W^{3\mu} + \frac{1}{8}g_1^2 v^2 B_\mu B^\mu + \frac{1}{4}g_1 g_2 v^2 W^3_\mu B^\mu + \frac{1}{4}g_2^2 v^2 W^+_\mu W^{-\mu}$$
$$+ \frac{1}{2}v(\partial^\mu G^0)(g_1 B_\mu + g_2 W^3_\mu) + \frac{i}{2}gv W^-_\mu \partial^\mu H^+ - \frac{i}{2}gv W^+_\mu \partial^\mu H^-. \tag{2.12}$$

The terms in the first line are rotated to mass eigenstates A_μ, Z_μ and $W^\pm_\mu$,

$$\begin{pmatrix} B_\mu \\ W^3_\mu \end{pmatrix} = \begin{pmatrix} \cos\Theta_W & \sin\Theta_W \\ -\sin\Theta_W & \cos\Theta_W \end{pmatrix}\begin{pmatrix} A_\mu \\ Z_\mu \end{pmatrix}, \quad W^\pm_\mu = \frac{W^1_\mu \mp W^2_\mu}{\sqrt{2}}, \tag{2.13}$$

where the Weinberg angle Θ_W is introduced,

$$\cos\Theta_W = c_W = g_2/\sqrt{g_1^2 + g_2^2}, \qquad \sin\Theta_W = c_W = g_1/\sqrt{g_1^2 + g_2^2}. \tag{2.14}$$

---

[2] In general, if Φ is a non-trivial representation of a group G with generators T^a and gauge fields G^a_μ, then $D_\mu\Phi = (\partial_\mu - igG^a_\mu T^a)\Phi$. If G is abelian, T^a is just a c-number.

This gives a vanishing mass term for the photon field A_μ and the following mass terms for W and Z,

$$\mathcal{L}_{\text{Higgs}} = \cdots + \frac{1}{2} M_Z^2 Z_\mu Z^\mu + M_W^2 W_\mu^+ W^{-\mu} + M_Z Z_\mu \partial^\mu G^0 + i M_W (W_\mu^- \partial^\mu G^+ - W_\mu^+ \partial^\mu G^-), \quad (2.15)$$

with masses

$$M_Z = \frac{1}{2} \sqrt{g_1^2 + g_2^2} v, \qquad M_W = \frac{1}{2} g_2 v. \quad (2.16)$$

The value of v is related to the Fermi constant $G_F = 1/(\sqrt{2} v^2)$ and can thus be calculated as $v = 246 \,\text{GeV}$ without knowledge of the Higgs mass. If unitary gauge is applied, the Goldstone fields disappear completely, but their real degrees of freedom live on in the longitudinal components of the now-massive vector bosons. This is sometimes described as the vectors "eating the Goldstone bosons" to acquire mass. In a general R_ξ gauge, explicit gauge fixing terms need to be added to the Lagrangian:

$$\mathcal{L}_{\text{GF}} = -\frac{1}{2\xi_G} (\partial^\mu G_\mu^a)^2 - \frac{1}{2\xi_A} (\partial^\mu A_\mu)^2 - \frac{1}{2\xi_Z} \left(\partial^\mu Z_\mu - \xi_Z M_Z G^0 \right)^2 - \frac{1}{\xi_W} \left| \partial^\mu W_\mu^- + i\xi_W M_W G^+ \right|^2 . \quad (2.17)$$

These terms are chosen to eliminate the terms of eq. (2.15) that mix scalars and vectors. This requires an integration by parts such as $\int \mathrm{d}^4 x (\partial^\mu Z_\mu) G^0 = -\int \mathrm{d}^4 x Z_\mu \partial^\mu G^0 + \int \mathrm{d}^4 x \partial^\mu (Z_\mu G^0)$. The terms in eq. (2.17) formally describe Goldstone masses, e.g. $M_{G^0}^2 = \xi_Z M_Z^2$. They don't have a physical meaning and cannot be observed. Goldstone fields are more like book-keeping devices that can simplify certain calculations. We now turn again to the potential V,

$$V(h, G^0 = H^\pm = 0) = \frac{\mu^2}{2} (v + h)^2 + \frac{1}{4} \lambda (v + h)^4. \quad (2.18)$$

The minimum requires

$$\frac{\partial V}{\partial h} \equiv t_h = \mu^2 (v + h) + \lambda (v + h)^3 = 0. \quad (2.19)$$

This condition is sometimes called a tadpole equation [70], because t_h is related to a one-point correlation function, which at one-loop looks like a tadpole, cf. fig. 2.1. Such tadpole diagrams are needed to determine the minimum of the potential including quantum corrections. Evaluated at
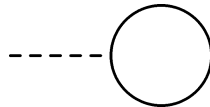
Figure 2.1: Tadpole diagram

$h = 0$, eq. (2.19) gives the relation between the VEV and the Lagrangian parameters, $\mu^2 = -\lambda v^2$, that can be used to eliminate one of these parameters. The remaining free field $h(x)$ is a physical,

massive field, called the Higgs boson. Its tree-level mass is equal to the second derivative of V,

$$\frac{\partial^2 V}{\partial h^2}\Big|_{\min} = \mu^2 v + 3\lambda v^2 = 2\lambda v^2 \equiv m_h^2, \qquad (2.20)$$

where the notation $\big|_{\min}$ means evaluation at the minimum, in this case using $\mu^2 = -\lambda v^2$. The existence of the Higgs boson is a well-established fact since its discovery in 2012 [21, 22] and its mass has become a precision observable with an average of [23–25]

$$m_h = (125.09 \pm 0.32)\,\text{GeV}. \qquad (2.21)$$

By the end of the LHC's second run at 13 TeV the precision will have further improved. Even more improvement can be expected from a future linear collider [78].

Through EWSB the Yukawa terms of eq. (2.2) split up into

$$\mathcal{L}_{\text{Yukawa}} = \frac{Y_u^{ij} v}{\sqrt{2}}\overline{u_{Li}}u_{Rj} + \frac{Y_d^{ij} v}{\sqrt{2}}\overline{d_{Li}}d_{Rj} + \frac{Y_e^{ij} v}{\sqrt{2}}\overline{e_{Li}}e_{Rj} + \text{h.c.} + \ldots, \qquad (2.22)$$

where the dots signify all non-mass terms. The masses of the fermions are determined by the scale v, defined by the Higgs sector, and the free parameters $Y_{u,d,e}$. Fermion masses exhibit a large hierarchy ranging from $\mathcal{O}\,(\text{MeV})$ for u, d quarks up to $m_{\text{top}} = 173\,\text{GeV}$ [79]. The SM offers no explanation to this peculiarity. Also, from the observation of flavour changing neutral currents (FCNC) it is proven that the mass eigenstates of the down quarks (or up quarks, only their combined effect is measureable) are not equal to the gauge eigenstates that take part in weak interactions. Instead,

$$\begin{pmatrix} d' \\ s' \\ b' \end{pmatrix} = V_{\text{CKM}} \begin{pmatrix} d \\ s \\ b \end{pmatrix} \qquad (2.23)$$

describe the weak eigenstates. The mixing is contained in the Cabibbo-Kobayahsi-Maskawa matrix V_{CKM} [80, 81] and is the only source of flavour violation within the SM. For completeness, we give the remaining terms of the Lagrangian,

$$\mathcal{L}_{\text{SM}} = \mathcal{L}_{\text{gauge}} + \mathcal{L}_{\text{Higgs}} + \mathcal{L}_{\text{fermion}} + \mathcal{L}_{\text{Yukawa}} + \mathcal{L}_{\text{GF}} + \mathcal{L}_{\text{ghost}}, \qquad (2.24\text{a})$$

$$\mathcal{L}_{\text{gauge}} = -\frac{1}{4}G_{\mu\nu}^a G^{a\mu\nu} - \frac{1}{4}W_{\mu\nu}^a W^{a\mu\nu} - \frac{1}{4}B_{\mu\nu}B^{\mu\nu}, \qquad (2.24\text{b})$$

$$\mathcal{L}_{\text{fermion}} = \sum_{\text{fermions}} i\overline{\psi}\gamma^\mu D_\mu \psi, \qquad (2.24\text{c})$$

$$\mathcal{L}_{\text{ghost}} = \text{see appendix A.2.} \qquad (2.24\text{d})$$

More details about the SM are not to be discussed here, as excellent reviews can be found in the literature [82–84].

2.2 Motivation for physics beyond the Standard Model

The Standard Model has been scrutinised by experiments and has produced astonishingly accurate predictions. Although the neglect of gravity is the most obvious shortcoming to the model, there are other shortcomings that are testable at present experiments. In this subsection

we summarise reasons to extend the Standard Model and highlight how supersymmetry is important in this context.

2.2.1 Neutrino masses

The three neutrinos ν_{Li} are massless Weyl fermions in the Standard Model and are the only fermionic particles that do not have a right-handed partner to form a Dirac mass term. Neutrino oscillations, first predicted in 1967 [85] as the expected disappearance of solar ν_e neutrinos and confirmed by several experiments [86–91], prove that they have masses. Oscillations of atmospheric neutrinos $\nu_\mu, \bar{\nu}_\mu$ were later confirmed by the Kamiokande experiment [89]. Those measurements fix the mass differences, but not their absolute values or their hierarchy. Recent observations from PLANCK tightly constrain the sum of masses $\sum m_\nu < 0.23\,\text{eV}$ [92]. The known neutrino parameters make up the "standard neutrino model" [93]. However, it is unclear how the Standard Model must be extended to incorporate neutrinos. A way of achieving this is to postulate heavy right-handed neutrino fields, which generate small neutrino masses through the seesaw mechanism [94]. The MSSM also does not explain neutrino masses. They can be incorporated by similiar means as in the SM, e.g. a seesaw mechanism. In the context of R-parity violation, neutrino masses might even be explained as the result of mixing with neutralinos via radiative corrections [95] without the need for additional right-handed neutrino fields.

2.2.2 Dark matter

Astronomical observations of the rotation speed of spiral galaxies, first discovered by Oort [32] and Zwicky [33, 34], are inconsistent with the effect of the gravitational force exerted by the observed amount of luminous matter within these galaxies [35, 37, 38]. There are different ways of explaining this observation. A common idea is that there is simply more matter distributed around galaxies than is visible by telescopes. The new, dark matter does not interact with light or via the strong force. An introduction is found in Ref. [96]. According to measurements of the cosmic microwave background by the WMAP [97] and PLANCK experiments [92, 98], dark matter accounts for roughly 23 % of the entire universe's energy density, while our observable universe makes up only 4.3 %. The rest is ascribed to the little-known dark energy, which is the driving force of the expansion of the universe. Neutrinos seem to fit the role of dark matter and can possibly explain large structure formation in the universe [99]. However, neutrinos as the dominant form of dark matter are ruled out, as they would produce too much large structure [100]. Dark matter thus demands new physics, in the form of one or more new neutral particles. Many SM extensions offer good dark matter candidates like Higgs singlets [101] or lightest Kaluza-Klein states [102, 103], while supersymmetric models have the lightest neutralino [104, 105], provided that R-parity is conserved to guarantee its stability. Other candidates are axions [106, 107] or gravitinos [108].

2.2.3 Baryon asymmetry

Particle interactions seem to produce matter and antimatter in equal amounts. Then it is an open question why the observable universe apparently contains no larger amounts of antimatter. Assuming a symmetric initial universe, the surplus of matter can be generated if the three Sakharov conditions [42] are fulfilled: C and CP must be violated, also baryon number B, and interactions have to occur out of thermal equilibrium. The Standard Model fulfils these conditions and could potentially explain the asymmetry via electroweak baryogenesis. At some

point in time in the early universe, a transition from a state with unbroken electroweak symmetry to the known state with massive gauge bosons occured. This electroweak phase transition could be of first order and mark the departure from thermal equilibrium (electroweak baryogenesis) [43]. However, the only source of CP violation in the SM lies in the CKM matrix and it is not enough to generate the observed amount of baryons [109–112]. BSM models like the MSSM offer new sources of CP violation which could fix this problem. Reviews of baryon asymmetry models can be found in Refs. [44, 45].

2.2.4 Flavour and electroweak precision observables

Processes in which the flavour of one participant changes are called flavour observables. In the SM, this mainly happens in the quark sector through the flavour mixing described by the CKM matrix (quark flavour violation, QFV). Lepton flavour violation is loop-suppressed, but possible e.g. through neutrino mixing. BSM effects can give sizeable contributions to these observables and strong deviations from the SM prediction can indicate new physics. On the other hand, flavour observables place strong constraints on new models [113]. The quark transition $b \to s$ is of high importance for constraining new physics. It occurs for example in the neutral mesons system $B_s^0 - \overline{B_s^0}$ and the decays $B_s \to \mu^+\mu^-$, $B \to X_s\gamma$. The impact of new physics on these observables is discussed in Refs. [114–117]. The properties of B mesons are investigated at specialised B-factories like Belle, BaBar and the LHCb experiment.

Another testing ground are electroweak precision observables (EWPO), of which we name two examples. The SM predicts a W boson mass that is slightly below the measured value [118]. The M_W prediction is sensitive to new physics contributions [119–121] and is thus an important indirect probe. A similar situation exists for the anomalous magnetic moment of the muon [122],

$$a_\mu^{\text{exp}} = \frac{g_\mu - 2}{2} = 11659209.1(5.4)(3.3) \times 10^{-10}, \tag{2.25}$$

which is one of the most precisely measured and theoretically best studied quantities. The first error is statistical, the second one systematic. The difference between theory and experiment [123],

$$\Delta a_\mu = a_\mu^{\text{exp}} - a_\mu^{\text{SM}} = 288(63)(49) \times 10^{-11}, \tag{2.26}$$

corresponds to an inconclusive 3.6 σ deviation, possibly a sign for new physics.

2.2.5 The hierarchy problem and fine-tuning

Probably the strongest feature of supersymmetry is that it provides a solution to the hierarchy problem [28–31]. In a renormalisable theory, finite results can be obtained even if the momenta of virtual particles in quantum corrections are extended all the way up to infinity. This makes the theory calculable for physical processes at infinitely high scales. However, the general belief is that the SM is not the ultimate theory and that some new physics happens at higher scales. Then, the SM should be considered as an effective theory valid up to some cut-off scale Λ. At the very least, some new physics must happen at the Planck scale M_P, when quantum gravity effects become relevant. But even if the scale of new physics is only a few orders of magnitude above the electroweak scale $v = 246\,\text{GeV}$, then there is a hierarchy problem in the SM. Since all masses in the SM are generated through the Higgs mechanism which determines the size of v, they should all be of the same order as v. This is true for the heaviest particles: the top quark, the Higgs boson and the gauge bosons W, Z. We now demonstrate how the Higgs mass is

(a) fermion loop ($i\Pi_a$)   (b) quartic scalar loop ($i\Pi_b$)   (c) cubic scalar loop ($i\Pi_c$)
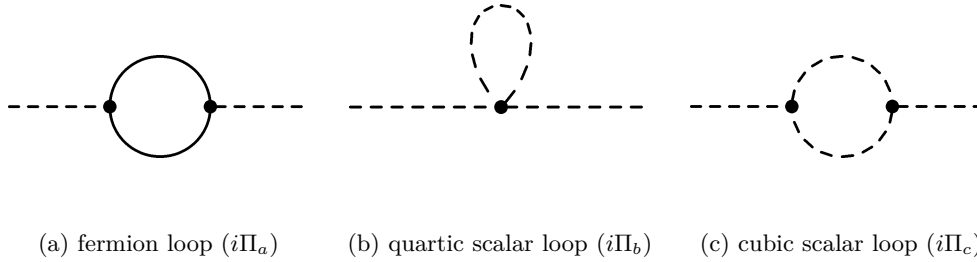
Figure 2.2: One-loop diagrams for scalar mass corrections

affected by the presence of large scales. The irreducible two-point diagrams of a scalar field like the Higgs boson h at one-loop level are shown in fig. 2.2 (considering only scalars and fermions in the loop). In the Standard Model, the diagram 2.2(a) with the top quark taking the role of f is the most important contributor. Let $i\Pi(p^2)$ be the sum of all 1PI[3] scalar self-energy diagrams. The resummation of 1PI diagrams to all orders gives the full scalar propagator

$$i\mathcal{G}(p^2) = \frac{i}{p^2 - m_0^2 + \Pi(p^2) + i\epsilon}. \tag{2.27}$$

The physical mass m_p is defined as the pole of the propagator, $m_p^2 = m_0^2 - \Pi(p^2 = m_p^2)$. All the diagrams in fig. 2.2 diverge for large loop momenta. These ultraviolet (UV) divergences are symptoms of the assumption that the theory is valid up to infinitely high scales or equivalently, small distances. They can be removed by the systematic procedure of renormalisation [124], resulting in a UV finite theory. For this, a UV regulator has to be employed. The simplest possibility is a cut-off at Λ. Considering first only the diagram 2.2(b), with a virtual scalar S of mass m_S, the corresponding expression for the self-energy (which is calculated later in this section) is

$$\Pi_b(p^2) = -\frac{\lambda_S}{16\pi^2}\Lambda^2 + \mathcal{O}\left(\ln(\Lambda^2/m_S^2)\right). \tag{2.28}$$

Because of momentum conservation this diagram is independent of the value of p^2. The one-loop corrected Higgs mass reads

$$m_h^2 = m_{h,\text{tree}}^2 + \frac{\lambda_S}{16\pi^2}\Lambda^2 + \mathcal{O}\left(\ln(\Lambda/m_S)\right). \tag{2.29}$$

Assuming that the couplings λ, λ_S are not much greater than 1 and in the perturbative regime, the correction term is huge, $\mathcal{O}\left((10^{19}\,\text{GeV})^2\right)$. Then the Lagrangian parameter μ^2 needs to be equally huge, and a remarkable cancellation between both terms has to take place to end up with a squared mass of $\mathcal{O}\left((100\,\text{GeV})^2\right)$. This large fine-tuning is considered *unnatural* (an interesting discussion of the naturalness criterion can be found in Ref. [125]). A natural behaviour would be to have a Higgs mass of the order of $\Lambda = M_P$. Other particles, such as fermions and vector bosons, do not have this illness: their mass corrections are protected by symmetries, ensuring that corrections are of the order of their own masses only. The concept of fine-tuning may be considered an aesthetic one and by itself it does not falsify a theory. It is rather an empirical

---

[3] 1PI=one-particle irreducible, meaning all diagrams that can not be cut into two separate diagrams by cutting one internal line

hint that the theory is incomplete, or that there is a hidden mechanism behind it. A quantitative measure of fine tuning has been established in Refs. [126, 127],

$$\Delta \equiv \max_{\alpha}\left(|\Delta_{\alpha}|\right), \qquad \Delta_{\alpha} \equiv \frac{\partial \ln M_Z^2}{\partial \ln \alpha} = \frac{\alpha}{M_Z^2}\frac{\partial M_Z^2}{\partial \alpha}. \tag{2.30}$$

Here, α is a set of independent parameters and Δ_{α}^{-1} estimates the accuracy to which α must be tuned to achieve the correct electroweak reference scale, M_Z. This definition is useful in the context of a model embedded in a high scale (e.g. GUT scale) model, at which the parameters α are defined. Supersymmetry solves the technical part of the hierarchy problem by systematically eliminating the dangerous Λ^2 corrections. In comparison, logarithmic contributions are very tame, e.g. $\ln(10^{19}/10^2) \approx 39$. We consider a toy model consisting of a complex scalar S, a Dirac fermion f with a mass obtained through the Higgs mechanism with $H = (v + h + ia)/\sqrt{2}$ (a similar calculation was done in Ref. [67]),

$$\mathcal{L} \supset -\lambda_S \left|H\right|^2 \left|S\right|^2 - \lambda_f H \overline{f} f \tag{2.31a}$$

$$\rightarrow -\frac{1}{2}\lambda_S h^2 \left|S\right|^2 - (\lambda_S v)h \left|S\right|^2 - \frac{\lambda_f}{\sqrt{2}} h \overline{f} f - \frac{\lambda_f v}{\sqrt{2}}\overline{f} f + \dots . \tag{2.31b}$$

The masses are m_S for S and $m_f = \lambda_f v/\sqrt{2}$ for f with vertex factors $\mathcal{C}\left[h, S^*, S\right] = -i\lambda_S$ and $\mathcal{C}\left[h, \overline{f}, f\right] = -i\lambda_S v$. The self-energies of fig. 2.2 are given by

$$i\Pi_a(p^2) = \left(-i\frac{|\lambda_f|}{\sqrt{2}}\right)^2 \int \frac{\mathrm{d}^4 q}{(2\pi)^4} \frac{-\mathrm{tr}\left[i(\slashed{q} + m_f)i(\slashed{q} + \slashed{p} + m_f)\right]}{(q^2 - m_f^2 + i\epsilon)((q+p)^2 - m_f^2 + i\epsilon)}$$

$$= -\frac{\lambda_f^2}{2}4 \int \frac{\mathrm{d}^4 q}{(2\pi)^4} \frac{q^2 + qp + m_f^2}{(q^2 - m_f^2 + i\epsilon)((q+p)^2 - m_f^2 + i\epsilon)}$$

$$= i\frac{|\lambda_f|^2}{16\pi^2}2\left(\Lambda^2 - \int_0^1 \mathrm{d}\alpha \left(2\Delta + 3\Delta \ln\left(\frac{\Delta + \Lambda^2}{\Delta}\right)\right)\right), \quad \Delta \equiv m_f^2 - \alpha(1-\alpha)p^2$$

$$\overset{p^2=0}{=} -i\frac{|\lambda_f|^2}{16\pi^2}\left(-2\Lambda^2 + 6m_f^2 \ln\left(\frac{\Lambda^2}{m_f^2}\right) + 4m_f^2\right) \tag{2.32a}$$

$$i\Pi_b(p^2) = (-i\lambda_S) \int \frac{\mathrm{d}^4 q}{(2\pi)^4} \frac{i}{q^2 - m_S^2 + i\epsilon} = -i\frac{\lambda_S}{16\pi^2}\mathbf{A_0}(m_S^2)$$

$$= -i\frac{\lambda_S}{16\pi^2}\left(\Lambda^2 - m_S^2 \ln\left(\frac{\Lambda^2}{m_S^2}\right)\right) \tag{2.32b}$$

$$i\Pi_c(p^2) = (-i\kappa)^2 \int \frac{\mathrm{d}^4 q}{(2\pi)^4} \frac{i}{q^2 - m_S^2 + i\epsilon}\frac{i}{(q+p)^2 - m_S^2 + i\epsilon} = i\frac{\kappa^2}{16\pi^2}\mathbf{B_0}(p^2, m_S^2, m_S^2)$$

$$\overset{p^2=0}{=} -i\frac{\kappa^2}{16\pi^2}\left(-\ln\left(\frac{\Lambda^2}{m_S^2}\right) - 1\right) \tag{2.32c}$$

The loop functions $\mathbf{A}_0, \mathbf{B}_0$ are defined in appendix B.1. Both Π_a and Π_b contain the dangerous Λ^2 contributions, but with opposite signs (λ_S has to be positive to ensure vacuum stability). To

make them cancel each other, we demand

$$\lambda_S = |\lambda_f|^2. \tag{2.33}$$

By assuming another scalar particle with the same properties as S, the terms of Π_b, Π_c are effectively multiplied by two. The coupling $\kappa = \lambda_S v$ can be re-expressed as $\kappa^2 = (\lambda_S v)^2 = (|\lambda_f|^2 v)^2 = |\lambda_f|^2 \cdot 2m_f^2$. The mass correction then reads (in the approximation $p^2 = 0$)

$$-(\Pi_a + 2(\Pi_b + \Pi_c)) \overset{p^2 \to 0}{=} \frac{\left|\lambda_f^2\right|}{16\pi^2} \left[-2\Lambda^2 + 2\Lambda^2 + 6m_f^2 \ln\left(\frac{\Lambda^2}{m_f^2}\right) + 4m_f^2 \right.$$
$$\left. -2m_S^2 \ln\left(\frac{\Lambda^2}{m_S^2}\right) - 4m_f^2 \ln\left(\frac{\Lambda^2}{m_S^2}\right) - 4m_f^2 \right] \tag{2.34}$$

Demanding $\lambda_S = |\lambda_f|^2$ along with another copy of the S particle, the quadratic contributions cancel. Imposing supersymmetry between the fermion f and two bosons S leads to exactly these conditions. The particles f and S would be each others superpartners. More precisely, the Dirac fermion f has four fermionic degrees of freedom, and they would be matched to four bosonic degrees of freedom, contained in two scalar fields S_1, S_2. SUSY transforms bosonic fields into fermionic ones and vice verse, so the equality of their degrees of freedom is necessary. The cancellation is not a coincidence, but a feature of the symmetry and persists throughout all orders of perturbation theory. Furthermore, in an unbroken SUSY model, the masses of superpartners are equal. Assuming $m_S^2 = m_f^2$, even the logarithmic terms in eq. (2.34) would cancel. An exact supersymmetry "shields" the scalar masses from any high scale. But, our world is not supersymmetric, since there are no superpartners of the same mass as the SM particles. The answer could be that we live in a spontaneously broken supersymmetry, just like the broken electroweak symmetry, in which the condition $m_f^2 = m_S^2$ does not hold. In that case, logarithmic divergences appear, but quadratic divergences still cancel. The corrections to the Higgs mass are then of the order $m_S^2 - m_f^2$. This type of SUSY breaking is called soft breaking [128], where eq. (2.33) still holds. The softly broken SUSY protects the Higgs mass from arbitrary high scales, but not from the mass scale of the superpartners (generalised as M_{SUSY}). If M_{SUSY} is much larger then $\mathcal{O}(1\,\text{TeV})$, the theory becomes less attractive. In that case, a little hierarchy problem [129, 130] would be reintroduced.

2.2.6 Grand unification

The unification of forces has been a guiding principle in physics, as in the formulation of electric and magnetic forces in Maxwell's equations or in the electroweak theory by Weinberg, Glashow and Salam [1–3]. The SM gauge group is the direct product of three simple Lie groups and the choice of representations in table 2.1 strongly hints at an embedding into a higher dimensional group. The idea of a grand unified theory (GUT) [66, 131–133] is to have a single group G_{GUT}, such as $SU(5)$ or $O(10)$, which is associated with a single coupling constant g and spontaneously broken down to G_{SM}. This predicts that the three forces of the SM appear as only one force at the GUT scale. From a bottom-up perspective, the gauge couplings g_1, g_2, g_3 can be evolved to a
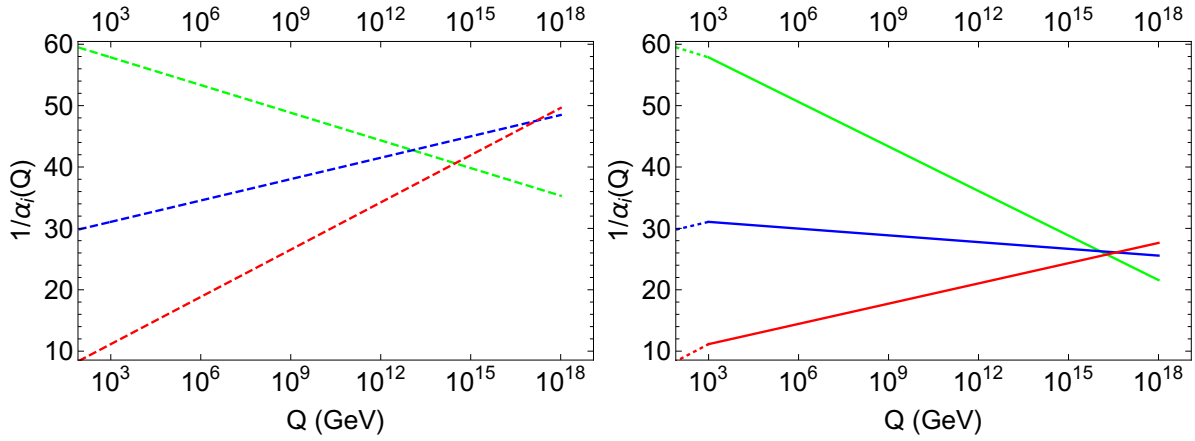
Figure 2.3: Evolution of gauge couplings (expressed through $\alpha_i^{-1} \equiv 4\pi g_i^{-2}$) in the SM (left) and MSSM (right). The colour code is red for g_3, blue for g_2 and green for g_1.

high scale. The evolution is described by the renormalisation group equations. [4] Physically, the coupling g_1 of $U(1)_Y$ increases with energy scale Q, while g_2, g_3 decrease with higher energies. In the Standard Model, the unification seems plausible, but is not very good (fig. 2.3, left). Including more particles into the model modifies the running of the couplings. In supersymmetry, the additional particle content makes just the right change (fig. 2.3, right, for the MSSM) and predicts unification at a scale $M_{\mathrm{GUT}} \sim 10^{16}\,\mathrm{GeV}$. The dependence of the gauge couplings $g_i(Q)$ on the scale Q is described by the so-called beta functions, which are calculated perturbatively. At one loop, their form is particularly simple,

$$\beta_i = Q\frac{\mathrm{d}}{\mathrm{d}Q}g_i(Q) = \frac{1}{16\pi^2}b_i g_i^3, \tag{2.35a}$$

$$Q\frac{\mathrm{d}}{\mathrm{d}Q}\alpha_i^{-1} = Q\frac{\mathrm{d}}{\mathrm{d}Q}\left(\frac{g_i^2}{4\pi}\right)^{-1} = -\frac{1}{2\pi}b_i, \tag{2.35b}$$

yielding a linear evolution of α_i^{-1} in terms of $\log Q$. The coefficients b_i for the SM [141] and MSSM [142] are as follows,

$$(b_1, b_2, b_3)_{\mathrm{SM}} = \left(\frac{41}{10}, -\frac{19}{6}, -7\right), \tag{2.36a}$$

$$(b_1, b_2, b_3)_{\mathrm{MSSM}} = \left(\frac{33}{5}, 1, -3\right). \tag{2.36b}$$

2.2.7 Uniqueness of supersymmetry

A relativistic gauge theory is invariant under the Poincaré group which describes the external symmetry of space-time. On the other hand there are the internal gauge symmetries, transforming the fields among themselves. There can also be discrete symmetries such as charge conjugation

---

[4] The idea of the renormalisation group dates back to Kadanoff [134] and Wilson [135]. Important achievements in its understanding were made in Refs. [136–138]. The equation by Callan and Symanzik [139, 140] led to a widespread application of the renormalisation group.

C, spatial inversion (parity) P and time reversal T. The Coleman-Mandula theorem [143] states that space-time symmetries and internal symmetries cannot be combined in any but a trivial way. The total local symmetry group of a consistent 4D quantum field theory can only be a direct product of the Poincaré group and an internal symmetry group. However, the theorem applies only to internal symmetries described by Lie algebras. A possible loophole to this no-go theorem is supersymmetry, which introduces a graded Lie algebra (Lie superalgebra) with fermionic generators $Q, Q^\dagger$ and anticommutator relations [51]. The generalisation to Coleman-Mandula is the theorem by Haag, Lopuszanski and Sohnius [144], stating that supersymmetry is the only loophole that allows the connection between the two groups. The operators $Q, Q^\dagger$ transform bosonic states into fermionic ones and vice versa,

$$Q|\text{Boson}\rangle = |\text{Fermion}\rangle, \qquad Q|\text{Fermion}\rangle = |\text{Boson}\rangle, \tag{2.37}$$

and must therefore be anticommuting two-component objects. The symmetry can be constructed using $\mathcal{N}$ different generators, but the case $\mathcal{N} = 1$ is mostly considered. Together with the Poincaré generators $P_\mu, M_{\mu\nu}$, they form the Lie superalgebra,

$$\{Q_\alpha, Q_{\dot\alpha}^\dagger\} = 2\sigma_{\alpha\dot\alpha}^\mu P_\mu, \tag{2.38}$$

$$\{Q_\alpha, Q_\beta\} = \{Q_{\dot\alpha}^\dagger, Q_{\dot\beta}^\dagger\} = 0, \tag{2.39}$$

$$[P^\mu, Q_\alpha] = \left[P^\mu, Q_{\dot\alpha}^\dagger\right] = 0, \tag{2.40}$$

with $\{A, B\} \equiv AB + BA$ being the anticommutator and $[A, B] \equiv AB - BA$ the commutator. For an introduction to the dotted and undotted spinor notation we refer to Ref. [145]. Especially eq. (2.38) is notable, as it relates the SUSY generators to the generator of space-time translations, P_μ. Allowing local SUSY transformations [146, 147] leads directly to curved space-time and the inclusion of gravity. In conclusion, supersymmetry is a unique extension to the total symmetry group of a theory and points towards further unification via supergravity. Historically, searching and formulating symmetries which could in principle be realised has been a promising concept.

2.3 Supersymmetry and the MSSM

This section introduces the MSSM [52, 53] with a focus on the Higgs sector and the scalar potential. There exists a wealth of literature about the model and supersymmetry in general, such as Refs. [51–67]. A popular introduction to the MSSM and the superfield notation is the supersymmetry primer by S. Martin [60]. The complete Lagrangian is given in Ref. [148] and a list of Feynman rules is found in Ref. [149].

A convenient framework to construct manifestly supersymmetric models is the superfield formalism [150]. It extends the concept of space-time (in which a point is described by a four-vector x) by introducing Grassmannian coordinates $\theta, \bar\theta$. A superfield $\mathbf{\Phi}(x, \theta, \bar\theta)$ contains both bosonic and fermion degrees of freedom and allows to write down manifestly supersymmetric expressions. The components are commonly labelled $\Phi, \widetilde{\Phi}$, where the field without a tilde is the known SM-like particle (if this connection can be made at all). The gauge group G is the same as in the SM. This fixes the necessary vector gauge fields and their fermionic superpartners, the *gauginos*. The matter particle content is a set of chiral supermultiplets. Table 2.2 shows the superfields and their components for the MSSM as well as the representations underneath which they transform. The construction of the supersymmetric Lagrangian follows quite different rules

superfield	spin 0	spin $1/2$	gen.	$SU(3)_C$	$SU(2)_L$	$U(1)_Y$
$\mathbf{H_u}$	$H_u = \begin{pmatrix} H^+ \\ H^0 \end{pmatrix}$	$\widetilde{H}_u = \begin{pmatrix} \widetilde{H}^+ \\ \widetilde{H}^0 \end{pmatrix}$	1	**1**	**2**	$\frac{1}{2}$
$\mathbf{H_d}$	$H_d = \begin{pmatrix} H^0 \\ H^- \end{pmatrix}$	$\widetilde{H}_d = \begin{pmatrix} \widetilde{H}^0 \\ \widetilde{H}^- \end{pmatrix}$	1	**1**	**2**	$-\frac{1}{2}$
$\mathbf{Q}$	$\widetilde{Q} = \begin{pmatrix} \widetilde{u}_L \\ \widetilde{d}_L \end{pmatrix}$	$Q = \begin{pmatrix} u_L \\ d_L \end{pmatrix}$	3	**3**	**2**	$\frac{1}{6}$
$\mathbf{U}$	$\widetilde{u}_R^*$	$u_R^\dagger$	3	$\mathbf{\bar{3}}$	**1**	$-\frac{2}{3}$
$\mathbf{D}$	$\widetilde{d}_R^*$	$d_R^\dagger$	3	$\mathbf{\bar{3}}$	**1**	$\frac{1}{3}$
$\mathbf{L}$	$\widetilde{L} = \begin{pmatrix} \widetilde{\nu}_L \\ \widetilde{e}_L \end{pmatrix}$	$L = \begin{pmatrix} \nu_L \\ e_L \end{pmatrix}$	3	**1**	**2**	$-\frac{1}{2}$
$\mathbf{E}$	$\widetilde{e}_R^*$	$e_R^\dagger$	3	**1**	**1**	1
superfield	spin 1	spin $1/2$	gen.	$SU(3)_C$	$SU(2)_L$	$U(1)_Y$
$\mathbf{B}_\mu$	B_μ	λ_B	1	adjoint of $U(1)_Y$		
$\mathbf{W}_\mu^a$	W_μ^a	λ_W^a	3	adjoint (**3**) of $SU(2)_L$		
$\mathbf{G}_\mu^a$	G_μ^a	λ_G^a	8	adjoint (**8**) of $SU(3)_C$		

Table 2.2: This table lists the left-chiral superfields of the MSSM and the representations of the gauge group G_{SM} underneath which they transform. The fermionic parts are given in terms of 2-component Weyl spinors.

than those of a non-supersymmetric one. It is derived from an auxiliary function $\mathcal{W}$ called the superpotential, a holomorphic and gauge invariant function of left-chiral superfields. All superfields in table 2.2 are chosen left-chiral, hence the use of conjugate components of $\mathbf{U}, \mathbf{D}, \mathbf{E}$. If the theory is supposed to be 4D-renormalisable, only terms up to the power of three in the superfields are allowed. This translates to Lagrangian terms up to mass dimension four.

The superpotential of the MSSM is given by

$$\mathcal{W}_{\mathrm{MSSM}} \equiv Y_u^{ij} \mathbf{Q}_i \mathbf{H_u} \mathbf{U}_j - Y_d^{ij} \mathbf{Q}_i \mathbf{H_d} \mathbf{D}_j - Y_e^{ij} \mathbf{L}_i \mathbf{H_d} \mathbf{E}_j + \mu \mathbf{H_u} \mathbf{H_d}. \tag{2.41}$$

The minus signs are chosen by convention, such that eq. (2.68) will have only plus signs. The Higgs field $\mathbf{H_d}$ plays the same role as its SM counterpart H. However, the MSSM requires a second Higgs doublet $\mathbf{H_u}$ with opposite quantum numbers for two reasons: First, the holomorphy requirement of the superpotential forbids the use of conjugated fields. The second reason is anomaly cancellation: In the SM, gauge anomalies of the type $SU(2)_L^2 U(1)_Y$ and $U(1)_Y^3$ vanish, i.e. the conditions $\mathrm{tr}\left[T_3^2 Y\right] = \mathrm{tr}\left[Y^3\right] = 0$ are fulfilled (the traces run over all left-handed Weyl degrees of freedom). This cancellation would be spoiled by introducing the fermionic partners of only one Higgs doublet. Adding a second Higgs doublet with opposite hypercharge makes the MSSM free of gauge anomalies.

The term $\mu \mathbf{H_u} \mathbf{H_d}$ is unique to the MSSM with a parameter μ of mass dimension one. Being a free parameter, its scale is in principle undetermined. However, it must be not much higher than the electroweak scale if we want to avoid another hierarchy problem. This means that μ has to be tuned to a value close to v_{ew} *before* EWSB takes place, which is known as the μ problem [151].

gauge eigenstates	mass eigenstates	name
$\left[\widetilde{u}, \widetilde{c}, \widetilde{t}\right]_{L,R}$	$\widetilde{u}_i \quad i = 1 \dots 6$	up-type squarks
$\left[\widetilde{d}, \widetilde{s}, \widetilde{b}\right]_{L,R}$	$\widetilde{d}_i \quad i = 1 \dots 6$	down-type squarks
$\left[\widetilde{e}, \widetilde{\mu}, \widetilde{\tau}\right]_{L,R}$	$\widetilde{e}_i \quad i = 1 \dots 6$	(charged) sleptons
$\widetilde{\nu}_e, \widetilde{\nu}_\mu, \widetilde{\nu}_\tau$	$\widetilde{\nu}_i \quad i = 1 \dots 3$	sneutrinos
$\widetilde{H}_u^0, \widetilde{H}_d^0, \widetilde{W}^3, \widetilde{B}$	$\widetilde{\chi}_i^0 \quad i = 1 \dots 4$	neutralinos
$\widetilde{H}_d^-, (\widetilde{H}_u^+)^\dagger, \widetilde{W}^-, (\widetilde{W}^+)^\dagger$	$\widetilde{\chi}_i^- \quad i = 1, 2$	charginos
H_u^0, H_d^0	$h, H, A^0 \,(, G^0)$	neutral Higgs, (Goldstone)
$H_d^-, (H_u^+)^*$	$H^\pm \,(, G^\pm)$	charged Higgs, (Goldstone)
$\widetilde{g}$	$\widetilde{g}$	gluino

Table 2.3: Gauge and mass eigenstates of the MSSM

In tab. 2.2 the fields are given in their gauge eigenstates. Fields with the same quantum numbers usually mix to form new mass eigenstates, which are shown in tab. 2.3. The total particle count of mass eigenstates yields 28 sparticles (not counting colour states or antiparticles as separate entities) plus three additional Higgs states, assuming that h is identified with the discovered 125 GeV state. In the MSSM with CP conservation in the Higgs sector, there will be two CP-even bosons h, H and one CP-odd A^0. In the more general CP-violating case, the states h, H, A^0 will mix.

In unbroken supersymmetry, particles and superpartners have the same mass. Since this is not observed in nature, supersymmetry has to be broken. The main motivation of supersymmetry, curing the hierarchy problem by cancelling quadratic divergences, should not get lost in the breaking process. This can be achieved by adding terms with dimensionful couplings to the Lagrangian, so-called soft SUSY breaking terms [128]. While the correct mechanism of SUSY breaking is unknown, its effect is parameterised by these soft breaking parameters. The soft-breaking Lagrangian of the MSSM is (using $\widetilde{D} = \widetilde{d}_R^*$, $\widetilde{U} = \widetilde{u}_R^*$ and $\widetilde{E} = \widetilde{e}_R^*$ alternatively)

$$
\begin{aligned}
-\mathcal{L}_{\text{soft}} = {} & m_{H_d}^2 \left|H_d\right|^2 + m_{H_u}^2 \left|H_u\right|^2 \\
& + \widetilde{Q}^\dagger m_q^2 \widetilde{Q} + \widetilde{L}^\dagger m_l^2 \widetilde{L} + \widetilde{D}^\dagger m_d^2 \widetilde{D} + \widetilde{U}^\dagger m_u^2 \widetilde{U} + \widetilde{E}^\dagger m_e^2 \widetilde{E} \\
& + \frac{1}{2} \left(M_1 \lambda_B \lambda_B + M_2 \lambda_W^a \lambda_W^a + M_3 \lambda_G^\alpha \lambda_G^\alpha + \text{h.c.}\right) \\
& + \left(T_u^{ij} \widetilde{Q}_i H_u \widetilde{U}_j + T_d^{ij} \widetilde{Q}_i H_d \widetilde{D}_j + T_e^{ij} \widetilde{L}_i H_d \widetilde{E}_j + b H_u H_d + \text{h.c.}\right),
\end{aligned}
\tag{2.42}
$$

with m_ϕ^2 a symmetric 3×3 matrix for $\phi = q, u, d, l, e$. All soft breaking terms have a coupling with mass dimension ≥ 1 and include mass terms for all scalar particles ($m_{\phi,ij}^2$, $m_{H_u}^2$, $m_{H_d}^2$), gaugino mass terms (M_1, M_2, M_3), and other couplings between scalar components (T_u, T_d, T_e, b) that are analogous to the superpotential terms. The large number of soft breaking parameters complicates realistic predictions and thus requires some simplifying assumptions. Similar to the SM, the Higgs mechanism is the necessary ingredient to provide masses for fermions and vectors. Because of the extended scalar sector, the MSSM Higgs mechanism is more complicated. In a general SUSY model with scalars φ_i and a gauge group made up of direct products of simple Lie groups G_A with gauge couplings g_A and generators T_A^a, a general formula for the scalar

potential can be given [60]:

$$V(\varphi_i) = \sum_j |W_j|^2 + \frac{1}{2} \sum_A g_A^2 \sum_{i,j} \sum_a \left(\varphi_i^\dagger T_A^a \varphi_i\right) \left(\varphi_j^\dagger T_A^a \varphi_j\right), \qquad W_j \equiv \frac{\partial \mathcal{W}}{\partial \varphi_j}. \tag{2.43}$$

φ_i assumes all non-singlet representations of the gauge subgroup G_A. Evaluating the general formula of eq. (2.43) for $\varphi_i = H_u, H_d$ with respect to $SU(2)_L$ and $\varphi_i = H_u^+, H_u^0, H_d^0, H_d^-$ with respect to $U(1)_Y$ gives the Higgs potential

$$V(H_u, H_d) = V_F + V_D, \tag{2.44a}$$

$$V_F(H_u, H_d) = \left(|\mu|^2 + m_{H_u}^2\right)|H_u|^2 + \left(|\mu|^2 + m_{H_d}^2\right)|H_d|^2 + (bH_uH_d + \text{h.c.}), \tag{2.44b}$$

$$V_D(H_u, H_d) = \frac{g_1^2 + g_2^2}{8}\left(|H_u|^2 - |H_d|^2\right)^2 + \frac{g_2^2}{2}\left|H_d^\dagger H_u\right|^2. \tag{2.44c}$$

In search for the minimum, $H_d^- = 0$ and $H_u^+ = 0$ can be assumed since nature does not exhibit a charged ground state:

$$\begin{aligned} V(H_u^0, H_d^0) &= \left(|\mu|^2 + m_{H_u}^2\right)\left|H_u^0\right|^2 + \left(|\mu|^2 + m_{H_d}^2\right)\left|H_d^0\right|^2 + \left(-bH_u^0H_d^0 + \text{h.c.}\right) \\ &\quad + \frac{g_1^2 + g_2^2}{8}\left(\left|H_d^0\right|^2 - \left|H_u^0\right|^2\right)^2. \end{aligned} \tag{2.45}$$

Without the SUSY-breaking parameters $m_{H_u}^2, m_{H_d}^2, b$ the minimum would be at the origin, $V(0) = 0$, and electroweak symmetry breaking would not take place. b can be assumed real and positive, because any phase can be absorbed into the relative phases of H_u^0, H_d^0. The condition that the potential is bounded from below leads to eq. (2.46a) and demanding that the origin is unstable leads to eq. (2.46b),

$$2b < 2|\mu|^2 + m_{H_d}^2 + m_{H_u}^2, \tag{2.46a}$$

$$b^2 > \left(|\mu|^2 + m_{H_d}^2\right)\left(|\mu|^2 + m_{H_d}^2\right). \tag{2.46b}$$

Assuming a breaking pattern of $H_i^0 = (v_i + \phi_i + i\sigma_i)/\sqrt{2}$ with $i = u, d$, the tadpole equations are

$$t_d \equiv \frac{\partial V}{\partial \phi_d}\bigg|_{\text{min}} = \left(m_{H_d}^2 + |\mu|^2\right)v_d - b\,v_u + \frac{g_1^2 + g_2^2}{8}\left(v_d^2 - v_u^2\right)v_d, \tag{2.47a}$$

$$t_u \equiv \frac{\partial V}{\partial \phi_u}\bigg|_{\text{min}} = \left(m_{H_u}^2 + |\mu|^2\right)v_u - b\,v_d - \frac{g_1^2 + g_2^2}{8}\left(v_d^2 - v_u^2\right)v_u. \tag{2.47b}$$

Similarly to the SM, the Higgs fields provide masses to the gauge bosons via the gauge covariant derivatives,

$$(D_\mu H_u)^\dagger(D^\mu H_u) + (D_\mu H_d)^\dagger(D^\mu H_d), \tag{2.48}$$

resulting in a tree-level mass

$$M_Z^2 = \frac{1}{4}(g_1^2 + g_2^2)(v_u^2 + v_d^2) \tag{2.49}$$

for the Z boson. From this, we can relate the VEVs of the MSSM with the SM one, i.e.

$v^2 = v_u^2 + v_d^2$. Using $\tan\beta = v_u/v_d$ and eq. (2.49), the tadpoles can be expressed as

$$\frac{t_d}{v_d} = m_{H_d}^2 + |\mu|^2 - b\tan\beta + \frac{1}{2}M_Z^2\cos 2\beta = 0, \tag{2.50a}$$

$$\frac{t_u}{v_u} = m_{H_u}^2 + |\mu|^2 - b\cot\beta - \frac{1}{2}M_Z^2\cos 2\beta = 0. \tag{2.50b}$$

Adding up eq. (2.50a) and eq. (2.50b) gives the relation

$$m_{H_u}^2 + m_{H_d}^2 + 2|\mu|^2 = \frac{2b}{\sin 2\beta}. \tag{2.51}$$

Considering the mass matrix of the imaginary Higgs components, we get

$$\mathcal{M}_A^2 = \left(\frac{\partial^2 V}{\partial\sigma_i\partial\sigma_j}\right) = \begin{pmatrix} m_{H_d}^2 + |\mu|^2 + \frac{1}{2}M_Z^2 c_{2\beta} & b \\ b & m_{H_u}^2 + |\mu|^2 - \frac{1}{2}M_Z^2 c_{2\beta} \end{pmatrix} = b\begin{pmatrix} \tan\beta & 1 \\ 1 & \cot\beta \end{pmatrix}, \tag{2.52}$$

where the last equality exploits the tadpole equations. This matrix is diagonalised by

$$\begin{pmatrix} \sigma_d \\ \sigma_u \end{pmatrix} = Z_A\begin{pmatrix} G^0 \\ A^0 \end{pmatrix} \qquad \text{with } Z_A \equiv \begin{pmatrix} \cos\beta & \sin\beta \\ -\sin\beta & \cos\beta \end{pmatrix}, \tag{2.53}$$

with two eigenvalues, 0 and $2b/\sin 2\beta$. In a general R_ξ gauge, the same gauge fixing terms as in the SM are added, eq. (2.17), changing the zero eigenvalue to $\xi_Z M_Z^2$, which corresponds to the neutral Goldstone boson G^0. The other state is a heavy Higgs boson A^0 with mass

$$m_A^2 = \frac{2b}{\sin 2\beta}. \tag{2.54}$$

Moving on to the charged Higgs fields $(H_d^-, (H_u^+)^*)$, we consider the mass matrix $\mathcal{M}_{H^\pm}^2$ with

$$(\mathcal{M}_{H^\pm}^2)_{11} = m_{H_d}^2 + |\mu|^2 + \frac{1}{2}M_Z^2 c_{2\beta} + \frac{1}{4}g_2^2 v_u^2 = b\tan\beta + M_W^2\sin\beta, \tag{2.55a}$$

$$(\mathcal{M}_{H^\pm}^2)_{22} = m_{H_u}^2 + |\mu|^2 - \frac{1}{2}M_Z^2 c_{2\beta} + \frac{1}{4}g_2^2 v_d^2 = b\cot\beta + M_W^2\cos\beta, \tag{2.55b}$$

$$(\mathcal{M}_{H^\pm}^2)_{12} = b + \frac{1}{4}g_2^2 v_d v_u = b + M_W^2 s_\beta c_\beta, \tag{2.55c}$$

$$\Rightarrow \mathcal{M}_{H^\pm}^2 = \mathcal{M}_A^2 + M_W^2\begin{pmatrix} s_\beta^2 & s_\beta c_\beta \\ s_\beta c_\beta & c_\beta^2 \end{pmatrix} \tag{2.55d}$$

With a field rotation

$$\begin{pmatrix} H_d^- \\ (H_u^+)^* \end{pmatrix} = Z^\pm\begin{pmatrix} G^- \\ H^- \end{pmatrix}, \qquad \text{with } Z^\pm \equiv \begin{pmatrix} \cos\beta & \sin\beta \\ -\sin\beta & \cos\beta \end{pmatrix}, \tag{2.56}$$

the mass matrix becomes diagonal. Very similar to the previous case, we obtain a massless field $G^\pm$ (whose unphysical mass becomes $\xi_W M_W^2$ when gauge fixing terms are added) and a new

massive charged Higgs $H^\pm$ with a mass

$$M_{H^\pm}^2 = M_W^2 + m_A^2. \tag{2.57}$$

The mass matrix $\mathcal{M}_h^2$ for the real Higgs components is given by

$$\left(\mathcal{M}_h^2\right)_{11} = \frac{\partial^2 V}{\partial \phi_d^2} = m_{H_d}^2 + |\mu|^2 + \frac{g_1^2 + g_2^2}{8}\left(3v_d^2 - v_u^2\right) = m_{H_d}^2 + |\mu|^2 + \frac{1}{2}M_Z^2(c_{2\beta} + 2c_\beta^2), \tag{2.58a}$$

$$\left(\mathcal{M}_h^2\right)_{22} = \frac{\partial^2 V}{\partial \phi_u^2} = m_{H_u}^2 + |\mu|^2 + \frac{g_1^2 + g_2^2}{8}\left(3v_u^2 - v_d^2\right) = m_{H_u}^2 + |\mu|^2 - \frac{1}{2}M_Z^2(c_{2\beta} - 2s_\beta^2), \tag{2.58b}$$

$$\left(\mathcal{M}_h^2\right)_{12} = \frac{\partial^2 V}{\partial \phi_u \partial \phi_d} = -b - \frac{g_1^2 + g_2^2}{4}v_d v_u = -b - M_Z^2 s_\beta c_\beta. \tag{2.58c}$$

Substituting the minimisation conditions (2.50a) and (2.50b) into $\mathcal{M}_h^2$, we get

$$\mathcal{M}_h^2 = \begin{pmatrix} m_A^2 s_\beta^2 + M_Z^2 c_\beta^2 & -(m_A^2 + M_Z^2)s_\beta c_\beta \\ -(m_A^2 + M_Z^2)s_\beta c_\beta & m_A^2 c_\beta^2 + M_Z^2 s_\beta^2 \end{pmatrix}. \tag{2.59}$$

Using the formula for the eigenvalues of a symmetric matrix $\begin{pmatrix} a & c \\ c & b \end{pmatrix}$,

$$\lambda_{1,2} = \frac{1}{2}\left(a + b \pm \sqrt{(a-b)^2 + 4c^2}\right), \tag{2.60}$$

we obtain the eigenvalues of $\mathcal{M}_h^2$:

$$m_{h,H}^2 = \frac{1}{2}\left(m_A^2 + M_Z^2 \mp \sqrt{(m_A^2 + M_Z^2)^2 - 4m_A^2 M_Z^2 c_{2\beta}^2}\right). \tag{2.61}$$

The rotation to the eigenstates h, H is described by the angle α,

$$\begin{pmatrix} h \\ H \end{pmatrix} = \begin{pmatrix} -\sin\alpha & \cos\alpha \\ \cos\alpha & \sin\alpha \end{pmatrix}\begin{pmatrix} h_d \\ h_u \end{pmatrix} \tag{2.62}$$

where α is determined by [152]

$$\sin 2\alpha = -\frac{m_A^2 + M_Z^2}{m_H^2 - m_h^2}\sin 2\beta, \tag{2.63}$$

$$\cos 2\alpha = -\frac{m_A^2 - M_Z^2}{m_H^2 - m_h^2}\cos 2\beta. \tag{2.64}$$

CP is conserved at tree level in the MSSM, but at higher orders, CP violation can be introduced. In that case a mixing of all neutral components $(\phi_d, \phi_u, \sigma_d, \sigma_u)$ has to be considered. The light state h is assumed to be the $125\,\text{GeV}$ Higgs boson. An important limit for its mass is obtained

by expanding m_h^2 for $m_A^2 \ll M_Z^2$ and $m_A^2 \gg M_Z^2$,

$$m_h^2 = m_A^2 \cos^2 2\beta + \mathcal{O}\left(\frac{m_A^2}{M_Z^2}\right), \tag{2.65a}$$

$$m_h^2 = M_Z^2 \left(\cos^2 2\beta - \frac{M_Z^2}{4m_A^2} \sin^2 4\beta + \mathcal{O}\left(\frac{M_Z^2}{m_A^2}\right)^2\right). \tag{2.65b}$$

In between those limits, m_h^2 has no stationary point. In the decoupling limit $m_A^2 \gg M_Z^2$, h has SM-like couplings to gauge bosons and fermions. Also, the angle α can be approximated by

$$\alpha \approx \beta - \frac{\pi}{2} \qquad \text{for } m_A^2 \gg M_Z^2. \tag{2.66}$$

The remarkable implication of eq. (2.65) is that the MSSM predicts a bounded tree-level Higgs mass

$$m_h \leq M_Z \left|\cos 2\beta\right|. \tag{2.67}$$

The masses of the other Higgses $A^0, H^0, H^\pm$ are unrestricted because they depend on the free parameter b. Fortunately, this does not rule out the MSSM because radiative corrections can be large enough to push m_h towards the measured value of $125\,\text{GeV}$, which will be discussed in section 3.1. After all, the MSSM Higgs sector is described by five parameters $m_{H_d}^2, m_{H_u}^2, b, v_d, v_u$, of which two can be eliminated by the tadpole equations. The remaining parameters are often chosen to be $\tan\beta$, M_Z, m_A. The mass M_Z is measured very precisely, leaving only two unknown parameters, m_A and $\tan\beta$.

We refer to Ref. [152] for the discussion of the mass matrices of the other sparticles, since they are not explicitly relevant for this thesis (except for the up-squark matrix, which is given in section 5.1). The quark and lepton masses are given by (flavour indices suppressed)

$$\mathcal{L}_{\text{Yukawa}} \supset \frac{Y_u v_u}{\sqrt{2}} \overline{u_L} u_R + \frac{Y_d v_d}{\sqrt{2}} \overline{d_L} d_R + \frac{Y_e v_d}{\sqrt{2}} \overline{e_L} e_R, \tag{2.68}$$

where the Yukawas are related to their SM counterparts via

$$Y_u^{\text{MSSM}} = Y_u^{\text{SM}} / \sin\beta, \qquad Y_{d,e}^{\text{MSSM}} = Y_{d,e}^{\text{SM}} / \cos\beta. \tag{2.69}$$

Some general remarks can be made based on the theoretical analysis and non-observation of sparticles in direct searches in the ATLAS and CMS experiments. The gluino $\tilde{g}$ is unique in the sense that it cannot mix with any other particle. Its mass is equal to M_3 at tree level, and it can be related to the other gaugino masses M_1, M_2 under simplified boundary conditions like mSUGRA [5] [153–156] or GMSB [6] [157–161]. This roughly implies $M_3 : M_2 : M_1 \approx 6 : 2 : 1$ at the TeV scale [60], making the gluino much heavier than the neutralinos and charginos. In a hadron collider it is most likely to detect coloured particles such as squarks and gluinos in strong pair production. During the first run of the LHC, the lower limits of the gluino mass have been driven far into the TeV range. For example, under the assumption $m_{\tilde{q}} = m_{\tilde{g}}$ in the CMSSM, the mass range $m_{\tilde{g}} < 1.85\,\text{TeV}$ is excluded [162].

---

[5] minimal super-gravity
[6] gauge mediated supersymmetry breaking

2.4 Effective potential

So far in the introduction to the SM and MSSM, $V(\phi)$ was treated like a function of semi-classical fields, which can be understood as the expectation value of their corresponding operators, $\phi_i = \langle 0|\hat{\phi}_i|0\rangle$. The Coleman-Weinberg effective potential [163–167] is a tool to include radiative corrections in the potential $V(\phi)$ and it is highly useful to the understanding of symmetry breaking and vacuum stability [168–176].

We briefly discuss its definition following Ref. [163]. Starting from the generating functional $Z[J]$ with an external source $J(x)$ in the path integral formalism,

$$Z[J] = \int \mathcal{D}\phi \exp\left(i \int \mathcal{L}\{\phi_i\} + J(x)\phi(x)\mathrm{d}^4x\right) = e^{iW[J]}, \tag{2.70}$$

the functional $W[J]$ can be expanded in a Taylor series

$$W[J] = \sum_n \frac{1}{n!} \int \mathrm{d}^4x_1 \ldots \mathrm{d}^4x_n G^{(n)}(x_1, \ldots, x_n) J(x_1) \ldots J(x_n) \tag{2.71}$$

with the coefficients $G^{(n)}(x_1, \ldots, x_n)$ being the n-point connected Green's functions. Let a classical field be defined by $\phi_c(x) \equiv \frac{\delta W}{\delta J(x)}$. This field corresponds to the vacuum expectation value $\langle 0|\hat{\phi}|0\rangle = \phi_c$. Now, define the Legendre transform of $W[J]$ with respect to J as the effective action $\Gamma[\phi_c]$,

$$\Gamma[\phi_c] \equiv W[J] - \int \mathrm{d}^4x J(x)\phi_c(x). \tag{2.72}$$

We can relate the conjugate variables $J(x)$ and $\phi_c(x)$ via

$$\phi_c(x) = \frac{\delta W}{\delta J(x)}, \qquad J(x) = -\frac{\delta\Gamma}{\delta\phi_c(x)}. \tag{2.73}$$

Now consider an expansion of $\Gamma[\phi_c]$ with respect to ϕ_c, similar to eq. (2.71),

$$\Gamma[\phi_c] = \sum_n \frac{1}{n!} \int \mathrm{d}^4x_1 \ldots \mathrm{d}^4x_n \Gamma^{(n)}(x_1, \ldots, x_n)\phi_c(x_1) \ldots \phi_c(x_n), \tag{2.74}$$

where we can identify $\Gamma^{(n)}$ as the 1PI[7] Green's functions, the sum of all 1PI Feynman diagrams with n external lines. A proof of this statement can be found in Refs. [177, 178]. An alternative expansion of $\Gamma[\phi_c]$ can be done with respect to external momenta about $\partial_\mu\phi_c = 0$,

$$\Gamma[\phi_c] = \int \mathrm{d}^4x \left(-V_{\text{eff}}(\phi_c) + \frac{1}{2}(\partial_\mu\phi_c)^2 A(\phi_c) + \ldots\right). \tag{2.75}$$

The leading order term, corresponding to zero external momenta, is the effective potential $-V_{\text{eff}}(\phi_c)$. For the special case of J and ϕ_c independent of x, we have $V'_{\text{eff}}(\phi_c) = J$, or, if the external source J is not there at all,

$$V'_{\text{eff}}(\phi_c) = 0. \tag{2.76}$$

This means that in the vacuum, the value of ϕ_c is determined by the minimum of V_{eff}. From

---

[7] One-particle irreducible Feynman diagrams are connected diagrams that can not be disconnected by cutting a single internal line. They are evaluated without propagators on the external lines by convention.

comparing eq. (2.74) to eq. (2.75) it follows that $\Gamma^{(n)}$ is related to V_{eff} in the case of vanishing external momentum by

$$\Gamma^{(n)} = -\frac{\delta^n V_{\text{eff}}}{\delta\phi_c(x_1)\dots\delta\phi_c(x_n)}. \tag{2.77}$$

The physical meaning of V_{eff} is the minimum of the energy-density expectation value in the class of all normalised states $|\psi\rangle$ that satisfy $\langle\psi|\phi|\psi\rangle = \phi_c$ [178], i.e.

$$V_{\text{eff}}(\phi_c) = \langle\psi|\mathcal{H}|\psi\rangle \quad \text{for} \quad \delta\langle\psi|\mathcal{H}|\psi\rangle = 0. \tag{2.78}$$

V_{eff} is calculated from vacuum loop diagrams with explicit dependence on ϕ_c [163]. Therefore, all masses and couplings have to be taken as functions of ϕ_c. The effective potential is expanded in loop orders,

$$V_{\text{eff}} = V^{(0)} + \frac{1}{16\pi^2}V^{(1)} + \left(\frac{1}{16\pi^2}\right)^2 V^{(2)} + \dots, \tag{2.79}$$

where the tree-level part $V^{(0)}$ is found in the Lagrangian. The effective potential of the SM has received increased interest recently, in the form of contributions at leading order in the top Yukawa couplings at three loops [179] and leading QCD corrections even up to four loops [180]. The effective potential obeys an RGE [171],

$$\left[\mu\frac{\partial}{\partial\mu} - \gamma_i\phi_i\frac{\partial}{\partial\phi_i} + \beta_i\frac{\partial}{\partial\lambda_i}\right]V_{\text{eff}} = 0, \tag{2.80}$$

with couplings λ_i and their β functions, and fields ϕ_i with their anomalous dimensions γ_i.

Two properties of the effective potential shall be further discussed, which are gauge dependence and the problems that can be caused by massless scalars such as Goldstone bosons in the Landau gauge ($\xi = 0$). The effective potential $V_{\text{eff}}(\phi_i)$ truncated at a fixed loop order is gauge dependent, but the physical properties derived from it are not. The evolution of V_{eff} with respect to the gauge parameter ξ can be described by a formula proposed by Nielsen [181],

$$\left(\frac{\partial}{\partial\xi_a} + C_{ai}(\phi,\xi)\frac{\partial}{\partial\phi_i}\right)V_{\text{eff}}(\phi,\xi_a) = 0, \tag{2.81}$$

where ξ_a is a general set of gauge parameters and ϕ_i a set of scalar field expectation values. If $C_{ai}(\phi,\xi)$ can be calculated, the Nielsen identity eq. (2.81) implies that, given a solution $\hat{\phi}(\phi,\xi)$ of the differential equations

$$\frac{\partial\hat{\phi}_i}{\partial\xi_a} = C_{ai}(\hat{\phi},\xi) \tag{2.82}$$

with the boundary condition $\hat{\phi}(\phi,\xi_0) = \phi$, the function V_{eff} can be reparameterised by $\phi \to \hat{\phi}$, resulting in

$$\hat{V}(\phi) \equiv V_{\text{eff}}(\hat{\phi}(\phi,\xi_a),\xi_a). \tag{2.83}$$

This new function $\hat{V}(\phi,\xi)$ is now gauge independent,

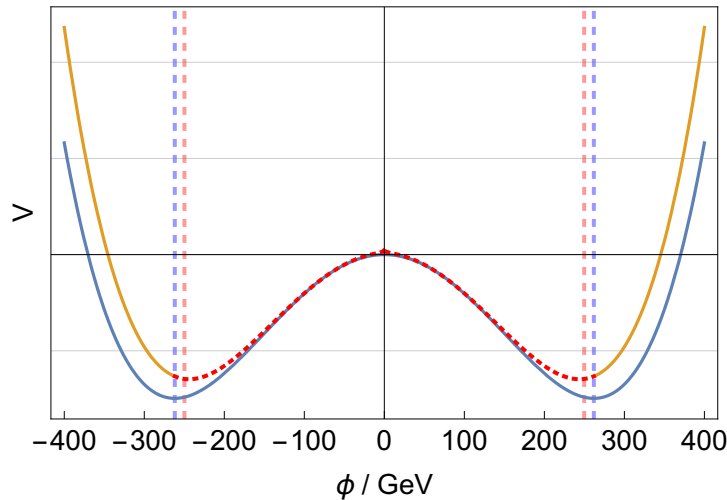$$\frac{\hat{V}(\phi,\xi)}{\partial\xi_a} = 0. \tag{2.84}$$

Figure 2.4: The effective potential of the SM at tree-level (blue) and one-loop (orange and red). The red dashed line marks the area where an imaginary part arises. The vertical blue (orange) dashed lines mark the minima at tree level (one-loop).

Also, it follows directly from eq. (2.81) that at the minimum of V_{eff}, i.e.

$$\left.\frac{\partial V_{\text{eff}}}{\partial \phi_i}\right|_{\phi=v} = 0, \tag{2.85}$$

eq. (2.81) reduces to

$$\left.\frac{\partial V_{\text{eff}}}{\partial \xi_a}\right|_{\phi=v} = 0, \tag{2.86}$$

which means that the minimum energy V_{min} is gauge invariant. The function $C_{ai}(\phi,\xi)$ can in fact be infinite at the minimum, which is why alternative treatments have been studied in Ref. [171], proving the same statement, eq. (2.86).

The preferred gauge for effective potential calculations is Landau gauge, $\xi = 0$, in which the Goldstones do not mix with the longitudinal vector modes and are massless. The masses and couplings entering the effective potential are field-dependent *tree-level* quantities. The squared Goldstone tree-level masses $m_{G^0}^2, m_{G^\pm}^2$ are zero at the minimum of $V^{(0)}$, but not at the minimum of the loop-corrected potential. For negative tree-level Goldstone masses, V_{eff} receives an imaginary part from the logarithms. A non-zero imaginary part of V_{eff} usually indicates instability [166], however this is not the case here. The field-dependent Goldstone mass can be obtained from the Higgs potential as $m_{G^0}^2 = \mu^2 + \lambda v^2 \equiv G$. To make the field dependence explicit, substitute $v \to \phi$, where $\phi = \Re(H(x))/\sqrt{2}$. We illustrate the tree-level and one-loop corrected potential of the SM in fig. 2.4 [8] The red-dashed line describes the region $-v^{(0)} \le \phi \le v^{(0)}$ where an imaginary part arises because of $G(\phi) < 0$. In this picture we consider the Lagrangian parameters as fixed while the VEVs change with loop corrections. Another way of treating the parameters is to demand that the VEVs keep their values throughout all loop orders, while the other Lagrangian parameters receive corrections. In practical calculations, the

---

[8] The numerical parameters are taken from Ref. [182] $\lambda = 0.12710$, $y_t = 0.93697$, $g_3 = 1.1666$, $\mu^2 = -(93.36\,\text{GeV})^2$, $g_2 = 0.6483$, $g_1 = 0.3587$, all taken at the scale $Q = m_t = 173.35\,\text{GeV}$. Only the dominant top quark contribution is taken into account.

spurious imaginary part of V_{eff} is often ignored and only the real part is minimised. By choosing a different renormalisation scale Q ($\overline{\text{MS}}$), the squared Goldstone mass can be tuned to a different value. Tuning it very close to zero produces a more serious practical problem. The terms with the lowest powers of G in the different loop orders of V_{eff} are as follows ($\overline{\ln}\,(m^2) \equiv \ln(m^2/Q^2)$),

$$V_{\text{SM}}^{(0)}(\phi) = \frac{1}{2}G^2\phi^2 + \dots, \tag{2.87}$$

$$V_{\text{SM}}^{(1)}(\phi) = \frac{3}{4}G^2\left(\overline{\ln}\,(G) - \frac{3}{2}\right) + \dots, \qquad (\overline{\text{MS}}) \tag{2.88}$$

$$V_{\text{SM}}^{(2)}(\phi) \sim G\,\overline{\ln}\,(G) + \dots. \tag{2.89}$$

The dots indicate all other terms, including higher powers of $G^n\,\overline{\ln}\,(G)^m$. In general the dependence at higher orders is [179]

$$V^{(\ell)}(\phi) \sim G^{3-\ell}\,\overline{\ln}\,(G), \qquad\qquad \ell = 1, 2, 3, \tag{2.90}$$

$$V^{(\ell)}(\phi) \sim G^{3-\ell}, \qquad\qquad \ell \geq 4. \tag{2.91}$$

For $\ell = 3$, the potential diverges logarithmically for $G \to 0$. For increasing powers $\ell \geq 4$, the divergence becomes even worse. The tadpole equations $V'(\phi) = 0$ already diverge at $\ell = 2$ for $G \to 0$. This is the so-called Goldstone boson catastrophe. However, this problem is rather a practical inconvenience than a theoretical problem. It is possible to obtain sensible mass corrections even from the IR-unsafe potential. The tree-level masses, such as G, depend on the renormalisation scale Q. If Q is chosen such that all tree-level masses are away from zero, the effect of the problem is minimal, as has been found in Ref. [183].

It is desirable to cure the problem by expressing V_{eff} in a IR-finite form. Recent treatments [184, 185] conclude that the divergence is an artefact of gauge dependence that arises because of the truncation at a fixed loop order. The potential is simply written down in a way that is of little use. The IR divergences can be rendered finite by resummation techniques involving higher order dressed Goldstone loops (daisy diagrams). In principle, this causes a shift $G \to G + \Pi_g$ in the terms of $V^{(\ell)}$ (Π_g is a well-defined contribution to the Goldstone mass that is calculated perturbatively [184]). Explicit expressions for the SM have been calculated in Ref. [185] and for the MSSM in Ref. [186]. In fact, if the loop corrections $V^{(n)} = V^{(n)}(G^0, G^\pm)$ are understood as a function of the field-dependent Goldstone masses $G^0, G^\pm$, it was found in Ref. [186] that the resummed potential $\widehat{V}_{\text{eff}}$ has the form

$$\begin{aligned}\widehat{V}_{\text{eff}} =& V^{(0)} + \frac{1}{16\pi^2}\left[V^{(1)}(0,0) + f(G^0 + \Delta^0) + 2f(G^\pm + \Delta^\pm)\right] \\ &+ \frac{1}{(16\pi^2)^2}\left[V^{(2)}(0,0) + \frac{1}{2}\Omega^0 G^0 + \Omega^\pm G^\pm\right]\end{aligned} \tag{2.92}$$

with the one-loop integral function

$$f(x) \equiv \frac{x^2}{4}\left(\overline{\ln}\,(x) - \frac{3}{2}\right). \tag{2.93}$$

The constants Δ^0, $\Delta^\pm$, Ω^0 and $\Omega^\pm$ are perturbatively calculated and depend on all masses and couplings. This equation was resummed to the order in G such that the first derivative can be taken safely. The result is that the tadpoles obtained from the resummed effective

potential do not change at one-loop, but at two-loop they receive a correction of the order $\Omega^0, \Omega^\pm$. Numerically, it turns out that the difference between using the resummed potential and using the IR-unsafe potential (or even just fixing $G^0 = G^\pm = 0$ from the start, neglecting their field dependence in the differentiation) is extremely small [186].

The field dependence of $G^0, G^\pm$ can be calculated from the mass matrices (tadpole equations must be inserted *after* differentiation) with the formula

$$\frac{\partial}{\partial x} \left[\mathcal{M}^2_{\text{diag}} \right]_{ii} = \left[U \frac{\partial \mathcal{M}^2}{\partial x} U^\dagger \right]_{ii}, \quad \text{no sum over } i, \quad \mathcal{M}^2_{\text{diag}} = U \mathcal{M}^2 U^\dagger. \tag{2.94}$$

Explicitly for the MSSM, we obtain

$$\frac{\partial G^0}{\partial v_i} = \frac{1}{4} (g_1^2 + g_2^2) v_i \cos(2\beta), \quad i = u, d, \tag{2.95}$$

$$\frac{\partial G^\pm}{\partial v_d} = \frac{1}{4} \left[g_1^2 v_d \cos(2\beta) + g_2^2 (v_d - v_u \sin(2\beta)) \right], \tag{2.96}$$

$$\frac{\partial G^\pm}{\partial v_u} = \frac{1}{4} \left[-g_1^2 v_u \cos(2\beta) + g_2^2 (v_u - v_d \sin(2\beta)) \right]. \tag{2.97}$$

These equations make clear that if one restricts oneself to the *gaugeless limit*,

$$g_1 = g_2 = 0, \tag{2.98}$$

the Goldstone masses $G^0, G^\pm$ are constant in the surroundings of the minimum. This way, the Goldstone problem is completely circumvented, but it works only for models in which the Higgs quartic potential is entirely determined by electroweak gauge couplings. In the NMSSM, this is already not the case and the Goldstone problem resurfaces. A more practical way of avoiding the divergence is to have the tree-level masses all away from zero. As pointed out earlier, this is usually the case if one works in the minimum of the full effective potential (including higher orders). Also the choice of Q allows to avoid the divergences, as has been analysed in Ref. [183]. Alternatively, one can use the full tadpole equations in combination with tree-level mass matrices without D-terms (i.e. gaugeless) to evaluate V_{eff}. This is the approach chosen in the implementation described in chapter 4, where also other arguments in favour of the gaugeless limit are discussed.

Radiative Higgs mass corrections

This chapter sets up the definitions needed for the Feynman diagrammatic approach and effective potential approach to obtain two-loop Higgs mass corrections in a model-independent way and presents the necessary calculations. One of the main contributions of this thesis is the description and implementation of these approaches into `SARAH` (previously published in Refs. [187, 188]). The approach itself and the generic formulae from literature have existed for a long time, but have never been utilised in an automated code in this way. An introduction to `SARAH` and `SPheno` is given in chapter 4, along with details of the implementation. As a motivation, we first explain the importance of radiative Higgs mass corrections and the achievements in this field.

3.1 Introduction

One of the features of the MSSM is that it predicts an upper bound for the tree-level Higgs mass (eq. (2.67)), $m_h \leq M_Z = 91.2\,\text{GeV}$. If the MSSM is to predict the measured $125\,\text{GeV}$ mass, there have to be large radiative corrections. Considering that masses add in squares, the corrections have to be about $\sim 88\%$ the size of the tree-level value.

$$(125\,\text{GeV})^2 \approx (91.2\,\text{GeV})^2 + (85\,\text{GeV})^2. \tag{3.1}$$

In recent decades a lot of effort has been taken in the calculation of Higgs mass corrections in the MSSM, which was initiated by the observation that corrections from the stop can lift the Higgs mass above the LEP bound of $114\,\text{GeV}$ [189–193]. In the decoupling limit $M_A \gg M_Z$ the top and stop contribution at one-loop is [189, 190, 194]

$$m_h^2 = m_h^{2,\text{tree}} + \delta m_h^2 \approx M_Z^2 \cos^2 2\beta + \frac{3}{4\pi^2} \frac{m_t^4}{v^2} \left[\log\left(\frac{m_{\tilde{t}_1} m_{\tilde{t}_2}}{m_t^2}\right) + \frac{X_t^2}{M_S^2} \left(1 - \frac{X_t^2}{12 M_S^2}\right) \right], \tag{3.2}$$

with $X_t \equiv T_t - \mu \cot \beta$. The geometric mean of the stop masses arises in the logarithm, $M_S = \sqrt{m_{\tilde{t}_1} m_{\tilde{t}_2}}$, which is identified as the SUSY scale. The shift δm_h^2 is maximised for $X_t = \pm\sqrt{6} M_S$ known as the maximal mixing case. It has been estimated before the Higgs discovery that $m_h \leq 140\,\text{GeV}$ is possible with radiative corrections in the MSSM [195], assuming that the sparticles do not exceed $2\,\text{TeV}$. In realistic models, reaching $125\,\text{GeV}$ is challenging and usually requires very heavy and/or highly mixed stops. Explaining the large radiative corrections at one-loop comes with a poor theoretical uncertainty. The dominant two- and

three-loop corrections can change the predicted pole mass by several GeV. It is remarkable that only the light Higgs mass is that sensitive to radiative corrections. In contrast, all other SM particles enjoy additional symmetries which ensure the smallness of their mass corrections. At tree-level and for $m_A > 300\,\mathrm{GeV}$, the heavy Higgs H^0 has a larger share of H_d^0 (70%) than of H_u^0 in terms of superposition, and its coupling to the top quark is therefore suppressed, leading to smaller corrections from the top Yukawa coupling.

The full diagrammatic calculation at one-loop was done over two decades ago in Refs. [196–199]. At two-loop, the leading corrections in the effective potential approach, or the equivalent diagrammatic approach at zero momentum, have also been available for a long time [183, 200–210]. Several calculations using renormalisation group equation (RGE) techniques have been made in Refs. [194, 211–216]. The contributions are classified by coupling order in terms of the strong coupling $\alpha_s \equiv g_3^2/(4\pi)$, the top (bottom, tau) Yukawa coupling $y_{t,b,\tau}$ ($\alpha_{t,b,\tau} \equiv y_{t,b,\tau}^2/(4\pi)$) and the weak coupling, defined by the fine structure constant $\alpha \equiv e^2/(4\pi)$. The dominant orders at two loops are $\mathcal{O}\left(\alpha_s \alpha_t\right)$ and $\mathcal{O}\left(\alpha_t^2\right)$. With these expressions known, it is straightforward to extend them to all third-generation fermions:

$$\mathcal{O}\left(\alpha_s(\alpha_t + \alpha_b + \alpha_\tau)\right), \qquad \mathcal{O}\left((\alpha_t + \alpha_b + \alpha_\tau)^2\right). \tag{3.3}$$

These contributions are widely used in different public codes such as `SoftSUSY` [217–220], `SPheno` [221, 222], `SuSpect` [223] or `FeynHiggs` [224–227]. In particular the results of Refs. [200] are the ones implemented in `SPheno` and serve as the benchmark for all extensions that we discuss here. Even three-loop results of $\mathcal{O}\left(\alpha_s^2 \alpha_t\right)$ for vanishing external momenta exist [228–230] and are part of the code `H3m` [229]. The electroweak contributions of the MSSM have been estimated to account for a shift of $\sim 1\,\mathrm{GeV}$ [195].

With the improving mass precision in the LHC Runs I and II came a new wave of advances in this field: diagrammatic two-loop orders $\mathcal{O}\left(\alpha_s \alpha_t\right)$ and $\mathcal{O}\left(\alpha_t^2\right)$ including external momenta exist [231–234]. Also, effective model calculations matched to the MSSM have been performed [235, 236]. A good review about Higgs mass calculations in different tools and renormalisation schemes is given in Ref. [237]. An earlier numerical comparison between `SPheno`, `SoftSUSY` and `SuSpect` was done in Ref. [236]. The focus of attention has been on the MSSM, followed by the NMSSM.

One motivation for models beyond the MSSM is for example that they can lift the Higgs mass already at tree-level beyond M_Z by new F-term contributions [238–246] (including the NMSSM) or D-term contributions [247–253]. This makes these models more natural by reducing the fine-tuning [240, 241, 244, 254–256]. A brief overview of beyond-MSSM Higgs sectors is found in Ref. [257]. Also, non-minimal models can weaken direct SUSY constraints from collider searches by either predicting compressed spectra or reducing the expected missing transverse energy [258–261].

Despite the impressive advancement in this field the task of stating a reliable theoretical uncertainty of m_h still poses a challenge. The problem is that the size of the missing higher order corrections is simply not known. One way of estimating them is to measure the variations of the running mass $m_h(Q)$ within the interval $Q/2$ and $2Q$, because the dependence on the renormalisation scale Q decreases with higher orders. Another way is to calculate the ratio of a one-loop correction to its tree-level value and assume the same scaling behaviour for higher orders. It is possible that certain $(N + 1)$ loop diagrams can be more important than some individual N loop contributions. For example, strong contributions at three loops can dominate over electroweak two-loop contributions. Finally, the Higgs mass prediction depends on the
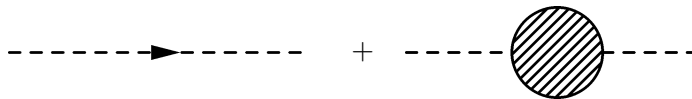
Figure 3.1: Diagrams contributing to the full scalar propagator

uncertainties of the other input parameters, mainly the top mass. There can be a sizeable discrepancy between calculations in different schemes, which are formally of higher order than the level to which they are calculated. The upside is that this discrepancy serves as another estimate of the theoretical uncertainty. In Ref. [195] several sources of uncertainties have been discussed, concluding that a total uncertainty of $3\,\mathrm{GeV}$ is a realistic estimate for the MSSM (including the contributions of eq. (3.3)). This number is smaller than the sum of all individual uncertainties because it is unlikely that they sum up coherently. Compared to the experimental uncertainty of a combined ATLAS and CMS analysis [23–25],

$$m_h = (125.09 \pm 0.32)\ \mathrm{GeV}, \tag{3.4}$$

which is below 0.3%, it is clear that theory has to catch up a lot. It has been estimated in Ref. [120] that the theoretical uncertainty in the MSSM could be reduced to $0.5\,\mathrm{GeV}$ given the inclusion of all two-loop effects with momentum dependence. The anticipated International Linear Collider (ILC) is expected to reduce the experimental uncertainty to $50\,\mathrm{MeV}$ [262].

In general, there are two main approaches to calculate radiative corrections: a fixed-order approach, including the Feynman diagrammatic (FD) and effective potential (EP) approach, and on the other hand the effective field theory (EFT) approach. The latter is used in the tool `SUSYHD` [263]. `FeynHiggs` uses a fixed order calculation in combination with large logarithm resummation. EFT methods are better suited for calculations with very large SUSY masses up to $100\,\mathrm{TeV}$ because they resum large logarithms. Currently the programs `SARAH`/`SPheno` use only fixed order calculations in the $\overline{\mathrm{DR}}'$ renormalisation scheme. The standard approach to obtain a loop-corrected mass spectrum is to calculate two-point Feynman diagrams (self-energies) of the particles. A full propagator is the sum of the tree-level propagator and all higher-order two-point functions, which are shown as a blob on the right hand side of fig. 3.1 for a scalar particle. Any two-point diagram can be repeated n times to form another two-point diagram. This infinite sum can be performed by virtue of the geometric series. Therefore, it suffices to consider only one-particle irreducible diagrams (1PI). Let $i\Pi_0(p^2)$ be the sum of all 1PI two-point diagrams up to a certain loop order, called the self-energy. After resummation the self-energy appears in the denominator of the full propagator.

$$i\mathcal{G}_0^{(2)}(p) = \frac{i}{p^2 - m_0^2 + i\epsilon} \sum_{n=0}^{\infty} \left[i\Pi_0(p^2) \frac{i}{p^2 - m_0^2 + i\epsilon} \right]^n = \frac{i}{p^2 - m_0^2 + \Pi_0(p^2) + i\epsilon} \tag{3.5}$$

The index 0 means that these are bare quantities which are formally divergent. In the renormalisation procedure they are exchanged for renormalised quantities $m, \Pi, \mathcal{G}^{(2)}$. The rescaling constants are free parameters and can be chosen to absorb the formal infinities into counterterms. Calculating diagrams with counterterm contributions renders loop expressions like $\Pi(p^2)$ finite. This is called renormalised perturbation theory, in which the Green's function takes the form

$$i\mathcal{G}^{(2)}(p) = \frac{i}{p^2 - m^2 + \Pi(p^2) + i\epsilon}. \tag{3.6}$$

This has the same form as eq. (3.5) with renormalised quantities instead of bare ones. So one might as well talk only about renormalised quantities, which is what we do from now on. The term m^2 is a running $\overline{\text{MS}}$ (or $\overline{\text{DR}}'$) mass. A short summary of the differences between those schemes is given in appendix A.1. The physical mass is defined by the pole of $\mathcal{G}^{(2)}$ in the complex plane. For $s = p^2$ a complex number, let the pole be at $s = m_{\mathrm{p}}^2 - im_{\mathrm{p}}\Gamma$. The real part of the pole is identified with the squared physical mass and Γ is identified with the total decay width. This leads to the pole mass condition

$$m_{\mathrm{p}}^2 - im_{\mathrm{p}}\Gamma - m^2 + \Pi(m_{\mathrm{p}}^2 - im_{\mathrm{p}}\Gamma) = 0. \tag{3.7}$$

In the case of a small width compared to the pole mass, $\Gamma \ll m_{\mathrm{p}}$, as is the case for the SM Higgs boson, a Taylor expansion is justified.

$$\Pi(m_{\mathrm{p}}^2 - im_{\mathrm{p}}\Gamma) = m_{\mathrm{p}}^2 \left(m_{\mathrm{p}}^{-2}\Pi(m_{\mathrm{p}}^2) - i\frac{\Gamma}{m_{\mathrm{p}}}\Pi'(m_{\mathrm{p}}^2) + \mathcal{O}\left(\Gamma/m_{\mathrm{p}}\right)^2 \right) \tag{3.8}$$

Inserting eq. (3.8) into eq. (3.7), both real and imaginary part have to vanish independently, leading to

$$m_{\mathrm{p}}^2 - m^2 + \Re[\Pi(m_{\mathrm{p}}^2)] + m_{\mathrm{p}}\Gamma\Im[\Pi'(m_{\mathrm{p}}^2)] = 0, \tag{3.9a}$$

$$-m_{\mathrm{p}}\Gamma + \Im[\Pi(m_{\mathrm{p}}^2)] = 0, \tag{3.9b}$$

in first order of Γ/m_{p}.

In a general theory with n real scalar fields ϕ_i the tree level mass matrix for scalars follows from the potential $V^{(0)}(\phi_i)$,

$$\mathcal{M}_{ij}^2 \equiv \frac{\partial^2 V^{(0)}}{\partial\phi_i\partial\phi_j}. \tag{3.10a}$$

It has to be evaluated at the minimum, defined by the tadpole equations

$$T_i^{(0)} \equiv \frac{\partial V^{(0)}}{\partial\phi_i} = 0. \tag{3.11}$$

The 1PI self-energies are then described by a matrix $\Pi_{ij}(p^2)$, which enters the inverse propagator

$$\Gamma_{ij}(p^2) = p^2\delta_{ij} - \mathcal{M}_{ij}^2 + \Pi_{ij}(p^2). \tag{3.12}$$

The matrix Π_{ij} is expressed in the basis ϕ_i, but it can also be expressed using mass eigenstates of the tree-level matrix $\mathcal{M}^2$. Either way, the complex poles $p^2 = s_k$ are found from

$$\det\left[p^2\delta_{ij} - \mathcal{M}_{ij}^2 + \Pi_{ij}(p^2) \right] = 0. \tag{3.13}$$

Since $\Pi_{ij}(p^2)$ is a highly non-trivial function of p^2, the roots of eq. (3.13) can only be determined numerically. This can be done by using $p^2 = m_{\text{tree}}^2$ as a starting value and computing the eigenvalues of $\mathcal{M}_{ij}^2 - \Pi_{ij}(p^2 = m_{\text{tree}}^2)$ as the next iteration. The simplest approximation to eq. (3.13) is to consider vanishing external momenta, i.e. using only $\Pi_{ij}(0)$ as was done in section 2.2.5. In that case, the values s_i are the eigenvalues of the matrix $\mathcal{M}_{ij}^2 - \Pi_{ij}(0)$ and can
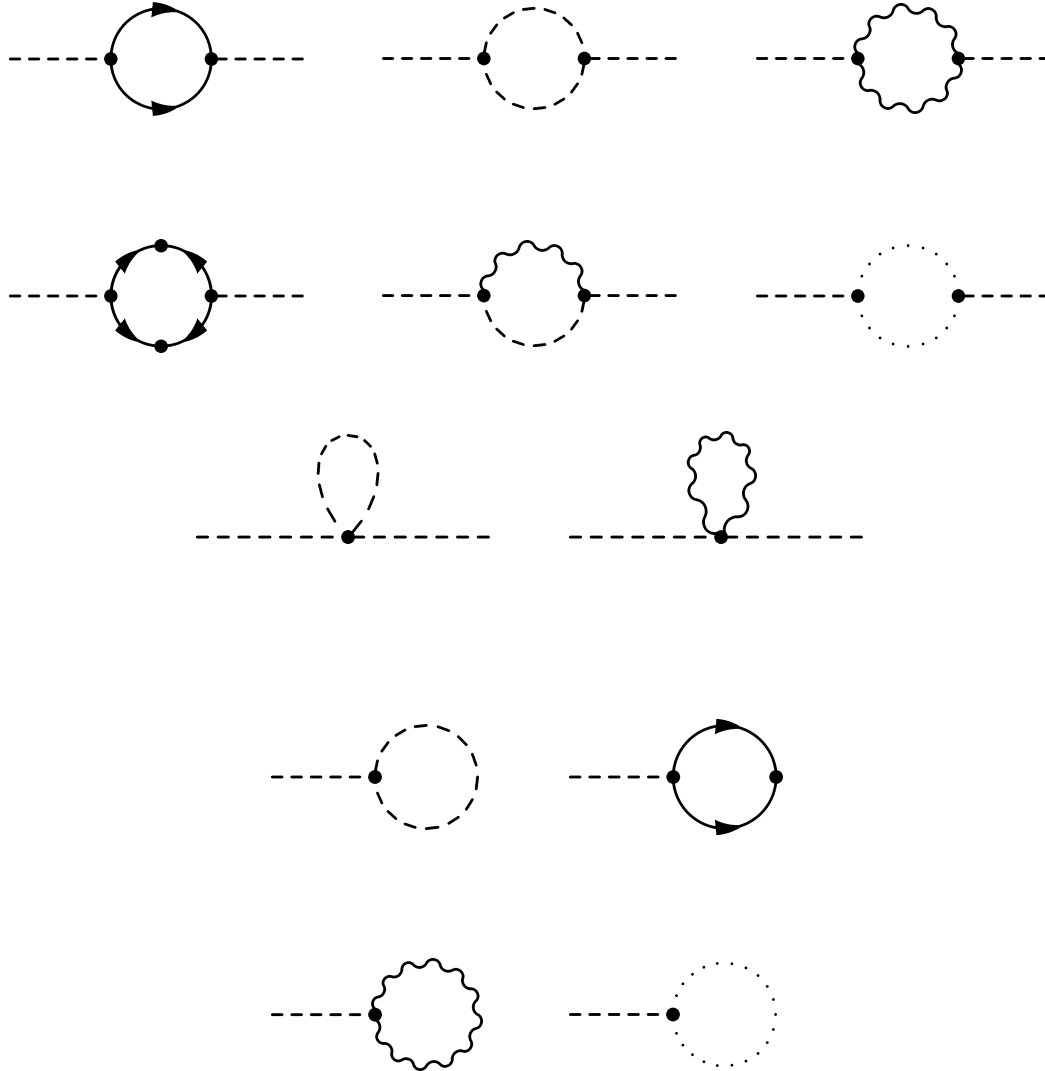
Figure 3.2: General one-loop self-energy and tadpole diagrams. The fermion arrows correspond to two-component spinor formalism. Dotted lines represent ghost fields.

be expressed in a closed form. The self-energy is calculated in loop orders,

$$\Pi_{ij}(p^2) = \frac{1}{16\pi^2}\Pi_{ij}^{(1)}(p^2) + \left(\frac{1}{16\pi^2}\right)^2 \Pi_{ij}^{(2)}(p^2) + \dots . \tag{3.14}$$

The one-loop case consists of only a few diagrams shown in fig. 3.2 that are easily calculated with Passarino-Veltman integrals [264]. The ghost loops need to be included in a general R_ξ gauge and also the tadpole diagrams are needed. The effective potential provides a shortcut to obtain $\Pi(0)$.

3.2 Notation

In order to write down the effective potential and subsequent calculations, we need to establish some notation. Since we rely heavily on the results of Ref. [265], we borrow his notation as well. A general renormalised theory consists of real scalars R_i', two-component Weyl fermions ψ_I' and real vector fields $A_\mu'^a$ with ghost fields $\omega^a, \overline{\omega}^a$. Any kind of symmetry breaking is assumed to have already been performed and the fields R_i' describe fluctuations around the chosen minimum. In case of the MSSM, the VEVs v_u, v_d can be thought of as already included in the mass matrices and couplings. The mass terms are

$$\mathcal{L}_{\text{kin,mass}} = -\frac{1}{2} m_{ij}^2 R_i' R_j' - \frac{1}{2} \left(m^{IJ} \psi_I' \psi_J' + \text{h.c.} \right) - \frac{1}{2} m_{ab}^2 A_a'^\mu A_{\mu b}'. \tag{3.15}$$

The gauge eigenstates, indicated by primes, are rotated to mass eigenstates via

$$R_i' = N_{ji}^{(S)} R_j, \tag{3.16a}$$

$$\psi_I' = N_{JI}^{(F)*} \psi_J, \tag{3.16b}$$

$$A_a'^\mu = N_{ba}^{(V)} A_b^\mu. \tag{3.16c}$$

The orthogonal rotations $N^{(S)}, N^{(V)}$ and the unitary $N^{(F)}$ diagonalise the mass matrices as follows:

$$N_{ik}^{(S)} m_{kl}^2 N_{jl}^{(S)} = m_i^2 \delta_{ij}, \tag{3.17a}$$

$$N_{IK}^{(F)} m_{KL}^2 N_{JL}^{(F)*} = m_I^2 \delta_{IJ}, \tag{3.17b}$$

$$N_{ac}^{(V)} m_{cd}^2 N_{bd}^{(V)} = m_a^2 \delta_{ab}. \tag{3.17c}$$

Here, m_{ij}^2 and m_{ab}^2 are real symmetric, m_{IK} is complex symmetric and $m_{IJ}^2 \equiv m_{IK}^* m^{KJ}$ is a Hermitean matrix. $N^{(F)}$ does not necessarily also diagonalise m^{IJ}. Instead, the mass insertion $M^{IJ} \equiv N_{II'}^{(F)*} N_{JJ'}^{(F)*} m^{I'J'}$ becomes block diagonal for Dirac masses, $\begin{pmatrix} 0 & m_D \\ m_D & 0 \end{pmatrix}$, and diagonal for Majorana masses. The interaction terms of the Lagrangian are defined as

$$\mathcal{L}_S = -\frac{1}{6} \lambda^{ijk} R_i R_j R_k - \frac{1}{24} \lambda^{ijkl} R_i R_j R_k R_l, \tag{3.18a}$$

$$\mathcal{L}_{SF} = -\frac{1}{2} y^{IJk} \psi_I \psi_J R_k + \text{h.c.}, \tag{3.18b}$$

$$\mathcal{L}_{SV} = -\frac{1}{2} g^{abi} A_\mu^a A^{\mu b} R_i - \frac{1}{4} g^{abij} A_\mu^a A^{\mu b} R_i R_j - g^{aij} A_\mu^a R_i \partial^\mu R_j, \tag{3.18c}$$

$$\mathcal{L}_{FV} = g_I^{aJ} A_\mu^a \psi^{\dagger I} \overline{\sigma}^\mu \psi_J, \tag{3.18d}$$

$$\mathcal{L}_{\text{gauge}} = g^{abc} A_\mu^a A_\nu^b \partial^\mu A^{\nu c} - \frac{1}{4} g^{abe} g^{cde} A^{\mu a} A^{\nu b} A_\mu^c A_\nu^d + g^{abc} A_\mu^a \omega^b \partial^\mu \overline{\omega}^c. \tag{3.18e}$$

The couplings λ^{ijk} and λ^{ijkl} are real and completely symmetric in their indices, while the Yukawa interactions y^{IJk} are symmetric under I, J. Lowered fermionic indices indicate complex conjugation (M^{IJ}, M_{IJ}^*), in all other cases the index height does not matter. The covariant

derivatives are given by

$$D_\mu \psi_I = \partial_\mu \psi_I - ig A^a_\mu (T^a)^J_I \psi_J, \tag{3.19a}$$

$$D_\mu R_i = \partial_\mu R_i + ig A^a_\mu \theta^a_{ij} R_j. \tag{3.19b}$$

T^a are the usual Hermitean generators of the gauge group with $\left[T^a, T^b\right] = if^{abc}T^c$. Because everything is expressed in terms of real bosons, the matrices θ^a are imaginary antisymmetric matrices obeying the Lie algebra. In the case of complex fields, θ^a has twice the dimension of T^a. The generators T^a and θ^a fulfil the conditions

$$(T^a T^a)^j_i = C(R)\delta^j_i, \tag{3.20a}$$

$$\mathrm{Tr}\,(T^a T^a) = C(R)d(R), \tag{3.20b}$$

$$\mathrm{Tr}\left[T^a T^b\right] = S(R)\delta^{ab}, \tag{3.20c}$$

where $C(R)$ is the quadratic casimir of the representation R and $d(R)$ is its dimension. $S(R)$ is the Dynkin index defined by convention in tab. 3.1. It is instructive to work out the coefficients

R of $SU(N)$	$C(R)$	$d(R)$	$S(R)$
fundamental	$(N^2-1)/(2N)$	N	$\frac{1}{2}$
adjoint	N	N^2-1	N

Table 3.1: Definition of group invariants

$g^{abij}, g^{aij}, g^{aJ}_I$ from the covariant derivative for an unbroken gauge group, such as $SU(3)_C$.

$$\begin{aligned}
\mathcal{L} \supset -\frac{1}{2}(D_\mu R_i)^2 &= -\frac{1}{2}(\partial_\mu R_i)^2 - ig(\partial^\mu R_i)\theta^a_{ij}R_j A^a_\mu + \frac{1}{2}g^2\theta^a_{ij}\theta^b_{ik}R_j R_k A^a_\mu A^{b\mu} \\
&= -\frac{1}{2}(\partial_\mu R_i)^2 - ig\theta^a_{ji}A^a_\mu R_i(\partial^\mu R_j) + \frac{1}{2}g^2\theta^a_{ki}\theta^b_{kj}R_i R_j A^a_\mu A^{b\mu} \tag{3.21a}
\end{aligned}$$

$$\mathcal{L} \supset i\psi^{\dagger I}\bar{\sigma}^\mu D_\mu \psi_I = i\psi^{\dagger I}\bar{\sigma}^\mu \partial_\mu \psi_I + g(T^a)^J_I A^a_\mu \psi^{\dagger I}\bar{\sigma}^\mu \psi_J \tag{3.21b}$$

$$g^{abij} = 2g^2(\theta^a \theta^b)_{ij} \tag{3.22a}$$

$$g^{aij} = -ig\theta^a_{ij} \tag{3.22b}$$

$$g^{abi} = 0 \tag{3.22c}$$

$$g^{aJ}_I = g(T^a)^J_I \tag{3.22d}$$

3.3 Effective potential approach

The effective potential, truncated at two loops,

$$V_{\mathrm{eff}}(\phi_i) = V^{(0)}(\phi_i) + \frac{1}{16\pi^2}V^{(1)}(\phi_i) + \left(\frac{1}{16\pi^2}\right)^2 V^{(2)}(\phi_i) + \dots \tag{3.23}$$

is calculated perturbatively through vacuum diagrams with no external lines. The topologies at one and two loops (fig. 3.3) are associated with the basic functions $J(x)$, $J(x,y)$ and $I(x,y,z)$.
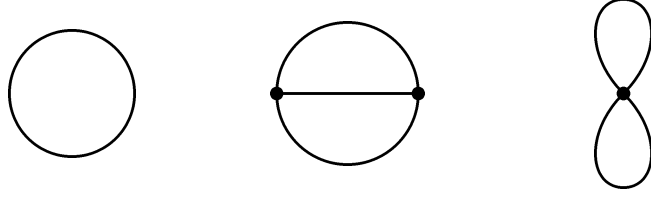
Figure 3.3: The circle topology at one-loop and "sunset" and "snowman" topologies at two-loop.

We use the definitions given in Ref. [266] which were also used in related works, Refs. [265, 267]. Earlier work on the evaluation of these functions was done in Ref. [268] [1].

The full definition of all necessary functions is given in appendix B.1. For now, the easiest cases are presented,

$$J(x) = x \left(\overline{\ln} \left(x \right) - 1 \right), \tag{3.24a}$$

$$J(x, y) = J(x)J(y). \tag{3.24b}$$

We express all diagrams in terms of finite loop function, where the divergent epsilon terms are subtracted by counterterms in the $\overline{\mathrm{DR}}'$ scheme. As a next step, the internal lines are populated by scalars, fermions and vectors. Note that the fermion arrows correspond to the two-component spinor formalism [150], where arrows signify chirality rather than quark/lepton number flow, and dots between clashing arrows denote mass insertions.[2] This gives the twelve diagrams shown in fig. 3.4 that completely describe $V^{(2)}$. All quantities such as masses and couplings must be expressed field-dependently. The loop corrected mass matrix at zero external momentum can be found from the second derivative,

$$\mathcal{M}_{ij}^2 - \Pi_{ij}(p^2 = 0) = \frac{\partial^2 V_{\mathrm{eff}}}{\partial \phi_i \partial \phi_j}. \tag{3.25}$$

Comparing this in loop orders, we have the important relation

$$\boxed{\Pi_{ij}^{(\ell)}(0) = -\frac{\partial^2 V^{(\ell)}}{\partial \phi_i \partial \phi_j}} \tag{3.26}$$

that allows to obtain mass corrections from V_{eff} at a certain loop order. The minus sign depends on the definition of Π. This is the effective potential approach and equivalent to calculating $\Pi_{ij}(0)$ with Feynman diagrams. Of course, $p^2 = 0$ is only an approximation and in the end has to give way to a full diagrammatic approach with momentum dependence. Nevertheless, $p^2 = 0$ is a useful choice at this point. Recent studies of momentum effects in two-loop QCD corrections [232, 234] have found that their impact on m_h is about a few hundred MeV, far below other sources of uncertainty. It has been noted earlier in Ref. [231] that neglecting momentum effects in the case of electroweak contributions might not be a good approximation, as both effects account for a shift of $\sim 1\,\mathrm{GeV}$. On the other hand, the contributions that become accessible

---

[1] The notation $\hat{I}$ (I) of Ref. [268] corresponds to our I ($\mathbf{I}$) for the finite (divergent) expressions.

[2] Fermion propagators with a mass insertion ($im/(p^2 - m^2)$) contribute a power of -2 to the diagram's superficial degree of divergence, while normal fermion propagators ($ip\sigma/(p^2 - m^2)$) contribute a power of -1.
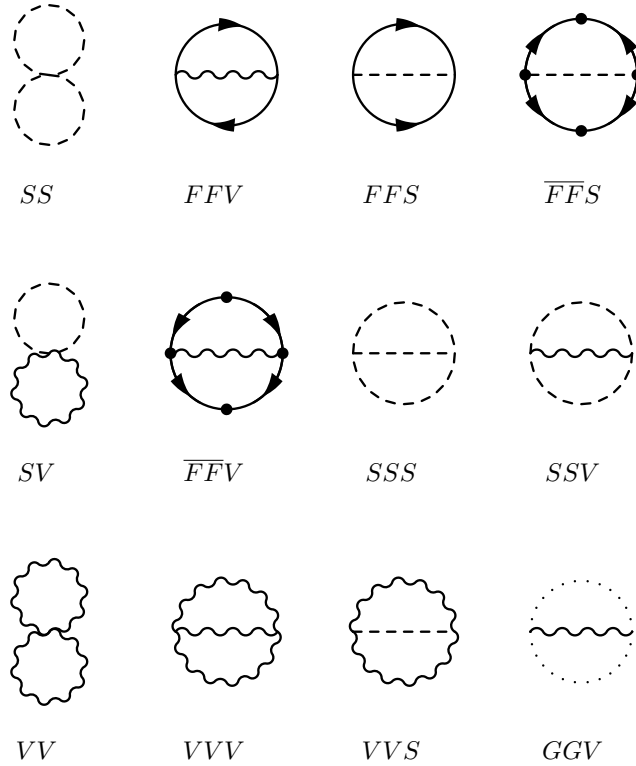
Figure 3.4: All diagrams contributing to the two-loop effective potential [265], using two-component notation for fermions.

with the effective potential approach can be much larger even in the gaugeless limit, and it is therefore a useful step towards two-loop precision. The easiest way to calculate the derivative is to use a numerical differentiation routine on the function V_{eff}.

The full two-loop effective potential from Ref. [265] consists of one term for each of the 12 diagrams in fig. 3.4, where the pure gauge diagrams VVV, VV and GGV are collectively written as V_{gauge},

$$V^{(2)} = V_{FFS} + V_{\overline{FF}S} + V_{SSS} + V_{SSV} + V_{FFV} + V_{\overline{FF}V} + V_{SS} + V_{SV} + V_{VVS} + V_{\text{gauge}}. \quad (3.27)$$

We use a shorthand notation for mass arguments like $f(i, j, k) \equiv f(m_i^2, m_j^2, m_k^2)$. If not stated otherwise, repeated indices are summed over. The individual contributions of the diagrams are

given by

$$V_{SSS} = \frac{1}{12}(\lambda^{ijk})^2 f_{SSS}(i,j,k), \tag{3.28a}$$

$$V_{SS} = \frac{1}{8}\lambda^{iijj} f_{SS}(i,j), \tag{3.28b}$$

$$V_{FFS} = \frac{1}{2}\left|y^{IJk}\right|^2 f_{FFS}(I,J,k), \tag{3.28c}$$

$$V_{\overline{FF}S} = \frac{1}{4}y^{IJk}y^{I'J'k}M_{II'}^*M_{JJ'}^* f_{\overline{FF}S}(I,J,k) + \text{c.c.}, \tag{3.28d}$$

$$V_{SSV} = \frac{1}{4}(g^{aij})^2 f_{SSV}(i,j,a), \tag{3.28e}$$

$$V_{VS} = \frac{1}{4}g^{aaii} f_{VS}(a,i), \tag{3.28f}$$

$$V_{FFV} = \frac{1}{2}\left|g_I^{aJ}\right|^2 f_{FFV}(I,J,a), \tag{3.28g}$$

$$V_{\overline{FF}V} = \frac{1}{2}g_I^{aJ}g_{I'}^{aJ'}M^{II'}M_{JJ'}^* f_{\overline{FF}V}(I,J,a), \tag{3.28h}$$

$$V_{\text{gauge}} = \frac{1}{12}(g^{abc})^2 f_{\text{gauge}}(a,b,c). \tag{3.28i}$$

The loop functions f_X are combinations of $J(x,y)$, $I(x,y,z)$ and polynomials in x,y,z. Diagrams without vectors (SSS, SS, FFS, $\overline{FF}S$) are equal in both $\overline{\text{MS}}$ and $\overline{\text{DR}}'$ schemes,

$$f_{SS}(x,y) = J(x,y), \tag{3.29}$$

$$f_{SSS}(x,y,z) = -I(x,y,z), \tag{3.30}$$

$$f_{FFS}(x,y,z) = J(x,y) - J(x,z) - J(y,z) + (x+y-z)I(x,y,z), \tag{3.31}$$

$$f_{\overline{FF}S}(x,y,z) = 2I(x,y,z). \tag{3.32}$$

Diagrams with vectors differ for $\overline{\text{MS}}$ and $\overline{\text{DR}}'$. Since we restrict ourselves to the gaugeless limit with massless vectors, the functions can be used in a simplified form with $z = 0$ (starting with the $\overline{\text{DR}}'$ parts),

$$f_{SSV}(x,y,0) = (x+y)^2 + 3(x+y)I(x,y,0) + 3J(x,y) - 2xJ(x) - 2yJ(y), \tag{3.33}$$

$$f_{VS}(x,y) = 3J(x,y), \tag{3.34}$$

$$f_{FFV}(x,y,0) = -(x+y)^2 + 2xJ(x) + 2yJ(y), \tag{3.35}$$

$$f_{\overline{FF}V}(x,y,0) = 6I(x,y,0). \tag{3.36}$$

The same functions in $\overline{\text{MS}}$ have to be understood as $f_X^{\overline{\text{MS}}} = f_X^{\overline{\text{DR}}'} + \Delta^{\overline{\text{MS}}}f_X$ with

$$\Delta^{\overline{\text{MS}}}f_{SSV}(x,y,0) = 0, \tag{3.37}$$

$$\Delta^{\overline{\text{MS}}}f_{VS}(x,y) = 2xJ(y), \tag{3.38}$$

$$f_{FFV}^{\overline{\text{MS}}}(x,y,0) = 0, \tag{3.39}$$

$$\Delta^{\overline{\text{MS}}}f_{\overline{FF}V}(x,y,z) = 2(x+y+z) - 4J(x) - 4J(y). \tag{3.40}$$

The function $f_{FFV}(x,y,0)$ vanishes completely in the $\overline{\text{MS}}$ scheme. The full expressions for

massive gauge bosons are given in appendix B.3.2. In the gaugeless limit with Landau gauge we can completely ignore the diagrams VVV, VV, GGV, VVS and also VS. The vector contributions for unbroken gauge symmetry can be expressed through group invariants, using eq. (3.22).

$$V_{SSV,g} = \frac{1}{4}(g^{aij})^2 f_{SSV}(i,j,a) \qquad = \frac{1}{4}g^2 C(i)d(i)f_{SSV}(i,i,a), \tag{3.41a}$$

$$V_{VS,g} = \frac{1}{4}g^{aaii}f_{VS}(a,i) \qquad = \frac{1}{2}g^2 C(i)d(i)f_{VS}(a,i), \tag{3.41b}$$

$$V_{FFV,g} = \frac{1}{2}\left|g_I^{aJ}\right|^2 f_{FFV}(I,J,a) \qquad = \frac{1}{2}g^2 C(I)d(I)f_{FFV}(I,I,a), \tag{3.41c}$$

$$V_{\overline{FF}V,g} = \frac{1}{2}g_I^{aJ}g_{I'}^{aJ'}M^{II'}M_{JJ'}^* f_{\overline{FF}V}(I,J,a) \qquad = -\frac{1}{2}g^2 C(I)d(I)m_I^2 f_{\overline{FF}V}(I,I,a), \tag{3.41d}$$

$$V_{\text{gauge},g} = \frac{1}{12}(g^{abc})^2 f_{\text{gauge}}(a,b,c) \qquad = \frac{1}{12}g^2 C(a)d(a)f_{\text{gauge}}(a,a,a). \tag{3.41e}$$

One can combine the fermion-vector diagrams to give

$$V_{FFV}^{(2)} + V_{\overline{FF}V}^{(2)} \equiv \frac{g^2}{2}d(I)C(I)F_{FV}(m_I^2), \tag{3.42}$$

$$F_{FV}(x) \equiv -4x^2 + 4xJ(x) - 6xI(x,x,0) + \delta_{\overline{\text{MS}}}4xJ(x), \tag{3.43}$$

where $\delta_{\overline{\text{MS}}}$ is zero for $\overline{\text{DR}}'$ and one for $\overline{\text{MS}}$. All of the above contributions to V have the form of one coupling c_1 (or two couplings $c_1 \cdot c_2$) multiplied by a prefactor k and a loop function f_X,

$$V_X^{(2)} = k \cdot (c_1 c_2) \cdot f_X(m_1^2, m_2^2, m_3^2), \qquad \text{for } X = FFS, FFV, SSV, VVS, \text{gauge}, \tag{3.44a}$$

$$V_X^{(2)} = k \cdot (c_1 c_2) \cdot m_{F1}m_{F2} \cdot f_X(m_{F1}^2, m_{F2}^2, m_3^2), \quad \text{for } X = \overline{FF}S, \overline{FF}V, \tag{3.44b}$$

$$V_X^{(2)} = k \cdot (c_1) \cdot f_X(m_1^2, m_2^2), \qquad \text{for } X = SS. \tag{3.44c}$$

For the implementation into the computer code `SARAH`, it is more convenient to recast the general expressions into a form that distinguishes Dirac and Majorana fermions as well as real and complex scalars. This amounts to a prefactor k for each of these cases. The calculations are found in appendix B.2. A vertex between particles A, B, C is understood as

$$\mathcal{C}[A,B,C] \equiv i\frac{\partial^3 \mathcal{L}}{\partial A \, \partial B \, \partial C} = i\begin{cases} c\,\Gamma & A, B, C \text{ bosons}, \\ c_L\,\Gamma_L + c_R\,\Gamma_R & A, B \text{ fermions}. \end{cases} \tag{3.45}$$

The matrix Γ is the kinematic part with spin structure. In case of fermionic couplings, $\Gamma_{L/R}$ indicate projection operators,

$$\Gamma_{L/R} = \begin{cases} P_{L/R} & FFS \text{ coupling} \\ \gamma^\mu P_{L/R} & FFV \text{ coupling} \end{cases}. \tag{3.46}$$

With the prefactors from appendix B.2 all the pieces for an implementation are in place. `SARAH` extracts the couplings c, c_L, c_R from the Lagrangian and populates the general diagrams of fig. 3.4 with particles. Also, a numerical differentiation routine is needed along with the analytic functions $J(x), J(x,y), I(x,y,z)$. Details about the implementation are given in section 4.2.

3.4 Analytic derivatives at two-loop

The diagrammatic approach requires many more diagrams and a system to reduce the two-loop tensor integrals to a set of basic integrals. Such a scheme has been proposed by Tarasov [269]. In fact, the nearly complete calculation by S. Martin of all scalar two-loop self-energies for a general renormalisable theory has been available for almost as long as the effective potential expressions [266, 267, 270]. The only parts that are missing are the remaining gauge contributions beyond the leading order ($\sim g^2$), i.e. from diagrams with more than one internal vector. Also, the two-loop self-energy of the Z boson is needed in order to fix the electroweak VEV, v. Even in the effective potential approach, these v corrections are necessary for gauge invariance. Recent works like Ref. [271] (full $\delta^{(2)} M_Z^2$ in the SM) indicate that this gap might be closed in the near future. Implementing the nearly-complete results of Refs. [266, 267, 270] would be a huge step. However, there is a simpler way to improve the effective potential approach, which consists of taking only analytic derivatives of the diagrams in fig. 3.4 corresponding to the terms in eq. (3.28). This has the clear advantage of being independent of numerical relics from a finite step size in the differentiation routine. The resulting expressions are equivalent to the diagrammatic approach in the limit $p^2 = 0$. In many cases, the expressions obtained by differentiating match those of the diagrammatic calculation as in Refs. [266, 267, 270] except for a non-zero p^2 in the loop functions. In a few cases, the results obtained by differentiation are much simpler than by the diagrammatic approach, but are fully equivalent.

Because of the equivalence to the diagrammatic approach, we refer to the method explained here as such. It was presented in Ref. [188] along with the calculations. Instead of reciting the lengthy calculations here, we rather explain how it is in principle done and which diagrams are included in the implementation. The purely scalar two-loop diagrams are shown in fig. 3.5, which are at the same time representatives for all possible two-point topologies. The naming scheme in terms of $M, S, T, U, V, W, X, Y, Z$ is borrowed from Refs. [266, 267, 270]. A minimal basis to express the loop diagrams is given by four functions S, T, U, M [266] and the one-loop functions A, B. All diagrams with fermions and vectors that do not vanish in the gaugeless limit are shown in fig. 3.6. The tadpole diagrams in section 3.4 are needed for the minimisation conditions at two loops. Recall that R_i' is a set of real scalar fields defined in eqs. (3.16) to (3.18) and R_i their mass eigenstates. The true minimum is at $R = 0$ and can have a broken symmetry. Consider a field configuration $R \neq 0$, slightly outside the minimum. We evaluate the field-dependent scalar masses and couplings at this point,

$$m_{ij}^2(R) = \frac{-\partial^2 \mathcal{L}}{\partial R_i \partial R_j} = m_i^2 \delta_{ij} + \lambda^{ijk} R_k + \frac{1}{2} \lambda^{ijkl} R_k R_l, \tag{3.47a}$$

$$\lambda^{ijk}(R) = \frac{m_{ij}^2(R)}{\partial R_k} = \lambda^{ijk} + \lambda^{ijkl} R_l, \tag{3.47b}$$

$$\lambda^{ijkl}(R) = \frac{\lambda^{ijk}(R)}{\partial R_l} = \lambda^{ijkl}. \tag{3.47c}$$
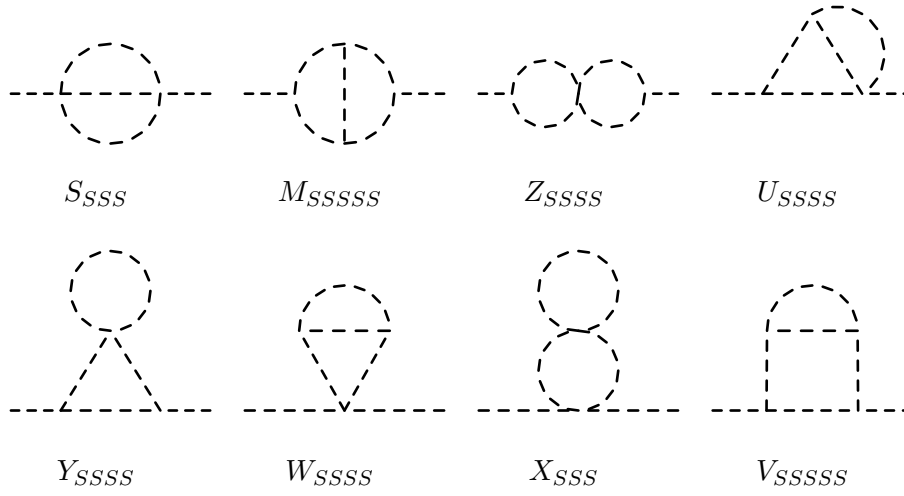
Figure 3.5: Two-loop self-energy diagrams involving only scalars. They also represent the basic topologies for any two-loop self-energy.
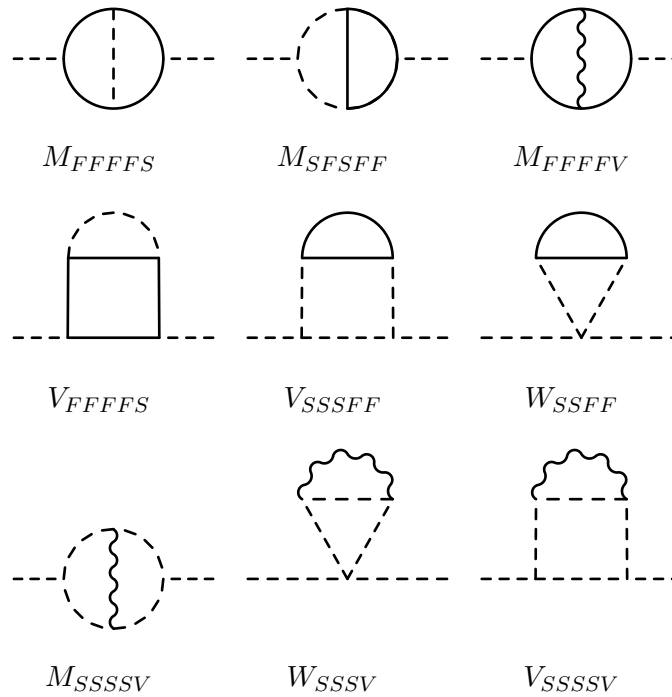
Figure 3.6: Mixed two-loop self-energy diagrams that do not vanish in the gaugeless limit. For every fermionic diagrams there exist variants with all combinations of chirality-flipping mass insertions.
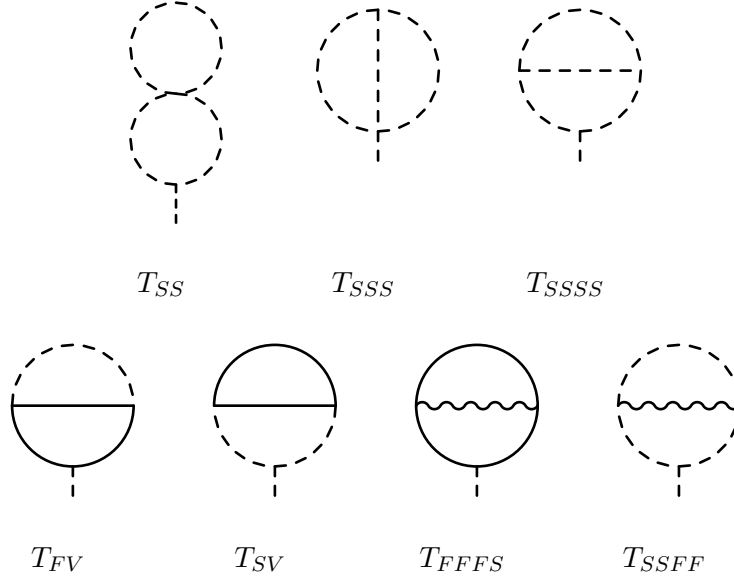
Figure 3.7: Tadpole diagrams at the two-loop level which do not vanish in the gaugeless limit.

This has to be done for the fermions and vector bosons, too:

$$M^{IJ}(R) = -\frac{\partial^2 \mathcal{L}}{\partial \psi_I \partial \psi_J} = M^{IJ} + y^{IJk} R_k, \tag{3.48a}$$

$$\frac{\partial}{\partial R_k} M^{IJ}(R) = y^{IJk}, \tag{3.48b}$$

$$\frac{\partial}{\partial R_r} \left[M^{IJ}(R) M^*_{JK}(R) \right] = y^{IJr} M^*_{JK}(R) + M^{IJ}(R) y^*_{JKr}, \tag{3.48c}$$

$$m_{ab}^2(R) g^{\mu\nu} = -\frac{\partial^2 \mathcal{L}}{\partial A_\mu^a \partial A_\nu^b} = \left(m_a^2 \delta^{ab} + g^{abi} R_i + \frac{1}{2} g^{abij} R_i R_j \right) g^{\mu\nu}, \tag{3.48d}$$

$$\frac{\partial}{\partial R_i} m_{ab}^2(R) = g^{abi}(R) = g^{abi} + g^{abij} R_j, \tag{3.48e}$$

$$\frac{\partial}{\partial R_j} g^{abi}(R) = g^{abij}. \tag{3.48f}$$

For a given configuration of the fields $R_i \neq 0$ the field-dependent mass matrix $m_{ij}^2(R)$ is again diagonalised by a field-dependent rotation matrix $\tilde{N}(R)$,

$$\tilde{R}_i = \tilde{N}_{ij}(R) R_j. \tag{3.49}$$

In the basis $\tilde{R}_i$, the couplings and masses are labelled $\tilde{m}_i(R), \tilde{\lambda}^{ijk}(R), \tilde{\lambda}^{ijkl}$. The field-dependent propagator of $R_i \to R_j$ is the ij entry of the inverse of the matrix $q^2 - \mathbf{m^2}(R)$. The derivative of this propagator can be calculated with a mathematical identity for an invertible matrix $\mathbf{A}(x)$,

$$\frac{\mathrm{d}}{\mathrm{d}x} \mathbf{A^{-1}} = -\mathbf{A}^{-1} \times \frac{\mathrm{d}\mathbf{A}}{\mathrm{d}x} \times \mathbf{A}^{-1}. \tag{3.50}$$

This implies

$$\frac{\partial}{\partial R_r} \left[\frac{1}{q^2 - \mathbf{m^2}(R)} \right]_{ij} = - \left[\frac{1}{q^2 - \mathbf{m^2}(R)} \right]_{ik} \frac{-\partial m_{kk'}^2(R)}{\partial R_r} \left[\frac{1}{q^2 - \mathbf{m^2}(R)} \right]_{k'j}. \tag{3.51}$$

After differentiation the limit $R \to 0$ is taken, which brings back the diagonal matrix, $\mathbf{m}^2(R)_{ik} \to m_i^2 \delta_{ik}$. The derivative of the mass matrix is $\lambda^{kk'r}$ following eq. (3.47a). Then, eq. (3.51) becomes

$$\to \frac{1}{q^2 - m_i^2} \frac{1}{q^2 - m_j^2} \lambda^{ijr} = \frac{1}{m_i^2 - m_j^2} \left(\frac{1}{q^2 - m_i^2} - \frac{1}{q^2 - m_j^2} \right) \lambda^{ijr}. \tag{3.52}$$

We see the appearance of the difference quotient operation defined by

$$f^{(1,0)}(x, y; z) = \mathcal{D}_{x,y} f(x, z) \equiv \frac{f(x, z) - f(y, z)}{x - y}, \tag{3.53a}$$

$$f^{(1,0,0)}(x, u; y, z) = \mathcal{D}_{x,u} f(x, y, z) \equiv \frac{f(x, y, z) - f(u, y, z)}{x - u}. \tag{3.53b}$$

The operator $\mathcal{D}_{x,u}$ obeys a product rule,

$$\begin{aligned} \mathcal{D}_{x,u}\left[f(x)g(x)\right] &= \frac{f(x)g(x) - f(u)g(u)}{x - u} \\ &= \left[\mathcal{D}_{x,u}f(x)\right]g(x) + f(u)\left[\mathcal{D}_{x,u}g(x)\right] \\ &= \left[\mathcal{D}_{x,u}f(x)\right]g(u) + f(x)\left[\mathcal{D}_{x,u}g(x)\right]. \end{aligned} \tag{3.54}$$

We can now analytically differentiate the individual contributions to $V^{(2)}$. The propagators of fields that are not mass eigenstates depend on all entries of the mass matrix $\mathbf{m}^2$. We will however tolerate an abuse of notation of the following kind,

$$f(m_{ij}^2) \sim \int \mathrm{d}^d q \left[\frac{1}{q^2 - \mathbf{m^2}} \right]_{ij}, \tag{3.55}$$

noting that f is not a function of just one real number but of all entries of $\mathbf{m}^2$. Self-energies can be calculated in the gauge eigenstate basis or mass eigenstate basis, but it is more convenient to take derivatives with respect to the mass eigenstates R_i. The self-energies Π_{ij} and tadpoles δT_k obtained this way can be rotated to the other basis via

$$\Pi'_{ij} = N_{ki}^{(S)} N_{lj}^{(S)} \Pi_{kl}, \tag{3.56a}$$

$$\delta T'_i = N_{ki}^{(S)} \delta T_k. \tag{3.56b}$$

We demonstrate the procedure on $V_{SS}^{(2)}$, expressed in terms of field-dependent quantities. The

first derivative with respect to R_r produces the tadpole expression $T_{SS,r}$,

$$
\begin{aligned}
T_{SS,r} = \frac{\partial}{\partial R_r} V_{SS}^{(2)} &= \frac{\partial}{\partial R_r}\left[\frac{1}{8}\tilde{\lambda}^{iijj} f_{SS}(\tilde{m}_i^2(R), \tilde{m}_j^2(R))\right] = \frac{\partial}{\partial R_r}\left[\frac{1}{8}\tilde{\lambda}^{ikjl}\delta_{ik}\delta_{jl} f_{SS}(\tilde{m}_i^2(R), \tilde{m}_j^2(R))\right] \\
&= \frac{\partial}{\partial R_r}\frac{1}{8}\tilde{\lambda}^{i'k'j'l'}\tilde{N}_{i'i}\tilde{N}_{k'k}\tilde{N}_{j'j}\tilde{N}_{l'l} f_{SS}(m_{ik}^2(R), m_{jl}^2(R)) \\
&= \frac{\partial}{\partial R_r}\frac{1}{8}\lambda^{ikjl} f_{SS}(m_{ik}^2(R), m_{jl}^2(R)) \\
&= \frac{1}{4}\lambda^{ikjl} f_{SS}^{(1,0)}(m_{im}^2(R), m_{nk}^2(R); m_{jl}^2(R))\frac{\partial m_{mn}^2(R)}{\partial R_r} \\
&= \frac{1}{4}\lambda^{ikjj}\lambda^{ikr} f_{SS}^{(1,0)}(m_i^2, m_k^2; m_j^2).
\end{aligned}
\tag{3.57}
$$

The new function $f_{SS}^{(1,0)}$ of three arguments needs to be examined. Recall that the finite part of the one-loop integral is given by $J(x) = \mathbf{J}(x) + \frac{x}{\epsilon}$.

$$
\begin{aligned}
f_{SS}^{(1,0)}(x, y; z) = \mathcal{D}_{x,y} J(x, z) &= \mathcal{D}_{x,y}\left(\mathbf{J}(x) + \frac{x}{\epsilon}\right)\left(\mathbf{J}(z) + \frac{z}{\epsilon}\right) \\
&= \left(-\frac{C}{i}\int d^d q \mathcal{D}_{x,y}\frac{1}{q^2 - x} + \frac{1}{\epsilon}\right)J(z) \\
&= \left(-\frac{C}{i}\int d^d q \frac{1}{q^2 - x}\frac{1}{q^2 - y} + \frac{1}{\epsilon}\right)J(z) \\
&= \left(-\mathbf{B}_0(x, y) + \frac{1}{\epsilon}\right)J(z) \\
&= -B_0(x, y)J(z)
\end{aligned}
\tag{3.58}
$$

The definition of $\mathbf{B}_0$ is given in appendix B.1.1. It is preferred to express the difference quotients in terms of basic loop functions, because the limit $x \to y$ is needed often. By repeated application of the $\mathcal{D}_{x,y}$ operator one can obtain loop functions corresponding to diagrams with more legs. The function C_0 is the one-loop, three-point function at $p^2 = 0$,

$$
C_0(x, y, z) \equiv -B_0^{(1,0)}(x, y; z) = -\frac{B_0(x, z) - B_0(y, z)}{x - y}.
\tag{3.59}
$$

Differentiating T_{SS} a second time gives the self-energy contributions,

$$
\begin{aligned}
&\frac{\partial^2}{\partial R_r \partial R_s} V_{SS}^{(2)} \\
&= \frac{1}{4}\lambda^{ikjj}\left(\lambda^{ikrs} f^{(1,0)}(i, k; j) + 2\lambda^{ikr}\lambda^{ii's} f_{SS}^{(2,0)}(i, i'; k, j) + \lambda^{ikr}\lambda^{jj's} f_{SS}^{(1,1)}(i, k; j, j')\right) \\
&= \frac{1}{4}\lambda^{ikjj}\left(\lambda^{ikrs} X_{SSS}(i, k, j) + 2\lambda^{ikr}\lambda^{ii's} Y_{SSSS}(i, i', k, j) + \lambda^{ikr}\lambda^{jls} Z_{SSSS}(i, k, j, l)\right),
\end{aligned}
\tag{3.60}
$$

where the new loop functions are given by

$$X_{SSS}(x,y,z) = f^{(1,0)}(x,y;z) = -B_0(x,y)J(z), \tag{3.61a}$$

$$Y_{SSSS}(x,y,z,u) = f_{SS}^{(2,0)}(x,y;z,u) = C_0(x,y,z)J(u), \tag{3.61b}$$

$$Z_{SSSS}(x,y,z,u) = f_{SS}^{(1,1)}(x,y;z,u) = B_0(x,y)B_0(z,u). \tag{3.61c}$$

The labels of the functions match those of the three diagrams of fig. 3.5 that represent the terms. Performing the differentiation on the sunrise diagram, we obtain the two-point topologies S, M, U, W, V. The purely-scalar diagrams are of course the easiest – the loop functions of more complicated diagrams with vectors contain also polynomials of the squared masses. For fermions, all combinations of propagators with or without chirality-flipping mass insertions M^{IJ} have to be distinguished. After this exercise in case of SS, we can formulate a rule how to quickly write down the derivatives. The terms of the effective potential have the general form $A^{ij}f_X(x_i,y_j)$ for snowman diagrams (fig. 3.3) and $(A^{ijk})^2 f_X(x_i,y_j,z_k)$ for sunrise diagrams. The derivative with respect to R_r is

$$\frac{\partial}{\partial R_r}A^{ij}f_X(x_i,y_j) = \frac{A^{ij}}{R_r}f_X(x_i,y_j) + A^{ij}\frac{m_{ii'}^2}{\partial R_r}f_X^{(1,0)}(x_i,x_{i'};y_j),$$

$$\frac{\partial}{\partial R_r}(A^{ijk})^2 f_X(x_i,y_j,z_k) = 2f_X(x_i,y_j,z_k)A^{ijk}\frac{\partial A^{ijk}}{\partial R_r}$$

$$+ A^{ijk}A^{i'jk}\left\{\frac{\partial m_{ii'}^2}{\partial R_r}f_X^{(1,0,0)}(x_i,x_{i'};y_j,z_k) + (x \leftrightarrow y) + (x \leftrightarrow z)\right\}. \tag{3.62}$$

Often the f_X are symmetric in two or more arguments and can be simplified. The total contribution to $\Pi_{ij}^{(2)}(0)$ in our gaugeless limit is given by

$$-\Pi_{ij}^{(2)}(0) = \Pi_{ij}^S + \Pi_{ij}^{S_2 F_2(W)} + \Pi_{ij}^{S_1 F_4(M)} + \Pi_{ij}^{S_2 F_3(M)} + \Pi_{ij}^{S_3 F_2(V)} + \Pi_{ij}^{S_1 F_4(V)} + \Pi_{ij}^{S_k V_1} + \Pi_{ij}^{F_4 V_1}. \tag{3.63}$$

The notation in superscript means the number of scalar (fermion, vector) propagators and the topology in parentheses. All of these contributions are listed in the appendix B. [3] The expressions are equivalent to those in Ref. [267] if $p^2 = 0$ is assumed. Because of the various relations between the loop functions, such results can be presented in many different ways. It turned out that the expressions for $\Pi_{ij}^{S_1 F_4(V)}, \Pi_{ij}^{S_k V_1}, \Pi_{ij}^{F_4 V_1}$ found with this method have a much simpler form than those in Ref. [267] for the gaugeless limit. It is in principle possible to extend this calculation to the case of massive gauge bosons. One step in this direction has been done in Ref. [188], consisting of the tadpole expressions for the neglected contributions. However, the explicit expressions for the various derivatives such as $f_{VVS}^{(1,0,0)}(x,y,z)$ were not given. We close this gap in this thesis and present the calculation of the missing functions in appendix B.3.2. In the likely case that the two-loop calculation of `SARAH` will be updated to massive gauge bosons or even momentum dependence, these expressions will still be required.

---

[3] To avoid having a minus sign in front of every expression for the components Π_{ij}^{XY} stemming from the definition of eq. (3.26), we introduce instead a minus sign in eq. (3.63).

Implementation details in `SARAH/SPheno`

4.1 The `SARAH/SPheno` framework
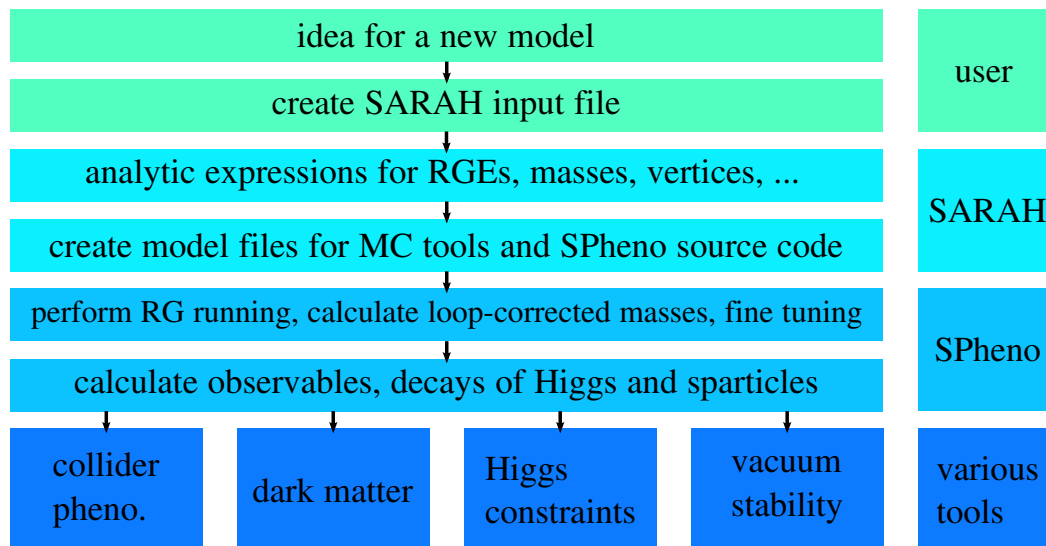
Figure 4.1: The workflow within the `SARAH/SPheno` framework.

4.1.1 Introduction

There exist several numerical spectrum generators that are able to solve renormalisation group equations and to diagonalise the mass matrices of a quantum field theory. This number-crunching job is best done in compiler languages like `Fortran` or C/C++. Depending on the tool, the available output can consist of much more: branching ratios, production cross sections, low-energy observables, etc. The interface between spectrum generators and other specialised tools (e.g. event generators) is realised by the SUSY Les Houches accord (SLHA) [272, 273]. Although the SLHA file format is inspired by supersymmetric parameters, its structure is general enough to be used for any model. A later extension was the Flavour Les Houches accord (FLHA) for flavour observables [274].

The spectrum generator of our choice is `SPheno` [221, 222][1], developed by W. Porod and F. Staub. It features full one-loop corrected mass spectra, two-loop RGE running, branching ratios and decay widths for all BSM particles and a set of low energy observables. The MSSM is supported with several high-scale boundary conditions (CMSSM [153–156], GMSB [157–161], AMSB [2] [275–277]) and extensions like see-saw or CP violation.

Spectrum generators are written for specific models, mostly the MSSM and NMSSM, using hard-coded expressions. The large amount of models requires more flexible ways of calculation than a fixed spectrum generator can offer. This inspired the creation of a meta-tool such as `SARAH` [68–74][3], written by F. Staub (2009). This tool uses the symbolic manipulation power of the `Mathematica` language to derive analytic expressions for a user-defined model.

By itself, `SARAH` calculates a complete Lagrangian for a renormalisable QFT from a minimal user input. Kinetic terms, gauge interactions and gauge fixing terms follow from fixed rules and are automatically added. In supersymmetry there are even more restrictions on the possible interactions because of holomorphy of the superpotential. At its heart a model is defined by:

- Local gauge group

- Global symmetries

- Particle content and representations

- Explicit non-gauge interaction terms / superpotential

If a model is embedded in a high scale theory, the boundary conditions at the GUT scale have to be added to the list. The part of the Lagrangian that defines non-gauge interactions (in SUSY theories, just the superpotential) has to be given explicitly by the user, so that individual conventions can be used. `SARAH` can check if any other interaction terms that respect the global and local symmetries are missing. Further, the mixing between particles with the same quantum numbers has to be defined by the user, because of the conventional choices that can be made for the ordering of the fields. Such a tool requires model-independent, generic expressions that have to be populated with particles of concrete models. The generic two-loop RGEs for all parameters of a softly broken SUSY model studied in Refs. [278–281] are one foundation of the code.

While it is possible to obtain important results from the analytic level alone, `SARAH` can export model files in the UFO format and in the file formats of `FeynArts` [282], `CalcHep/CompHep` [283] and `WHIZARD` [284]. The event generator `MadGraph` [285] can import UFO files. The most important feature is the link to `SPheno`: Analytic expressions are cast into `Fortran` source code, which can then be compiled as an add-on within the stock version of `SPheno`, resulting in a customised spectrum generator. The automatised workflow is illustrated in fig. 4.1. The tool chain can be extended by passing the SLHA spectrum file produced by `SPheno` to other tools like event generators. The consistency of the Higgs sector with experimental data is checked by `HiggsBounds/HiggsSignals` [286–288]. Vacuum stability can be tested with `Vevacious` [289].

In 2014 another meta-tool was born with `FlexibleSUSY` [290, 291], which imports `SARAH`-generated β-functions, mass matrices, self-energies, EWSB conditions and parameter boundary conditions to generate a C++ spectrum generator related to `SoftSUSY`. Both `SPheno/SARAH`

---

[1] available at `https://spheno.hepforge.org`

[2] anomaly mediated supersymmetry breaking

[3] available at `https://sarah.hepforge.org`

and `FlexibleSUSY` use the $\overline{\mathrm{DR}}'$ renormalisation scheme. This toolbox eliminates the tedious task for model builders of deriving the expressions for RGEs, mass matrices, vertices etc. and only requires the idea and physical intuition for a model.

4.1.2 Spectrum calculation

We will describe the procedure of spectrum calculation in `SPheno` in more detail.

1. Start from a set of running parameters at the renormalisation scale Q. This can be a direct input from the user (low scale input) or the result of RGE running from a high scale input. The established SM parameters are read in from the `SMINPUTS` block of the SLHA file.

2. Use the parameters to solve the n tree-level tadpole equations $T_i = 0$. They allow to fix n Lagrangian parameters. The easiest solutions are usually found for the soft-breaking scalar masses, but other choices can be made by the user within the model file.

3. The parameters, now fixed to the minimum, are used to calculate the tree-level mass spectrum.

4. The one-loop correction to the Z boson, $\delta M_Z^{(1)}$, is calculated using the tree-level spectrum.

5. The electroweak VEV v is obtained by the measured pole mass of the Z boson, M_Z^{pole}, via

$$v^2 = \frac{M_Z^{2,\mathrm{pole}} + \delta M_Z^2}{f(g_i)}, \tag{4.1}$$

   with $f(g_i) = \frac{1}{4}(g_1^2 + g_2^2)$ in the MSSM. This point is crucial for two-loop mass corrections of any kind, because v depends on δM_Z^2, which is currently only known at one-loop (for a general model).

6. The tree-level spectrum is recalculated with the new values for the VEVs.

7. The tadpole corrections at one- and two-loop, $\delta T_i^{(1)}$, $\delta T_i^{(2)}$, are calculated and used to solve the minimisation conditions again.

$$T_i + \delta T_i^{(1)} + \delta T_i^{(2)} = 0 \tag{4.2}$$

8. The one-loop self-energies for all particles are evaluated at a fixed value of p^2 (starting with $p^2 = m_X^{2,\mathrm{tree}}$). For the neutral Higgs, also the two-loop self-energies $\Pi_{h,ij}^{(2)}(0)$ are evaluated using one of the available methods.

9. In an iterative procedure the poles of the propagator matrices in p^2 are determined, satisfying

$$\det\left[p^2 \delta_{ij} - \mathcal{M}_{ij}^2 + \Pi_{ij}^{(1)}(p^2) + \Pi_{ij}^{(2)}(0)\right] = 0. \tag{4.3}$$

   The real parts of these poles are returned as the pole masses.

The initial guess for the pole masses is $s_i^{(0)} = m_i^{2,\mathrm{tree}}$. At the k-th order, the pole masses $s_i^{(k)}$ are the eigenvalues of

$$\mathcal{M}^2 - \Pi^{(1)}(p^2 = s_i^{(k-1)}) - \Pi^{(2)}(0). \tag{4.4}$$

The iteration continues until a relative precision of 10^{-5} is reached.

4.2 Two-loop self-energy and tadpole calculation

4.2.1 Numerical approach

Calculation of effective potential

The problem amounts to a combinatorial exercise of populating the relevant diagrams and generating an expression for each diagram from generic formulae. A topology in `SARAH` is defined as a two element list $\{A, B\}$ with A a list of vertices and B a list of replacement rules that describe which particles are external and internal. The following example has no external lines and describes the sunrise topology.

```
topology={ C[FieldToInsert[1], FieldToInsert[2], FieldToInsert[3]],
             C[AntiField@FieldToInsert[1], AntiField@FieldToInsert[2],
               AntiField@FieldToInsert[3]]},
            {Internal[1]->FieldToInsert[1],
              Internal[2]->FieldToInsert[2],
              Internal[3]->FieldToInsert[3]}  }
```

A call of the function `InsFields[topology]` returns a list of populated diagrams. The diagrams are sorted into categories $SS, SSS, FFS, FFV, VS, VVV, VV, GGV$. In the gaugeless limit the last three types are not used, and from FFV, VS the diagrams with massive gauge bosons are discarded. At this step, particles are represented by placeholder expressions without explicit generation indices. It must be determined whether bosons are real or complex and whether fermions are Majorana or Dirac to choose the appropriate prefactor. Also it is necessary to determine the colour factor for each contribution. With this information, a string of Fortran code is cast for each diagram and written into a file `EffectivePotential_MODEL.f90` as part of the subroutine

`CalculateEffPot2Loop(vd, vu, ...).`

which returns the value of $V^{(2)}$ (the dots indicate additional VEVs and all other parameters). As an example, we show the contribution of the SSS sunrise diagram with down-type squarks (`Sd`) and Higgs pseudoscalar (`Ah`) in the MSSM. The variables i_1, i_2, i_3 are used to sum over generation indices and `coup1` is assigned the coupling of the three particles. The function name `Fep_SSS` refers to $f_{SSS}(m_1^2, m_2^2, m_3^2)$ (eq. (3.32)), which also depends on the renormalisation scale Q. The contribution of the individual diagrams is saved in the array `results1` for sunrise topologies (snowman topology contributions in `results2`).

```
! ——— diagrams of type SSS, 8 ———
! ——— Ah,Sd,conj[Sd] ———
temp=0._dp
Do i1=1,2
  Do i2=1,6
     Do i3=1,6
coup1 = cplAhSdcSd(i1,i2,i3)
colorfactor=3
```

```
 9  temp=temp+colorfactor*0.5_dp*abs(coup1)**2*Fep_SSS(MAh2(i1), ↪
         ↪ MSd2(i2),MSd2(i3),Qscale)
10    if (.not.(temp.eq.temp)) write(*,*) 'NaN at SSS C[Ah, Sd, ↪
         ↪ conj[Sd]]'
11      End Do
12    End Do
13  End Do
14  results1(1)=temp
```

In fig. 4.2 we show a simplified workflow of the two-loop calculation in `SPheno`, to which we will refer in the following explanations.

Figure 4.2: Flowchart of `SPheno` subroutines for two-loop calculation. The modules ending in `MODEL` are dynamically created by `SARAH`, while the other modules contain hard-coded functions. All methods return two arrays describing the two-loop tadpoles and self-energies.

Numerical derivatives

Let Φ_i be the scalar fields that receive a VEV,

$$\Phi_i = \frac{1}{\sqrt{2}} \left(v_i + \phi_i + i\sigma_i \right). \tag{4.5}$$

If CP conservation is assumed, the real parts ϕ_i do not mix with the imaginary parts σ_i. The first derivatives are the corrections to the tadpole equations,

$$\delta T_i^{(2)} = \frac{\partial V^{(2)}}{\partial v_i}. \tag{4.6}$$

The self-energies $\Pi^{(2)}(0)$ are obtained by numerically differentiating $V^{(2)}$ twice with respect to the VEVs,

$$\Pi_{ij}^{(2)}(0) = -\frac{\partial^2 V^{(2)}}{\partial v_i \partial v_j} \tag{4.7}$$

evaluated at the minimum of the potential. The negative sign follows from the sign convention of the self-energy fixed in eq. (3.5) and is consistent with

$$\begin{aligned}
\mathcal{M}_{ij}^2 = \mathcal{M}_{\text{tree},ij}^2 - \Delta\mathcal{M}_{ij}^2 =& \mathcal{M}_{\text{tree},ij}^2 - \Pi_{ij}^{(1)}(p^2) - \Pi_{ij}^{(2)}(0) \\
=& \frac{\partial^2 V_{\text{tree}}}{\partial \phi_i \partial \phi_j} - \Pi_{ij}^{(1)}(p^2) + \frac{\partial^2 V^{(2)}}{\partial \phi_i \partial \phi_j}
\end{aligned} \tag{4.8}$$

A straightforward way to calculate the derivative is using a finite step method on the full $V^{(2)}(v_d, v_u, \dots)$ function (dots signify additional VEVs and all other parameters). This approach was also chosen in Ref. [183]. Our code uses Ridders' method of polynomial extrapolation with dynamical step size [292] for the numerical derivation (function `dfridr` in fig. 4.2). It requires an initial step size that covers a region where the function varies significantly. The algorithm then decreases the step size dynamically to reach the desired precision. However, a too small or too large initial step size can lead to unstable results as discussed below. Note that changing the values of v_u, v_d also changes the masses and couplings, which is why they have to be calculated anew with each call of `EffPotFunction2Loop`. An auxiliary function, named `CalculateCorrectionsEffPot` (cf. fig. 4.2), calls the first derivative routine on the function for $V^{(2)}$, resulting in an array `ti_ep2L` of dimension n that stores the value of the two-loop tadpoles (n is the number of VEVs). Similarly, the second derivatives are stored in an $n \times n$ array `Pi2S_Effpot`, corresponding to the self-energy matrix $\Pi_{ij}^{(2)}(0)$. This is the purely-numerical method (method 1).

Semi-analytical derivative

A complication lies in the fact that the absolute value of the loop functions is of the order $\mathcal{O}\left(M_{\text{SUSY}}^4\right)$ and might change only in the decimals under a small variation of the VEVs. This is numerically unfavourable and prone to errors. A way to improve the numerical situation is to split up the derivatives of the expressions in eq. (3.44) using the product rule. For example, the first derivative of eq. (3.44c) is

$$\frac{\partial V_{SS}^{(2)}}{\partial v_i} = k\left[\frac{\partial c_1}{\partial v_i} f_{SS}(m_1^2, m_2^2) + c_1\left(f'_{SS}(m_1^2, m_2^2)\frac{\partial m_1^2}{\partial v_i} + f'_{SS}(m_2^2, m_1^2)\frac{\partial m_2^2}{\partial v_i}\right)\right], \tag{4.9}$$

where $f'_{SS}(x, y) \equiv \partial f_{SS}(x, y)/\partial x$. The fact that f_{SS} is symmetric in its arguments requires only one first derivative $f'_{SS}(x, y)$. For other loop functions, more derivatives are needed. The point is that the derivatives of the loop functions can be calculated analytically. This is numerically more stable in the presence of large hierarchies in the VEVs. The downside is that the first and second derivatives of all the masses and couplings have to be calculated, which is again done with the finite step method. This requires more differentiation, but hardly upscales the computing time. In the subroutine `SecondDerivativeEffPot2Loop` the first and second derivatives of the individual $V^{(2)}$ diagrams are calculated from the product rule, which requires different rules for the diagram classes. The rules are written in auxiliary functions in the

module `DerivativesEffPotFunctions.f90` together with the analytical derivatives of the loop functions (method 2 in fig. 4.2).

Goldstone bosons

While the loop functions are all regular for real arguments, their derivatives diverge for zero masses. This infrared (IR) divergence is the Goldstone problem mentioned in section 2.4. The terms that arise in the semi-analytical approach have the form

$$\frac{\partial m_G^2}{\partial v_i} f'(m_G^2, y, z). \tag{4.10}$$

If m_G^2 does not depend on v_i at all, the term is zero and the problem does not occur. This is the case in the MSSM if one works in the gaugeless limit, as was shown in eq. (2.95). In models with an extended Higgs sector this does not hold necessarily. The problem has to be circumvented by ensuring that no tree-level mass of a scalar becomes very close to zero. This depends on the renormalisation scale Q and has been analysed in Ref. [183] in the MSSM, concluding that the common choice $Q = \sqrt{m_{\tilde{t}_1} m_{\tilde{t}_2}}$ is fine. Ref. [183] compared the case of the full EP approach (including electroweak contributions) with the gaugeless limit. In the first case, IR divergences are clearly visible for certain values of Q in the prediction for m_h. On the other hand, the m_h prediction in the gaugeless limit has no divergences even at the problematic values of Q, which is a strong motivation of using this limit. We chose to work in the minimum of the full effective potential (with $g_1, g_2 \neq 0$), but calculating tree-level masses in the gaugeless limit. This ensures non-zero $\overline{\mathrm{DR}}'$ Goldstone masses.

In the case presented in Ref. [183], the difference in m_h for the gaugeless and full EP case is about $1\,\mathrm{GeV}$, showing that the electroweak corrections are clearly necessary to reach a theoretical uncertainty that matches the experimental one. However, the missing $\delta^{(2)} M_Z^2$ corrections (which influence the value of v) have to be included as well, as their effects on m_h are of the same order. For a general model, this calculation was not available in literature at the time of writing.

4.2.2 Diagrammatic approach

A third analytical approach in the spirit of section 3.4 was supplemented to `SARAH` in version `4.5.0` [188]. Similarly to the previous case, the set of all two-loop tadpole diagrams is populated with particles and then classified according to the diagrams in section 3.4. The same procedure is done for the self-energy topologies according to figs. 3.5 and 3.6. Expressions for the individual tadpoles and self-energies are written into the subroutine `CalculatePi2S` of the module `Pole2L_MODEL.f90` (fig. 4.2, method 3). They require the two-point loop functions defined in `2LPoleFunctions.f90`. In the `SPhenoInput` block of a Les Houches input file the flag number 8 can be set to 3 to choose the diagrammatic method, which has become the default setting. Because the most expensive operation is the evaluation of loop functions, unnecessary calls should be avoided. Loop functions need to be evaluated for every combination of generation indices on internal lines, but not for each external scalar index, as long as p^2 dependence is neglected. Therefore, the calculation must be performed in the order (1) sum over internal indices, (2) loop function evaluation, (3) sum over external indices. There is also a check that the coupling multiplying the loop function is non-zero to skip unnecessary calls of the loop routines. It is possible to generalise the code to include momentum dependence. Instead of calling the functions from `2LPoleFunctions.f90`, one can link to the package TSIL [293] to calculate loop

functions for arbitrary p^2. In an unofficial test version we found that this significantly increases the computing time up to several minutes.

4.2.3 Validation

The following control flags were added to the Les Houches input file for `SARAH/SPheno` version `4.4.0`.

```
Block SPhenoInput #
...
  7  ... # Skip two loop masses
  8  ... # Choose two-loop method
  9  ... # Gaugeless limit
 10  ... # Safe mode
...      #
400  ... # Step-size for purely-numerical method
401  ... # Step-size for semi-analytic method
```

The following values are possible:

- `SPhenoInput[7]`:
    - 0: Don't skip two-loop masses
    - 1: Skip two-loop masses

- `SPhenoInput[8]`:
    - 1: Two-loop calculation with purely numerical derivation
    - 2: Two-loop calculation with analytical derivation of loop functions
    - 3: Two-loop diagrammatic calculation
    - 9: Use routines based on Refs. [200]

- SPhenoInput[9]:
    - 0: Turn off gauge-less limit
    - 1: Use gauge-less limit (default)

- SPhenoInput[10]:
    - 0: Turn off the safe-mode (default)
    - 1: Use safe-mode

- `SPhenoInput[400]`: a real number (default: 0.5)

- `SPhenoInput[401]`: a real number (default: 0.001)

To use the two-loop routines of Refs. [200]
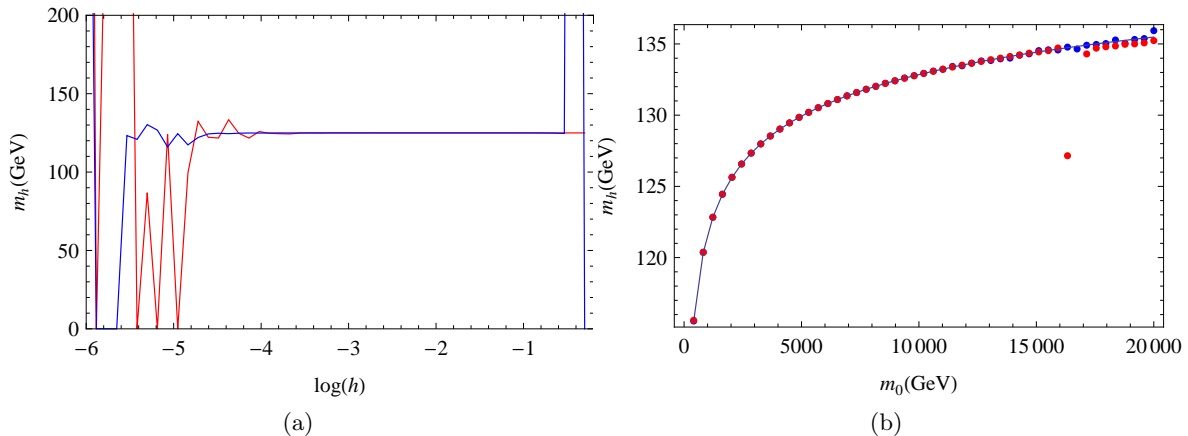
```
UseHiggs2LoopMSSM = True;
```

Figure 4.3: Test of the numerical stability: on the left side the initial step-size h is varied. The blue line corresponds to the semi-analytical approach and red for the purely numerical calculation. The right figure shows m_h for large m_0 (with $M_{1/2} = -A_0 = m_0$ and $\tan\beta = 10, \mu > 0$). The solid line is based on Refs. [200], the blue points are based on our semi-analytical method and the red ones on the purely numerical one.

must be set in the `SPheno.m` file. The flags `SPhenoInput[400]` and `SPhenoInput[401]` set the initial step size for differentiation. The algorithm reduces this quantity iteratively, but the starting value must be large enough to cover an area with significant variations. For the fully numerical method we found that the initial step size needs to be larger compared to the semi-analytical method, especially for heavy SUSY spectra, because the potential is of the order $\mathcal{O}\left(M_{\mathrm{SUSY}}^4\right)$ (cf. fig. 4.3(a)). The second method usually operates acceptably with a smaller initial step size because objects of at most order $O(M_{\mathrm{SUSY}}^2, M_Z^2)$ are derived numerically. Also, we make the approximation of treating loop masses smaller than $10^{-5} \times m_{\mathrm{heaviest}}$ in the loop to be zero for the purely numerical method ($< 10^{-8} \times m_{\mathrm{heaviest}}$ for the semi-analytical method), where m_{heaviest} is the heaviest mass in the loop. The flag `SPhenoInput[9]` (gaugeless limit) switches off D-term contributions to mass matrices and couplings. This is enabled by default to be consistent with the potential $V^{(2)}$ itself, which is gaugeless in any case.

The numerical routines were validated against the well-established routines of Refs. [200] for a variation of m_0, $M_{1/2}$, $\tan\beta$ and A_0 in the context of the CMSSM (fig. 4.4),

$$M_0 = M_{1/2} = 1\,\mathrm{TeV}, \quad A_0 = -2\,\mathrm{TeV}, \quad \tan\beta = 10, \quad \mathrm{sgn}(\mu) = 1. \tag{4.11}$$

For the comparison one has to make some modifications to ensure that the codes use equivalent definitions of parameters. This requires to set all couplings of the first two generations to zero. Further, the values of μ and M_A are calculated in the minimum of the gaugeless potential. That means, they solve the tadpole equations without D-terms (by default, the calculation based on Refs. [200] uses μ, M_A calculated in the minimum with D-terms). Table 4.1 shows that the methods agree very well. There are small numerical differences with no visible impact on the Higgs mass, stemming from the numerical derivatives and the treatment of Goldstones. Also, including D-terms in the tree-level mass matrices hardly makes a difference. The routines were also validated for the NMSSM using existing Refs. [294] for the $\alpha_s(\alpha_t + \alpha_b)$ corrections [187]. The differences between the two methods are compared in fig. 4.3, showing an improved stability for smaller initial step sizes h (fig. 4.3(a)) and heavy spectra (fig. 4.3(b)). Note that both
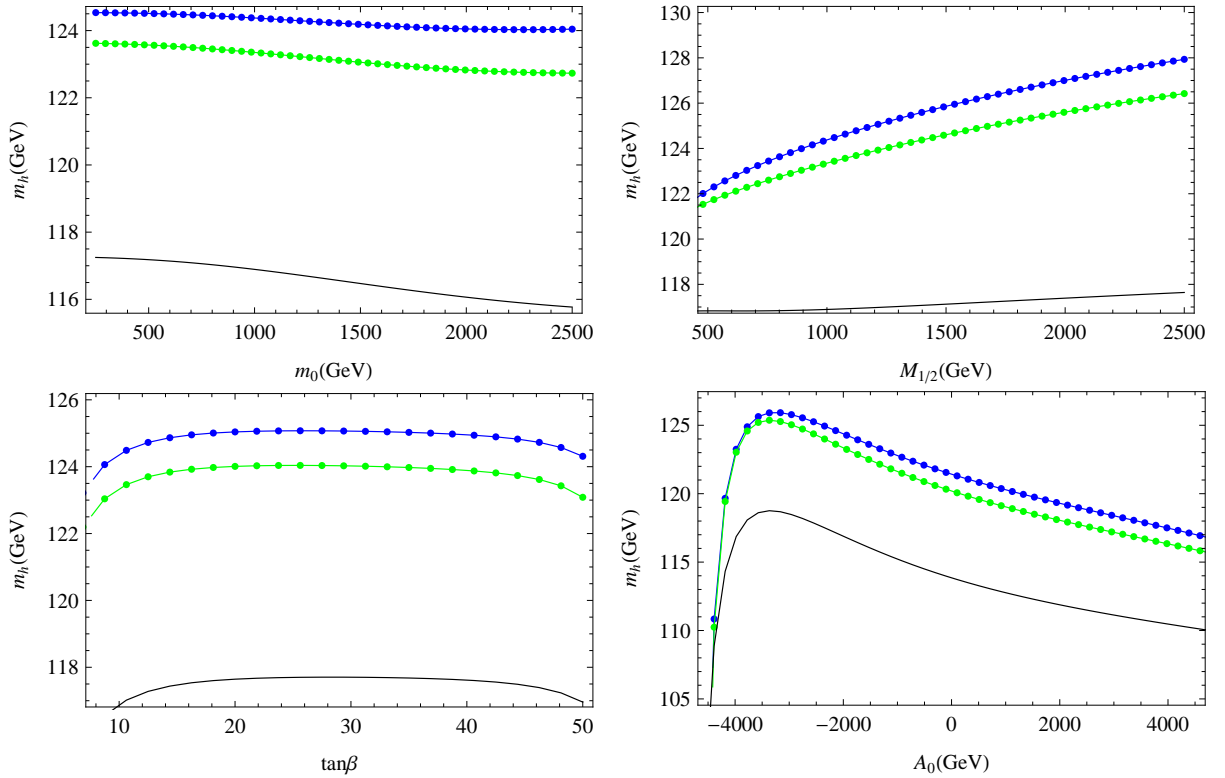
Figure 4.4: The Higgs mass at one-loop (black) and two-loop (blue, green) for variation of the CMSSM parameters $m_0, M_{1/2}, \tan\beta, A_0$. The unvaried parameters are fixed to $m_0 = M_{1/2} = 1$ TeV, $\tan\beta = 10$, $\mu > 0$, $A_0 = -2$ TeV. Blue lines include $\alpha_s(\alpha_t + \alpha_t)$ corrections while green includes all dominant two-loop corrections. The full lines are the results from the routines of Refs. [200], while the dots were calculated with the routines generated by `SARAH` presented here.

methods reveal instabilities and deviations from the solid line for scales above 15 TeV, where even the top mass is treated as massless in the loops. In this regime our setup suffers from a large uncertainty anyway. It should be considered in the context of an effective theory [295] with heavy particles decoupled. This statement applies for most SUSY spectrum generators with fixed-order calculations.

The method based on the diagrammatic approach was validated in Ref. [188] and is shown in fig. 4.5, comparing it to all other methods. We stress that the three methods are equivalent and independent, so they can be used to cross-check each other. This is important for models beyond the MSSM and NMSSM, because no other codes exist.

	Purely-numerical method (with D-terms)	Purely-numerical method	Semi-analytical method (with D-terms)	Semi-analytical method	Reference
$\Pi_{11}^{(2)}$ [GeV^2]	3475.21	3462.95	3475.18	3462.87	3460.45
$\Pi_{12}^{(2)}$ [GeV^2]	-299.21	-297.92	-299.21	-297.92	-297.70
$\Pi_{22}^{(2)}$ [GeV^2]	1954.32	1954.06	1954.32	1954.06	1954.03
m_{h_1} [GeV]	124.69	124.69	124.69	124.69	124.69
m_{h_2} [GeV]	1963.56	1963.55	1963.56	1963.56	1963.55

Table 4.1: Two-loop self energies and loop-corrected masses calculated with the two numerical methods in the gaugeless limit. We used $m_0 = M_{1/2} = 1$ TeV,$\mu > 0$, $\tan \beta = 10$, $A_0 = -2$ TeV. The reference value is the one using the routines of Refs. [200]. This was presented in Ref. [187].
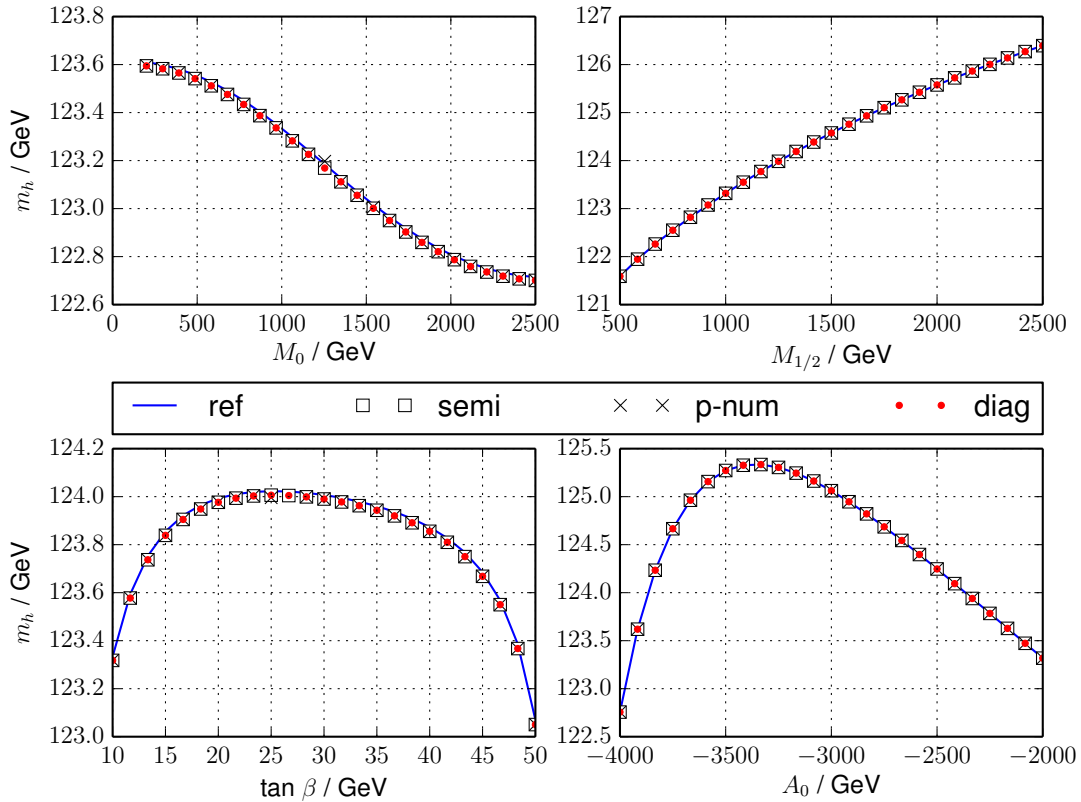
Figure 4.5: Comparison between the diagrammatic calculation ("diag") of the two-loop Higgs masses and both EP calculations ("p-num": purely numerical, "semi": semi-analytical) and the routines based on Refs. [200] ("ref"). The fixed parameters are as in eq. (4.11).

Application to SUSY models

Models beyond the MSSM introduce additional parameters and particles which can influence the Higgs mass at two-loop level. These corrections could not be studied with numerical tools prior to Ref. [187]. We revisited several common SUSY models and studied the impact of the new corrections in different regions of parameter space. The models under consideration are:

- Section 5.1: MSSM with large flavour violation [296]

- Section 5.2: NMSSM [297]

- Section 5.3: MSSM with RPV [298]

- Section 5.4: MSSM extended by vectorlike tops [299]

The last model is also explored with respect to fine-tuning, embedded in minimal GMSB. The results of the papers [296–299] are the content of this chapter.

5.1 MSSM with large flavour violation

5.1.1 Introduction

The MSSM is certainly the most studied extension of the Standard Model, with a theoretical uncertainty of the Higgs mass of a few GeV including dominant two-loop corrections [120, 195, 224, 300]. The established corrections prior to Ref. [187] are of the order

$$\alpha_s(\alpha_t + \alpha_b), \quad (\alpha_t + \alpha_b + \alpha_\tau)^2\,, \tag{5.1}$$

which do not take into account a possible flavour mixing (or flavour violation, FLV) in the squark sector between the third generation and the first and second generation. This assumption is safe in the context of minimal flavour violation [301–303] where the only source of flavour violation is the CKM matrix of the SM. The three generations of sfermions are then aligned with their partner fermions and the soft-breaking terms do not introduce any additional flavour violation.

However, there is no real reason for this simplifying assumption and there are some well-motivated non-minimal scenarios. For example, in models with gravity-mediated SUSY breaking minimal FLV is hard to obtain [304, 305]. In recent years there has been an interest in non-minimal gauge-mediating models [306–311] with direct couplings between the messenger and visible sectors, which can lead to large FLV. In the MSSM, non-minimal FLV was studied in terms of collider phenomenology [312] and flavour precision observables [313]. Large FLV can have a big effect on the Higgs mass already at one-loop [119, 120, 314–318]. For example, in Refs. [317, 318] corrections of $\mathcal{O}(10\,\text{GeV})$ were found due to large flavour mixing in the squark sector. They can even be as high as 60 GeV if more mixing parameters are included. On the other hand, large flavour violation is constrained by precision observables such as $B_s \to \mu^+\mu^-$, $B \to X_s\gamma$ and ΔM_{B_s}, see e.g. Ref. [313]. It is known that flavour effects can be large already at one loop, but it was not yet studied how significant they are at two loops. We close this gap here by considering a sample of parameter points with explicit deviations from the minimal FLV scenario, leading to a highly mixed up-squark sector. We identify the relevant parameters that lead to a large shift in the Higgs mass from flavour effects and study the dependence on these parameters.

5.1.2 The model

The superpotential of the MSSM was introduced in section 2.3,

$$\mathcal{W}_{\text{MSSM}} \equiv Y_u^{ij}\mathbf{Q}_i\mathbf{H_u}\mathbf{U}_j - Y_d^{ij}\mathbf{Q}_i\mathbf{H_d}\mathbf{D}_j - Y_e^{ij}\mathbf{L}_i\mathbf{H_d}\mathbf{E}_j + \mu\mathbf{H_u}\mathbf{H_d}. \tag{5.2}$$

In absence of lepton flavour violation, the matrix $Y_e = \text{diag}(y_e, y_\mu, y_\tau)$ must be diagonal. In the quark sector, the fields can be rotated into the super-CKM basis [319],

$$\mathbf{u}_{Li} \to (U_L^u)_{ij}\mathbf{u}_{Lj}, \qquad \mathbf{d}_{Li} \to (U_L^d)_{ij}\mathbf{d}_{Lj} \tag{5.3}$$

where Y_d, Y_u become diagonal as well,

$$Y_d = \text{diag}(y_d, y_s, y_b), \quad Y_u = \text{diag}(y_u, y_c, y_t). \tag{5.4}$$

The unitary Cabibbo-Kobayashi-Maskawa [81] matrix

$$V_{\text{CKM}} = (U_L^u)^\dagger U_L^d \tag{5.5}$$

contains all information about flavour violation. Adopting the soft-breaking terms from eq. (2.42), the case of minimal flavour violation is described by trilinear couplings proportional to the corresponding Yukawas, $T_i = A_i Y_i$ for $i = u, d, e$ and a constant A_i. Here we study large deviations from this limit. Consider the mass matrix of the up-type squarks $\mathcal{M}_u^2$ in the basis $(\widetilde{u}_L, \widetilde{c}_L, \widetilde{t}_L, \widetilde{u}_R, \widetilde{c}_R, \widetilde{t}_R)$,

$$\mathcal{M}_u^2 = \begin{pmatrix} V_{\text{CKM}} m_q^2 V_{\text{CKM}}^\dagger + \frac{1}{2} v_u^2 Y_u^2 + D_{LL} & X^\dagger \\ X & m_u^2 + \frac{1}{2} v_u^2 Y_u^2 + D_{RR} \end{pmatrix}, \tag{5.6}$$

with a 3×3 matrix

$$X = -\frac{v_d}{\sqrt{2}} \mu^* Y_u + \frac{v_u}{\sqrt{2}} T_u \tag{5.7}$$

and D_{LL}, D_{RR} are diagonal matrices with D-term contributions. We focus only on mixing between third and second generation in the up-quark sector. This is described by trilinear couplings $T_{u,23}, T_{u,32} \neq 0$ and all other off-diagonal $T_{u,ij} = 0$ for simplicity. The up-squark sector (of the 2nd and 3rd generation) is parameterised by four soft squark masses $m_{u,33}^2$, $m_{u,22}^2$, $m_{q,33}^2$, $m_{q,22}^2$. We will write the square root of these parameters for notational convenience in the following. The tree-level gluino mass M_3 is a free parameter. All other soft masses are set to a universal mass $\widetilde{m}$. Hence the parameter space is spanned by

$$m_{u,33}, \ m_{u,22}, \ m_{q,33}, \ m_{q,22}, \widetilde{m},$$
$$T_{u,33}, \ T_{u,32}, \ T_{u,23},$$
$$M_1, \ M_2, \ M_3,$$
$$M_A^2, \ \tan\beta.$$

5.1.3 Numerical results

The combination `SARAH`/`SPheno` is employed for spectrum generation using the dominant two-loop calculation described in chapter 4, taking into account all generation of sfermions. The output for the Higgs mass will be referred to as m_h^{full}, in contrast to the previous standard calculation (m_h^{approx}) including the dominant contributions of eq. (5.1) based on Refs. [200] [1]. Note that we use the label "full" even though the mentioned limitations exists (in particular the gaugeless limit). In the following we fix the parameters of lesser importance for the Higgs mass corrections to be

$$M_1 = 100\,\text{GeV}, \ M_2 = 200\,\text{GeV}, \ \tilde{m} = 1\,500\,\text{GeV},$$
$$\mu = 500\,\text{GeV}, \ M_A^2 = (1000\,\text{GeV})^2, \ \tan\beta = 10.$$

---

[1] The specific settings in `SPheno` used for the two values of the Higgs mass are in the Flag 8 of `Block SPhenoInput`: the value is set to 3 for m_h^{full} (diagrammatic calculation) and to 9 for m_h^{approx} (2-loop dominant, 3rd generation contributions).
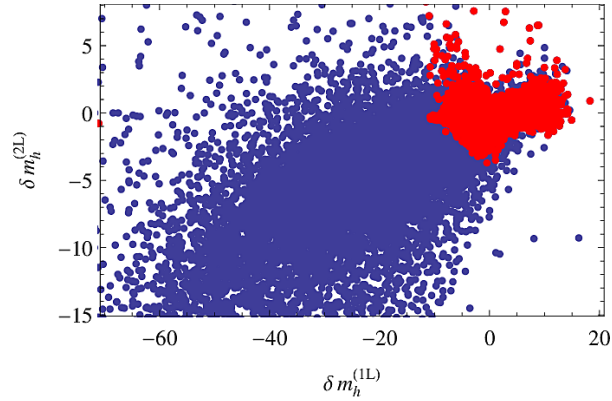
Figure 5.1: Correlation between $\delta m_h^{(1L)}$ and $\delta m_h^{(2L)} \equiv \delta m_h$. The blue points are all points which give a tachyon-free spectrum without any further restrictions. The red points provide at two loops a Higgs mass with $m_h > 120$ GeV.

For the other parameters, we scan over the following ranges:

$$M_3 \in [1,3] \text{ TeV},$$
$$m_{u/q,33} \in [0.2, 2] \text{ TeV}, \, m_{u/q,22} \in [1.2, 2.5] \text{ TeV},$$
$$T_{u,ij} \in [-4,4] \text{ TeV} \, (i,j = 2,3).$$

To be consistent with LHC collider limits, the second generation mass parameters are chosen larger than 1.2 TeV. The choice of $m_{u/q,33}$ leads to small stop masses which could also be excluded by direct searches at the LHC. However, these bounds are highly dependent on the mass of the LSP and its mass difference to the stop. In the case of a splitting below 85 GeV, the bounds are not very severe, $m_{\tilde{t}_1} > 245$ GeV [320]. Therefore, the third generation can be much lighter. It is always possible to choose M_1 such that the LSP mass is close to the stop mass, which has almost no impact on the Higgs mass. The quantity of interest is the difference between the two calculations

$$\delta m_h^{(2L)} \equiv \delta m_h = m_h^{\text{full}} - m_h^{\text{approx}}. \tag{5.8}$$

If we impose no cut upon the Higgs mass (i.e. do not require it to have the observed value of 125 GeV) then we can have very large shifts in its value through flavour effects. To begin with, we consider a rough scan over 250k points, where the only requirement is that the spectrum contains no tachyons, leaving 95k points. If large differences are found at two-loop level, they might already be present at one-loop level. To observe this we show $\delta m_h^{(1L)}$ (the difference between a full one-loop calculations and the one-loop calculation neglecting flavour effects) against $\delta m_h^{(2L)}$ in fig. 5.1. There is a weak correlation between the one- and two-loop effects. The more realistic points are those with a Higgs mass of $m_h > 120$ GeV (red points in fig. 5.1). With this cut we obtain a set of points in which the differences at one- and two-loop level are of similar size.

As a next step, a larger, finer scan for potentially relevant models was done within the $m_h > 120$ GeV bound. This scan included 5 million points using a flat prior. To avoid the issue of undersampling in a scan with six free parameters, at least 10^6 points have to be sampled, which is exceeded by this number. From the total number of points, a selection of about 50k points have $m_h > 120$ GeV and $|\delta m_h| > 0.5$ GeV, as well as fulfilling flavour constraints from

(a)

(b)

(c)
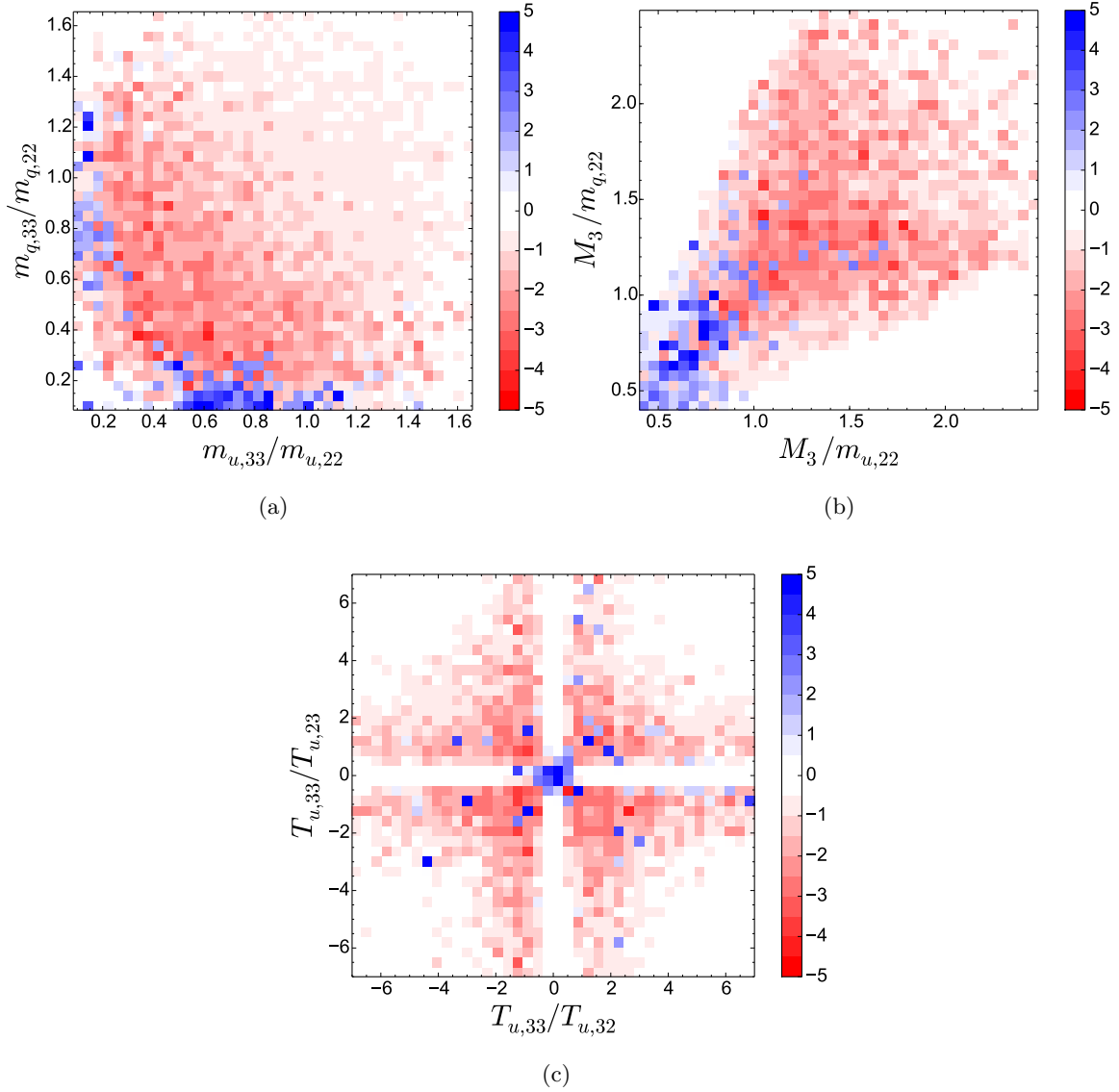
Figure 5.2: δm_h (in GeV) of the point with the maximal $|\delta m_h|$ per bin is shown, as function of different ratios of important soft-breaking parameters.

important B observables, which were calculated with `FlavorKit` [321]. The strongest constraint comes from $b \to s\gamma$. This selection is used in the following plots. It is useful to define the ratios $r_u \equiv m_{u,33}/m_{u,22}$ and $r_q \equiv m_{q,33}/m_{q,22}$ of soft mass parameters. We show in fig. 5.2 the value of δm_h with the largest absolute value per bin. These plots indicate regions where the *largest* corrections, positive as well as negative, can be obtained, possibly among other points with smaller corrections residing in the same bin which are not shown. Therefore, each plot in fig. 5.2 projects out a certain amount of points and the remaining number equals the number of bins. Complementary, fig. 5.3 shows histograms of the number of points (normalised to one) which survive the cut $|\delta m_h| \in [0.8, 7]$GeV. Figure 5.3(a) (red hue) shows only points with negative δm_h and the other plot, fig. 5.3(b), (blue hue) shows only positive δm_h. These
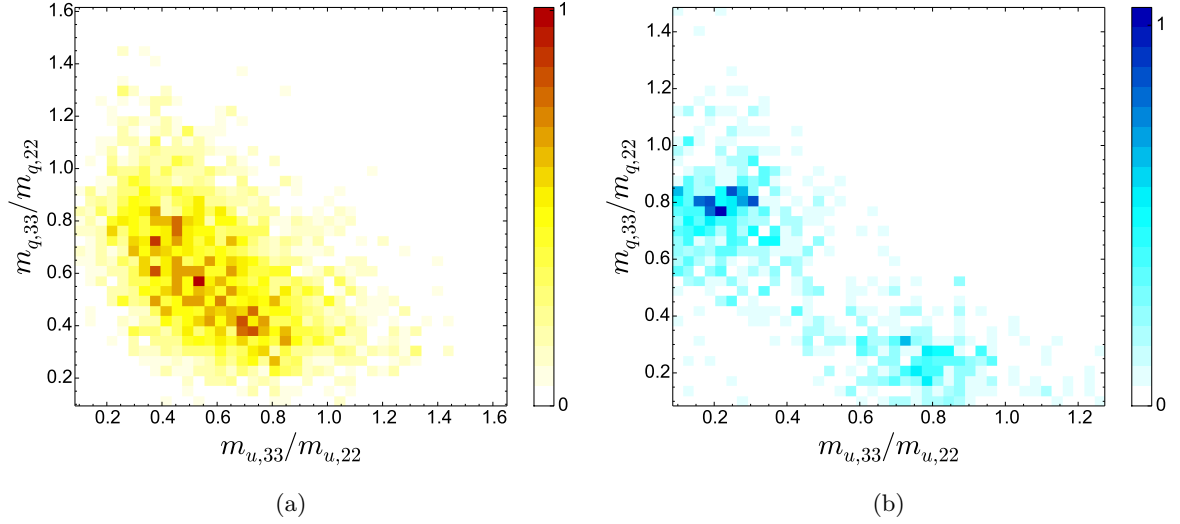
Figure 5.3: These plots show normalised histograms of points from the generated sample that fulfil $|\delta m_h| \in [0.8, 7]$ GeV (color bars range from 0 to 1). The left plot shows points with negative δm_h (red hue) and the right plot shows points of positive δm_h (blue hue).
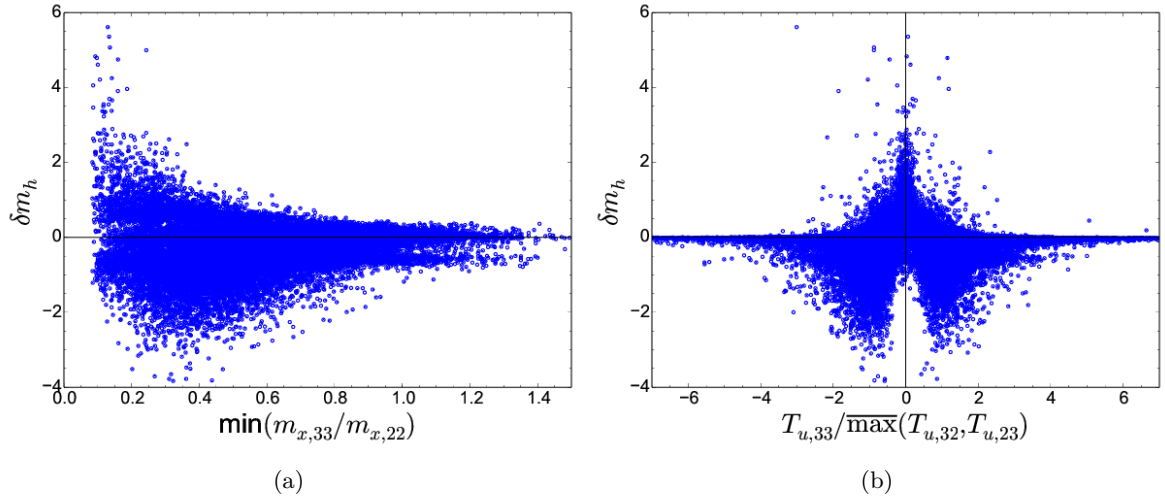
Figure 5.4: The plots show δm_h as function of $\min(m_{x,33}/m_{x,22})$ $(x = q, u)$ in (a) and as a function of $T_{u,33}/\overline{\max}(T_{u,32}, T_{u,23})$ in (b), where $\overline{\max}$ picks the entry whose absolute value is larger independent of the sign.

plots do not show the magnitude of the corrections, but rather the general location in parameter space where positive and negative corrections can be found. We find the following behaviour:

1. From fig. 5.2(a) it can be seen that a necessary condition for a large deficit of several GeV in m_h^{approx} (i.e. $\delta m_h > 0$) is a large hierarchy between the third and second generation of the soft-masses m_q or m_u. In particular, many such points reside in a region around $(r_u, r_q) = (0.8, 0.2)$ and $(0.8, 0.2)$ which is visible in fig. 5.3(b). On the other hand, if r_q or r_u is ≥ 0.4, one finds negative δm_h. This can be seen in fig. 5.3(a), where the bulk of points is within the area of $r_u \geq 0.4, r_q \geq 0.4$. It is also visible in fig. 5.4(a), where δm_h is displayed against $\min(r_u, r_q)$: Large negative values of δm_h are found around 0.4.

2. In the case that the gluino is lighter than the second generation of soft masses ($M_3/m_{x,22} < 1$, $x = q, u$), δm_h is found positive (blue area within fig. 5.2(b)), while for a heavier gluino ($M_3/m_{x,22} > 1$, $x = q, u$) the additional corrections from flavour violation are negative (red area within fig. 5.2(b)).

3. The sign of the additional corrections depends strongly on the ratio of $T_{u,33}$ and the two off-diagonal couplings $T_{u,32}$ and $T_{u,23}$. If $|T_{u,32}|$ or $|T_{u,23}|$ are much bigger than $|T_{u,33}|$, the flavoured two-loop corrections are usually large and positive, fig. 5.2(c). Negative corrections appear in particular for the case that $\max(|T_{u,32}|, |T_{u,23}|) \simeq |T_{u,33}|$. This is shown in fig. 5.4(b). We checked that a similar pattern as in fig. 5.4(b) also exists at one loop: positive (negative) corrections can be found around $T_{u,33}/\overline{\max}(T_{u,32}, T_{u,23}) = 0$ (at ± 1, respectively), but the magnitude can be much larger.

We investigate the dependence on the different parameters for two example points, one with positive shift and one with negative shift to the Higgs mass. The first point with positive shift is given by

$$m_{u,33} = 300 \text{ GeV}, \, m_{q,33} = 2000 \text{ GeV},$$
$$m_{u,22} = m_{q,22} = 2300 \text{ GeV},$$
$$T_{u,33} = T_{u,32} = -1800 \text{ GeV}, \, T_{u,23} = 0,$$
$$M_3 = 1550 \text{ GeV}. \tag{5.9}$$

This is not a point that maximises the shift. Note that this choice of parameters respects direct collider bounds by the same reasoning that was given earlier. Depending on the used two-loop calculation, we find the following values for the SM-like Higgs mass:

$$m_h^{\text{full}} = 123.1 \text{ GeV}, \tag{5.10}$$
$$m_h^{\text{approx}} = 121.1 \text{ GeV}. \tag{5.11}$$

The third-generation-only approximation gives a result which is 2 GeV too small compared to the full calculation. We checked the difference at one-loop and found $m_h^{\text{full,(1L)}} = 116.4$ GeV, $m_h^{\text{approx,(1L)}} = 119.5$ GeV. Thus, the effects are of similar size but with different sign. For this benchmark point, the dependence on the individual parameters is displayed in fig. 5.5. The discrepancy δm_h quickly increases for smaller values of $m_{u,33}$ and M_3 as well as for large negative $T_{u,32}$. Going from smaller to larger negative values of $T_{u,33}$, the sign change of δm_h is visible at about $T_{u,33} = -1.2 \text{ TeV}$. Points with large flavour violation and sizeable splitting in the soft masses can trigger charge and colour breaking minima [322–326]. Therefore we checked
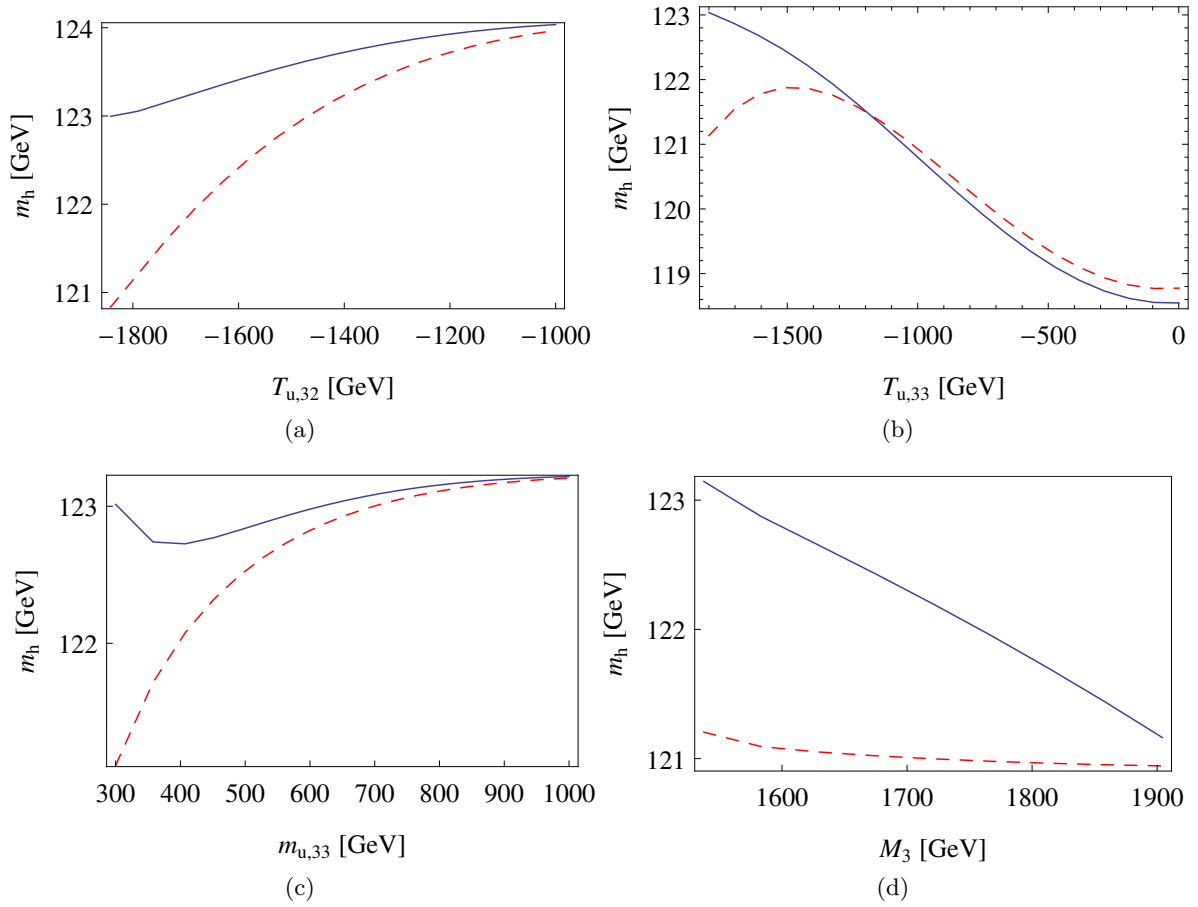
Figure 5.5: m_h^{full} (solid blue) and m_h^{approx} (dashed red) as functions of $T_{u,32}$, $T_{u,33}$, $m_{u,33}$ and M_3. The other parameters are fixed to the values in eq. (5.9).

the vacuum stability of all surviving points within the sample with `Vevacious` [289] allowing that the second and third generation of up-squarks can receive VEVs. Indeed, the benchmark point at hand exhibits a colour breaking global minimum, but the lifetime calculated with `CosmoTransitions` [327] turns out to be many times the age of the universe.

We consider a second benchmark point with negative contributions from flavour effects:

$$
\begin{aligned}
m_{u,33} &= 720\,\mathrm{GeV},\ m_{q,33} = 875\,\mathrm{GeV},\\
m_{u,22} &= m_{q,22} = 2\,500\,\mathrm{GeV},\\
T_{u,33} &= 1\,200\,\mathrm{GeV},\ T_{u,32} = -1\,900\,\mathrm{GeV},\ T_{u,23} = 0,\\
M_3 &= 2\,600\,\mathrm{GeV}.
\end{aligned}
\tag{5.12}
$$

Here, the minimum of the scalar potential is stable. The discrepancy between the Higgs mass

calculations turns out to be about $3\,\mathrm{GeV}$,

$$m_h^{\mathrm{full}} = 121.2\,\mathrm{GeV}, \tag{5.13}$$

$$m_h^{\mathrm{approx}} = 124.0\,\mathrm{GeV}. \tag{5.14}$$

Comparing this to the one-loop level, we find a difference of about $1\,\mathrm{GeV}$: $m_h^{\mathrm{full,(1L)}} = 117.3\,\mathrm{GeV}$, $m_h^{\mathrm{approx,(1L)}} = 118.3\,\mathrm{GeV}$. For this point, the flavour violation effects at two-loop are even more important than at one-loop. The dependence on $T_{u,32}$ and $T_{u,33}$ as well as on $m_{u,33}$ and M_3 is shown in fig. 5.6. Note that in the region of large $|T_{u,32}|$ and δm_h in fig. 5.6(a), the electroweak potential becomes meta-stable and even short-lived. These constraints have to be taken into account and they can be more restricting than flavour observables.
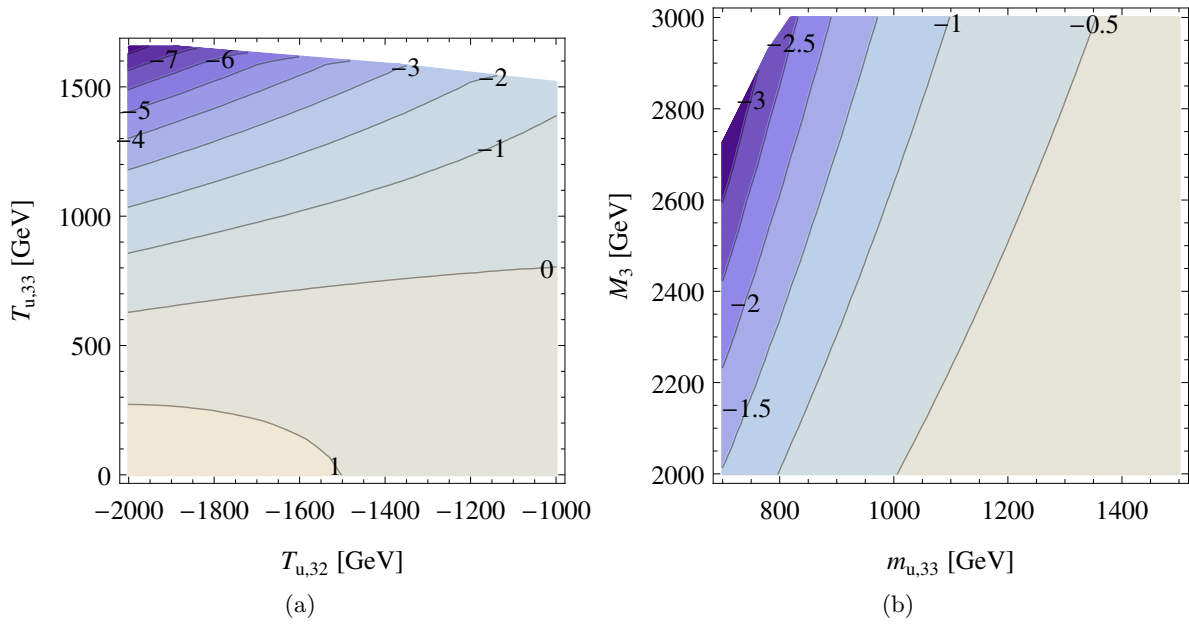
Figure 5.6: δm_h in the $(T_{u,32}, T_{u,33})$ and $(m_{u,33}, M_3)$ plane. The other parameters are fixed to the values in eq. 5.12.

5.1.4 Discussion

We have analysed the effect of large flavour mixing on the two-loop Higgs mass calculation, compared to the third-generation-only approximation. The difference can be several GeV for parameter points that are consistent with bounds from flavour observables, direct collider searches and vacuum stability. The size and the sign of the flavoured two-loop contributions depends mainly on the hierarchy in the soft-breaking squark masses, the size of the flavour violating trilinear soft-terms and the gluino mass. We address some further questions in the following.

1. *Do the shifts at two loops correlate with those at one loop?* In fig. 5.1 we saw that there is a relationship between the shifts at one and two-loops for the rough scan. For the

points of the fine scan shown in fig. 5.7(b) we can identify roughly two branches of points: the horizontal one exhibits small two-loop differences that seem uncorrelated to $\delta m_h^{(1L)}$. The other branch shows a positive correlation between one- and two-loop shifts. Broadly speaking, the points that show a large difference from flavour effects between approximate and full calculation at two loops also show a discrepancy already at one loop. One could naively assume that a large gluino mass suppresses the differences at two loops. However, it turns out that the points of the correlated branch tend to have a gluino mass that is much larger than the stop masses. Gluinos have the effect of enhancing the two-loop corrections in general.

2. *Are the corrections proportional to the full Yukawa ($y_{u,d,c,s} \neq 0$) couplings?* To investigate this, we recalculated the corrections with only the top/bottom mass terms in the Yukawa couplings non-zero, and found very little difference. In fact, only $y_t \equiv Y_u^{33}$ is relevant. This means that the only the off-diagonal trilinear couplings $T_{u,ij}$ are responsible for the shifts.

3. *Are the differences mostly in α_t^2 or $\alpha_t \alpha_s$ corrections?* Using modified versions of our code we have compared the difference between "full" and third-generation-only results for these two cases. The strong contribution exhibits the largest differences.

Another question is whether the found discrepancies are correlated to the one-loop shifts to the stop masses caused by flavour violation. To look at this superficially, we consider the difference between $m_{\tilde{t}}^{1L}$ and the same mass with flavour violating terms forced to zero,

$$\delta m_{\tilde{t}} \equiv m_{\tilde{t}}^{1L} - m_{\tilde{t}}^{1L}\big|_{T_{23}=T_{32}=0}. \tag{5.15}$$

Figure 5.7(a) shows a 2D histogram of points with respect to $\delta m_{\tilde{t}}/m_{\tilde{t}}$ and δm_h. There is no clear sign of a correlation between the two, but rather a spread of points. This is not a conclusive result and the correlation might still be there for some of the points. To investigate this a bit more, we use a refined measure. A guess for the order of magnitude of the two-loop shift in the Higgs mass can be obtained by plugging the one-loop stop masses into the one-loop Higgs mass expressions,

$$\Delta^{2L} m_h^2 = \delta^{1L} m_h^2(m_{\tilde{t}_i}^{1L}) - \delta^{1L} m_h^2(m_{\tilde{t}_i}^{\overline{DR}'}), \tag{5.16}$$

with $\delta^{1L} m_h^2(M)$ being the one-loop correction to the Higgs mass-squared computed using the effective potential method found, for example, in [200]. In the presence of large flavour mixing, a stop isn't well defined. We consider instead the two up-type squarks with the largest components of $\tilde{t}_L, \tilde{t}_R$ as stops. We stress that Δ^{2L} is not a true two-loop value, but merely an estimate of the order of magnitude. However we can use it to see whether shifting both the stop masses may correlate with the Higgs mass shift.

$$\delta^{(1L)^2} m_h^2 \equiv \Delta^{2L} m_h^2 - \Delta^{2L} m_h^2\big|_{T_{32}=T_{23}=0}, \tag{5.17}$$

$$\Rightarrow \delta m_h^{(1L)^2} \equiv \left((m_h^{\text{approx}})^2 + \delta^{(1L)^2} m_h^2 \right)^{1/2} - m_h^{\text{approx}},$$

where $\delta m_h^{(1L)^2}$ is derived from $\delta^{(1L)^2} m_h^2$ as a parameter of mass dimension 1. The size of $\delta m_h^{(1L)^2}$ gives the would-be "two-loop" shift in the Higgs mass when the generation-mixing trilinear couplings are turned on. It describes the same shift as the actual δm_h used before, but is roughly

(a)

(b)

(c)
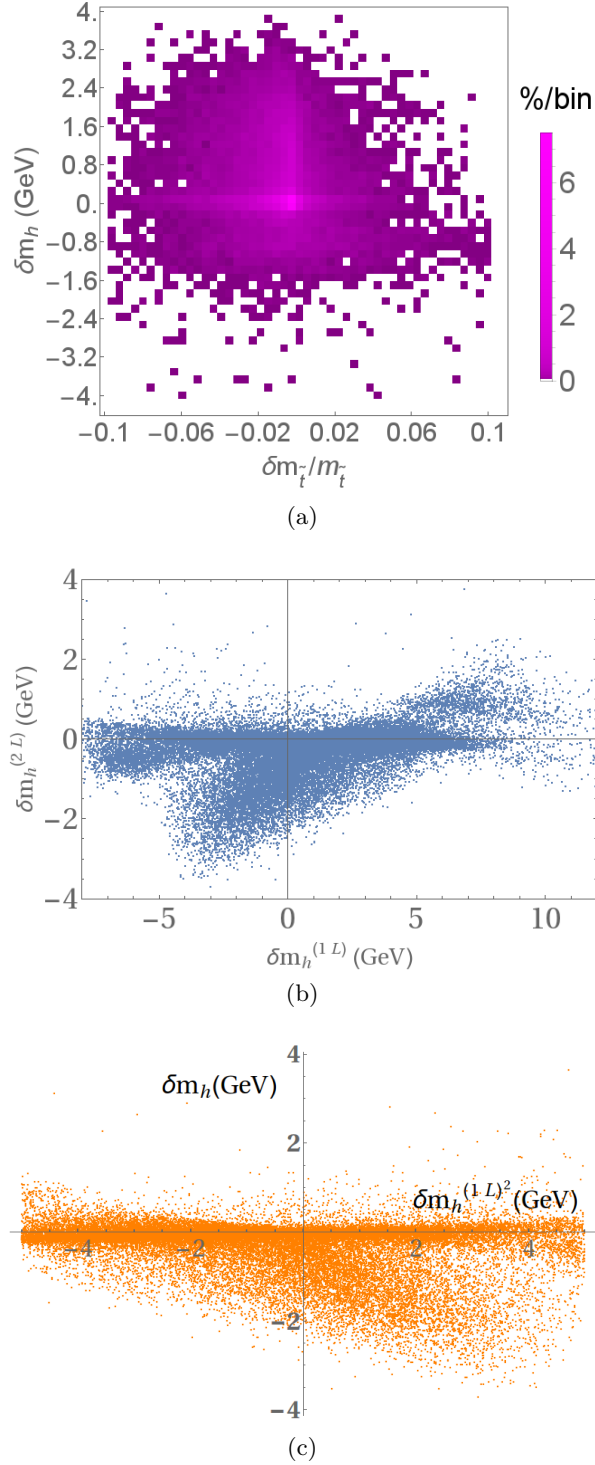
Figure 5.7: (a): δm_h against proportional shift in lightest stop mass ($\delta m_{\tilde{t}_1}/m_{\tilde{t}_1}$) compared to model with $T_{23} = T_{32} = 0$, colours show percentage of points in each bin in a 50 by 50 grid, bins with zero points shown as white. (b): Correlation between the off-diagonal flavour induced shift in the Higgs mass at one and two loops. (c): δm_h (ordinate) against approximation for shift from inserting on-shell stop masses into the one-loop Higgs mass expression (abscissa) as given in equation (5.17).

estimated only from one-loop expressions. The plot shown in fig. 5.7(c) is also not clearly conclusive, but it does show a weak anti-correlation between $\delta m_h^{(1\mathrm{L})^2}$ and δm_h, which appears to be the inverse of the relationship shown in fig. 5.7(b). The fact that large two-loop discrepancies δm_h can be related to a one-loop shift in the stop masses implies that the discrepancies have an uncertainty stemming from the use of the $\overline{\mathrm{DR}}'$ scheme (which would be of higher order). Passing to the on-shell scheme for at least the stop masses could reduce the observed differences, where everything would be expressed in terms of stop pole masses. A full $\overline{\mathrm{DR}}'$ calculation is much simpler and can be written down for generic models, but it can suffer from unphysical large contributions if there are large hierarchies between the masses of particles in the loops [200]. The Higgs mass calculation in the on-shell scheme on the other hand can have a smaller theoretical uncertainty, but requires the inclusion of new counterterms at two loops and is less practical. This issue has recently been studied in the case of Dirac gaugino models [328].

From considering the above it can be concluded that a sizeable contribution to δm_h arises from the new diagrams involving the trilinear couplings T_{23}, T_{32} . These effects can only be obtained if all generations of sfermions are taken into account. In the case of trilinear terms of a magnitude comparable to the other soft terms, we can no longer trust the third-generation-only approximation.

5.2 NMSSM Higgs mass beyond $\mathcal{O}\left(\alpha_s(\alpha_t + \alpha_b)\right)$

5.2.1 Introduction

In this section we consider the NMSSM [238] and the impact of the two-loop corrections beyond $\mathcal{O}\left(\alpha_s(\alpha_b + \alpha_t)\right)$ on the Higgs mass. The model involves one additional superfield **S**, which is a singlet under all gauge groups. Its components, the scalar singlet S and the singlino $\widetilde{S}$, extend the Higgs sector and neutralino sector, respectively. One of the crucial restrictions of the MSSM is the upper bound on the tree-level Higgs mass (eq. (2.67)) and the need for large quantum corrections. The NMSSM enhances the Higgs mass already at tree level [238, 239] compared to the MSSM, reducing the fine-tuning [240, 241, 244, 254–256]. Further, the μ problem of the MSSM [151] is solved by the additional singlet, which generates an effective μ term. The NMSSM has a rich collider phenomenology [329] and it has been shown recently that light singlinos could explain why SUSY has remained hidden from the LHC [260]. The Higgs mass precision in the NMSSM has received a lot of attention, with full one-loop calculations available in the $\overline{\mathrm{DR}}'$ scheme [294, 330] and in different on-shell schemes [331, 332]. At the two-loop level the dominant corrections $\alpha_s(\alpha_b + \alpha_t)$ have been calculated in Ref. [294]. The state-of-the art codes written specifically for the NMSSM are `NMSPEC` [333] and Next-to-Minimal `SOFTSUSY` [217–220], which use the known MSSM-like corrections $(\alpha_b + \alpha_t + \alpha_\tau)^2$. Advanced techniques are also implemented in `FeynHiggs` [224–227] and `NMSSMCALC` [334]. There are two-loop contributions that are exclusive to the NMSSM, which we could address here for the first time [297]. After introducing the model, we analyse the significance of the new corrections in a few scenarios with heavy and light singlets.

5.2.2 The model

The NMSSM is constructed from the MSSM by adding a chiral superfield **S** with representations $(\mathbf{1}, \mathbf{1}, 0)$. The superpotential reads (with flavour indices suppressed)

$$\mathcal{W}_{\mathrm{NMSSM}} = Y_u \mathbf{Q} \mathbf{H}_u \mathbf{U} - Y_d \mathbf{Q} \mathbf{H}_d \mathbf{D} - Y_e \mathbf{L} \mathbf{H}_d \mathbf{E} + \lambda \mathbf{H}_u \mathbf{H}_d \mathbf{S} + \frac{1}{3} \kappa \mathbf{S}^3. \tag{5.18}$$

Without further restrictions, gauge invariance and renormalisability allow terms $\mathbf{S}^k$ up to $k = 3$. Only the cubic term is used here, because no other dimensionful parameters should be introduced. If the singlet receives a VEV, $\langle S \rangle = v_s/\sqrt{2}$, then the term $\lambda \mathbf{H}_u \mathbf{H}_d \mathbf{S}$ generates an effective μ-term. In this setup, the superpotential satisfies a discrete $\mathbb{Z}_3$ symmetry acting on all chiral superfields as $\mathbf{\Phi} \rightarrow \exp(i\, 2\pi/3)\mathbf{\Phi}$ [335]. This symmetry is spontaneously broken by the VEV of S. As a consequence of this breaking, the universe would be allowed to form *domain walls* during its evolution, where different patches of space-time occupy different vacua [336]. The existence and interactions of such domain walls can have interesting effects (e.g. in the context of baryogenesis [337]), but in this case they would overdominate the energy density of the universe [335] and contradict our observations of cosmic microwave background. A possible solution to the domain wall problem is an *explicit* breaking of the $\mathbb{Z}_3$ symmetry (e.g. Ref. [336]). However, our study concerns itself only with the minimal version of the NMSSM defined by eq. (5.18).

The soft-breaking terms are given by

$$
\begin{aligned}
-\mathcal{L}_{\text{soft},2} &= m_{H_u}^2 |H_u|^2 + m_{H_d}^2 |H_d|^2 + m_S^2 |S|^2 \\
&\quad + \widetilde{Q}^\dagger m_Q^2 \widetilde{Q} + \widetilde{L}^\dagger m_L^2 \widetilde{L} + \widetilde{D}^\dagger m_D^2 \widetilde{D} + \widetilde{U}^\dagger m_U^2 \widetilde{U} + \widetilde{E}^\dagger m_E^2 \widetilde{E}, \\
&\quad + \frac{1}{2} \left(M_1 \lambda_B \lambda_B + M_2 \lambda_W^a \lambda_W^a + M_3 \lambda_G^\alpha \lambda_G^\alpha + \text{h.c.} \right), \quad (5.19) \\
-\mathcal{L}_{\text{soft},3} &= T_u^{ij} \widetilde{Q}_i H_u \widetilde{U}_j + T_d^{ij} \widetilde{Q}_i H_d \widetilde{D}_j + T_e^{ij} \widetilde{L}_i H_d \widetilde{E}_j + T_\lambda H_u H_d S + \frac{1}{3} T_\kappa S^3. \quad (5.20)
\end{aligned}
$$

After EWSB, the singlet and the Higgs fields split into CP-even and odd components and a VEV,

$$
S(x) = \frac{1}{\sqrt{2}} \left(v_s + \phi_s(x) + i\sigma_s(x) \right), \quad (5.21)
$$

$$
H_i^0(x) = \frac{1}{\sqrt{2}} \left(v_i + \phi_i(x) + i\sigma_i(x) \right), \qquad i = d, u. \quad (5.22)
$$

We choose a phase convention such that all VEVs are real. The VEV of the singlet triggers effective μ- and b-terms

$$
\mu_{\text{eff}} = \frac{1}{\sqrt{2}} \lambda v_s, \qquad b_{\text{eff}} = \frac{1}{\sqrt{2}} T_\lambda v_s + \frac{1}{2} \kappa \lambda v_s^2. \quad (5.23)
$$

μ_{eff} and λ shall be treated as input parameters from which $v_s = \sqrt{2}\mu_{\text{eff}}/\lambda$ is calculated. The tadpole equations at tree level are given by

$$
T_i^{(0)} = \left. \frac{\partial V}{\partial \phi_i} \right|_{\text{min}} = 0, \qquad i = d, u, s \quad (5.24)
$$

with

$$
\frac{1}{v_d} \frac{\partial V}{\partial \phi_d} = m_{H_d}^2 + \frac{1}{8}\left(g_1^2 + g_2^2\right)\left(v_d^2 - v_u^2\right) + \frac{1}{2}\left(v_s^2 + v_u^2\right)|\lambda|^2 - \frac{1}{2}v_s^2 \tan\beta \Re[\kappa\lambda^*] - \frac{1}{\sqrt{2}}v_s \tan\beta \Re[T_\lambda],
$$
$$(5.25a)$$

$$
\frac{1}{v_u} \frac{\partial V}{\partial \phi_u} = m_{H_u}^2 + \frac{1}{8}\left(g_1^2 + g_2^2\right)\left(v_u^2 - v_d^2\right) + \frac{1}{2}\left(v_d^2 + v_s^2\right)|\lambda|^2 - \frac{1}{2}v_s^2 \cot\beta \Re[\kappa\lambda^*] - \frac{1}{\sqrt{2}}v_s \cot\beta \Re[T_\lambda],
$$
$$(5.25b)$$

$$
\frac{1}{v_s} \frac{\partial V}{\partial \phi_s} = m_S^2 - v_d v_u \Re[\lambda\kappa^*] + v_s^2|\kappa|^2 + \frac{1}{2}(v_d^2 + v_u^2)|\lambda|^2 - \frac{1}{\sqrt{2}}\frac{v_d v_u}{v_s}\Re[T_\lambda] + \frac{1}{\sqrt{2}}v_s \Re[T_\kappa]. \quad (5.25c)
$$

As usual all parameters are running parameters at the scale Q. The tadpole equations receive corrections at loop level ($\delta T_i^{(n)}$) and the corrected minimum is defined by the vanishing sum

$$
T_i^{(0)} + \delta T_i^{(1)} + \delta T_i^{(2)} = 0 \qquad \text{for} \quad i = d, u, s. \quad (5.26)
$$

Here we choose to solve for the squared soft masses, $m_{H_d}^2, m_{H_u}^2, m_S^2$. This leaves the free input parameters of the Higgs sector to be

$$
\lambda, \kappa, \mu_{\text{eff}}, T_\lambda, T_\kappa, \tan\beta.
$$

It is sometimes convenient to define

$$T_\lambda \equiv \lambda A_\lambda, \qquad T_\kappa \equiv \kappa A_\kappa.$$

The tree-level mass matrices of the CP-even Higgs bosons are calculated from the scalar potential via

$$\mathcal{M}^2_{h,ij} = \left.\frac{\partial^2 V}{\partial \phi_i \partial \phi_j}\right|_{\min}, \tag{5.27}$$

with $i, j = u, d, s$.

$$\mathcal{M}^2_{h,\phi_d\phi_d} = \frac{1}{2}\left(v_s^2 + v_u^2\right)|\lambda|^2 + \frac{1}{8}\left(g_1^2 + g_2^2\right)\left(3v_d^2 - v_u^2\right) + m_{H_d}^2$$

$$\mathcal{M}^2_{h,\phi_d\phi_u} = \frac{1}{4}\left(-2\sqrt{2}v_s\Re\left(T_\lambda\right) + \left(4v_dv_u\lambda - v_s^2\kappa\right)\lambda^* - v_s^2\lambda\kappa^*\right) - \frac{1}{4}\left(g_1^2 + g_2^2\right)v_dv_u$$

$$\mathcal{M}^2_{h,\phi_u\phi_u} = \frac{1}{2}\left(v_d^2 + v_s^2\right)|\lambda|^2 - \frac{1}{8}\left(g_1^2 + g_2^2\right)\left(-3v_u^2 + v_d^2\right) + m_{H_u}^2$$

$$\mathcal{M}^2_{h,\phi_d\phi_s} = -\frac{1}{\sqrt{2}}v_u\Re\left(T_\lambda\right) + v_s\left(\left(-\frac{1}{2}v_u\kappa + v_d\lambda\right)\lambda^* - \frac{1}{2}v_u\lambda\kappa^*\right)$$

$$\mathcal{M}^2_{h,\phi_u\phi_s} = \frac{1}{2}\left(-v_d\left(\sqrt{2}\Re\left(T_\lambda\right) + v_s\lambda\kappa^*\right) - v_s\left(-2v_u\lambda + v_d\kappa\right)\lambda^*\right)$$

$$\mathcal{M}^2_{h,\phi_s\phi_s} = \frac{1}{2}\left(2\sqrt{2}v_s\Re\left(T_\kappa\right) + \left(6v_s^2\kappa - v_dv_u\lambda\right)\kappa^* + \left(\left(v_d^2 + v_u^2\right)\lambda - v_dv_u\kappa\right)\lambda^*\right) + m_S^2 \tag{5.28}$$

This matrix is diagonalised by an orthogonal matrix Z_H,

$$Z_H \mathcal{M}_h^2 (Z_H)^T = \text{diag}(m_{h_1}^2, m_{h_2}^2, m_{h_3}^2). \tag{5.29}$$

The three eigenvalues of $\mathcal{M}_h^2$ correspond to the squares of the tree-level masses $m_{h_1}^2$, $m_{h_2}^2$, $m_{h_3}^2$ which are ordered by their mass. The lightest Higgs mass m_{h_1} is bounded from above at tree level [238],

$$m_{h,\text{tree}}^2 \leq M_Z^2 \cos^2 2\beta + \frac{1}{2}\lambda^2 v^2 \sin^2 2\beta = M_Z^2\left(\cos^2 2\beta + \frac{2\lambda^2}{g_1^2 + g_2^2}\sin^2 2\beta\right). \tag{5.30}$$

The extra contribution to the tree-level Higgs mass $\sim \lambda^2 v^2 \sin^2 2\beta$ is helpful in the sense that radiative corrections can be smaller in order to reach $125\,\text{GeV}$. However, the extra term is only relevant for small $\tan\beta$. The mass matrix of the CP-odd states reads

$$\mathcal{M}^2_{A,ij} = \left.\frac{\partial^2 V}{\partial \sigma_i \partial \sigma_j}\right|_{\phi_k=0,\sigma_k=0}, \tag{5.31}$$

with

$$\mathcal{M}^2_{A,\sigma_d\sigma_d} = \frac{1}{2}\left(v_s^2 + v_u^2\right)|\lambda|^2 + \frac{1}{8}\left(g_1^2 + g_2^2\right)\left(-v_u^2 + v_d^2\right) + m_{H_d}^2, \tag{5.32}$$

$$\mathcal{M}^2_{A,\sigma_u\sigma_u} = \frac{1}{2}\left(v_d^2 + v_s^2\right)|\lambda|^2 - \frac{1}{8}\left(g_1^2 + g_2^2\right)\left(-v_u^2 + v_d^2\right) + m_{H_u}^2, \tag{5.33}$$

$$\mathcal{M}^2_{A,\sigma_s\sigma_s} = \frac{1}{2}\left(v_u^2 + v_d^2\right)|\lambda|^2 + v_s^2|\kappa|^2 + v_dv_u\Re[\lambda\kappa^*] + m_S^2 - \sqrt{2}v_s\Re[T_\kappa], \tag{5.34}$$

$$\mathcal{M}^2_{A,\sigma_d\sigma_u} = \frac{1}{2}v_s^2\Re[\lambda\kappa^*] + \frac{1}{\sqrt{2}}v_s\Re[T_\lambda], \tag{5.35}$$

$$\mathcal{M}^2_{A,\sigma_d\sigma_s} = -v_sv_u\Re[\lambda\kappa^*] + \frac{1}{\sqrt{2}}v_u\Re[T_\lambda], \tag{5.36}$$

$$\mathcal{M}^2_{A,\sigma_u\sigma_s} = -v_sv_d\Re[\lambda\kappa^*] + \frac{1}{\sqrt{2}}v_d\Re[T_\lambda]. \tag{5.37}$$

The matrix $\mathcal{M}^2_A$ is diagonalised by Z_A,

$$Z_A\mathcal{M}^2_A(Z_A)^\dagger = \mathrm{diag}(m^2_{A_1}, m^2_{A_2}, m^2_{A_3}). \tag{5.38}$$

The spectrum contains a massless state, which we identify as the Goldstone boson $G^0 = A_1$. Including the gauge-fixing term

$$\mathcal{L}_{\mathrm{GF}} \supset -\frac{1}{2\xi_Z}\left(\partial^\mu Z_\mu + \xi_Z M_Z G^0\right)^2, \tag{5.39}$$

the Goldstone boson mass becomes $\xi_Z M_Z^2$. Working in the gaugeless limit, we can isolate this state by performing a preliminary rotation,

$$\sigma_u = \sigma_{ud}\cos\beta - G^0\sin\beta, \qquad \sigma_d = \sigma_{ud}\sin\beta + G^0\cos\beta. \tag{5.40}$$

with $\tan\beta = v_u/v_d$. Upon substituting the tadpoles, the mass matrix reads

$$\begin{pmatrix} \xi_Z M_Z^2 & 0 & 0 \\ 0 & \star & \star \\ 0 & \star & \star \end{pmatrix}. \tag{5.41}$$

Let us take the derivatives of the first eigenvalue (before applying the tadpoles) with respect to the VEVs and with $g_1 = g_2 = 0$ (applying eq. (2.94)),

$$\frac{\partial m^2_{G^0}}{\partial v_d} = \lambda^2\sin^2\beta \; v_d,$$

$$\frac{\partial m^2_{G^0}}{\partial v_u} = \lambda^2\cos^2\beta \; v_u,$$

$$\frac{\partial m^2_{G^0}}{\partial v_s} = \left(\lambda^2 - \Re[\lambda\kappa^*]\sin(2\beta)\right) \; v_s - \frac{\Re[T_\lambda]}{\sqrt{2}}\sin(2\beta). \tag{5.42}$$

These clearly never all vanish, even in the gaugeless limit, unless $\lambda = 0$. In our approach we solve the full tadpole equations (including gauge contributions), but use the mass matrices of scalars and pseudo-scalars in the gaugeless limit. This way, the Goldstone mass becomes negative, because it is effectively evaluated outside the minimum.

$$\left.\frac{\partial^2 V^{(0)}_{\mathrm{gaugeless}}}{\partial(G^0)^2}\right|_{\mathrm{min}} = -\frac{M_Z^2}{2}\cos^2 2\beta. \tag{5.43}$$

This avoids the problem of massless scalars in derivatives of the effective potential (Goldstone problem) and is valid only in the gaugeless limit. With CP conservation, the Higgs sector of the NMSSM exhibits three CP-even Higgses (h_1, h_2, h_3), two CP-odd ones (A_1, A_2) and a charged

(a)

(b)

(c)
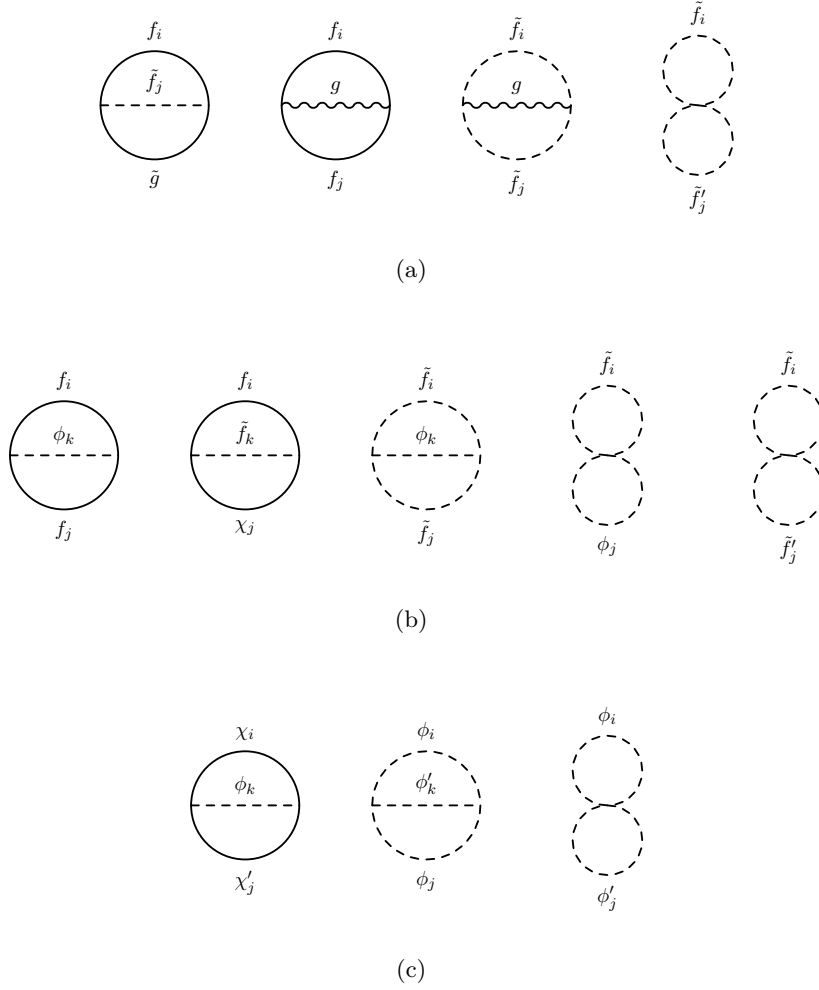
Figure 5.8: Feynman diagrams contributing to the effective potential at two-loop level. **(a):** Strong corrections $\alpha_s(\alpha_t + \alpha_b)$ involving coloured SM fermions ($f_i, f_i' = d_i, u_i$) and SUSY sfermions ($\tilde{f}_i, \tilde{f}_i' = \tilde{d}_i, \tilde{u}_i$). **(b):** Diagrams involving Yukawa couplings with SM fermions ($f_i, f_i' = d_i, u_i, l_i, \nu_i$), SUSY sfermions ($\tilde{f}_i, \tilde{f}_i' = \tilde{d}_i, \tilde{u}_i, \tilde{l}_i, \tilde{\nu}_i$), neutralinos/charginos ($\chi_i = \tilde{\chi}_i^0, \tilde{\chi}_i^+$) and Higgs particles ($\phi_i = h_i, A_i^0, H_i^+$). **(c):** Diagrams contributing at the order $(\alpha_\lambda + \alpha_\kappa)^2$ to the effective potential. They involve the neutralinos/charginos ($\chi_i, \chi_i' = \tilde{\chi}_i^0, \tilde{\chi}_i^+$) and Higgs particles ($\phi_i, \phi_i' = h_i, A_i^0, H_i^+$). A sum over all flavour combinations is assumed, but all CP and charge violating diagrams are not considered.

one $H^\pm$. Because the h_i are linear combinations of ϕ_u, ϕ_d, ϕ_s, they can be called doublet-like or singlet-like if the corresponding coefficient is much larger than the others. If the mixings are not too large, one of states h_i can be called a singlet, or more precisely a singlet-like state. In the following, we will distinguish two regimes: A singlet that is much heavier than the SM-like Higgs, and a singlet of comparable or smaller mass.

5.2.3 Numerical results

The dominant strong corrections $\mathcal{O}\left(\alpha_s(\alpha_t + \alpha_b)\right)$ stemming from the diagrams in fig. 5.8(a) had already been calculated for the NMSSM [294] and they were cross-checked against the

corresponding contributions from our code (Ref. [187]). To do this, we applied a few changes to the code to be able to switch off individual contributions. Let $\delta_s^{(2L)} m_h$ be the two-loop shift of the Higgs mass described the diagrams in fig. 5.8(a). In our calculation of $V_{\text{eff}}^{(2)}$ the diagrams of figs. 5.8(b) and 5.8(c) are also included, but with $g_1 = g_2 = 0$. The diagrams shown in fig. 5.8(b) have so far only been calculated in the MSSM [200], but not in the NMSSM, where the vertices have extra terms with λ, κ. Furthermore, the contributions of fig. 5.8(c) vanish in the MSSM (in the gaugeless limit), but in the NMSSM they contribute at the order $\mathcal{O}\left((\alpha_\lambda + \alpha_\kappa)^2\right)$. All of these corrections combined lead to a correction $\delta_{\text{full}}^{(2L)} m_h$. We are interested in the difference between the two calculations,

$$\Delta_M = \delta_{\text{full}}^{(2L)} m_h - \delta_s^{(2L)} m_h, \tag{5.44}$$

as well as in the ratio $\Delta_R = \Delta_M / \delta_s^{(2L)} m_h$, which gives an estimate of the importance of the new corrections.

Heavy singlet with moderate λ

We test the importance of the two-loop corrections beyond $\mathcal{O}\left(\alpha_s(\alpha_t + \alpha_b)\right)$ with a parameter point in the constrained NMSSM. In this setup, universal boundary conditions at the GUT scale are applied,

$$M_1 = M_2 = M_3 \equiv M_{1/2},$$
$$m_D^2 = m_U^2 = m_Q^2 = m_E^2 = m_L^2 \equiv m_0^2 \mathbb{1}_3,$$
$$T_i \equiv A_0 Y_i, \quad i = u, d, e.$$

$M_{1/2}$, m_0, A_0, A_λ and A_κ are defined at the unification scale, while λ, κ, μ_{eff} and $\tan\beta = \frac{v_u}{v_d}$ are defined at the SUSY scale. As an example we pick the parameter point fixed by

$$m_0 = 1.4 \text{ TeV}, \quad M_{1/2} = 1.4 \text{ TeV}, \quad \tan\beta = 2.9, \quad A_0 = -1.35 \text{ TeV},$$
$$\lambda = 0.56, \quad \kappa = 0.33, \quad A_\lambda = -390 \text{ GeV}, \quad A_\kappa = -280 \text{ GeV}, \quad \mu_{\text{eff}} = 200 \text{ GeV}. \tag{5.45}$$

The results for the Higgs masses at different loop levels are summarised in table 5.1. Here, h_2 is the predominantly singlet scalar (about 96%) at two-loop,

$$\phi_s = 0.09 \, h_1 - 0.98 \, h_2 + 0.17 \, h_3.$$

The SM-like Higgs is h_1 and does not substantially mix with the singlet-like state. In table 5.1 it is shown that the strong two-loop corrections give a positive mass shift, but adding the full corrections afterwards reduces the masses. We compare this to the CMSSM [54] with the same input parameters ($m_0 = M_{1/2} = 1.4 \text{ TeV}$, $\tan\beta = 2.9$, $\mu > 0$, $A_0 = -1.35 \text{ TeV}$): The contributions involving the strong interaction cause a shift by 11.3 GeV, while the purely Yukawa corrections reduce the mass by -1.4 GeV. This is almost the same as the numbers in table 5.1, therefore for this point the two-loop corrections are MSSM-dominated.

	Tree	one-loop	two-loop $(\alpha_s(\alpha_b + \alpha_t))$	full two-loop
m_{h_1}	93.8	117.6 (+ 25.4%)	126.1 (+7.2%)	124.7 (-1.1%)
m_{h_2}	214.5	209.2 (-2.4%)	209.2 ($\pm$ 0%)	208.7 (-0.2%)
m_{h_3}	555.5	541.9 (-2.4%)	542.3 (+0.1%)	541.4 (-0.2%)

Table 5.1: Higgs masses at tree-level, one-loop and two-loop for the parameter point of eq. (5.45) in GeV. The state h_2 is singlet-like.

We now analyse the dependence of the shifts on λ and κ. The mass of h_1 at different loop levels is shown in figs. 5.9(a) and 5.9(b). To compare the effect of the new contributions, we show Δ_M in figs. 5.9(c) and 5.9(d) and the relative shift, Δ_R, in figs. 5.9(e) and 5.9(f). The new corrections are small compared to the strong ones in this scenario: For the above parameter point they are about 10%–20% the size of the strong corrections. To give an impression of the remaining uncertainty from higher order corrections we show the Higgs mass in fig. 5.10 as a function of the renormalisation scale Q. As expected, the scale dependence is reduced at the two-loop level. For $M_{\text{SUSY}} = \sqrt{m_{\tilde{t}_1} m_{\tilde{t}_2}} \approx 2\,\text{TeV}$ we observe a variation in the range $\frac{1}{2}M_{\text{SUSY}}$ and $2M_{\text{SUSY}}$ of 2.3 GeV, which can be taken as a rough estimate of the remaining uncertainty.

Heavy singlet with large λ

So far we concentrated on moderate values of λ, which are consistent with gauge coupling unification and do not exhibit a Landau pole below the GUT scale. However, if one surrenders this condition then λ can assume larger values. These so-called λSUSY scenarios are popular because they predict very moderate values for the fine-tuning [338] and have interesting phenomenological consequences [339, 340]. Typically, λSUSY models are defined with more general soft-breaking and superpotential terms, but we consider only the minimal version of the NMSSM here. We choose the parameter point given by

$$\lambda = 1.6, \quad \kappa = 1.6, \quad \tan\beta = 3, \quad T_\lambda = 600\,\text{GeV}, \quad T_\kappa = -2\,650\,\text{GeV}, \quad \mu_{\text{eff}} = 614\,\text{GeV}. \tag{5.46}$$

All sfermion squared soft-masses are fixed to $2 \cdot 10^6$ GeV^2, the gaugino masses are

$$M_1 = 200\,\text{GeV}, M_2 = 400\,\text{GeV}, M_3 = 2\,000\,\text{GeV},$$

while the trilinear couplings T_u, T_d, T_e are set to zero. The corresponding masses at different loop levels are shown in table 5.2. Again the state h_2 is mostly singlet-like with a mass of about 700 GeV and h_1 is the SM-like Higgs boson. For this point all two-loop shifts to h_1 have the same sign (positive), implying that the NMSSM-specific corrections become more important.

	Tree	one-loop	two-loop $(\alpha_s(\alpha_b + \alpha_t))$	full two-loop
m_{h_1}	144.8	122.6 (-15.3%)	126.5 (+3.2%)	128.0 (+1.2%)
m_{h_2}	713.2	745.9 (+4.6%)	745.8 (+0.0%)	747.9 (+0.3%)
m_{h_3}	1454.5	1421.1 (-2.3%)	1420.1 (-0.1%)	1420.3 (+0.0%)

Table 5.2: Higgs masses at tree-level, one-loop and two-loop for the parameter point of eq. (5.46). The state h_2 is mostly singlet-like and h_3 is the MSSM-like heavy Higgs.
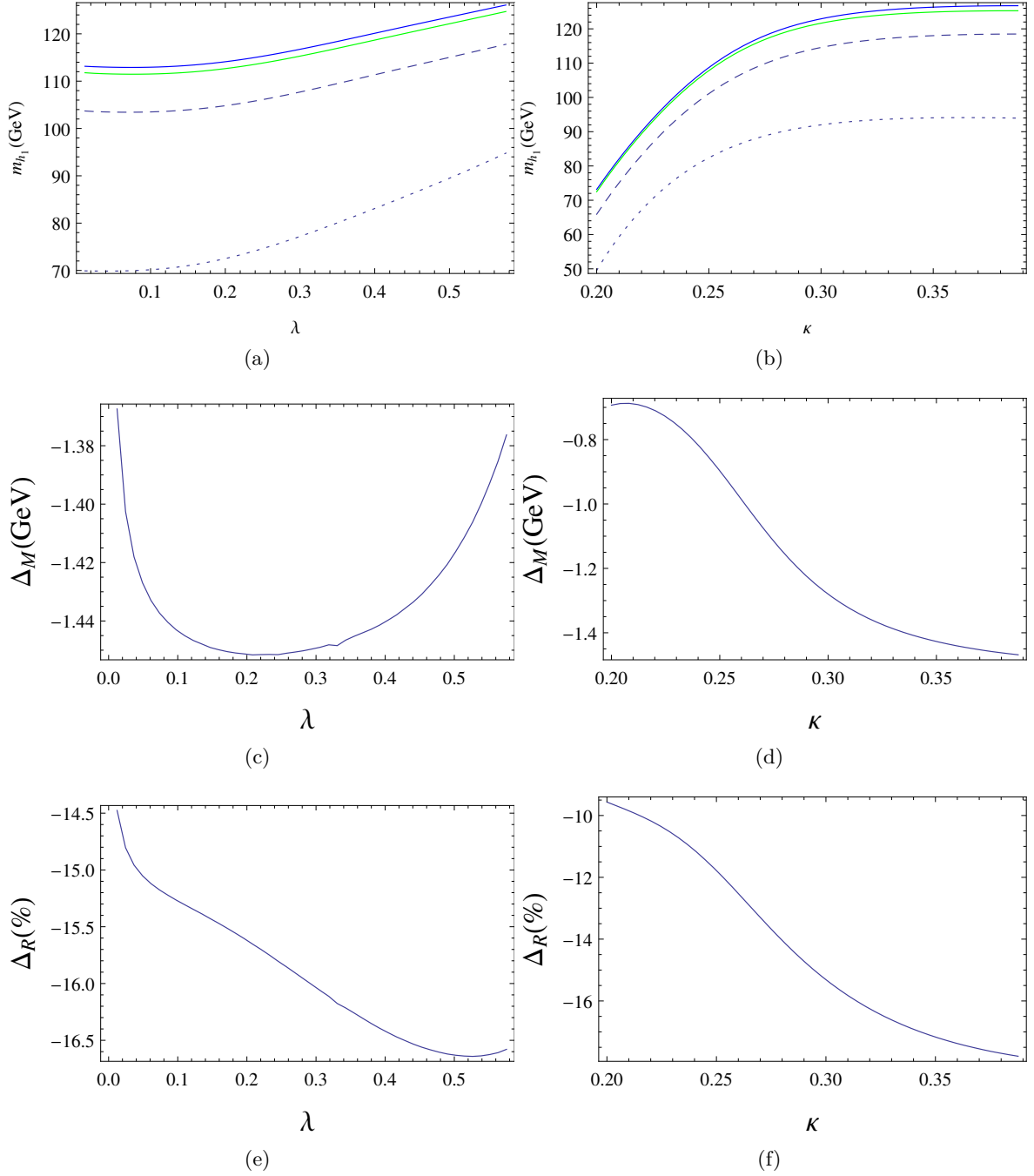
Figure 5.9: **First row:** Light Higgs mass based on the parameter point of eq. (5.45) for a variation of λ and κ. The Higgs mass is shown at tree-level (dotted line), one-loop (dashed line) and two-loops (full line). At two-loop level we distinguish between the $\alpha_s(\alpha_b + \alpha_t)$ corrections (blue) and the full calculation in the NMSSM (green). **Second row:** The absolute size of the two-loop contributions beyond $\mathcal{O}\left(\alpha_s(\alpha_b + \alpha_t)\right)$. **Third row:** The relative size of these corrections normalised to the $\alpha_s(\alpha_b + \alpha_t)$ ones.
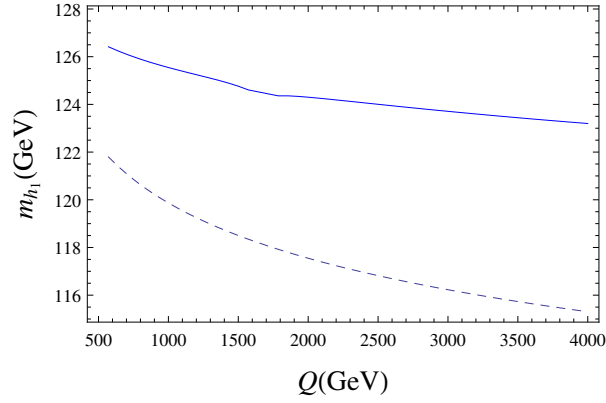
Figure 5.10: The light Higgs mass m_{h_1} based on the point (5.45) is shown for a variation of the renormalisation scale Q at one-loop (dashed line) and two-loop (full line).
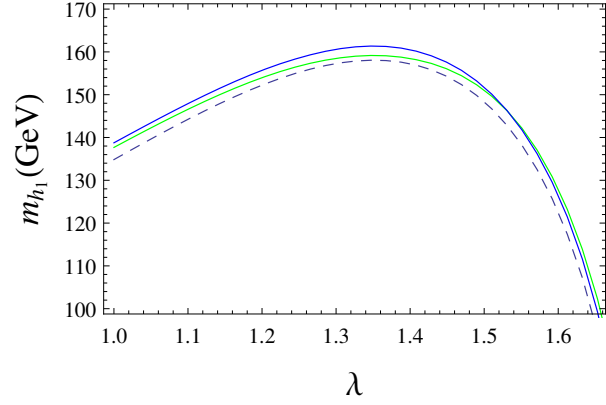
(a)
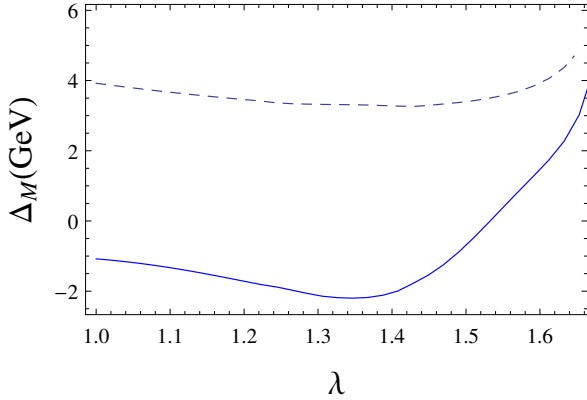
(b)
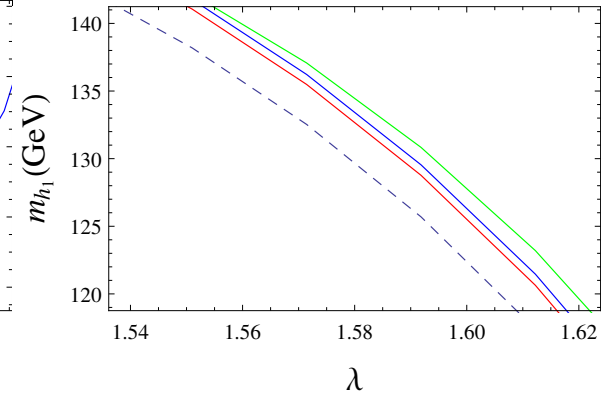
(c)

Figure 5.11: (a): The light Higgs mass based on the parameter point of eq. (5.46) for a variation of λ. The colour and line coding is the same as in fig. 5.9. (b): Absolute size of the strong corrections (dashed) and full ones (full line), i.e. Δ_M as defined in eq. (5.44). (c): Zoom into the interesting region of (a). The red line corresponds to the approximation of MSSM-like Yukawa correction plus strong contributions.

	Tree	one-loop	two-loop $(\alpha_s(\alpha_b + \alpha_t))$	full two-loop
m_{h_1}	19.4	67.8 (+249.5%)	74.5 (+9.9%)	74.2 (-0.4%)
m_{h_2}	122.7	123.5 (+0.7%)	124.3 (+0.6%)	123.3 (-0.8%)
m_{h_3}	177.4	188.2 (+6.1%)	192.7 (+2.3%)	191.1 (-0.8%)

Table 5.3: Higgs masses at tree-level, one-loop and two-loop for the parameter point of eq. (5.47).

We show again the dependence of m_{h_1} on λ in fig. 5.11(a). The shift Δ_M changes its sign at $\lambda \simeq 1.5$ from negative to positive in fig. 5.11(b). We zoom into the interesting mass range in fig. 5.11(c), in which the additional red line shows an approximation where the strong corrections are extended by the MSSM-like Yukawa contributions $\mathcal{O}\left((\alpha_t + \alpha_b + \alpha_\tau)^2\right)$, which modify only the upper 2×2 block of the Higgs mass matrix. This approximation is not a good one for large λ, because the predicted shift is in the other direction. Leaving out the MSSM-like Yukawa contributions would give a result closer to the full calculation. In conclusion, for large λ the difference between the full (blue) and the strong (green) calculation is notable (about $1\,\mathrm{GeV}$), although the strong corrections themselves are much more important.

Light singlet case

Finally the effects in a light singlet scenario are discussed. The benchmark point BMP-A of Ref. [341] has the interesting feature that all three scalars h_i are lighter than $200\,\mathrm{GeV}$,

$$\lambda = 0.596, \quad \kappa = 0.596, \quad T_\lambda = -27 \text{ GeV}, \quad T_\kappa = -240 \text{ GeV}, \quad \mu_{\mathrm{eff}} = 130 \text{ GeV},$$
$$T_t = -3\,050\,\mathrm{GeV}, \quad T_b = T_\tau = -1\,000\,\mathrm{GeV}, \quad \tan\beta = 1.68,$$
$$m_{Q,33}^2 = 9.0 \cdot 10^5 \text{ GeV}^2, \quad m_{U,33}^2 = 1.05 \cdot 10^6 \text{ GeV}^2. \tag{5.47}$$

The Higgs masses at different loop levels are summarised in table 5.3. At tree-level, the SM-like m_{h_2} is already quite close to $125\,\mathrm{GeV}$ and loop corrections play a minor role. The mixing with the lighter singlet as well as the F-term contribution $\delta m_h \sim \lambda^2(v^2/2)\cos^2 2\beta$ give it a sizeable push. The remarkable feature is that one- and two-loop corrections are of comparable size. To find a better understanding of the different two-loop effects, the masses of h_1, h_2 are shown as a function of λ in fig. 5.12. There is a very strong dependence on λ for both masses which is mainly dictated by the tree-level (dotted line). For small λ, there is a large mass gap between h_1 and h_2 and none of them is SM-like. With increasing λ, h_2 becomes lighter and for $\lambda \simeq 0.55$ a level crossing takes place. We zoom into this region in fig. 5.13.

The composition of h_1 and h_2 in terms of ϕ_d (blue), ϕ_u (green) and ϕ_s (red) components is shown in fig. 5.14 together with Δ_M. There is a direct correlation between the singlet fraction and Δ_M: For a larger singlet admixture, $|\Delta_M|$ decreases. Thus, despite the sizeable value of λ, the main contribution to the two-loop masses is again dominated by the strong interaction. Interestingly, for a light state below $80\,\mathrm{GeV}$ (i.e. $\lambda > 0.592$) which is 60% singlet, the $\alpha_s(\alpha_b + \alpha_t)$ contributions still give a sizeable push to m_{h_1} while Δ_M nearly vanishes. But if we look beyond $\lambda > 0.58$ for the state h_2 the picture reverses (fig. 5.13): The new corrections shown here can even compensate the strong corrections and produce an overall shift towards lower masses. Using only the strong corrections one would obtain the wrong conclusion that the mass is increased at two-loop.

Finally, we comment on the approximation of carrying over the known two-loop Yukawa
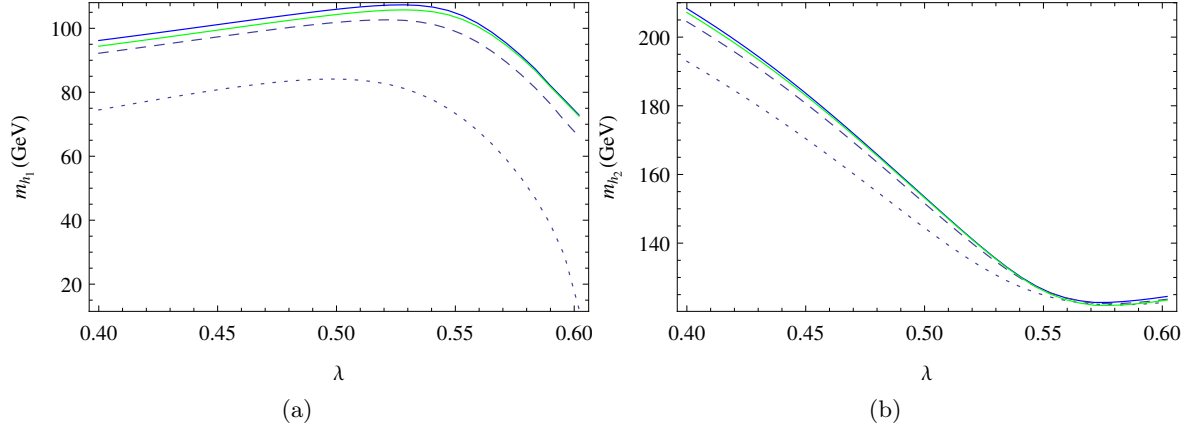
Figure 5.12: The two lightest Higgs masses based on the point of eq. (5.47) for a variation of λ. The colour code is the same as in fig. 5.9.
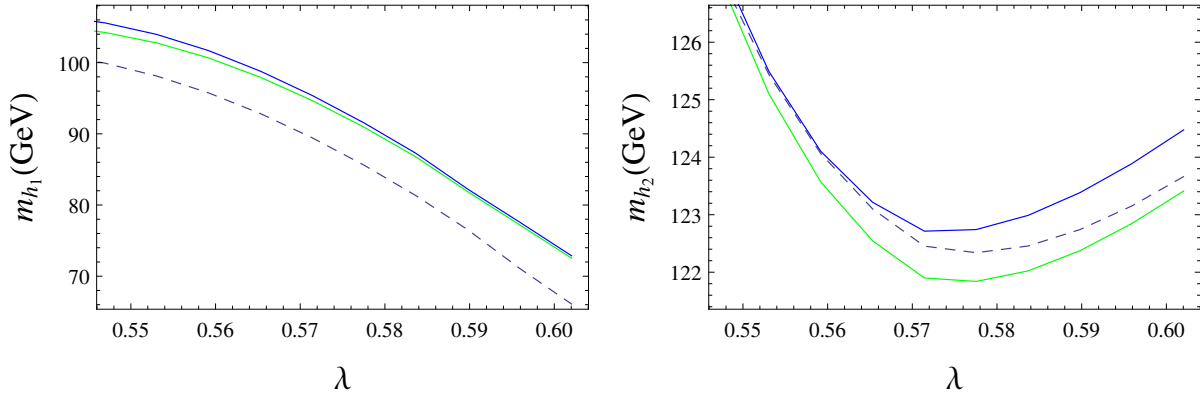
Figure 5.13: The masses of h_1 and h_2 for the light singlet case are shown (zoom into the interesting range). The colour coding is the same as in fig. 5.9.
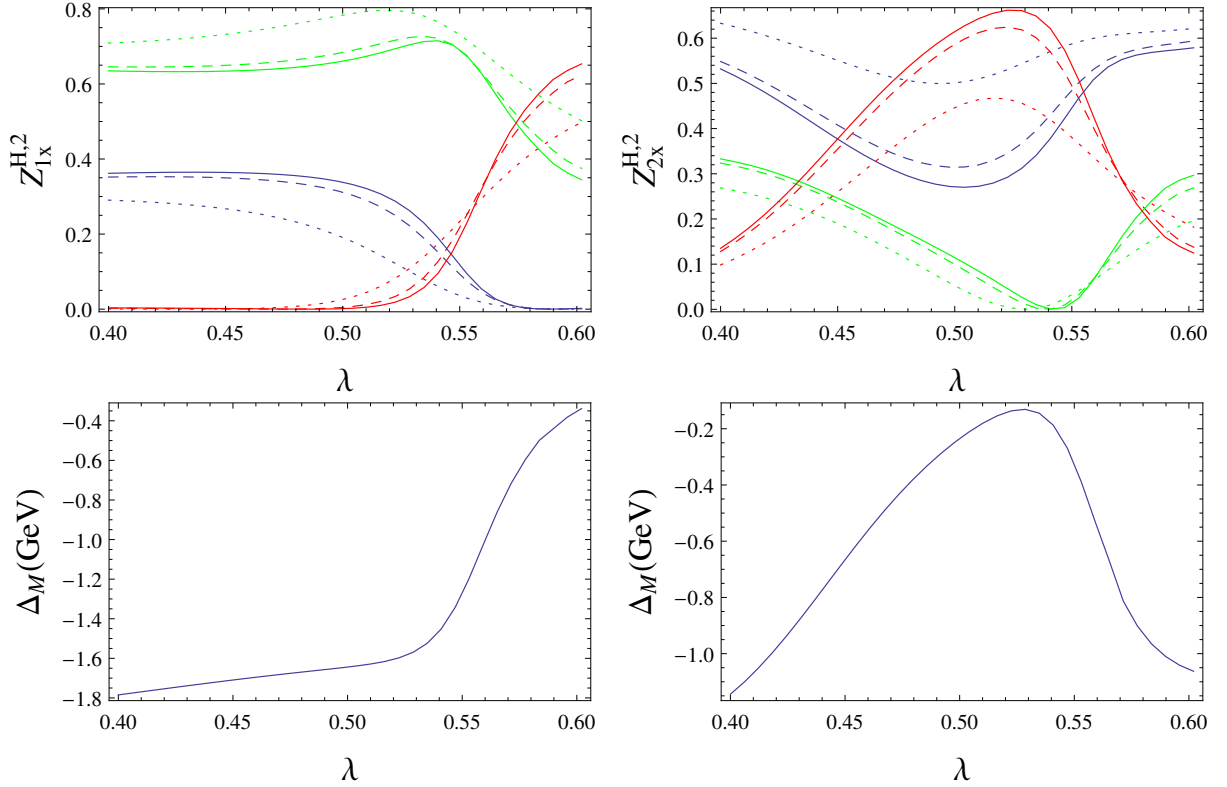
Figure 5.14: The left column is for h_1, the right column for h_2. **First row:** down- (blue), up- (green) and singlet- (red) fraction (i.e. squared entry of mixing matrix Z_{1i}^H and Z_{2i}^H, $i = d, u, s$) of the Higgs particles h_1, h_2 at tree-level (dotted), one-loop (dashed) and two-loop (full line). **Second row:** absolute size of the two-loop corrections compared to only the strong interaction.
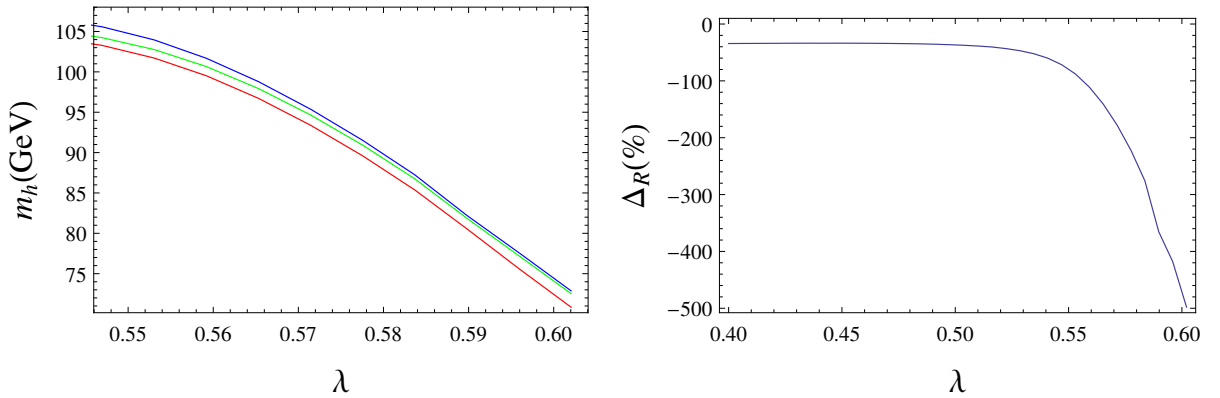
Figure 5.15: Left: the lightest Higgs mass at two loops based on the parameter point of eq. (5.47) for a variation of λ. The blue line is the mass using only $\alpha_s(\alpha_t + \alpha_b)$ corrections, the green line corresponds to our full calculation and the red line gives the result from the approximation of using the MSSM expressions for the pure Yukawa contributions. On the right we show the ratio of the correction from the MSSM approximation and the full correction.

corrections of the MSSM to the upper 2×2 block of the Higgs mass matrix. Using the same parameter point in the regime of large $\lambda > 0.55$, we show the MSSM approximation plus the strong contributions as the red line in fig. 5.15 (left). We also compare the ratio of the shift caused by these MSSM-like contributions to the shift by our full contribution in fig. 5.15 (right). It turns out that the approximation works for small λ, but fails above $\lambda > 0.55$ where it predicts a Higgs mass with $2\,\text{GeV}$ difference to the full calculation. This is mainly due to the missing corrections to the $(1,3)$ and $(2,3)$ elements of the Higgs mass matrix. Since the corrections are negative for these entries and therefore reduce the mixing between the doublets and the singlet, the incomplete approximation predicts a mixing that is too large, which reduces the lighter mass eigenstate.

5.2.4 Discussion

We have examined the impact of the previously unavailable contributions from the diagrams in figs. 5.8(b) and 5.8(c) with full dependence on the superpotential parameters in the NMSSM, in comparison to the existing (and dominant) strong corrections $\mathcal{O}\left(\alpha_s(\alpha_t + \alpha_b)\right)$ [294]. As a step in between we also considered the approximation of adding the pure MSSM Yukawa contributions $\mathcal{O}\left((\alpha_t + \alpha_b + \alpha_\tau)^2\right)$ to the strong corrections. This approximation works for small λ, but in the case of a significant mixing between singlet and doublet states and/or large λ, the approximation is poor and has an error of approximately $2\,\text{GeV}$. This is to be expected, because important contributions to the entries $(1,3)$ and $(2,3)$ of the Higgs mass matrix are missing. Further, we observed that by including the MSSM Yukawa part, the prediction is generally shifted in the other direction (towards lower masses) compared to the full case, as can be seen in fig. 5.11(c) and fig. 5.15.

The new corrections, although limited to the gaugeless limit, are essential to obtain a more accurate calculation of the Higgs mass in the NMSSM, in particular for large λ and/or substantial mixing between singlet and doublet Higgses. It is likely that the two-loop effects are even more significant in other singlet extensions like the generalised NMSSM [241] for large λ, where a large singlet scalar mass can be accommodated along with a splitting between the scalar and higgsinos.

5.3 Higgs mass at two-loop in the RPV-MSSM

5.3.1 The MSSM extended by R-parity violation

From the particle content of the MSSM, we can construct additional gauge invariant terms,

$$\mathcal{W}_{\mathrm{RPV}} = \frac{1}{2}\lambda_{ijk}\mathbf{L}_i\mathbf{L}_j\mathbf{E}_k + \lambda'_{ijk}\mathbf{L}_i\mathbf{Q}_j\mathbf{D}_k + \frac{1}{2}\lambda''_{ijk}\mathbf{U}_i\mathbf{D}_j\mathbf{D}_k + \kappa_i\mathbf{L}_i\mathbf{H}_u, \tag{5.48}$$

which violate either baryon number (B) or lepton number (L). The simultaneous violation of B and L can lead to rapid proton decay, which is not observed in nature. Therefore, the potentially dangerous terms are forbidden in the usual MSSM by imposing a discrete symmetry, called R-parity [95, 342–344]

$$R_p = (-1)^{3(B-L)+2s}, \tag{5.49}$$

where s is the spin of a component field. Under this symmetry, all SM fields and scalar Higgs bosons are even, while the superpartners are odd. As a consequence, the decay products of one sparticle must contain an odd number of sparticles. The lightest sparticle then must be stable and provides a dark matter candidate. This is *not* the case in R-parity violation, but it is equally well motivated as the R_p conserving MSSM [344–351]. Equivalently, one can define matter parity of a superfield as $P_M = (-1)^{3(B-L)}$. This implies that the superfields $\mathbf{L}, \mathbf{E}, \mathbf{Q}, \mathbf{U}, \mathbf{D}$ are all odd under P_M, while $\mathbf{H}_u, \mathbf{H}_d$ are even, forbidding the terms of eq. (5.48). The MSSM extended by RPV operators has a rich collider phenomenology [352–356] and the existing mass bounds from colliders can be significantly weakened in this setup [357–360]. Concerning the Higgs mass, the additional RPV couplings become relevant in two-loop self-energies and could possibly increase the radiative corrections, thus improving the fine-tuning situation. The RPV couplings also appear in the two-loop renormalisation group equations [361], meaning that they modify the running of the parameters compared to the (R_p conserving) MSSM. In this section we study the impact of RPV couplings on the light Higgs mass at two-loop in the effective potential approach, with the restriction that only RPV interactions involving coloured states are considered [298].

Since the top Yukawa coupling is the dominant source of higher order Higgs mass corrections, it can be expected that the operators LQD and UDD will give the most relevant contributions. We restrict ourselves to trilinear RPV terms with baryon number violation,

$$\mathcal{W} = \mathcal{W}_{\mathrm{MSSM}} + \lambda'_{ijk}\mathbf{L}_i\mathbf{Q}_j\mathbf{D}_k + \frac{1}{2}\lambda''_{ijk}\mathbf{U}_i\mathbf{D}_j\mathbf{D}_k, \tag{5.50}$$

and more specifically to couplings to third generation particles. The λ'_{ijk}-tensor has no symmetries and 27 independent components. λ''_{ijk} must be antisymmetric in j, k because the contraction of colour indices $(\epsilon_{\alpha\beta\gamma}\mathbf{U}_i^\alpha\mathbf{D}_j^\beta\mathbf{D}_k^\gamma)$ is also antisymmetric in j, k. This leaves 9 independent components for λ''_{ijk}. In the following we consider only one non-zero component at a time and its antisymmetric component, if it exists. This avoids proton decay as well as constraints from flavour changing neutral currents [346, 362, 363]. The additional soft-breaking terms in this model read

$$-\mathcal{L}_{\mathrm{SB,RPV}} = T'_{\lambda,ijk}\widetilde{L}_i\widetilde{Q}_j\widetilde{D}_k + \frac{1}{2}T''_{\lambda,ijk}\widetilde{U}_i\widetilde{D}_j\widetilde{D}_k + \mathrm{h.c.}, \tag{5.51}$$

where the trilinear couplings T'_λ, T''_λ are 3×3 matrices of mass dimension one. As for the MSSM trilinears $T_{u,d,e}$, they can be assumed proportional to the corresponding superpotential terms, $T_X = A_X Y_X$ for $X = u, d, e$ and $T'_\lambda = A'\lambda'$, $T''_\lambda = A''\lambda''$.
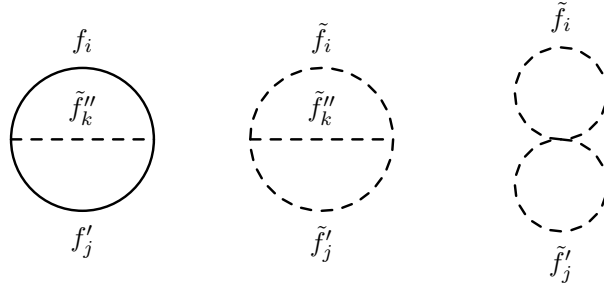
Figure 5.16: Two-loop corrections to the effective potential involving trilinear RPV couplings. f_i are SM fermions and $\tilde{f}_i$ are sfermions. The graph on the left involves superpotential couplings λ', λ'', the middle graph involves soft breaking terms T'_λ, T''_λ, and the graph on the right λ', λ'' from the F-term scalar potential.

5.3.2 Numerical results

The new diagrams that enter the effective potential in the presence of RPV are shown in fig. 5.16. We neglect the possibility that sneutrinos develop a VEV through the LQD operator, because the VEVs are restricted to be below $\sim 10\,\mathrm{MeV}$ by the smallness of neutrino masses [345]. But the effective potential is not the only thing that is changed by the presence of RPV couplings. They also enter the quark self-energies at one-loop, $\Sigma_L^q, \Sigma_R^q, \Sigma_S^q$ with $q = u, d$, which are related to the Yukawa couplings as [199]

$$\frac{v_q}{\sqrt{2}} Y_q \;=\; U_L^{q,T} m_q^{\mathrm{pole}} U_R^q + \Sigma_S^q + \Sigma_L^{q,T} \left(\frac{v_q}{\sqrt{2}} Y_q \right) + \left(\frac{v_q}{\sqrt{2}} Y_q \right) \Sigma_R^q + \dots, \qquad (5.52)$$

where the dots represent two-loop corrections that are relevant only for the top quark. The matrix m_q^{pole} is diagonal with the pole masses as entries. U_L^q, U_R^q are unitary matrices that diagonalise the Yukawa matrix Y_q. The condition (5.52) has to be solved iteratively for Y_q. The change of Y_q stemming from this matching condition can be considered a one-loop effect, which (formally) has a two-loop effect on the Higgs mass. This is called a *threshold correction* which will become more relevant in the context of vectorlike quark extensions of the MSSM (section 5.4). Consider the parameter point given by

$$\tan \beta = 10, \quad M_1 = M_2 = \frac{1}{2} M_3 = 1\,\mathrm{TeV}, \quad \mu = 0.5\,\mathrm{TeV},$$
$$M_A = 1\,\mathrm{TeV}, \quad \widetilde{m} = 1.5\,\mathrm{TeV}, \quad T_{u,33} = -2.5\,\mathrm{TeV}. \qquad (5.53)$$

All trilinear couplings $T_{u,d,e}$ are zero except $T_{u,33}$ which leads to a large stop mixing. All slepton soft masses and the squark soft masses of the first two generations are set to $\widetilde{m}$. For the third generation, we distinguish two hierarchies,

(i) $m_{q,33} = 1.5\,\mathrm{TeV}, \qquad m_{u,33} = m_{d,33} = 0.5\,\mathrm{TeV}$,

(ii) $m_{q,33} = m_{u,33} = m_{d,33} = 2.5\,\mathrm{TeV}$.

In (i) the third generation is lighter than the other sfermions, in (ii) it is heavier. The presence of large trilinear couplings ($T_{u,33}$) in combination with small soft masses can lead to an unstable
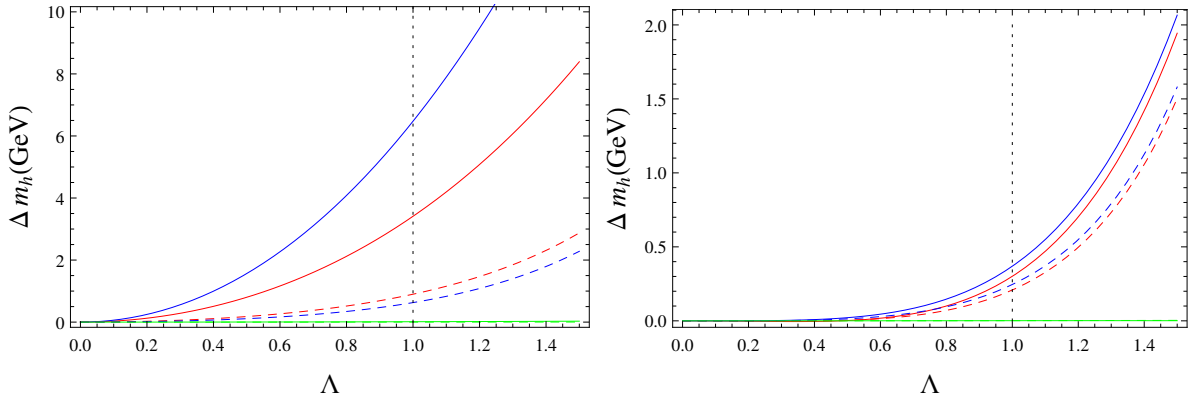
Figure 5.17: Δm_h is shown for the two mass hierarchies (i) [left], and (ii) [right]. The shift is shown as a function of $\Lambda = \lambda'_{ijk}, \lambda''_{ijk}$, with the colour code: λ''_{313} (full red), λ''_{312} (full blue), λ''_{213} (full green), λ'_{333} (dashed red), λ'_{331} (dashed blue), λ'_{313} (dashed green). The two green lines are degenerate in both plots.

vacuum [322, 325, 364]. Using the public code `Vevacious` [289] we found that point (i) has a meta-stable vacuum with a lifetime longer than the age of the universe, while point (ii) is stable. For the RPV couplings we choose

$$T'_{\lambda,ijk} = A_0 \lambda'_{ijk}, \quad T''_{\lambda,ijk} = A_0 \lambda''_{ijk}, \tag{5.54}$$

with $A_0 = -2.5\,\text{TeV}$. The renormalisation scale is $Q = \sqrt{m_{\tilde{t}_1} m_{\tilde{t}_2}}$. The SM parameters are

$$m_t^{\text{pole}} = 173.1\,\text{GeV}, \ m_b^{\overline{\text{MS}}}(m_b) = 4.18\,\text{GeV}, \ m_\tau^{\text{pole}} = 1.777\,\text{GeV}, \ \alpha_s^{\overline{\text{MS}}}(M_Z) = 0.1184. \tag{5.55}$$

We consider the difference between the two-loop Higgs mass $m_h(\Lambda)$ in the presence of RPV couplings and without,

$$\Delta m_h \equiv m_h(\Lambda) - m_h(0), \tag{5.56}$$

with $\Lambda = \lambda', \lambda''$. The two benchmark points predict the masses

(i) $m_h(0) = 110.0\,\text{GeV}$,

(ii) $m_h(0) = 124.3\,\text{GeV}$.

in the R_p-conserving case. The points were not tuned to reproduce the experimental mass well, but serve to demonstrate the effect of RPV couplings. In the following we modify only the couplings

$$\lambda''_{313}, \ \lambda''_{312}, \ \lambda''_{213}, \ \lambda'_{333}, \lambda'_{331}, \lambda'_{313}, \tag{5.57}$$

for which we use dashed lines in the following plots for λ' entries and full lines for λ'' entries. In fig. 5.17 we show δm_h for variations of these couplings. In case (i) we find large positive corrections of several GeV to the Higgs mass, but only for $\lambda''_{313}, \lambda''_{213}$ where stops are involved. The LQD operators only have a minor effect for large couplings $\lambda'_{333}, \lambda'_{331}$, while the contribution from $\lambda''_{213}, \lambda'_{313}$ (green lines) do not show any visible effect in this setup. For heavier stops in case (ii) the effects are much smaller. Large corrections are only found for relatively large couplings, above the perturbativity limit that we assume to be approximately 1 at the SUSY scale (see Refs. [365, 366]). In Ref. [365] the authors require perturbativity up to the unification scale
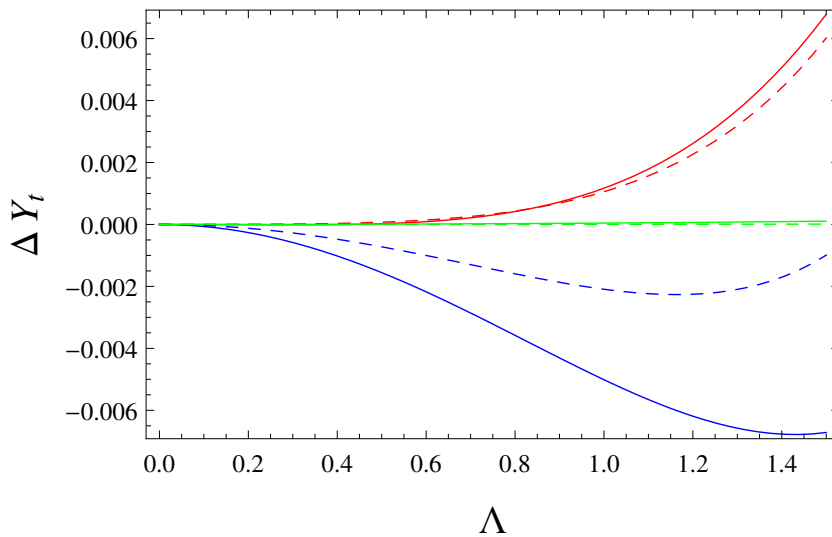
Figure 5.18: The change in the top Yukawa coupling, $\Delta Y_t(\Lambda)$, is shown for the mass hierarchy (i). The colour code is the same as in fig. 5.17.

$\sim 10^{16}$ GeV. If this condition is relaxed, one could also consider $\Lambda < \sqrt{4\pi} \approx 3.54$ as the upper limit for perturbativity. The couplings involving stops are hardly constrained by flavour physics, in particular for non-stop masses in the TeV range [367]. We have also checked that for large $\tan\beta = 25$, the change in the Higgs mass shift in the λ''_{312} case does not change substantially (less than 5%).

As pointed out earlier, the Yukawa couplings are subject to one-loop changes by the RPV couplings. We define

$$\Delta Y_t(\Lambda) \equiv Y_t(\Lambda) - Y_t(0), \qquad (5.58)$$

with $Y_t(0) = 0.85$ for $\tan\beta = 10$. The effect is very small: We see from fig. 5.18 that Y_t changes less than 1% even for large RPV couplings.

To analyse the dependence on the involved stop mass parameters, we consider the cases $\lambda''_{313} = 1$, $T''_{\lambda,313} = -2.5$ TeV and $\lambda'_{333} = 1$, $T'_{\lambda,333} = -2.5$ TeV starting with fixed $m_{q,33} = m_{u,33} = m_{d,33} = 1.5$ TeV and varying the individual soft masses in fig. 5.19. For large UDD coupling and small m_u we see the largest Higgs mass corrections. In the LQD case, there is a similarly large dependence on m_q. The value of m_d plays a sub-dominant role in both cases.

Finally we consider the dependence of m_h on the strength of the trilinear couplings, determined by A_0. With a light right-handed stop ($m_{u,33} = 0.5$ TeV) and with all other soft masses set to $\tilde{m} = 1.5$ TeV, we show m_h as a function of A_0 for vanishing RPV couplings as well as $\lambda''_{313} = 1$, $T''_{\lambda,313} = A_0$ and $\lambda'_{333} = 1, T'_{\lambda,333} = A_0$ in fig. 5.20. Again, the RPV couplings of order 1 can easily shift the Higgs mass prediction by several GeV. For λ''_{313}, the difference $m_h(\Lambda) - m_h(0)$ depends strongly on A_0, while this is not the case for λ'_{333}. This is consistent with the observation of fig. 5.19 and we would expect a stronger dependence on A_0 in the second case if smaller values of $m_{q,33}$ were chosen.

5.3.3 Conclusion

We have discussed the impact of the trilinear RPV couplings λ', λ'' on the light CP-even Higgs mass at two-loop level. Their contribution is significant only if the new couplings allow loop
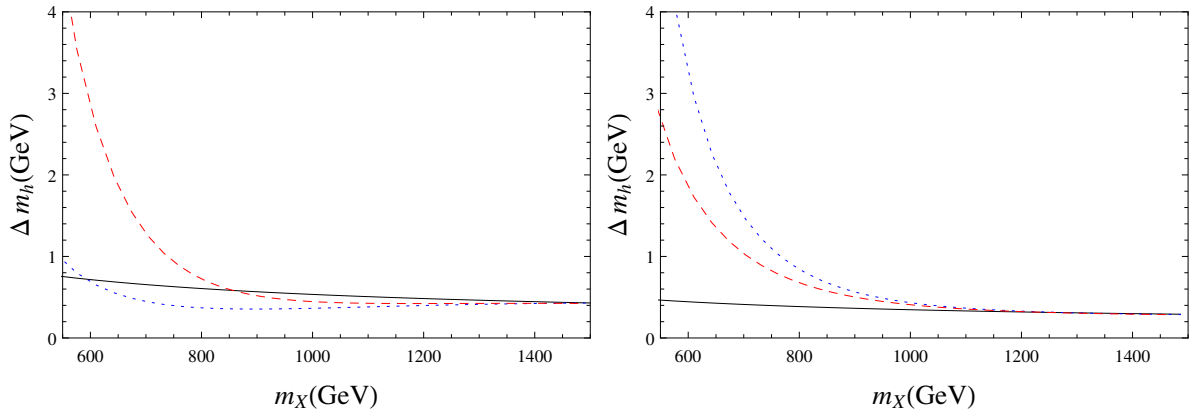
Figure 5.19: The two-loop RPV contributions to the light Higgs mass as a function of the soft squark masses (m_X) is shown. All soft masses are set to 1.5 TeV, while m_q (blue), m_u (red) and m_d (black) are individually varied. **Left:** $\lambda''_{313} = 1$, $T''_{\lambda,313} = -2.5$ TeV. **Right:** $\lambda'_{333} = 1$ and $T'_{\lambda,333} = -2.5$ TeV.
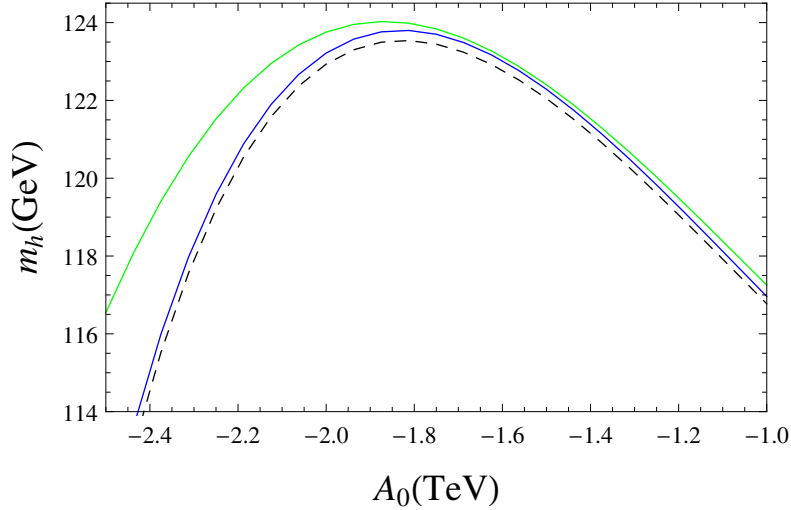
Figure 5.20: The CP-even Higgs mass m_h as a function of A_0 is shown for vanishing RPV couplings (dashed), for $\lambda'_{333} = 1$, $T'_{\lambda,333} = A_0$ (blue) and for $\lambda''_{313} = 1$, $T''_{\lambda,313} = A_0$ (green). $m_{\tilde{U},33} = 0.5$ TeV and all other soft masses are set to 1.5 TeV.

diagrams that involve the stops. In particular, we found that if λ''_{313}, λ''_{312} are close to 1 and the soft mass parameters of the third generation squarks are relatively light (500 GeV), the two-loop correction to the Higgs mass can be several GeV. It is important to note that the Yukawa couplings change in the presence of RPV couplings (compared to the R-parity conserving MSSM) via one-loop quark self-energies, however these threshold corrections are numerically small here.

5.4 Vectorlike tops and naturalness in minimal GMSB

5.4.1 Introduction

One way to accommodate the 125 GeV Higgs mass in the MSSM without excessive fine-tuning is to enhance the tree-level mass by new F-term or D-term contributions. At the loop level corrections involving the top Yukawa coupling are dominant due to the hierarchy amongst the Yukawas. If there were another heavy quark like the top with a similarly large couplings, this would clearly give a boost to the radiative corrections of the Higgs mass and lead to reduced fine-tuning. Fourth generation quarks are a standard item in the exotic particle search agenda of the LHC. Current lower mass limits are at 800 GeV [368]. A vectorlike quark (VLQ) is defined as a left-handed and right-handed fermion pair with opposite gauge quantum numbers. In contrast to a chiral quark, a vectorlike quark does not generate a chiral anomaly and does not have a large effect on Higgs production and decay [369]. Apart from their effect on the Higgs mass, VLQs have also indirect effects on electroweak precision observables and flavour physics [370–373].

When dealing with models with a large number of parameters, such as SUSY with its soft-breaking sector, one is forced to make simplifying assumptions to study the parameter space. There are several ideas about how SUSY breaking could occur at a high scale, described by only few parameters. From this minimal input, the values of the different soft-breaking parameters can be obtained by solving the RG equations. SUSY breaking is said to occur in a hidden sector and is transmitted to the visible sector via a specific mechanism. In gauge mediated SUSY breaking (GMSB) [157–161], messenger fields that take part in the SM gauge interactions couple to states from the hidden sector. The soft-breaking terms of the MSSM are then generated by loop corrections to MSSM fields involving the messengers.

In a study presented in Ref. [374] the maximum mass of the light Higgs boson was calculated for several simplified versions of the MSSM assuming $M_{\text{SUSY}} < 3$ TeV. For GMSB, the maximum mass was determined as $m_h^{\text{max}} = 121.5$ GeV, which is too low. Obtaining a Higgs mass of 125 GeV comes at the price of multi-TeV stop masses and an enormous fine-tuning [375]. In this section we analyse how much the fine-tuning can be reduced in the vectorlike quark setup.

Prior to Ref. [299], the effects of vectorlike tops had only been studied at one-loop without momentum dependence [376]. We consider the missing effects from one-loop momentum dependence and dominant two-loop effective potential contributions. There is another relevant effect, which stems from translating the Standard Model input parameters (i.e. fermion masses, gauge couplings, Weinberg angle) at the M_Z-threshold into running gauge and Yukawa couplings in the $\overline{\text{DR}}'$ scheme. Before any RGE running can take place, one needs the initial conditions in the form of a complete set of Lagrangian parameters at a scale Q in the same renormalisation scheme. The procedure of preparing this set is quite complicated, however a good explanation can be found in Ref. [377], as it involves multi-loop perturbative corrections depending on the model. As a consequence, the initial parameters (e.g. the top Yukawa coupling Y_t) will be different in the MSSM than in the model at hand. It is well known that these threshold corrections can alter m_h by several GeV in the MSSM [199]. With the `SARAH`/`SPheno` framework we can address both the two-loop and threshold corrections to the CP-even light Higgs mass in an automated fashion with a precision comparable to the standard calculations of Refs. [200] usually employed for the MSSM.

superfield	spin 0	spin ½	gen.	$SU(3)_C$	$SU(2)_L$	$U(1)_Y$
$\mathbf{T'}$	$\widetilde{t}'$	t'	1	$\mathbf{\bar{3}}$	$\mathbf{1}$	$-\frac{2}{3}$
$\mathbf{\overline{T}'}$	$\widetilde{\bar{t}}'$	$\bar{t}'$	1	$\mathbf{3}$	$\mathbf{1}$	$\frac{2}{3}$

Table 5.4: The superfields in this table are added to the MSSM particle content of table 2.2.

superfield	spin 0	spin ½	gen.	$SU(3)_C$	$SU(2)_L$	$U(1)_Y$
$\mathbf{Q'}$	$\widetilde{Q}'$	Q'	1	$\mathbf{3}$	$\mathbf{2}$	$\frac{1}{6}$
$\mathbf{\overline{Q}'}$	$\widetilde{\bar{Q}}'$	$\bar{Q}'$	1	$\mathbf{\bar{3}}$	$\mathbf{2}$	$-\frac{1}{6}$
$\mathbf{E'}$	$\widetilde{E}'$	E'	1	$\mathbf{1}$	$\mathbf{1}$	1
$\mathbf{\overline{E}'}$	$\widetilde{\bar{E}}'$	$\bar{E}'$	1	$\mathbf{1}$	$\mathbf{1}$	-1

Table 5.5: These superfields can be added to restore gauge unification in the vectorlike-top MSSM.

Besides the effects on the Higgs mass, we also consider the fine-tuning in a UV complete model with additional spectator superfields embedded in the $\mathbf{5}$ and $\overline{\mathbf{10}}$ multiplets of $SU(5)$. The resulting model has been studied to some extent in [378–380]. Here, we apply GMSB boundary conditions and study the parameter space that predicts the right Higgs mass and at the same time offers low fine-tuning.

5.4.2 The MSSM with vectorlike tops

The MSSM is extended by two chiral superfields $\mathbf{T'}, \overline{\mathbf{T}}'$, where $\mathbf{T'}$ has the same quantum numbers as $\mathbf{U}$ of the MSSM. They can be combined to form new interaction terms in the superpotential,

$$\mathcal{W} = \mathcal{W}_{\text{MSSM}} + Y_{t'}^i \mathbf{Q}_i \mathbf{H}_u \mathbf{T'} + M_{T'} \mathbf{T'} \overline{\mathbf{T}}' + m_{t'}^i \mathbf{U}_i \overline{\mathbf{T}}'. \tag{5.59}$$

The additional soft-breaking terms are given by

$$-\mathcal{L}_{\text{soft}} = -\mathcal{L}_{\text{soft,MSSM}} + \left(T_{t'}^i \widetilde{Q}_i H_u \widetilde{t}' + B_T \widetilde{t}' \widetilde{\bar{t}}' + B_t^i \widetilde{u}_{Ri}^* \widetilde{\bar{t}}' + \text{h.c.} \right) \tag{5.60}$$

$$+ m_{\tilde{t}'}^2 \left| \widetilde{t}' \right|^2 + m_{\tilde{\bar{t}}'}^2 \left| \widetilde{\bar{t}}' \right|^2 + \left(m_{ut}^2 \widetilde{u}_{Ri} \widetilde{t}' + \text{h.c.} \right). \tag{5.61}$$

Here, we consider only couplings to the third generation: $Y_{t'}^i = (0, 0, Y_{t'})$ and $T_{t'}^i = (0, 0, T_{t'})$. Also, all parameters are taken to be real in the soft sector, neglecting CP violation. Adding only the vectorlike tops spoils the prospect of gauge coupling unification. To reconcile this, one can add more fields that complete the multiplets of a unified gauge group, e.g. $SU(5)$. In the MSSM, the fields $\mathbf{Q}, \mathbf{E}, \mathbf{U}$ fit into one $\overline{\mathbf{10}}$-plet of $SU(5)$. Assuming that $\mathbf{T'}, \overline{\mathbf{T}}'$ are each part of such a $\overline{\mathbf{10}}$-plet, we can complete the multiplets with superfields $\mathbf{Q'}, \overline{\mathbf{Q}}', \mathbf{E'}, \overline{\mathbf{E}}'$ (table 5.5). The resulting superpotential is extended only by the mass terms

$$\Delta\mathcal{W} = M_{Q'} \mathbf{Q'} \overline{\mathbf{Q}}' + M_{E'} \mathbf{E'} \overline{\mathbf{E}}', \tag{5.62}$$

where we assume no other interactions of the new fields. This makes them spectator fields that only influence the RGEs and threshold corrections, as will be explained shortly. The beta

functions of the gauge couplings are expanded in loop orders,

$$\beta_{g_i} \equiv \frac{1}{16\pi^2} \beta_{g_i}^{(1)} + \frac{1}{(16\pi^2)^2} \beta_{g_i}^{(2)} + \dots, \tag{5.63}$$

where the one-loop contribution is

$$\beta_{g_1}^{(1)} = \left(\frac{41}{5} + \frac{7}{5} \, \delta_{\text{UV}} \right) g_1^3, \tag{5.64}$$

$$\beta_{g_2}^{(1)} = (1 + 3 \, \delta_{\text{UV}}) \, g_2^3, \tag{5.65}$$

$$\beta_{g_3}^{(1)} = (-2 + 2 \, \delta_{\text{UV}}) \, g_3^3, \tag{5.66}$$

with $\delta_{\text{UV}} = 1$ for the UV complete model and 0 in the minimal case. All beta functions have been calculated automatically by `SARAH`/`SPheno` using generalised formulas [278] up to two loops. Note that the strong coupling g_3 has a vanishing one-loop beta function in the UV completion. Figure 5.21 exemplifies the gauge coupling evolution in both model versions. The one-loop β
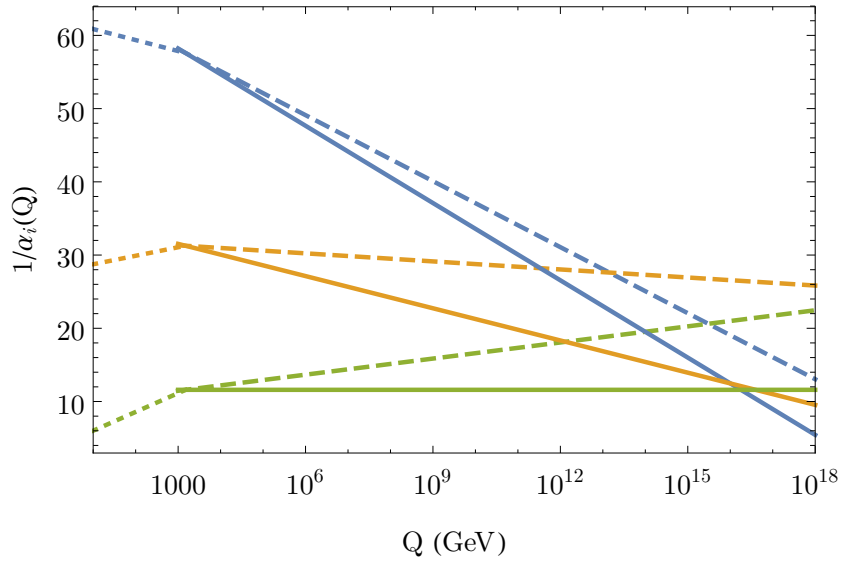

Figure 5.21: The running of the gauge couplings $\alpha_i^{-1}(Q)$ (with $i = 1$ (blue), 2 (orange), 3 (green)) at one-loop is shown. The dashed lines represent the minimal vectorlike top model and the full lines the UV-complete model. The dotted lines represent the SM-only running up to $M_{\text{SUSY}} = 1\,\text{TeV}$.

functions of the Yukawa couplings are the same in both model versions and read

$$\beta_{Y_d,ij}^{(1)} = \left[Y_d \left(3Y_d^\dagger Y_d + Y_u^\dagger Y_u + 3\mathrm{Tr}\left(Y_d Y_d^\dagger\right) - \frac{16}{3}g_3^2 - 3g_2^2 - \frac{7}{15}g_1^2 + \mathrm{Tr}\left(Y_e Y_e^\dagger\right) \right) \right]_{ij}$$
$$+ Y_{t',j}\left(Y_d Y_{t'}^*\right)_i, \tag{5.67}$$

$$\beta_{Y_e}^{(1)} = 3Y_e Y_e^\dagger Y_e + Y_e\left(3\mathrm{Tr}\left(Y_d Y_d^\dagger\right) - 3g_2^2 - \frac{9}{5}g_1^2 + \mathrm{Tr}\left(Y_e Y_e^\dagger\right)\right), \tag{5.68}$$

$$\beta_{Y_{t'}}^{(1)} = \left(3Y_u^T Y_u^* + 3\mathrm{Tr}\left(3Y_u Y_u^\dagger\right) + Y_d^T Y_d^* + 6\left(Y_{t'} Y_{t'}^*\right) - \frac{13}{15}g_1^2 - 3g_2^2 - \frac{16}{3}g_3^2\right)Y_{t'}, \tag{5.69}$$

$$\beta_{Y_u,ij}^{(1)} = \left[Y_u \left(3Y_u^\dagger Y_u + Y_d^\dagger Y_d + 3\mathrm{Tr}\left(Y_u Y_u^\dagger\right) + 3\left(Y_{t'} Y_{t'}^*\right) - \frac{13}{15}g_1^2 - 3g_2^2 - \frac{16}{3}g_3^2 \right) \right]_{ij}$$
$$+ 3Y_{t',j}\left(Y_u Y_{t'}^*\right)_i. \tag{5.70}$$

The new particle content in the UV-complete model allows additional soft-breaking terms (flavour indices suppressed):

$$-\Delta\mathcal{L}_{\mathrm{soft}} = m_{\tilde{E}'}^2 |\tilde{E}'|^2 + m_{\tilde{\bar{E}}'}^2 |\tilde{\bar{E}}'|^2 + m_{\tilde{Q}'}^2 |\tilde{Q}'|^2 + m_{\tilde{\bar{Q}}'}^2 |\tilde{\bar{Q}}'|^2$$
$$+ \left(m_{eE'}^2 \tilde{e}_R \tilde{E}' + m_{QQ'}^2 (\tilde{Q})^\dagger \tilde{Q}' + \mathrm{h.c.} \right). \tag{5.71}$$

More terms are allowed by gauge invariance which mix the scalar components of $\mathbf{E}, \mathbf{E}', \bar{\mathbf{E}}'$ and $\mathbf{Q}, \mathbf{Q}', \bar{\mathbf{Q}}'$. They are left out here, because the GMSB boundary conditions will force them to be zero.

5.4.3 Gauge mediated SUSY breaking and boundary conditions

In this subsection we briefly describe the idea of gauge mediated SUSY breaking and give the resulting GMSB boundary conditions for the soft parameters. We assume two messenger superfields $\mathbf{\Phi}_1, \mathbf{\Phi}_2$,

$$\mathbf{\Phi}_i = \phi_i + \sqrt{2}\theta\psi_i + \theta^2 F_i, \tag{5.72}$$

that take part in SM gauge interactions and also couple to a singlet field $\mathbf{S}$ of the hidden sector,

$$\mathcal{W} = \lambda\mathbf{S}\mathbf{\Phi}_1\mathbf{\Phi}_2, \tag{5.73}$$

where $\mathbf{\Phi}_1$ and $\mathbf{\Phi}_2$ have opposite quantum numbers. The field $\mathbf{S}$ acquires a VEV along its scalar and auxiliary component,

$$\langle\mathbf{S}\rangle = M' + \theta^2 F'. \tag{5.74}$$

The hidden mechanism that generates this VEV is left unspecified. The scales M' and $\sqrt{F'}$ can vary from several tens of TeV to almost M_{GUT} [161]. The coupling λ is absorbed into $M \equiv \lambda M'$ and $F \equiv \lambda F'$. We can integrate out the auxiliary degrees of freedom F_1, F_2 to obtain the mass

terms of the messenger fields,

$$
\begin{aligned}
\mathcal{L} &= \left[\mathbf{\Phi}^{i\dagger} \mathbf{\Phi}_i \right]_D + ([\mathcal{W}]_F + \text{h.c.}) \\
&\supset - M^2 \left(|\phi_1|^2 + |\phi_2|^2 \right) + (F\phi_1\phi_2 - M\psi_1\psi_2 + \text{h.c.}) \\
&= - (M^2 + F) |\phi_+|^2 - (M^2 - F) |\phi_-|^2 - (M\psi_1\psi_2 + \text{h.c.}) \,.
\end{aligned}
\tag{5.75}
$$

The scalar components can be diagonalised by defining

$$
\phi_\pm \equiv \frac{\phi_1 \pm \phi_2^*}{\sqrt{2}} \,.
\tag{5.76}
$$

The fermionic messengers have mass M, while the scalars $\phi_\pm$ have masses $m_\pm = \sqrt{M^2 \pm F}$. This requires $M^2 > F$. The soft-breaking terms in the MSSM are generated by loop corrections that involve the messenger particles, and are therefore fully determined by the scales M, F and the gauge structure. The gaugino masses are generated at one loop and while the scalar masses $m_{\tilde{f}}^2$ are generated at two loops. We use the leading approximations from literature [161] for the gaugino masses,

$$
M_i(t) = \frac{\alpha_i(t)}{4\pi} \Lambda_G,
\tag{5.77}
$$

and for the scalar soft masses,

$$
m_{\tilde{f}_i}^2 = 2 \sum_{r=1}^{3} C_2(r, \tilde{f}) \left(\frac{\alpha_r(t)}{4\pi} \right)^2 \Lambda_S^2,
\tag{5.78}
$$

with running couplings $\alpha_i(t) = g_i(t)^2/(4\pi)$ and a scale $t = \ln(M^2/Q^2)$. C_2 is the quadratic Casimir of the representation of $\tilde{f}$ with respect to the gauge group $r = 1, 2, 3$, meaning $U(1)_Y$, $SU(2)_L$ and $SU(3)_C$. In the case of an Abelian group $U(1)_Y$, the quadratic Casimir is defined as $C_2 = (3/5) \, Y^2$. For the fundamental representation of $SU(N)$, we have $C_2 = (N^2 - 1)/(2N)$, i.e. $4/3$ for $N = 3$ and $3/4$ for $N = 2$. We define the scale

$$
\Lambda \equiv \frac{F}{M}
\tag{5.79}
$$

to which Λ_G, Λ_S are related by

$$
\Lambda_G = \Lambda \cdot g(\Lambda/M), \qquad \Lambda_S^2 = \Lambda^2 \cdot f(\Lambda/M),
\tag{5.80}
$$

with the functions calculated in Refs. [381, 382],

$$
g(x) = 1 + \frac{x^2}{6} + \frac{x^4}{15} + \mathcal{O}\left(x^6\right), \quad f(x) = 1 + \frac{x^2}{36} - \frac{11x^4}{450} + \mathcal{O}\left(x^6\right).
\tag{5.81}
$$

For $F \ll M^2$ this implies $\Lambda_G = \Lambda_S = \Lambda$. Evaluating the general equation (5.78) gives

$$m_{l,ii}^2 = m_{H_u}^2 = m_{H_d}^2 = \kappa^2 \left(\frac{3}{10}g_1^4 + \frac{3}{2}g_2^4 \right) \Lambda_S^2, \tag{5.82a}$$

$$m_{q,ii}^2 = m_{\tilde{Q}'}^2 = m_{\bar{\tilde{Q}}'}^2 = \kappa^2 \left(\frac{1}{30}g_1^4 + \frac{3}{2}g_2^4 + \frac{8}{3}g_3^4 \right) \Lambda_S^2, \tag{5.82b}$$

$$m_{u,ii}^2 = m_{\tilde{t}'}^2 = m_{\bar{\tilde{t}}'}^2 = \kappa^2 \left(\frac{8}{15}g_1^4 + \frac{8}{3}g_3^4 \right) \Lambda_S^2, \tag{5.82c}$$

$$m_{e,ii}^2 = m_{\tilde{E}'}^2 = m_{\bar{\tilde{E}}'}^2 = \kappa^2 \frac{6}{5}g_1^4 \Lambda_S^2, \tag{5.82d}$$

$$m_{d,ii}^2 = \left(\frac{2}{15}g_1^4 + \frac{8}{3}g_3^4 \right) \Lambda_S^2, \tag{5.82e}$$

with $i = 1, 2, 3$ and $\kappa \equiv 1/(16\pi^2)$. The other soft-breaking parameters are zero up to two-loop order:

$$T_x = 0 \quad (x = d, u, e, t'),$$
$$B_X = 0 \quad (X = t', T),$$
$$m_{ut}^2 = m_{eE'}^2 = m_{QQ'}^2 = 0. \tag{5.83a}$$

This constitutes the main problem of GMSB, because a large T_t is needed to accommodate the Higgs mass. We will furthermore assume unification of all mass bilinears of the vectorlike states to a common mass $M_{V'}$ at the reference scale M,

$$M_{T'} = M_{Q'} = M_{E'} = M_{V'} \qquad \text{at } Q = M. \tag{5.84}$$

This leaves five free parameters for the GMSB model:

$$M, \quad \Lambda, \quad \tan\beta, \quad M_{V'}, \quad Y_{t'}. \tag{5.85}$$

In general GMSB predicts a gravitino LSP, which gives rise to the cosmological gravitino problem. We assume that one of the proposed solutions from literature work [381, 383–388].

The fine-tuning (FT) measure Δ based on Refs. [126, 127] was defined earlier in eq. (2.30) and is implemented in `SPheno`. The smaller the value of Δ, the more natural is the model under consideration. First, Δ_α is calculated individually with respect to

$$\alpha = \{\Lambda, \ M_{V'}, \ Y_{t'}, \ Y_t, \ g_3, \ \mu, \ b\}. \tag{5.86}$$

The overall fine-tuning is given as the largest absolute value of all Δ_α.

5.4.4 Tree-level properties

The tadpole equations are identical to the MSSM, as well as all mass matrices except for up-quarks and up-squarks. As a convention, the tadpoles are solved for μ, b (cf. sec. 2.3) in the UV-completion of the model, and for the soft masses $m_{H_u}^2, m_{H_d}^2$ for SUSY scale input in the minimal version. The new squarks mix with the MSSM up-type squarks. Their mass matrix is

given by

$$
\mathcal{M}_{\tilde{u}}^2 = \begin{pmatrix}
\left[m_{\tilde{u}_L \tilde{u}_L^*}^2\right]_{ij} & \cdot & \cdot & \cdot \\
\left[\frac{1}{\sqrt{2}}\left(v_u T_u - v_d Y_u \mu^*\right)\right]_{ij} & \left[m_{\tilde{u}_R \tilde{u}_R^*}^2\right]_{ij} & \cdot & \cdot \\
\frac{1}{\sqrt{2}}\left(v_u T_{t'} - v_d \mu^* Y_{t'}\right) & \frac{1}{2}\left(2\left(M_{T'} m_{t'}^* + m_{\tilde{u}\tilde{t}'}^2\right) + v_u^2 Y_u^* Y_{t'}\right) & m_{\tilde{t}'\tilde{t}'^*} & \cdot \\
\frac{1}{\sqrt{2}} v_u \left(M_{T'}^* Y_{t'} + Y_u^T m_{t'}^*\right) & B_{t'}^* & B_T^* & m_{\tilde{t}'^*\tilde{t}}
\end{pmatrix}
\tag{5.87}
$$

with the diagonal entries

$$
m_{\tilde{u}_L \tilde{u}_L^*} = -\frac{1}{24}\left(-3g_2^2 + g_1^2\right)\mathbb{1}\left(-v_u^2 + v_d^2\right) + \frac{1}{2}\left(2m_q^2 + v_u^2\left(Y_{t'}^* Y_{t'} + Y_u^\dagger Y_u\right)\right),
\tag{5.88}
$$

$$
m_{\tilde{u}_R \tilde{u}_R^*} = \frac{1}{2}\left(2\left(m_{t'}^* m_{t'} + m_u^2\right) + v_u^2 Y_u Y_u^\dagger\right) + \frac{1}{6}g_1^2\mathbb{1}\left(-v_u^2 + v_d^2\right),
\tag{5.89}
$$

$$
m_{\tilde{t}'\tilde{t}'^*} = \frac{1}{2}\left(2\left(m_{\tilde{t}'}^2 + |M_{T'}|^2\right) + v_u^2 |Y_{t'}|^2\right) + \frac{1}{6}g_1^2\left(-v_u^2 + v_d^2\right),
\tag{5.90}
$$

$$
m_{\tilde{t}'^*\tilde{t}} = \left(m_{\tilde{t}'}^2 + |M_{T'}|^2 + |m_{t'}|^2\right) + \frac{1}{6}g_1^2\left(-v_d^2 + v_u^2\right).
\tag{5.91}
$$

$\mathcal{M}_{\tilde{u}}^2$ contains eight mass eigenstates $\widetilde{u}_i$. The mass matrix of the up-type quarks reads

$$
\mathcal{M}_u = \begin{pmatrix}
\frac{1}{\sqrt{2}} v_u Y_u^T & \frac{1}{\sqrt{2}} v_u Y_{t'} \\
m_{t'} & M_{T'}
\end{pmatrix}.
\tag{5.92}
$$

Here, we need two rotation matrices U_L^u and U_R^u to diagonalise this matrix,

$$
U_L^{u\,*}\mathcal{M}_u U_R^{u,\dagger} = \mathcal{M}_u^{\mathrm{diag}}.
\tag{5.93}
$$

The four generations of mass eigenstates are called u_i, where the first three generations correspond to the up, charm and top quark. In this model, the CKM matrix is a 4×3 matrix with the additional entries $V_{t'b}, V_{t's}, V_{t'd}$, which can lead to new flavour mixing effects. While a full study of flavour physics is beyond the scope of the paper presented here, we checked that these matrix entries are within the current bounds,

$$
|V_{t'd}| < 0.01, \qquad |V_{t's}| < 0.01, \qquad |V_{t'b}| < 0.27,
\tag{5.94}
$$

which are given in Ref. [389] at 3σ. In fig. 5.22 we show that this condition is fulfilled.

5.4.5 Loop corrections

At one-loop, the Higgs mass receives corrections of the order $\mathcal{O}\left(\alpha_{t'}\right)$. They have been discussed widely in literature in the limit of vanishing momenta and are known to give a push of many GeV. `SARAH`/`SPheno` uses a generalisation of the renormalisation procedure described in Ref. [199] to calculate the full momentum dependence at one loop.

At two loops the dominant corrections of the MSSM are $\mathcal{O}\left(\alpha_s \alpha_t\right)$. Similar contributions from the new heavy top, $\mathcal{O}\left(\alpha_s \alpha_{t'}\right)$ are expected to be equally important ($\alpha_{t'} \equiv Y_{t'}^2/(4\pi)$). The diagrams are shown in fig. 5.23 and have to be understood as a sum over generation indices. Also the Yukawa-like contributions $\mathcal{O}\left(\alpha_t^2\right)$ of the MSSM are extended by more generations of
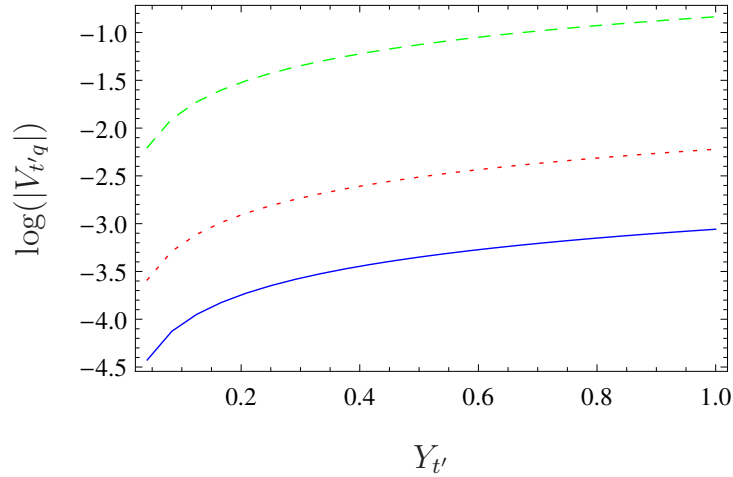
Figure 5.22: Absolute size $|V_{t'q}|$ of the CKM entries (logarithm with basis 10 is shown) between the vectorlike top states and the SM down quarks $q = d, s, b$. The colour code is $|V_{t'd}|$ (full blue), $|V_{t's}|$ (dotted red), and $|V_{t'b}|$ (dashed green). We fixed here $M_{T'} = 1$ TeV.
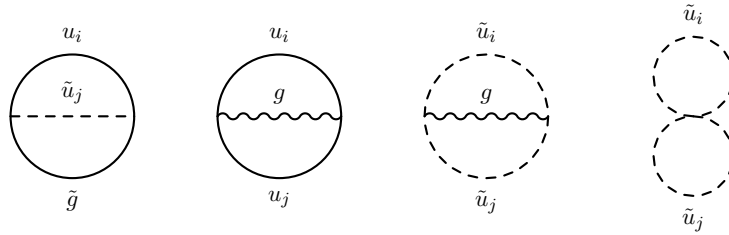
Figure 5.23: Two-loop diagrams giving contributions to the effective potential $\mathcal{O}\left((\alpha_t + \alpha_{t'})\alpha_s\right)$. Here, the indices of up-quark generations (u_i) run from 1 to 4, and those of up-squark generations $(\tilde{u}_i)$ from 1 to 8.

(s)quarks. They are described by the diagrams given in fig. 5.24 and introduce new corrections $\mathcal{O}\left(\alpha_{t'}^2\right)$ and $\mathcal{O}\left(\alpha_t\alpha_{t'}\right)$. All other sub-dominant combinations of Yukawa couplings are also included in our calculation.

5.4.6 Threshold corrections

To perform any RGE-based study, one needs a full set of running parameters at a given scale. However, these quantities are usually not directly measured in experiments. Instead, the parameters that we know with a very high precision are the electromagnetic coupling $\alpha_{\text{em}}(M_Z)$, the Fermi constant G_F, the Z pole mass M_Z and the strong coupling $\alpha_S(M_Z)$. The pole masses of the charged leptons are also well known. In the case of quarks, a pole mass is not well defined, because a quark is always bound in a hadron and can never be directly observed. Only the top pole mass can be directly measured, because its lifetime is shorter than the timescale at which the non-perturbative hadronisation process takes place. The light quark masses m_d, m_u, m_s are only known as running masses at a certain scale [377]. The matching in `SARAH`/`SPheno` follows the generalised procedure of Ref. [199], which we describe in more detail in appendix A.3. To summarise the effect, it can be said that the parameters $\alpha^{\overline{\text{DR}}'}(M_Z)$, $\alpha_s^{\overline{\text{DR}}'}(M_Z)$, v, $\sin^2\Theta_W^{\overline{\text{DR}}'}$ and

Figure 5.24: Two-loop diagrams giving contributions to the effective potential at $\mathcal{O}\left((\alpha_t + \alpha_{t'})^2\right)$. Here, $\Phi^0 = \{h, H, G^0, A^0\}$, $\Phi^\pm = \{H^\pm, G^\pm\}$, $\Phi = \{\Phi^0, \Phi^\pm\}$. The index ranges are: $\Phi(1,2)$; $\tilde{\chi}^0(1-4)$; $\chi^\pm(1,2)$; $u(1-4)$; $d(1-3)$; $\tilde{u}(1-8)$; $\tilde{d}(1-6)$.

the Yukawas are all slightly different than they would be in the normal MSSM after matching. In particular the change in $Y_t = Y_u^{33}$ should be notable, since it is the dominant parameter in the Higgs mass corrections. We show the effect of the threshold correction on Y_t in fig. 5.25 as a function of $Y_{t'}$. The effect makes a few percent difference in Y_t and it is stronger for smaller $M_{T'}$. This already has a large effect on the MSSM-like corrections and results in a few GeV change to the Higgs mass, as we will see in the following. At $Y_{t'} = 0$, the values of the two curves in fig. 5.25 do not agree. This is because g_3 receives threshold corrections, which depends on $M_{T'}$, even if no other couplings are introduced. The change in g_3 enters the RGE running as well as one-loop self-energies of the fermions.

Figure 5.25: The top Yukawa coupling (Y_u^{33}) at the SUSY scale is shown as a function of $Y_{t'}$ for two different values of $M_{T'}$: 1.0 TeV (blue) and 3.0 TeV (dotted red). All soft masses are set to 1.5 TeV and $\tan\beta = 3$.

5.4.7 Numerical results

Comparing one-loop, two-loop and threshold effects

Before we consider the fine-tuning in the UV complete model, we discuss the importance of the different Higgs mass corrections in the minimal vectorlike quark extension of the MSSM. The following parameters are assumed,

$$m_u^2 = m_q^2 = m_d^2 = m_e^2 = m_l^2 = 1 \cdot (1.5 \, \text{TeV})^2,$$
$$M_1 = 0.5 \, \text{TeV}, \quad M_2 = 1.0 \, \text{TeV}, \quad M_3 = 2.0 \, \text{TeV},$$
$$T_u = T_d = T_e = 0,$$
$$\mu = 1.0 \, \text{TeV}, \quad M_A^2 = (1 \, \text{TeV})^2,$$

and for the new sector

$$T_{t'} = m_{t'} = m_{ut}^2 = B_{t'} = 0, \quad M_{T'} = 1 \, \text{TeV},$$
$$m_{\tilde{t}'}^2 = m_{\tilde{\bar{t}}'}^2 = (1.5 \, \text{TeV})^2,$$

unless stated otherwise. It was checked that all benchmark points satisfy the bounds from flavour observables using `FlavorKit` [321]. The important SM input parameters are

$$\alpha_S^{\overline{\text{MS}}}(M_Z) = 0.1180, \quad m_b^{\overline{\text{MS}}}(m_b) = 4.2 \, \text{GeV}, \quad m_t^{\text{pole}} = 173.2 \, \text{GeV}.$$

We choose $M_{T'} = 1 \, \text{TeV}$ for the mass term to be consistent with limits from direct collider searches, which rule out heavy quark masses below $800 \, \text{GeV}$ [390]. It is expected that the LHC Run II will be sensitive to a mass range $m_{t'} < 1.5 \, \text{TeV}$ [391]. In the numerical results we distinguish the different effects on the Higgs mass:

- one-loop, vanishing momenta, with thresholds (red)

- one-loop, with momentum dependence, without thresholds (orange)

- one-loop, with momentum dependence and thresholds (blue)

- all the above effects and two-loop corrections (green)

In the following we show these effects for each of three benchmark points in four perspectives, which require some explanation. An overview plot (top left) shows m_h against $Y_{t'}$. To see explicitly the effect stemming only from the vectorlike quarks, the difference in m_h between including and neglecting vectorlike quark contributions is shown in the top right picture. The bottom left plot shows the absolute shift in m_h from one- and two-loop corrections stemming only from the vectorlike states, and the bottom right shows the relative size of this shift compared to the purely MSSM-like corrections.

First, we consider variations of $Y_{t'}$ using the benchmark point

$$\tan\beta = 2 \text{ or } 10, \quad M_{T'} = 1 \, \text{TeV}, \quad B_T = 0, \tag{5.95}$$

for two values of $\tan\beta$, shown in fig. 5.26. The value $m_h = 125 \, \text{GeV}$ is found for $Y_{t'} = 0.9(0.6)$ in these cases. The changes made by momentum dependence at one-loop can be up to $2 \, \text{GeV}$ for large $Y_{t'}$ and they are negative. In contrast, the two-loop corrections cause a positive shift
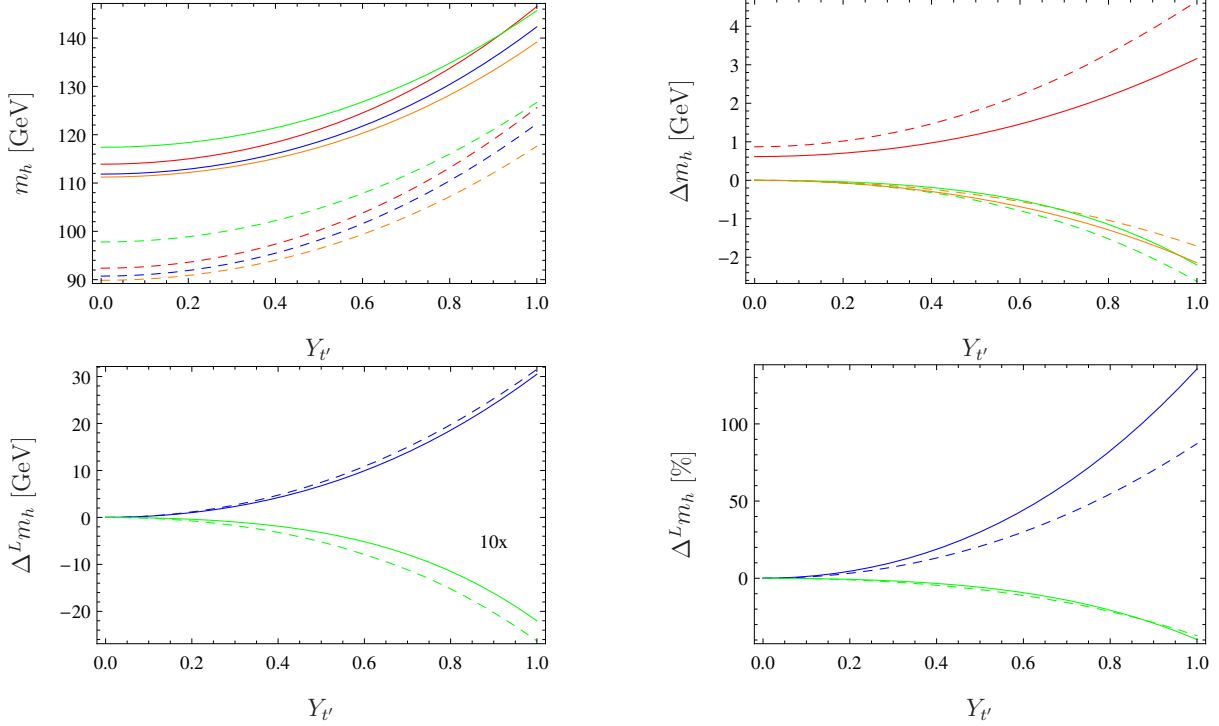
Figure 5.26: The full lines are for $\tan\beta = 10$ and the dotted ones are for $\tan\beta = 2$, both with $M_{T'} = 1.0$ TeV and $B_T = 0$. **Top left:** m_h is shown as a function of $Y_{t'}$. The red line corresponds to one-loop with $p^2 = 0$ and thresholds, orange is one-loop with $p^2 \neq 0$ without thresholds, blue is full one-loop with both p^2 and thresholds and green includes full one-loop with dominant two-loop corrections. **Top right:** This plot shows the difference in m_h between including and neglecting vectorlike tops for the same cases as before. **Bottom left:** This plot shows the absolute size of the one- (blue) and two-loop (green, multiplied by 10) corrections stemming from the vectorlike states. **Bottom right:** This plot shows the relative importance of the one- (blue) and two-loop (green) corrections normalised to the size of the purely MSSM-like corrections.

Figure 5.27: The plots show the same results as in fig. 5.26, but for $T_{t'} = 2.0$ TeV $\cdot Y_{t'}$, $\tan\beta = 5$ and $T_{u,33} = -2500$ GeV. The full lines are for $B_T = 0$, while the dashed ones correspond to $B_T = (1.5 \text{ TeV})^2$.

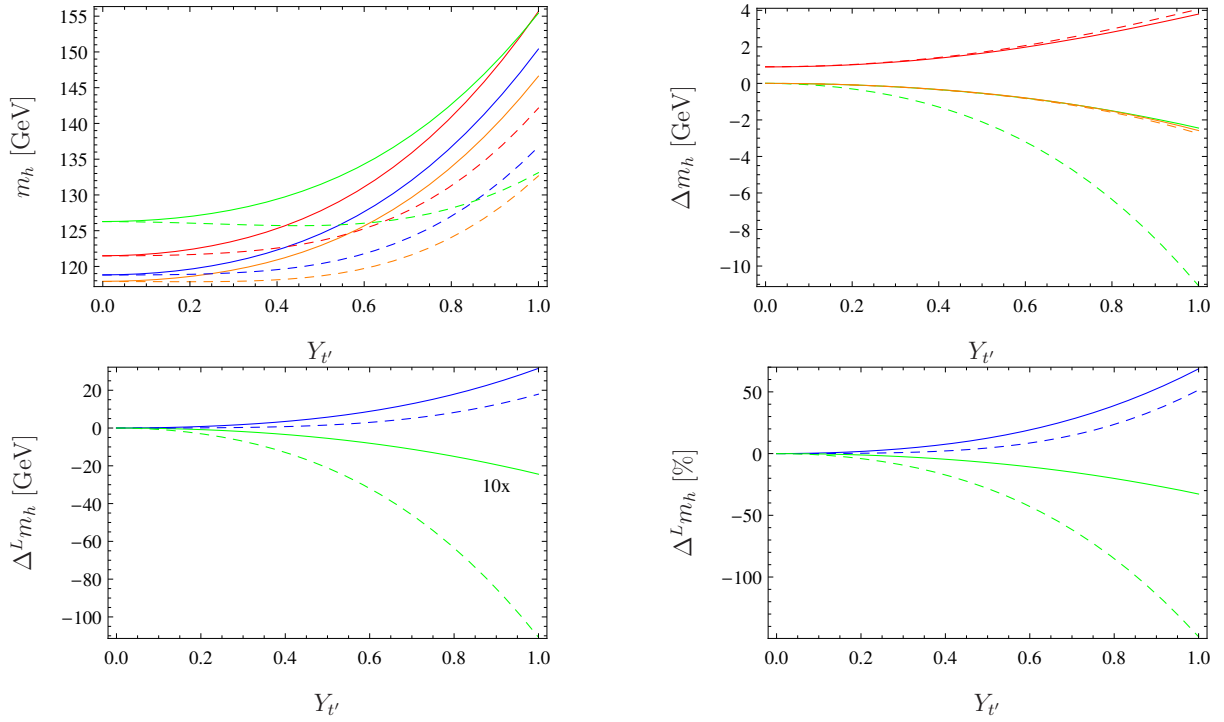of similar size. The biggest contribution comes from threshold corrections (top right, red line in fig. 5.26), which can change the mass by up to 5 GeV. The effect is stronger for small $\tan\beta$. Even for $Y_{t'} = 0$ there is a shift because α_s (and Y_t) is modified by the threshold corrections, cf. eq. (A.8). The absolute shifts at one-loop can be as large as 30 GeV, while the two-loop shifts are smaller by a factor of 10 (bottom left, fig. 5.26). In the bottom right of fig. 5.26 we observe that the one-loop vectorlike contributions are as important as the MSSM ones, while the two-loop contributions can reach about half their size.

As the second benchmark point, we consider

$$T_{t'} = 2 \text{ TeV} \cdot Y_{t'}, \quad B_T = 0 \text{ or } (1.5 \text{ TeV})^2, \tag{5.96}$$

for a variation of $Y_{t'}$ in fig. 5.27. In the case $B_T = 0$ there is no big difference to the previous benchmark point. The largest changes are again due to the threshold corrections. For $B_T \neq 0$ however, the picture changes: Because of the induced mass splitting between the vectorlike stops, the two-loop effects become large for $Y_{t'} \to 1$ to the extent that they can even cancel out the purely-MSSM two-loop contributions.

The third benchmark point has a rather small M_A^2,

$$M_A^2 = 10^5 \text{ GeV}^5, \quad B_T = 0 \text{ or } (1.5 \text{ TeV})^2, \quad T_{t'} = T_u = 0, \quad \tan\beta = 3, \tag{5.97}$$

where we consider again the two values $B_T = 0$ and $B_T = (1.5 \text{ TeV})^2$. The result is shown in fig. 5.28. The green line, representing the two-loop corrections, clearly makes the largest difference for $Y_{t'} \to 1$, especially for $B_T = (1.5 \text{ TeV})^2$ (solid line). They can cancel out the other MSSM-like two-loop contributions such that it becomes impossible to reach the preferred mass
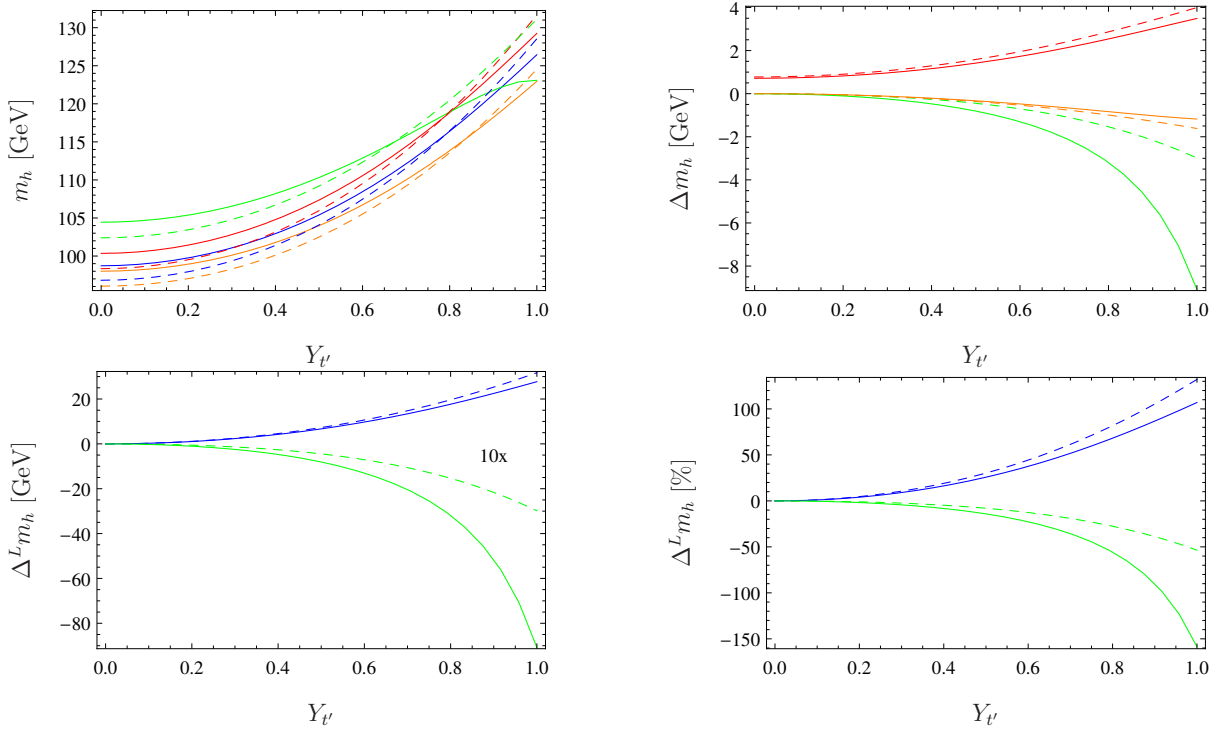
Figure 5.28: The plots show the same results as in fig. 5.26 for smaller $M_A^2 = 10^5$ GeV^2 and $T_{t'} = T_u = 0$, $\tan \beta = 3$. The dashed lines are for $B_T = 0$, while the full ones correspond to $B_T = (1.5$ TeV$)^2$.
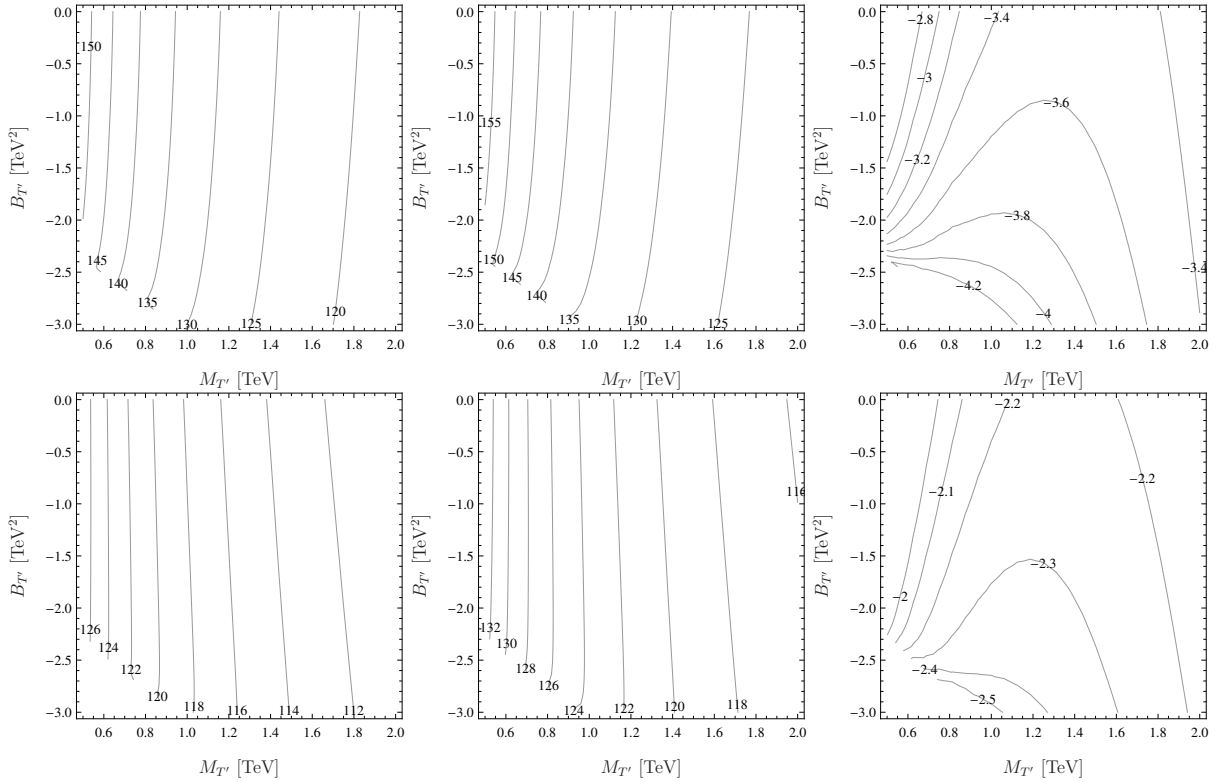
Figure 5.29: Contour lines of constant m_h at one- (left) and two-loop (middle) in the $(M_{T'}, B_{t'})$ plane. The plots in the right column show the size of the two-loop corrections stemming from vectorlike states. The plots in the first row are for $Y_{t'} = 1.0$ with $T_{t'} = 0$ and in the second for $Y_{t'} = 0.7$ with $T_{t'} = 1.4\,\text{TeV}$.

of $125\,\text{GeV}$ with this benchmark point. If B_T is taken to be zero, the effect is less severe and the MSSM contributions at two-loop are only partially cancelled out, still giving a sizeable push to the mass.

Dependence on the vectorlike masses, stop masses and the gaugino mass

As a next step we illustrate the dependence of the new loop corrections in the $(M_{T'}, B_{T'})$ plane (fig. 5.29). It shows that at both loop levels the Higgs mass decreases with larger $M_{T'}$, while the dependence on $B_{T'}$ is very mild. Of course, the two-loop values are higher, which is the result of the dominating MSSM-like contributions. The right column of fig. 5.29 singles out only the vectorlike two-loop contributions, which are negative, but slightly increase for higher masses $M_{T'} > 1\,\text{TeV}$ or larger $B_{T'}$. Comparing the first row ($Y_{t'} = 1.0, T_{t'} = 0$) and second row ($Y_{t'} = 0.7, T_{t'} = 1.4\,\text{TeV}$), we see a similar dependence, but the absolute values in the second row are much smaller.

So far we have concentrated on the new parameters from the vectorlike sector. Since the MSSM contributions are often dominant, we also consider the dependence on the gluino mass parameter M_3 and the soft squared mass of the left-handed stop, $m_{q,33}$. Starting with the gluino mass M_3, we can see in fig. 5.30 that the two-loop corrections from vectorlike quarks become more negative with increasing M_3 and can reach up to $4\,\text{GeV}$. On the other hand, their impact at one loop is tiny. However, the $\mathcal{O}(\alpha_{t'}^2)$ corrections are dominant, so the Higgs mass is
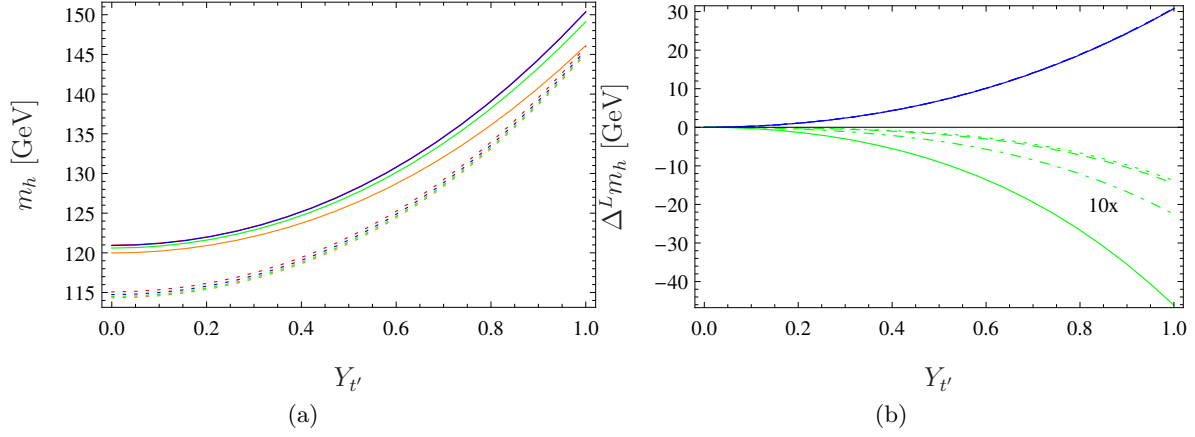
Figure 5.30: **(a):** The plot shows m_h vs $Y_{t'}$ for different M_3: 1 TeV (red), 2 TeV (blue), 3 TeV (green), 4 TeV (orange). The full lines are the two-loop results, the dotted ones the one-loop result.
(b): The absolute shift from the one- (blue) and two-loop (green) corrections involving vectorlike states is shown. The line coding is dashed, dotted, dot-dashed, full for increasing M_3. $M_{T'}$ is set to 1.5 TeV.

Figure 5.31: **(a):** The plot shows m_h vs $Y_{t'}$ for different values of $m_{q,33}$: 1 TeV (red), 2 TeV (blue), 3 TeV (green), 4 TeV (orange). The full lines are the two-loop results, the dotted ones the one-loop result.
(b): The absolute shift from the one- (blue) and two-loop (green) corrections involving only vectorlike states is shown. The line coding is dashed, dotted, dot-dashed, full for increasing $m_{q,33}$. $M_{T'}$ is set to 1.5 TeV.
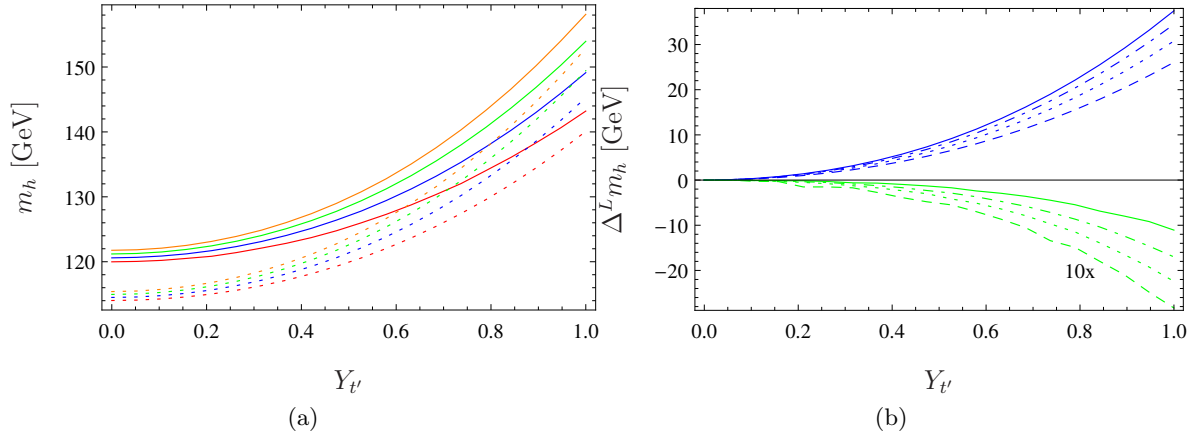
still increased by the overall two-loop effect.

Concerning the soft stop masses, we show the same setup in fig. 5.31 for increasing $m_{q,33}$. Their impact is huge: the one-loop corrections increase by a factor of 1.5 when going from 1 to 4 TeV, and the two-loop corrections increase by a factor of nearly 3. Interestingly, the pure vectorlike contributions show a different scaling behaviour: at one-loop they become larger for increasing $m_{q,33}$, while they decrease at two-loop. This concludes the analysis of the radiative Higgs mass corrections in the minimal vectorlike quark MSSM.

Fine-tuning in GMSB

Minimal GMSB has the general problem that it predicts small trilinear couplings. As a result, the Higgs mass is below 125 GeV for moderate stop masses in the TeV range. The only way to enhance m_h is to have very high stop masses, at the cost of a fine-tuning well above 1000. A recent study (Ref. [375]) nicely shows that typical values in minimal GMSB are $\Delta \sim \mathcal{O}(10^5)$. From a probabilistic point of view [392], one could consider a FT below 100 as acceptable. However, this is not a strict limit. Typical values for the MSSM are about 800–1000 [393]. With additional large loop corrections from heavy vectorlike quarks, the stop masses are allowed to be smaller and the fine-tuning is expected to improve. The full set of input parameters for this high scale model is

$$M, \Lambda, \tan\beta, M_{V'}, Y_{t'}. \tag{5.98}$$

We made a parameter scan for $\tan\beta, Y_{t'}, \Lambda$ with a fixed $M = 10^7$ GeV and two values for $M_{V'} = 0.5$ TeV and 1 TeV. Of the total set of points we take slices with different Higgs masses of 122, 125 and 128 GeV and show their projections in the $(\tan\beta, Y_{t'})$ plane in fig. 5.32. The desired Higgs mass can be achieved with a fine-tuning between 100 and 1000 in this part of parameter space and it decreases quickly with increasing $Y_{t'}$. Also, even for $Y_{t'} = 0$, the fine-tuning is reduced compared to the MSSM alone. The reason is that due to the different running of the couplings, g_3 at the messenger scale is larger than it would be in the MSSM. Therefore, the squarks are heavier for the same value of Λ, leading to larger Higgs corrections. Comparing the right column with $M_{T'} = 1$ TeV with the left column with $M_{T'} = 0.5$ TeV, we find that the fine-tuning increases with $M_{T'}$. In fig. 5.32 we also overlay red contours that show the gluino mass, which is directly related to Λ_G:

$$M_i(Q) = M_i(M) \frac{g_i^2(Q)}{g_i^2(M)} = \frac{g_i^2(Q)}{16\pi^2} \Lambda_G. \tag{5.99}$$

Since the LHC has set lower bounds on the gluino mass for several scenarios in the order of ~ 1.5 TeV, the majority of points shown here are excluded. The gluino mass can only be raised by increasing Λ, which also increases the fine-tuning. Going to larger messenger masses M does not help, since $\beta_{M_3}^{(1)}$ vanishes in this model and the mass actually decreases slightly with increasing M. We show in fig. 5.33 the fine-tuning of a selection of points in the $(m_{\tilde{g}}, m_h)$ plane, where in each bin the point with the lowest fine-tuning is chosen. It is interesting to see that there are points with $m_h = 128$ GeV with a lower fine-tuning than other points with $m_h = 125$ GeV and large $m_{\tilde{g}}$. Most importantly, the gluino mass is the bottleneck: Requiring a heavier gluino directly leads to a larger fine-tuning.

A large $Y_{t'}$ improves the FT, but the theory might not be perturbative up to the GUT scale. However, if we drop this condition, we must not insist on gauge coupling unification and additional spectator fields. This alters the running of the couplings such that g_3 becomes smaller
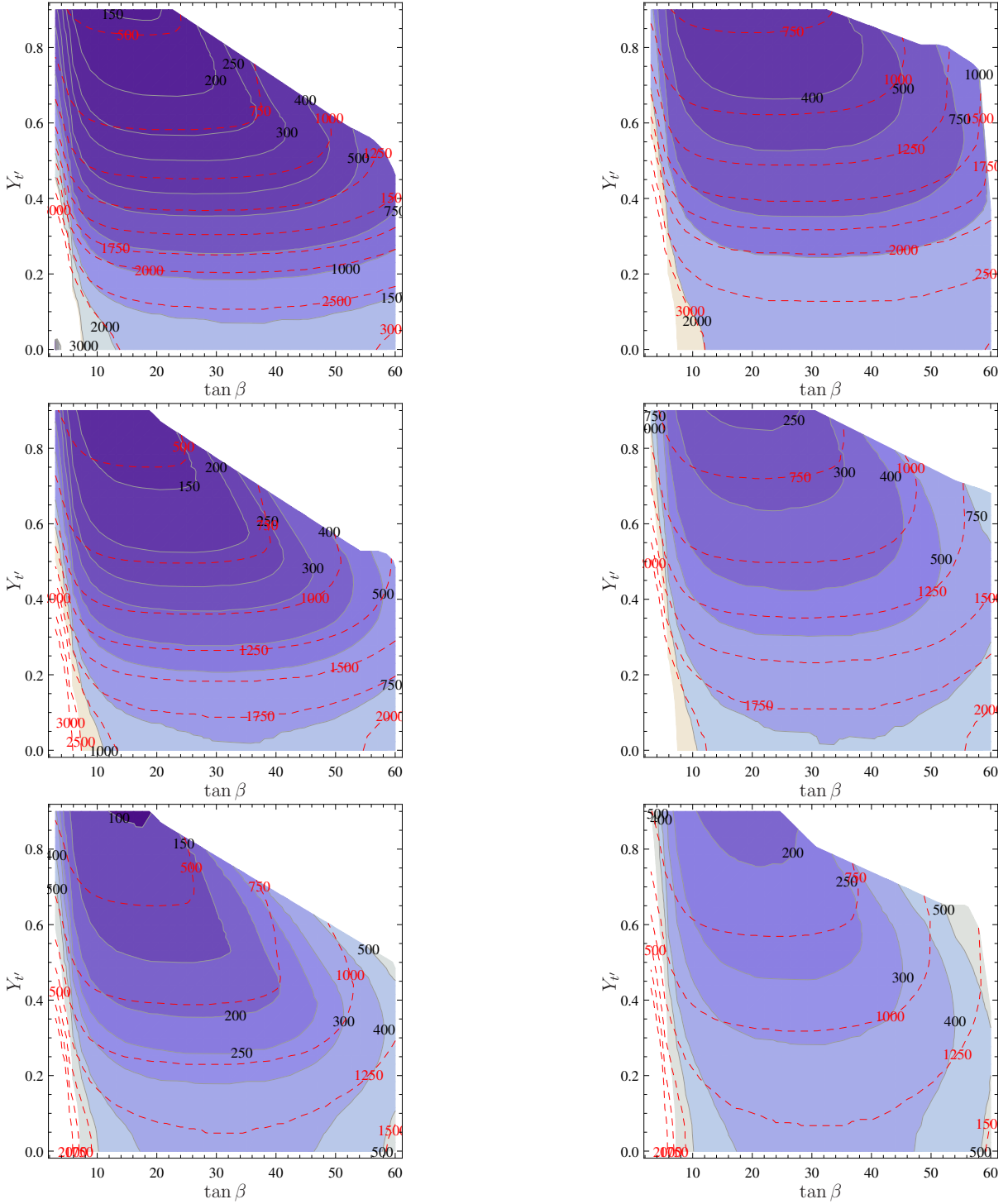
Figure 5.32: Contours of overall fine-tuning Δ in the $(\tan\beta, Y_{t'})$-plane demanding a Higgs mass $m_h = 128$ GeV (top), $m_h = 125$ GeV (middle), and $m_h = 122$ GeV (bottom) for the UV complete version of the model. We fixed here $M = 10^7$ GeV and $M_{V'} = 0.5$ TeV (left column), respectively, $M_{V'} = 1.0$ TeV (right column). The red dashed lines indicate the gluino mass in GeV.
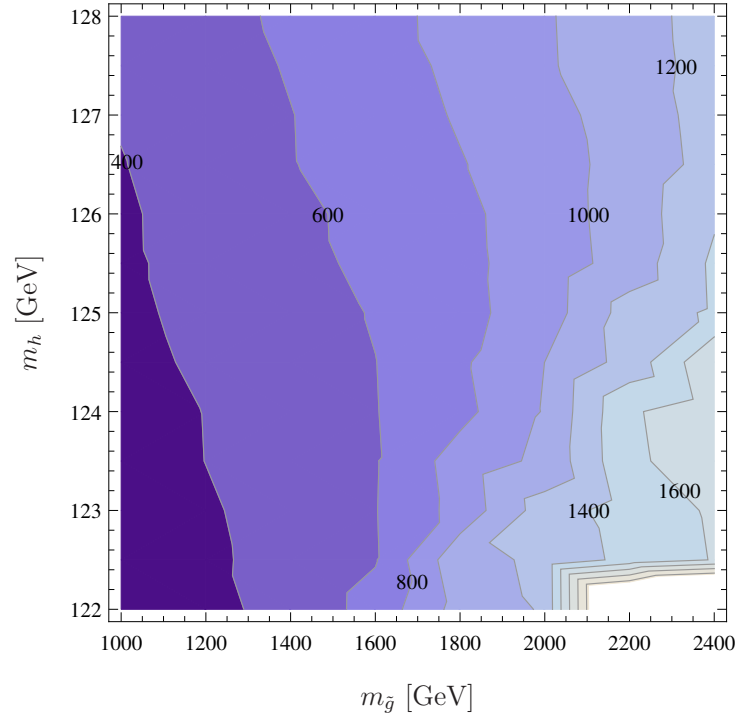
Figure 5.33: Minimal fine-tuning for a given Higgs mass m_h and gluino mass $m_{\tilde{g}}$. We fixed here $M = 10^7$ GeV and $M_{T'} = 1$ TeV and scanned over $\tan\beta$, $Y_{t'}$ and Λ.
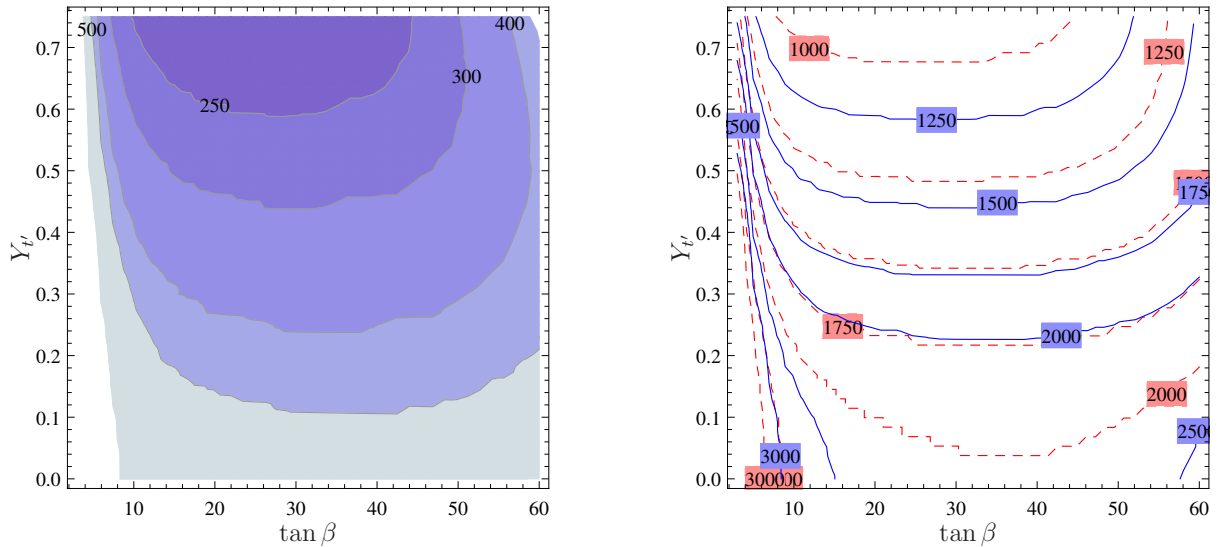
Figure 5.34: Contours of the overall fine-tuning Δ (left) and the mass of the lightest up-squark (right, full blue lines) and gluino (right, dashed red lines) in the $(\tan\beta, Y_{t'})$-plane demanding a Higgs mass $m_h > 122$ GeV for the version of the model without spectator fields. We fixed here $M = 10^7$ GeV.
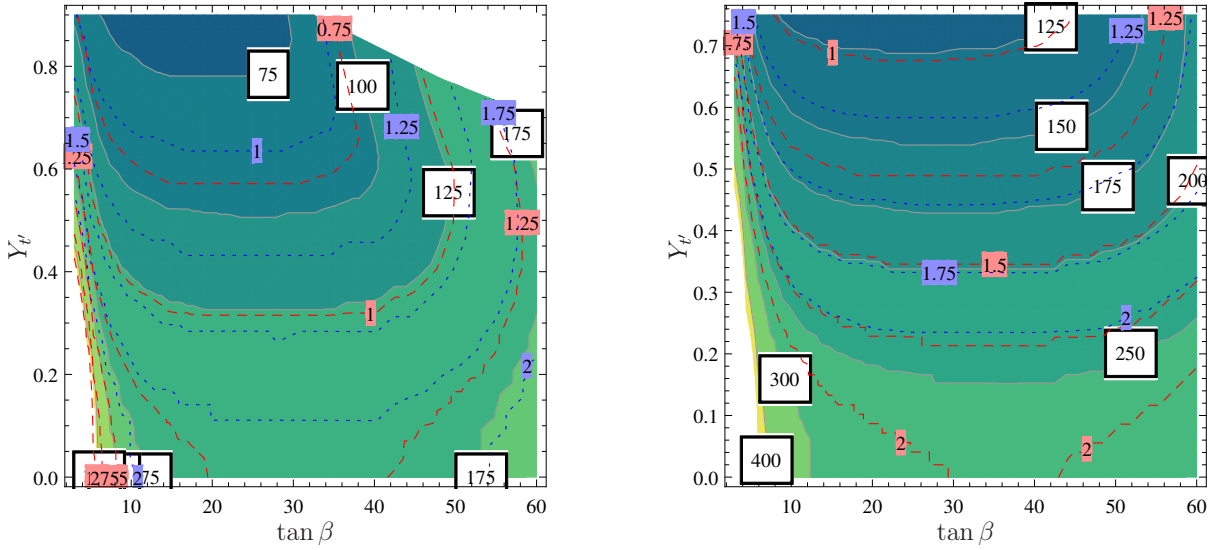
Figure 5.35: Contours of constant Λ (grey), the lightest top-squark mass (small-dashed blue lines) and gluino mass (dashed red lines) in the $(\tan\beta, Y_{t'})$-plane demanding a Higgs mass $m_h > 122$ GeV. All contours are given in units of TeV. On the left side the UV complete model is shown, on the right the model with only vectorlike tops. We fixed $M = 10^7$ GeV.

at the messenger scale for the same values of M and Λ (cf. fig. 5.21). As a consequence the squarks become lighter and the Higgs mass corrections are reduced. To reconcile this, a higher Λ is necessary, which leads to larger gluino masses. We show in fig. 5.34 contours of fine-tuning, gluino mass and lightest up-squark mass in the $(\tan\beta, Y_{t'})$ plane for the minimal model with vectorlike quarks for points which satisfy $m_h > 122$ GeV. Compared to the UV complete model, the fine-tuning does not change a lot, but the gluino masses are pushed to higher values because of the higher Λ. We find the following fine-tuning for the minimal model,

$$\Delta = (230, 275, 320, 380) \quad \text{for} \quad m_{\tilde{g}} = (1.0, 1.2, 1.4, 1.6) \text{ TeV} \tag{5.100}$$

and $m_h > 122$ GeV. To make the change in Λ visible, we show in fig. 5.35 both models, UV complete and minimal, side by side with contour lines of Λ (meaning the minimal Λ to obtain $m_h > 122$ GeV), $m_{\tilde{g}}$ and the lightest up-squark mass.

5.4.8 Conclusion

The main source of fine-tuning in this model is the gluino mass. While the inclusion of vectorlike quarks helps to reach the desired Higgs mass with a lower fine-tuning than the MSSM provides, the need for heavy gluinos in the > 1.5 TeV range set by collider bounds excludes many low fine-tuned points. In the minimal model, where grand unification is not enforced, one can accommodate larger gluino masses (1.6 TeV) with a moderate fine-tuning ($\Delta = 380$). It might be interesting to combine vectorlike (s)quarks with a GMSB variant in a model which predicts heavier gluinos without the cost of increasing Λ. An interesting feature is that for a given gluino mass, the best fine-tuning is not necessarily found for the lowest Higgs mass. For example, for $m_{\tilde{g}} = 1.8$ TeV, the lowest fine-tuning is found for a 125 GeV Higgs mass.

Concerning the loop corrections to the light Higgs mass, we have improved the existing calculations in three respects: (i) threshold corrections from vectorlike states to SM gauge and

Yukawa couplings, (ii) one-loop corrections with full momentum dependence and (ii) dominant two-loop corrections from the effective potential approach presented in Refs. [187, 188]. The momentum effects can change the mass by several GeV, but often the threshold corrections are even more important. At two-loop, the dominant corrections are often MSSM-like, but we have identified certain parameter regions where the vectorlike contributions are comparable or larger. In these regions the two-loop shift to the mass can be up to 10 GeV.

Long-lived particles at the LHC with a missing transverse energy signature

The content of this chapter was published in Ref. [394].

6.1 Introduction

Various BSM models predict new long-lived particles (LL), such as neutralinos in SUSY with weak R-parity violation [344], gluinos in split-SUSY [395], "hidden valley" models [396], and LL heavy neutrinos in the minimal $B - L$ extension of the SM [397]. Searches for neutral long-lived particles at the LHC have been conducted using reconstructed displaced vertices produced by particles that decay inside the detector volume. If the LL particle lifetime is of the order of picoseconds to nanoseconds, then its decay can yield striking signatures of displaced leptons, jets, photons or charged tracks. Based on these signatures, many searches have been performed at the LHC by the ATLAS (e.g. [398–400]) and CMS collaborations (e.g. [401, 402]). However, the efficiency of these searches is reduced if an increasing proportion of the LL particles decay outside the detector due to longer lifetimes, leading to weaker cross section limits. If more particles decay outside the detector, this will be visible as an increased missing transverse energy. This collider study considers this complementary signature (large E_T^{miss}) to set cross section limits for arbitrarily long lifetimes of LL particles. We concentrate on the results of two CMS papers which searched for displaced vertices within the CMS tracker, produced either by two leptons [399] or a quark-antiquark pair [400]. These papers set limits for a number of benchmark points in two models: (i) a model with a heavy non-standard model Higgs boson decaying into two LL scalar bosons X, which then decay either into pairs e^+e^-, $\mu^+\mu^-$ or $q\bar{q}$, and (ii) an R-parity violating SUSY model with an LL neutralino, decaying to either $\ell^+\ell^-\nu$ or $q\bar{q}^{(')}\mu$. We use measurements of the E_T^{miss} signature from CMS and ATLAS analyses at the 8 TeV LHC to set upper limits at the 95% confidence level (CL) on the production cross sections for a detector stable LL particle. Using the geometric properties of the detectors and the energy and pseudorapidity distribution of the LL particle, we extrapolate the cross section limits to finite lifetimes including when the mean decay distance is within the detector. This approach extends the LHC coverage to arbitrary long lifetimes. The limits obtained from E_T^{miss} signals are comparable to those from displaced vertex searches for decay distances above a few metres. In addition they are more model independent in the sense that they do not depend on the specific decay channel of the LL particle. We provide limits in a two-dimensional grid spanned by the

mass of the LL particle and the mass of the mediating particle up to $2\,\text{TeV}$. The results are made available in a data table which can be used for the interpretation of various other new physics models.

6.2 Setup

6.2.1 Models

To be able to directly compare our limits to the ones from displaced vertex searches, we use the same signal models that were studied by CMS in Refs. [399, 400]. It is important to stress that in these papers the LL particles were allowed to decay, while in our study we simulate stable particles. In doing this we conservatively assume that there is only a contribution to E_T^{miss} if both LL particles leave the detector. Therefore we do not need to specify the decay channel of the LL particles. We consider two signal models:

(1) A simplified model with a heavy, non-SM Higgs boson H^0 produced via gluon fusion (via an effective vertex from $\frac{1}{2}\text{Tr}[G^2]H^0$), with $G_{\mu\nu}^a$ the gluon field strength tensor) and decaying to two long-lived, heavy, neutral, spinless bosons X. In the CMS analyses, the X bosons are assumed to decay into either two leptons [399] or a quark-antiquark pair [400], while our simulation treats them as stable.

$$gg \to H^0 \to XX \tag{6.1}$$

$$X \to e^+e^-, \mu^+\mu^-, q\bar{q} \quad \text{(in the CMS analyses)} \tag{6.2}$$

The production channels are shown in fig. 6.1. The decay width of the heavy Higgs is assumed to be much smaller than its mass, $\Gamma_H \ll m_H$. Thus we only consider processes where the heavy Higgs is produced on-shell and the mass relation $m_X \le \frac{1}{2}m_H$ holds. We will call this model HXX for short.
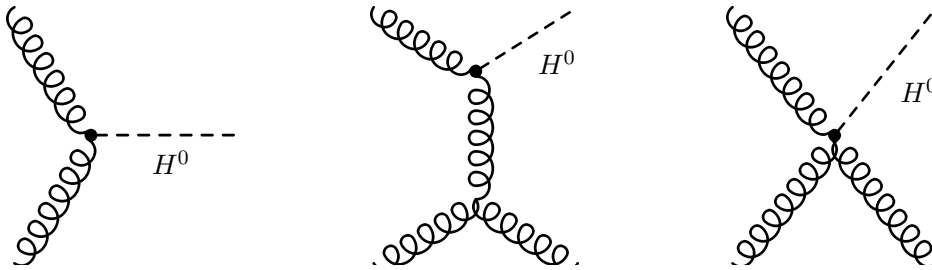
Figure 6.1: Production channels of H^0 in the HXX model, including up to 1 jet in the final state

(2) The MSSM with R-parity violating couplings and a long-lived lightest neutralino $\tilde{\chi}^0$. The signal channel is the decay of a pair of squarks $\tilde{q}$ of arbitrary flavour ($\tilde{u}_L$) (strongly produced), where each squark decays into a quark q and a neutralino $\tilde{\chi}^0$,

$$pp \to \tilde{q}\tilde{q}^*, \quad \tilde{q} \to q\tilde{\chi}^0. \tag{6.3}$$

In the CMS analyses, the neutralino decays either to $\ell^+\ell^-\nu$ [399] or to $u\bar{d}\mu^-$ [400], via $\lambda_{ijk}\mathbf{L}_i\mathbf{L}_j\mathbf{E}_k$ or $\lambda'_{ijk}\mathbf{L}_i\mathbf{Q}_j\mathbf{D}_k$ violating terms, respectively [344]. In the simulation the neutralinos are treated as stable. The production diagrams for the squark pair are shown

in fig. 6.2. There are three types of squark pairs $\tilde{q}\tilde{q}$, $\tilde{q}\tilde{q}^*$ or $\tilde{q}^*\tilde{q}^*$, which we collectively denote as $\tilde{Q}\tilde{Q}$ with $\tilde{Q} = \tilde{q}, \tilde{q}^*$. The branching ratio of $\tilde{q} \to q\tilde{\chi}^0$ is assumed to be 100% for all events.
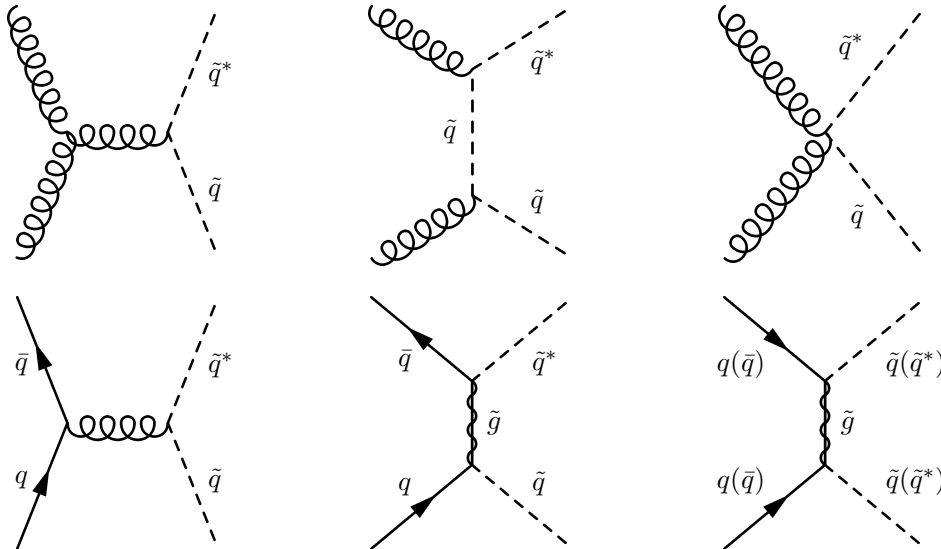
Figure 6.2: Strong production of squark pairs in SUSY at tree level

6.2.2 Event generation

We look for signals where the neutral LL particle, either X or $\tilde{\chi}^0$, leaves the detector before decaying which should show a large E_T^{miss} signature. For the HXX model, this can only happen if a high P_T jet is produced from initial state radiation (ISR) and recoils against the XX pair, providing a mono-jet signature. For the simulation we used a model generated with the `LanHEP` package [403–405], with an effective vertex between gluons and the heavy Higgs H^0 described by a Lagrangian term $\frac{1}{2}\mathrm{Tr}[G^2]H^0$.

In the RPV scenario, if there is small mass gap between the squark and the neutralino, one can again use a mono-jet signature because the quark produced by the squark decay is soft and not reconstructed as a jet. If there is a large gap, the quark from the decay $\tilde{q} \to q\tilde{\chi}^0$ can have a high P_T and appear as an energetic jet. The resulting signature will be of the type 'E_T^{miss} + jets'. To simulate this scenario the standard MSSM can be used, because the decay of the neutralino does not have to be modelled. All SUSY masses except $m_{\tilde{\chi}^0}, m_{\tilde{q}}$ are set to 5 TeV to match the model used by CMS.

In both cases we used `MadGraph5 v2.1.2` [285] for the event generation with `Pythia 6.4` [406, 407] for parton showering and hadronisation. To accurately simulate hard ISR jets, we allow an additional matrix element jet which is matched using the k_T MLM scheme [407].

6.2.3 Used CMS and ATLAS E_T^{miss} Analyses

E_T^{miss} signatures were frequently used in several dedicated studies by ATLAS and CMS in the context of SUSY searches with decays into LSPs. To find out which search provides the strongest cross section limits on the two models, we would have to implement the analyses of multiple

such publications and compare the resulting bounds. Fortunately, this work is simplified by `CheckMATE` [408–416], which has many results of such papers implemented and allows easy use of the searches. The tool takes a sample of Monte Carlo events in the HEP or HEPMC format after parton showering (PYTHIA/HERWIG) level of simulation and performs a detector simulation for the sample using `Delphes-3 [409]`. `CheckMATE` then applies each analysis as described in the experimental papers on the generated signal events.

The resulting efficiencies are compared with the information about signal counts provided by the publication to produce a statement on whether a point is excluded at 95% C.L. or not. As this depends on the assumed cross section for the signal (which has to be given by the user), this result can also be used to establish exclusion cross section limits. Here, we do not account for systematic uncertainty on the signal selection efficiency, because this would be model dependent. The analyses which we used have all been validated by using published results including available cut-flows.

In each analysis paper, CMS and ATLAS typically divide the signal space (in terms of final state observables) into smaller signal regions. For example, these can be defined by different intervals of E_T^{miss}. The signal region that gives the best *expected* limit is the one we use. Using the expected instead of the observed limit avoids the 'look elsewhere' effect.

It turns out that from the long list of available analyses, three are particularly important, giving the strongest limits (a fourth paper, a CMS monojet study [417], is potentially interesting, but was not yet available in `CheckMATE`). Their selection cuts and signal regions are briefly outlined below.

1. ATLAS E_T^{miss} + multi-jet analysis [418].
   This analysis uses 20.3 fb^{-1} of $\sqrt{s} = 8$ TeV data. E_T^{miss} must be above 160 GeV, the leading jet must have $p_T(j_1) > 130$ GeV and the second hardest jet $p_T(j_2) > 60$ GeV. The signal regions are distinguished by jet multiplicity 2,3,4,5,6, corresponding to signal region codes A,B,C,D,E, while only jets with $p_T > 60$ GeV are valid in this count. Given one of these five categories, signals are then subjected to loose (L), medium (M) or tight (T) constraints. In our case, the signal regions AM, BM, BT, CM, CT are relevant. For full details, cf. **Page 3, Table 1 of [418]**.

2. ATLAS E_T^{miss} + monojet analysis [419].
   This analysis uses 20.3 fb^{-1} of $\sqrt{s} = 8$ TeV data. Events must have at least one jet with $p_T > 120$ GeV and $|\eta| < 2.0$ and no charged leptons (of $p_T > 7$ GeV). For the leading jet, $p_T/E_T^{\mathrm{miss}} > 0.5$ must hold ($E_T^{\mathrm{miss}} > 150$ GeV required). The number of jets is unrestricted, but the leading jet is only considered (monojet-like selection). Nine signal regions are defined between 150 GeV $< E_T^{\mathrm{miss}} < 700$ GeV, labelled *SR1* through *SR9*. Complete definitions, cf. **Page 7, Table 2, of [419]**

3. CMS analysis using the α_T variable [420].
   This analysis uses 11.7 fb^{-1} of $\sqrt{s} = 8$ TeV data. Instead of E_T^{miss}, this analysis uses the related variable α_T [421, 422] to suppress multijet background events. This variable is used to be more independent of mismeasurements of E_T^{miss}. For two back-to-back jets with $E_T^{j_1} = E_T^{j_2}$, α_T is equal to 0.5. A value greater than 0.5 signifies that the jets are recoiling against significant E_T^{miss}. For further details of the α_T variable see [420–422]. Events with e or μ with $p_T > 10$ GeV are vetoed as well as those with an isolated photon with $p_T < 25$ GeV. To cut out multijet background events, $\alpha_T > 0.55$ is required. Also, the scalar sum of all transverse jet energies, $H_T = \sum_{i=1}^{n_{\mathrm{jet}}} E_T^{j_i}$, must be larger than 275 GeV.

The two leading jets must each have $p_T > 100\,\text{GeV}$ and the leading jet satisfies $|\eta| < 2.5$, but these conditions are also relaxed for some signal regions. The signal regions are named after the number of jets (`23j_` for 2-3 jets or `4j_` for ≥ 4 jets) + number of b-jets (`0b_` or `1b_`) + lower limit of H_T bin (`275, 325, 375, 475` etc.). Example: `23j_0b_325`.

6.2.4 Escape Probability

With the events and analyses described in section 6.2.3 we obtain the 95% cross section limits for stable LL particles that both leave the detector. In order to extrapolate these limits for a given finite lifetime, we need the probability for an LL particle to decay outside the detector. Apart from the lifetime, this also depends on the direction of emission of the particle and the speed it is travelling with. To take into account this information, we edited the `CheckMATE` code so that on an event by event basis for each simulated event which passed the selection cuts we calculated the probability of each LL particle leaving the detector before decaying, taking into account their energy E and pseudorapidity η. The probability to leave the detector is

$$p(D) = \exp\left(\frac{-D}{c\beta\gamma\tau}\right), \tag{6.4}$$

where D is the distance from the interaction point to the periphery of the detector, which depends on the size and shape of the detector and the pseudorapidity of the particle. Here, $\beta = v/c$ and $\gamma = E/m$ are the relativistic factors and τ the lifetime of the particle. The dependence of D on the pseudorapidity η is shown in fig. 6.3. For this calculation, the ATLAS and CMS detectors are assumed to be cylindrical in shape, with ATLAS having a length of 46 m and a diameter of 25 m, and CMS having a length of 21 m and a diameter of 15 m. Each event
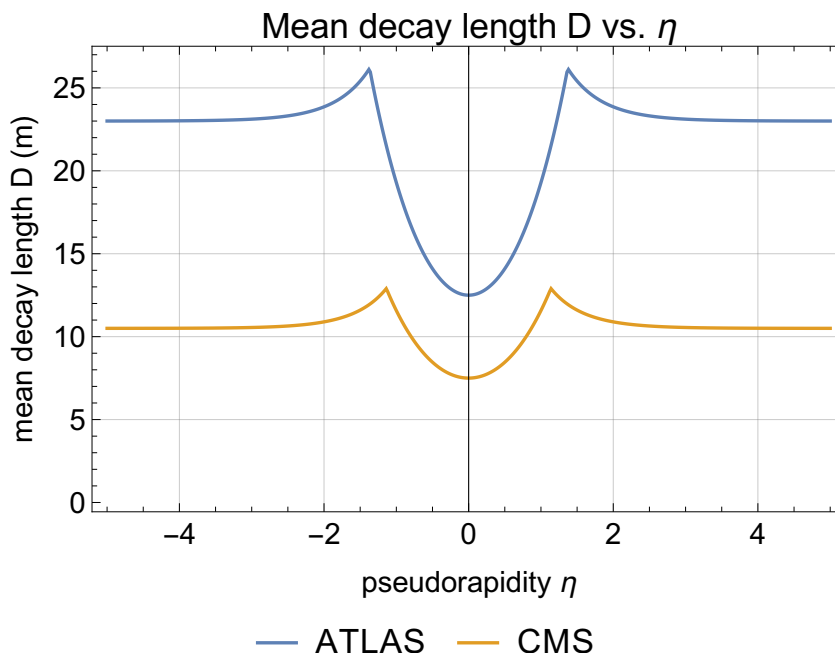

Figure 6.3: The dependence of the mean decay length D on η for ATLAS and CMS is shown.

is weighted according to the probability that both LL particles leave the detector undecayed,

$$w = p_1(D_1)p_2(D_2), \tag{6.5}$$

with p_1, p_2 denoting the probabilities for particle 1 and 2 respectively. Averaging the weights for all events gives the proportion P of these events which would have given an E_T^{miss} signature. From this we can calculate the 95% C.L. limit on the signal cross section for any lifetime,

$$\sigma_{c\tau}^{95\%} = \frac{1}{P}\sigma_{\mathrm{stable}}^{95\%}, \tag{6.6}$$

where $\sigma_{\mathrm{stable}}^{95\%}$ is the cross section limits calculated using `CheckMATE` by assuming stable LL particles. There is a simpler approximation to obtain the lifetime dependent limit $\sigma_{c\tau}^{95\%}$, which can be used by other researchers to approximate similar limits as those shown in figs. 6.4-6.5. If one assumes isotropic production of the LL pair, it requires only an energy distribution of the LL particles to approximate the limits. This is described in detail in the appendix C.1. We found that this method gives a reasonable agreement with our more accurate results and it can be applied to the limits in the result tables in C.2.

Events in which only one LL particle escapes the detector could also yield a missing energy signature and could therefore be used to improve the limits. This has not been done here, as it requires an understanding of how the detectors would react to the decaying particle and its decay products. Whether they contribute to the missing energy depends on the event reconstruction algorithms and the selection requirements of the individual analyses.

6.3 Results

We have performed the event generation described in section 6.2 and run the CMS and ATLAS analyses using `CheckMATE` for the benchmark points (BPs) used in the studies [399] and [400]. The points are defined by the mass of the LL particle and of the mediating particle: (m_X, m_H) in the first model and $(m_{\tilde{\chi}^0}, m_{\tilde{q}})$ in the RPV-SUSY model. The results are the cross section limits $\sigma_{\mathrm{stable}}^{95\%}$ for the $\sigma(pp \to H^0 \to XX)$ in table 6.1 and $\sigma(pp \to \widetilde{Q}\widetilde{Q} \to \tilde{\chi}^0\tilde{\chi}^0 + \mathrm{jets})$ processes in table 6.2.

For every BP in the HXX model, the ATLAS monojet + E_T^{miss} paper [419] provides the best sensitivity, as expected. In the RPV model there are different analyses that give best results. For $m_{\tilde{q}} = 120, 350$, the CMS paper [420], which uses the α_T variable, provides the best limit. On the other hand, for $m_{\tilde{q}} = 1000, 1500$ GeV, the best limit is provided by using the ATLAS paper [418] (large E_T^{miss} + multi-jet signal). In this model, the E_T^{miss} does not depend on ISR and there can be multiple hard jets in general. The limits for the HXX model are weaker than those obtained for the RPV-SUSY model, because only a small fraction of events contain the hard ISR on which the HXX limits rely.

From the limits $\sigma_{\mathrm{stable}}^{95\%}$ for each benchmark point we subsequently calculate the limits for arbitrary lifetimes, $\sigma_{c\tau}^{95\%}$ by the procedure described in section 6.2.4. The results are shown in figs. 6.4 and 6.5. Each colour corresponds to a different BP, with the thin solid curves denoting the limits found using the CMS detector dimensions and CMS analyses, and the dashed thin line corresponding to the ATLAS limit. For comparison, the published results from the CMS displaced vertex analyses [399, 400] are shown as the thick curves. These cross section limits from displaced vertices increase in proportion to a power of the LL particle lifetime, so they
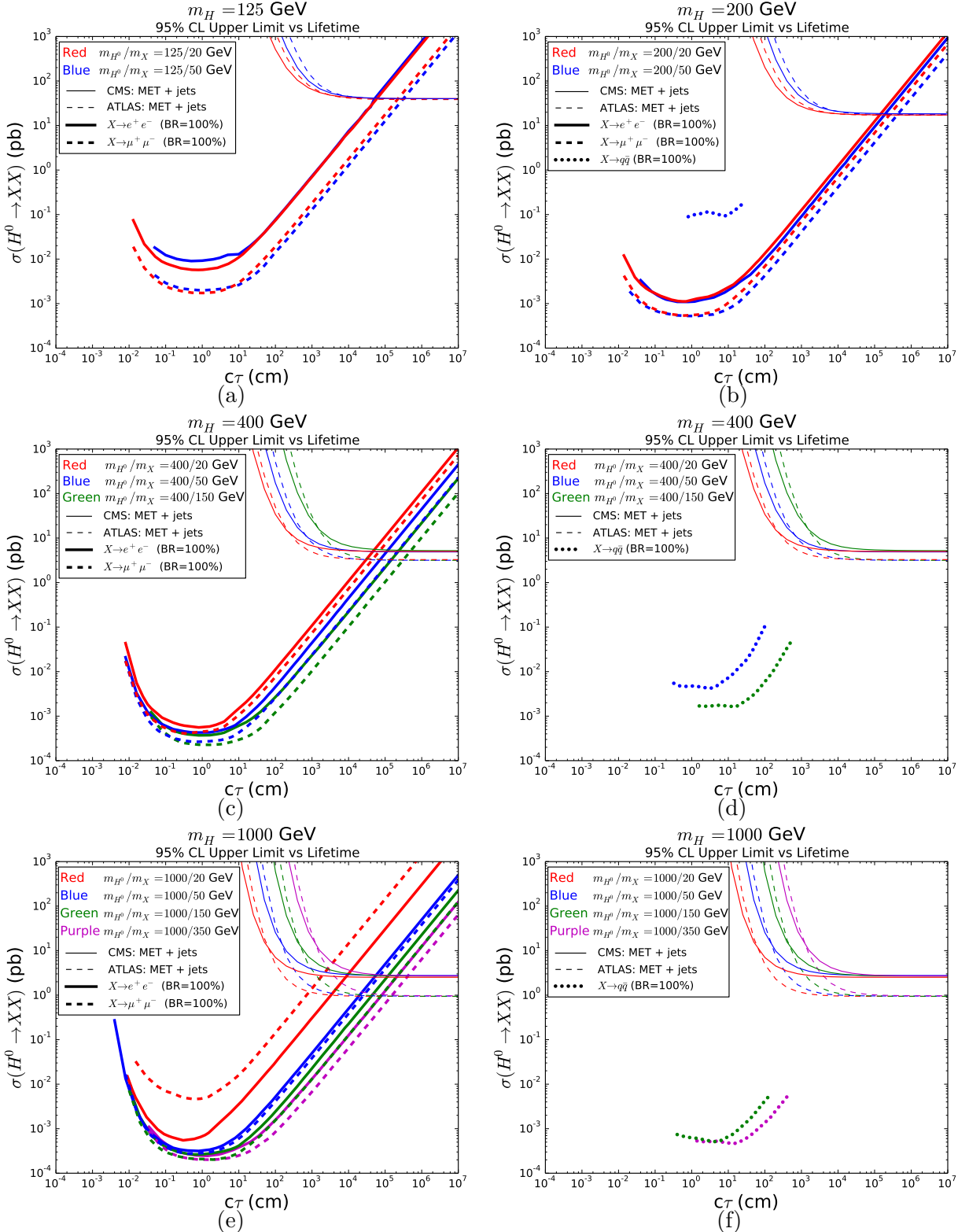
Figure 6.4: 95% CL upper limits on cross sections for the heavy Higgs model (HXX) with $m_H = 125$ GeV (a), 200 GeV (b), 400 GeV (c,d) and 1000 GeV (e,f) are shown. The colour red (blue) indicates $m_X = 20$ GeV (50 GeV) *for all curves*. The thin curves in the upper-right corner of all figures show our new E_T^{miss}-derived limits on LL particle cross sections for each detector (solid: CMS, dashed: ATLAS). For comparison, the cross section limits from the CMS displaced vertex searches, under the assumption of 100% branching ratios, are shown by thick curves: displaced leptons searches ($X \rightarrow \ell^+\ell^-$) [399] are indicated by the solid curves for $\ell = e$ and by dashed curves for $\ell = \mu$; whereas displaced jet searches ($X \rightarrow q\bar{q}$) [400] are indicated by dotted curves. Our new limits are identical in (c) and (d) as well as in (e) and (f) and have been split for clarity.

Benchmark Point	m_H (GeV)	m_X (GeV)	$\sigma^{95\%}_{\text{stable}}$ (pb)	Analysis - SR
1a	125	20	38.3	ATLAS monojet [419] – SR4
1b	125	50	39.9	ATLAS monojet [419] – SR4
2a	200	20	17.1	ATLAS monojet [419] – SR4
2b	200	50	17.5	ATLAS monojet [419] – SR4
3a	400	20	3.29	ATLAS monojet [419] – SR6
3b	400	50	3.17	ATLAS monojet [419] – SR6
3c	400	150	3.16	ATLAS monojet [419] – SR6
4a	1000	20	0.94	ATLAS monojet [419] – SR7
4b	1000	50	0.96	ATLAS monojet [419] – SR7
4c	1000	150	0.94	ATLAS monojet [419] – SR7
4d	1000	350	0.97	ATLAS monojet [419] – SR7

Table 6.1: Benchmark points from Ref. [399] and Ref. [400] (Model 1, HXX) and their 95% CL upper limit on cross section are shown, together with the CMS or ATLAS E_T^{miss} analysis paper from which this limit was derived.

Benchmark Point	$m_{\tilde{q}}$ (GeV)	$m_{\tilde{\chi}^0}$ (GeV)	$\sigma^{95\%}_{\text{stable}}$ (pb)	Analysis - SR
1	120	48	33.5	CMS α_T [420] – 4j_0b_325
2	350	148	0.57	CMS α_T [420] – 23j_0b_325
3	700	150	0.041	ATLAS multijet [418] – AM
4	700	500	0.24	CMS α_T [420] – 23j_0b_375
5	1000	148	0.0086	ATLAS multijet [418] – AM
6	1000	500	0.025	ATLAS multijet [418] – AM
7	1500	150	0.0018	ATLAS multijet [418] – CT
8	1500	494	0.0024	ATLAS multijet [418] – CT

Table 6.2: Benchmark points from Ref. [399] and Ref. [400] (Model 2, RPV-SUSY model) and their 95% CL upper limit on cross section are shown, together with the CMS or ATLAS E_T^{miss} analysis paper from which this limit was derived.
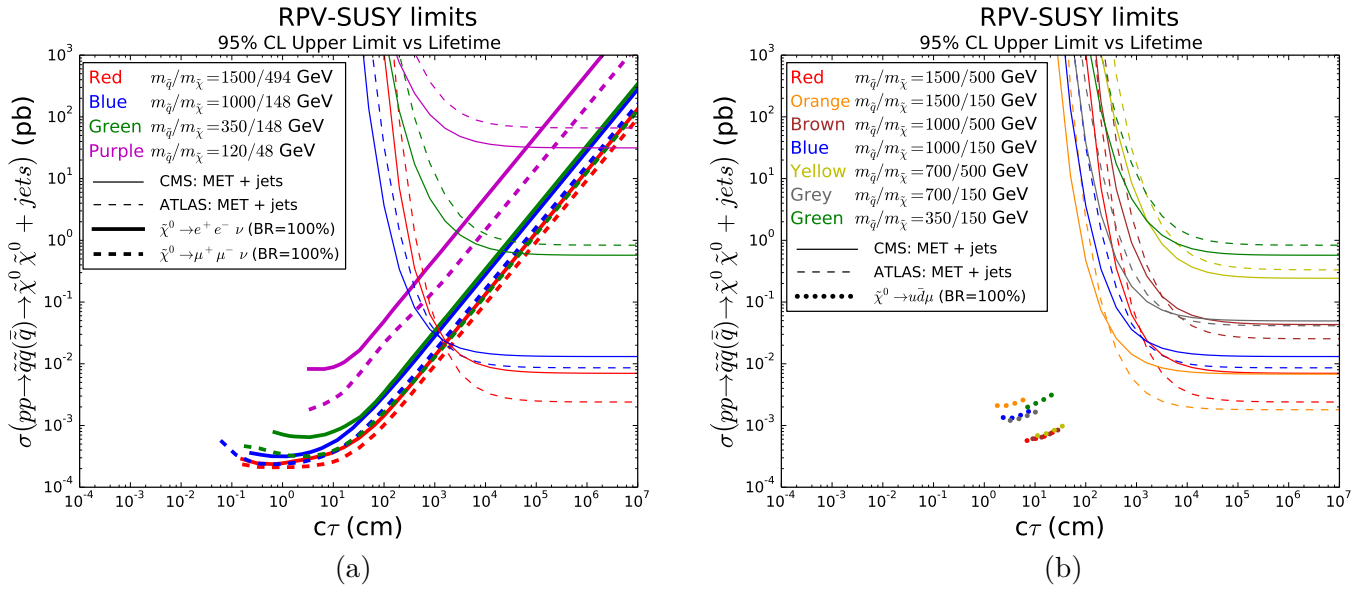
Figure 6.5: 95% CL upper limits on cross sections for the RPV-SUSY model with colours indicating various mass points are shown. The thin curves in the upper-right corner of both (a) and (b) show our new E_T^{miss}-derived limits on LL particle cross sections for each detector (solid: CMS, dashed: ATLAS). For comparison, the cross section limits from the CMS displaced vertex searches, under the assumption of 100% branching ratios are shown by thick curves: (a) for displaced dilepton searches ($\tilde{\chi}^0 \to \ell^+ \ell^- \nu$) [399], with the solid curves indicating $\ell = e$ and the dashed curves indicating $\ell = \mu$; and (b) for displaced dijet searches [400] searches ($\tilde{\chi}^0 \to u\bar{d}\mu$) shown by dotted curves.

appear as a straight line in the double logarithmic plot. This can be understood from the following consideration. Assuming that the detector is only sensitive to particles decaying within a distance L from the centre, the probability that a particle decays within this volume is given by $1 - \exp(\frac{-LM}{Pc\tau})$, which tends to $\frac{-LM}{Pc\tau}$ in the limit of long lifetimes. In an analysis such as Ref. [399], where the displaced vertex is reconstructed for just one LL particle per event, the resulting cross section limits will scale inversely to the acceptance. This scaling behaviour allows to extrapolate the CMS limits beyond the lifetimes in their original publications, under the condition that their results covered long enough lifetimes to to reach this asymptotic behaviour. For the CMS displaced dijet vertex search [400] this was not the case and no such extrapolation was done.

The smallest cross section limits from displaced vertex searches are found at $c\tau = \mathcal{O}(1\,\text{cm})$ and are of the order of fb, while the limits from E_T^{miss} searches are of the order of a pb or more. In general, both become comparable for larger lifetimes $c\tau = 10^3 - 10^5$ cm, depending on the benchmark point. Above the crossing point of two corresponding lines, the limits from E_T^{miss} searches are better. When making such comparisons, it is important to note that the CMS displaced vertex limits assume a branching ratio of 1 for the decays of the LL particles, which is made explicit. In our approach, this decay is unspecified and the limits are independent of the branching ratio. As an example, if in a realistic scenario the X particle would decay to e^+e^- with a branching ratio of 0.01, the presented CMS displaced vertex limits would be weakened by a factor 100. This would make our limits from E_T^{miss} signals comparable at smaller proper decay lengths at about 1 metre or less for certain benchmark points.

What is also noteworthy is that although the ATLAS analyses give better results for $\sigma_{\text{stable}}^{95\%}$ in figs. 6.4 and 6.5 (dashed lines), in the extrapolation to smaller lifetimes the CMS results become better (full lines). This is because the CMS detector is smaller and therefore a larger fraction of the decays will occur outside the detector. This nicely demonstrates the complementarity of the two machines.

Furthermore one can see in fig. 6.4(e,f) a relativistic effect related to the LL particle mass. The cross section limits for very large $c\tau$ are of the same order of magnitude for all values of m_X, because in every case nearly all decays occur outside the detector. However, the curves for smaller masses m_X are shifted to the left towards smaller values of $c\tau$ compared to larger masses m_X. Because of relativistic time-dilation, a lighter X is more likely to escape the detector than a heavier X of equal energy.

To give a more complete result beyond the shown benchmark points, we repeated the procedure of obtaining $\sigma_{\text{stable}}^{95\%}$ for many values of the LL mass and mediator mass, shown in a grid in fig. 6.6 for the HXX model and fig. 6.7 for the RPV-SUSY model, where the $\sigma_{\text{stable}}^{95\%}$ limits are indicated by the colour chart. The figures show different patterns: In fig. 6.6 for the HXX model the cross section limits depend only on the mass of the heavy Higgs H^0, while in fig. 6.7 they depend largely on the mass gap $\Delta m = m_{\tilde{q}} - m_{\tilde{\chi}^0}$. This can be explained by the production and decay channels of the two models. In the HXX model, the H^0 is produced on-shell before decaying into two X bosons. The missing transverse energy is basically just p_T of the H^0. With increasing m_H, also the average p_T increases, leading to better cross section bounds for larger values of m_H.

On the other hand, in the SUSY model each squark decays into a neutralino and a quark ($\tilde{q} \to q\tilde{\chi}^0$), producing jets and E_T^{miss}. For small mass gaps $\Delta m = m_{\tilde{q}} - m_{\tilde{\chi}^0}$ the decay products are soft, giving a low E_T^{miss} and a low signal efficiency. In these parameter regions, the monojet searches give the best limits (or α_T analyses with 2-jet signatures for low values of $m_{\tilde{q}}$), which are similar in size as for the HXX model. As Δm increases, the E_T^{miss} and jet p_T increase as well,
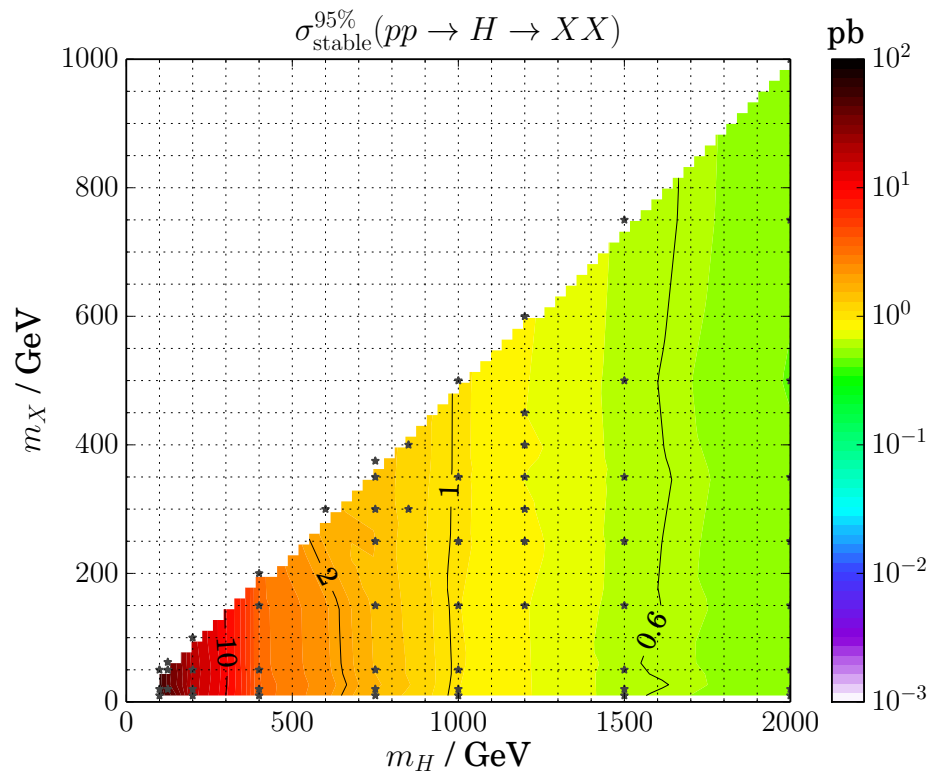
Figure 6.6: The figure shows the upper limit of the production cross section of XX+jets final states for the HXX–model in units of pb in the (m_H, m_X) plane.
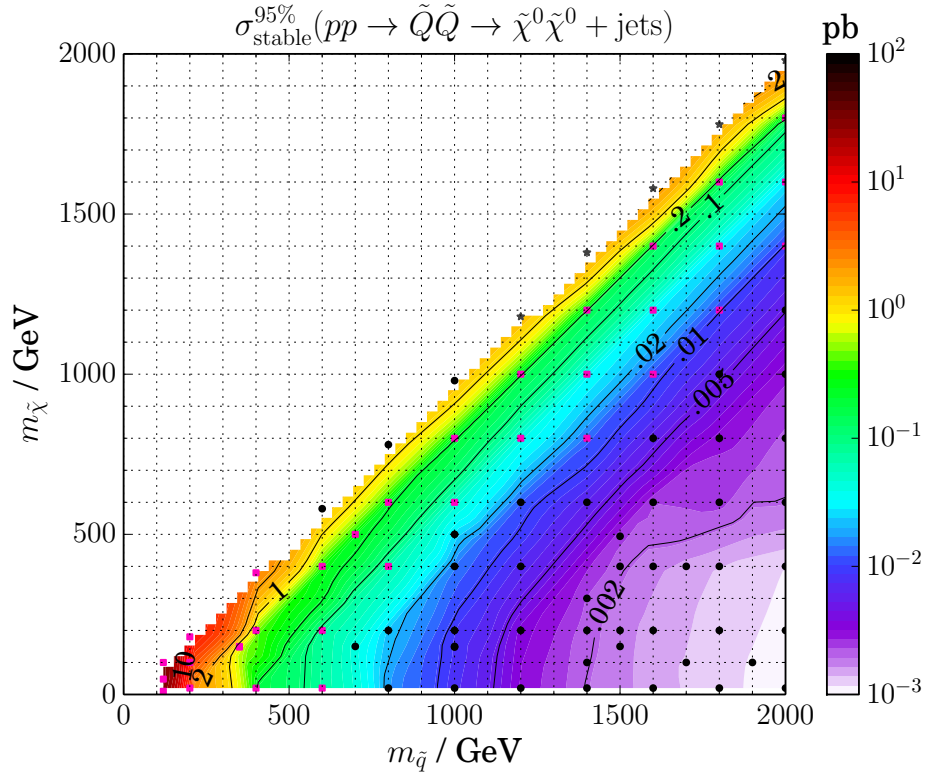
Figure 6.7: The figure shows the upper limit of the production cross section of $\tilde{\chi}^0\tilde{\chi}^0$+jets final states for the MSSM in units of pb in the $(m_{\tilde{q}}, m_{\tilde{\chi}^0})$ plane. Black dots indicate sample points where the ATLAS multijet paper [418] performed best, grey stars indicate the ATLAS monojet paper [419], and pink squares indicate best performance with the CMS α_T paper [420]. A similar plot indicating the best signal regions is shown in the fig. 6.8.
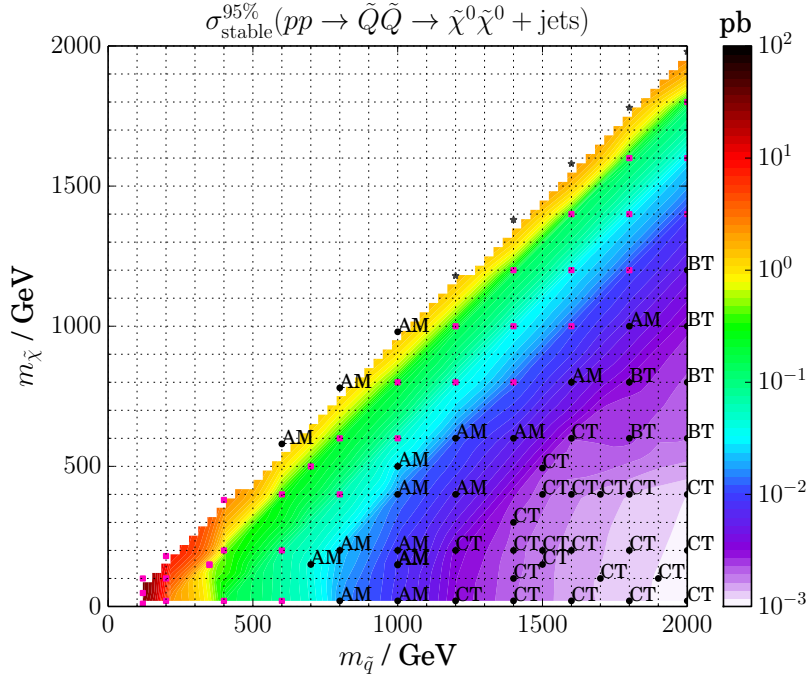
Figure 6.8: The figure shows the upper limit of the production cross section of $\tilde{\chi}^0\tilde{\chi}^0$+jets final states for the MSSM. The dots have the same meaning as in fig. 6.7, but in addition we show the best signal regions for the ATLAS multijet analysis.

giving a larger signal cut efficiency and thus better cross section limits. Δm appears to be the most important parameter to describe the behaviour seen in fig. 6.7. We present another plot of the SUSY grid scan in fig. 6.8, which also indicates which signal region gives the best result for each point. The data points of both grid scans have been published in Ref. [394], along with an approximation for calculating the escape probabilities, which is explained in appendix C.1.

Events in which one LL particle decays inside and the other one outside the detector were not considered in this study. This gives more conservative bounds, as such events could potentially give an additional E_T^{miss} signature, in particular for the HXX model where the requirement of recoiling against a high-p_T jet would no longer be needed. This scenario has the potential to produce stronger limits, but is more technically difficult to realise in detector simulations.

6.4 Conclusion

We have shown that the traditional searches for long-lived neutral particles using displaced vertices can be complemented by using missing transverse energy analyses, which extend the cross section limits to arbitrarily long lifetimes. For the two signal models considered in Refs. [399, 400], we obtained 95% cross section limits from a E_T^{miss} signature which are comparable to those from displaced vertex searches for values of $c\tau$ as short as a few metres (nanosecond lifetimes), although for most of the benchmark points they are comparable at larger distances from 10m – 100m. The approach shown here is more model independent because the cross section limits found with this approach are independent of the specific decay channels of the LL particles and their branching ratios. This is not the case for the displaced vertex searches

of Refs. [399, 400] since for realistic cases with branching ratios of a few percent or less, the CMS limits from displaced vertices are significantly weakened, making the limits from E_T^{miss} signatures much more competitive. In this case, our limits for stable particles can be better than the minimum obtained from displaced vertex searches for any $c\tau$ and they can be comparable for decay distances below 1 metre.

Also the spin of the LL particle does not affect the limits in the HXX model, because the spinless H decays isotropically into X pairs in its own rest frame. In fact, the bounds found for the HXX model are valid for any model in which a narrow width scalar H is produced via an effective vertex $\frac{1}{2}\mathrm{Tr}[G^2]H$ and decays into a pair of LL particles. Also in the SUSY case the results are independent of whether the neutralino decays via RPV operators or any other interaction, as long as the model has the same production channel assuming negligible effect from heavy intermediate gluino exchange.

Summary and Conclusion

The MSSM predicts a light Higgs mass $\leq 91.2\,\text{GeV}$ at tree level and thus requires large radiative corrections. As of July 2012, the bar has been set high with the discovery of the $125\,\text{GeV}$ Higgs boson at the LHC [21, 22]. Large quantum corrections require heavy sparticles above $1\,\text{TeV}$ and/or a large mixing between the stops. This raises the issue of naturalness and fine-tuning that SUSY was expected to solve. As the Higgs mass m_h has become a precision observable with a relative uncertainty below 0.3%, phenomenological tools struggle to provide comparably accurate predictions. However there has been a lot of improvement in the field of precision calculations lately. In particular the advanced tool `FeynHiggs` [227, 423] states an uncertainty of $2\,\text{GeV}$ for its Higgs mass calculation in the MSSM [224, 300] and also the NMSSM has received a lot of attention (e.g. Ref. [424] contains a detailed comparison of state-of-the-art NMSSM spectrum calculators). The full one-loop corrections with momentum dependence are well established [196–199] and implemented in many spectrum generators. The dominant MSSM two-loop corrections, eq. (7.1), in the zero momentum limit have also been around for several years [200]. At three-loop level, corrections of the order $\mathcal{O}\left(\alpha_s^2\alpha_t\right)$ [228–230] have been incorporated into the code `H3m` [229]. While SUSY phenomenologists have several choices of tools when it comes to the MSSM and NMSSM, for models beyond that the only stop is `SARAH` [68–74]. It is a tool that creates the full Lagrangian of a user-defined model from minimal input using `Mathematica`'s symbolic manipulation. From the Lagrangian, mass matrices and couplings between the particles are extracted analytically. It also employs generic formulae to calculate other key quantities such as two-loop RGEs and radiative corrections. While the program can be used in a stand-alone way for analytic studies at tree level, the most powerful feature is the ability to export Fortran source code to the program `SPheno` [221, 222], which creates a tailor-made spectrum generator for numerical studies beyond tree-level. This makes it a meta-tool that can also create model files for other tools. Since 2014, `FlexibleSUSY` [290, 291] offers an alternative to `SPheno` by producing its own customised spectrum generator. However, it is also linked to `SARAH` and requires some of its output.

The main contribution of this thesis is the following:

- We have implemented a model-independent, two-loop Higgs mass calculation into `SARAH`/`SPheno`, which allows to study models beyond the MSSM with an increased Higgs mass precision.

- Using this calculation, we studied two-loop contributions to the Higgs mass in the case of four supersymmetric models and identified parameter regions where the novel contributions are significant. Some of them have been studied here for the first time because they were

    unavailable in other public tools.

- We obtained production cross section limits for long-lived particles at the LHC using analyses written by ATLAS and CMS that focus on a large E_T^{miss} signature. This establishes a complementary approach to traditional searches for displaced vertices.

The extension to `SARAH` includes two-loop corrections to neutral Higgs bosons in the effective potential approach, where contributions from broken gauge groups are neglected (gaugeless limit). The idea of a numerical differentiation of the effective potential was used earlier (Ref. [183]) and the generic expressions for the full two-loop effective potential have been available for a long time [265]. However, they were not utilised in a computer code before. There are three independent methods implemented into `SARAH`/`SPheno` to calculate the entries of the two-loop self-energy matrix of the neutral Higgs components. In the simplest, purely-numerical approach, the effective potential function is numerically differentiated as a whole with respect to the VEVs. The semi-analytical approach uses a mixture of analytical derivatives of the loop functions and numerical derivatives of masses and couplings. In the third, diagrammatic approach we obtained self-energies (and tadpoles) by analytically differentiating the effective potential, which is equivalent to calculating the two-point (and one-point), two-loop Feynman diagrams with vanishing external momentum. This leads in some cases to simpler (but equivalent) expressions than the corresponding results from literature [267] with $p^2 = 0$. The effective potential and its derivatives can suffer from divergences in the case of massless scalars, which are present in the Landau gauge (Goldstone problem). We circumvented this by working in the minimum of the full effective potential along with tree-level scalar mass matrices in the gaugeless limit, which results in non-zero tree-level Goldstone masses. All approaches are independent and calculate the same quantity but differences arise because of the involved numerics. The methods have been presented and validated in Refs. [187, 188]. A next possible step towards further improvement could be the inclusion of contributions from massive vector bosons to the effective potential. The tadpoles of these contributions were partially published in Ref. [188], however the derivatives of the loop functions have not been calculated explicitly. This is done in this thesis and constitutes a previously unpublished result. At some point, one might want to exchange the effective potential approximation for a full momentum dependent calculation. We stress that even in this case, the tadpole expressions obtained from the effective potential will still be required.

    For many years the established precision of the Higgs mass in the MSSM was determined by the full one-loop corrections plus the dominant two-loop corrections stemming from the strong interaction and pure Yukawa interactions:

$$\mathcal{O}\left(\alpha_s(\alpha_t + \alpha_b)\right), \quad \mathcal{O}\left((\alpha_t + \alpha_b + \alpha_\tau)^2\right). \tag{7.1}$$

They were calculated in Ref. [200] in the limit of zero external momentum and are used in many public codes. To be more precise, $\mathcal{O}\left(\alpha_s\alpha_t\right)$ and $\mathcal{O}\left(\alpha_t^2\right)$ are really dominant, while the other corrections in eq. (7.1) are much smaller, because $y_t \gg y_b, y_\tau$. With our code it is possible to study many models beyond the MSSM with a similar precision.

    Using only the contributions of eq. (7.1) means neglecting the first two generations of sfermions. This is reasonable unless there is a large mixing in the squark sector between generations. The third-generation-only approximation can lead to a Higgs mass prediction that deviates by 2 GeV or more from the full contribution. This happens for large trilinear couplings and large hierarchies between the soft masses. Points in this part of parameter space can suffer from

vacuum instability and flavour violating decay ratios that are outside of their experimental bounds. These conditions have to be checked in any realistic study.

We have explored the effects of the new corrections to the Higgs mass in various models beyond the MSSM and found throughout that they can change the mass prediction by several GeV under certain circumstances. In the NMSSM, the strong contributions $\mathcal{O}\left(\alpha_s(\alpha_t + \alpha_b)\right)$ and top Yukawa contributions $\mathcal{O}\left(\alpha_t^2\right)$ are dominant, similar to the MSSM. The newly accessible corrections are the Yukawa-like corrections with full dependence on the superpotential parameters λ, κ as well the NMSSM-specific orders $\mathcal{O}\left((\alpha_\lambda + \alpha_\kappa)^2\right)$. We found a difference of 1–2 GeV between the new and old calculation in the case of large λ and a significant mixing between the singlet and doublet scalar states of the Higgs sector. The remaining theoretical uncertainty of m_h was estimated by variation of the renormalisation scale as 2.3 GeV, which is almost certainly an underestimation. For example, the experimental uncertainty of the top mass has to be taken into account as the main source of uncertainty. Also, there could be higher order corrections that are scale-independent, and these would not show up in the estimate.

In the MSSM with R-parity violating operators $\lambda'\mathbf{LQD}$ and $\lambda''\mathbf{UDD}$, the new couplings λ', λ'' enter explicitly the Higgs self-energies at two-loop, but not at one-loop. As expected, large RPV couplings can change the Higgs mass prediction by several GeV. There is another (formally two-loop) effect due to the fact that RPV couplings (represented by Λ) enter the fermion one-loop self-energies. The matching conditions between the measured fermion pole masses and the Yukawa couplings depends on Λ and thus the top Yukawa coupling Y_t becomes a function of Λ, however this effect is very small in the NMSSM.

The MSSM can be extended by a pair of superfields with the same quantum numbers as the up-type superfield $\mathbf{U}$. This adds a fourth generation heavy top quark to the model along with two more up-type squarks. Because the impact of the top Yukawa coupling on the Higgs mass is already huge, adding another quark with similar coupling strength is an effective way to raise the Higgs mass. Previous calculations for this model included only the one-loop corrections with vanishing external momentum. We extended this calculation in three respects: (i) Full one-loop momentum dependence, (ii) threshold corrections and (iii) dominant two-loop corrections. As expected, all of these effects have a profound impact on the mass. In some regions, the two-loop shift alone accounts for a 10 GeV change. While in many cases the dominant two-loop corrections are purely MSSM-like (cf. eq. (7.1)), we identified regions where the contributions from the vectorlike quarks alone are comparable or larger. In addition vectorlike quarks reduce the fine-tuning (defined by eq. (2.30)) compared to the MSSM. For an embedding of the model in GMSB boundary conditions, we find a fine-tuning of ~ 600 for gluino masses around 1.5 TeV and a Higgs mass of 125 GeV. A higher gluino mass is accompanied by a higher fine-tuning: Requiring a 2 TeV gluino leads to a fine-tuning above 1000 and makes the model unfavourable. For comparison, realistic benchmark points in the MSSM typically have a FT of $800 - 1000$ [393], while in the context of minimal GMSB it can easily be of the order 10^5 [375]. A model with a fine-tuning below 100 could be called natural [392], however this number is somewhat arbitrary. Of course, fine-tuning can not be used to falsify a model, but it is rather an indication that a there is a hidden mechanism that is poorly described by the model.

In conclusion, the two-loop corrections that became available with the update to `SARAH` in Refs. [187, 188] are a step towards a precision calculation of the neutral Higgs mass. They contain all two-loop contributions except those that involve couplings of broken gauge groups, such as the electroweak couplings, and they are calculated for vanishing external momentum. The accuracy that could be reached with the corrections of eq. (7.1) for the MSSM ($\Delta m_h^{\text{th}} \sim 3$ GeV [195]) is

now extended to all models that can be handled by `SARAH`. Since the estimates that have been made for the MSSM do not necessarily carry over to other models, the real theoretical uncertainty is probably larger. Obviously, the gap between the experimental uncertainty $\Delta^{\mathrm{exp}} m_h = 320\,\mathrm{MeV}$ and a few GeV is still large. To close it, future work should be directed towards full electroweak corrections and more efficient ways to evaluate momentum dependence, because this is very time consuming. It can be expected that the theoretical uncertainty of m_h in the MSSM can drop to $0.5\,\mathrm{GeV}$, if all the mentioned two-loop effects are taken into account [120]. Several steps in this direction have been taken for MSSM codes. Also, `SARAH` can be extended to momentum dependent loop functions with an external library like TSIL [293]. However this approach is not yet well suited for useful applications because of computing time but it is likely that more efficient ways of evaluating momentum dependent loop functions will be developed. On the theoretical side, one must escape the gaugeless limit: Generic formulae for two-loop scalar self-energies and tadpoles are needed with full gauge coupling dependence. Additionally, the complete two-loop self-energy of the Z-boson is required, because it influences the electroweak VEV and these contributions are needed to ensure gauge invariance. With regard to precision, it is possible that dominant three-loop corrections are as important as the missing electroweak ones at two loop. However one must always remember that a limiting factor to the theoretical uncertainty of m_h is the error of the top quark mass m_t, which enters Higgs mass calculations via Y_t.

In chapter 6 of this thesis we have presented an approach to obtain upper production cross section limits on long-lived particles in the ATLAS and CMS detectors at the LHC. The idea is to simulate pairs of stable particles that escape undetected, leading to large quantities of missing transverse energy in the events. The production mechanism is model dependent and we considered two quite general scenarios: (i) strong production of a heavy scalar H^0 from effective vertices with subsequent decay $H^0 \to XX$ with X being the LL particle, and (ii) strong production of squark pairs $\tilde{Q}\tilde{Q}$ with subsequent decay into neutralinos and jets, $\tilde{Q} \to q\tilde{\chi}_1^0$. Applying several analyses from ATLAS and CMS on the generated signal events, we obtain 95% CL upper cross section limits by comparing the resulting efficiencies with the information provided in the corresponding publications of the analyses. This process is greatly simplified and automatised by the software `CheckMATE` [408]. The limits are valid for stable particles, but they can be extrapolated to smaller finite lifetimes by calculating the probability of both unstable particles escaping the detector. This requires the energy and rapidity distribution of the LL particles, which we extract from the Monte Carlo events, along with the dimensions of the detectors. Going to smaller lifetimes, the limits become weaker (larger), which is complementary to traditional long-lived particle searches focusing on displaced vertices. Combining both methods, the coverage of the LHC in terms of cross section limits can be extended to arbitrary lifetimes. In addition in displaced vertex searches assumptions about the decays of the LL particles must be made and for smaller assumed branching ratios the limits become weaker. This is not the case in our simple approach, because the decay of the LL particle happens outside the detector and has no influence on the missing transverse energy. Therefore, our limits are independent of the decay process and its branching ratio.

At the end of 2015, the ATLAS and CMS collaborations reported an excess at $750\,\mathrm{GeV}$ in the spectrum of diphoton final states [425, 426], which caused a tremendous amount of excitement in the scientific community. If this excess turns into a true discovery, this would be the first sign of physics beyond the Standard Model. In the aftermath of this announcement there was a tsunami of papers proposing extensions to the SM and MSSM to accommodate the diphoton

excess [427]. Dealing with a variety of different models is exactly the strength of the generic expressions implemented into `SARAH`, and the two-loop Higgs corrections might prove valuable to future studies in that field. For example, vectorlike quarks in combination with large Yukawa couplings are frequently used in attempts to describe the diphoton excess, from which we have learned that they have a large two-loop impact on the Higgs mass.

We hope that the 13 TeV era of the LHC holds even more surprises and the first proof of new physics.

Additional information

A.1 Renormalisation schemes

In the Standard Model and other non-supersymmetric models the modified minimal subtraction scheme $\overline{\text{MS}}$ [428] is the standard choice, using dimensional regularisation (DREG) in $d = 4 - 2\epsilon$ dimensions. Vector fields also have $4 - 2\epsilon$ degrees of freedom in this scheme. In a supersymmetric model, the use of DREG leads to a mismatch in the degrees of freedom between the vector fields and gaugino fields and thus to a violation of supersymmetry. The problem is solved by giving the vector fields the full four degrees of freedom, but still integrating over $d = 4 - 2\epsilon$ spacetime dimensions. This is known as dimensional reduction (DREG) [429, 430]. The extra 2ϵ components of the vector fields transform like scalars (known as epsilon scalars) in the adjoint representation of the gauge group. This scheme is called $\overline{\text{DR}}$ [429, 430] and used for models with unbroken supersymmetry.

However, every realistic model has to involve SUSY breaking, usually by explicit soft-breaking terms. In these models, the epsilon scalars do not have the same masses and dimensionful couplings as the corresponding vector fields. The unphysical scalars have to be carried around as independent particles, making this scheme inconvenient for broken SUSY. With a slight modification of the parameters, the masses of the epsilon scalars can be completely decoupled from all RG equations and the expressions for physical observables. This scheme known as $\overline{\text{DR}}'$ [431] is the best choice for all realistic SUSY models. Sometimes in literature this distinction is not made clear and authors stating to use $\overline{\text{DR}}$ in fact use the modified $\overline{\text{DR}}'$.

A.2 Ghost Lagrangian of the Standard Model

For completeness, we quote the definition of the ghost Lagrangian of Ref. [432] following the Fadeev-Popov description. Recalling the gauge fixing Lagrangian,

$$\mathcal{L}_{\text{GF}} = -\frac{1}{2\xi_G}F_G^2 - \frac{1}{2\xi_A}F_A^2 - \frac{1}{2\xi_Z}F_Z^2 - \frac{1}{\xi_W}F_-F_+, \tag{A.1}$$

$$F_G^a = \partial^\mu G_\mu^a, \quad F_A = \partial^\mu A_\mu, \tag{A.2}$$

$$F_Z = \partial^\mu Z_\mu - \xi_Z M_Z G^0, \tag{A.3}$$

$$F_\pm = \partial^\mu W_\mu^\pm \mp i\xi_W M_W G^\pm, \tag{A.4}$$

the ghost Lagrangian is given as

$$\mathcal{L}_{\text{ghost}} = \sum_{i=1}^{4} \left[\bar{c}_+ \frac{\partial(\delta F_+)}{\partial \alpha^i} + \bar{c}_- \frac{\partial(\delta F_+)}{\partial \alpha^i} + \bar{c}_Z \frac{\partial(\delta F_Z)}{\partial \alpha^i} + \bar{c}_A \frac{\partial(\delta F_A)}{\partial \alpha^i} \right] c_i$$
$$+ \sum_{a,b=1}^{8} \bar{\omega}^a \frac{\partial(\delta F_G^a)}{\partial \beta^b} \omega^b. \tag{A.5}$$

The ω^a are the ghosts associated with $SU(3)_C$ transformations

$$U = e^{-iT^a \beta^a} \quad (a = 1, \ldots, 8) \tag{A.6}$$

and $c_\pm, c_A, c_Z$ are the electroweak ghosts associated with the transformations

$$U = e^{-ig_2 T^a \alpha^a} \quad (a = 1, 2, 3), \qquad U = e^{+ig_1 Y \alpha^4}. \tag{A.7}$$

The notation δF denotes an infinitesimal gauge transformation.

A.3 Threshold corrections in the MSSM with vectorlike quarks

We discussed the importance of threshold corrections in the context of the MSSM extended by vectorlike quarks in section 5.4. They are the result of the matching between the measured quantities ($\alpha_{\text{em}}(M_Z)$, G_F, M_Z, $\alpha_s(M_Z)$, fermion masses) and the running parameters in the $\overline{\text{DR}}'$ scheme. We describe how the matching is done in `SARAH`/`SPheno`, following the generalised procedure of Ref. [199].

First, the α and α_s, given in the $\overline{\text{MS}}$ scheme in the five flavour approximation need to be matched to their $\overline{\text{DR}}'$ counterparts,

$$\alpha^{\overline{\text{DR}}'}(M_Z) = \frac{\alpha^{(5),\overline{\text{MS}}}(M_Z)}{1 - \Delta\alpha(M_Z)}, \tag{A.8a}$$

$$\alpha_s^{\overline{\text{DR}}'}(M_Z) = \frac{\alpha_s^{(5),\overline{\text{MS}}}(M_Z)}{1 - \Delta\alpha_s(M_Z)}. \tag{A.8b}$$

The quantities $\Delta\alpha(\mu)$ and $\Delta\alpha_s(\mu)$ for the minimal vectorlike quark model read

$$\Delta\alpha(\mu) = \frac{\alpha}{2\pi} \left[\frac{1}{3} - \frac{16}{9} \sum_{i=3}^{4} \log \frac{m_{u_i}}{\mu} - \frac{4}{9} \sum_{i=1}^{8} \log \frac{m_{\tilde{u}_i}}{\mu} + \Delta\alpha^{\text{MSSM}}(\mu) \right], \tag{A.9}$$

$$\Delta\alpha_s(\mu) = \frac{\alpha_s}{2\pi} \left[-\frac{2}{3} \sum_{i=3}^{4} \log \frac{m_{u_i}}{\mu} - \frac{1}{6} \sum_{i=1}^{8} \log \frac{m_{\tilde{u}_i}}{\mu} + \Delta\alpha_s^{\text{MSSM}}(\mu) \right]. \tag{A.10}$$

Here, $\Delta\alpha^{\text{MSSM}}(\mu), \Delta\alpha_s^{\text{MSSM}}(\mu)$ contain all corrections that appear in the MSSM (Ref. [199]), except for the up-quark and up-squark terms, which are explicitly written out. The vectorlike quarks enter these expressions in the extended sum ranges. To relate $\alpha^{\overline{\text{DR}}'}(M_Z)$ to the running couplings g_1, g_2, the running Weinberg angle $\sin\Theta_W^{\overline{\text{DR}}'}$ is needed along with the electroweak VEV

v. The latter depends on the loop corrections δM_Z^2 of the Z boson.

$$v^2 = (M_Z^2 + \delta M_Z^2) \frac{(1 - \sin^2 \Theta_W^{\overline{\text{DR}}'}) \sin^2 \Theta_W^{\overline{\text{DR}}'}}{\pi \alpha^{\overline{\text{DR}}'}} \tag{A.11}$$

$$\sin^2 \Theta_W^{\overline{\text{DR}}'} = \frac{1}{2} - \sqrt{\frac{1}{4} - \frac{\pi \alpha^{\overline{\text{DR}}'}}{\sqrt{2} M_Z^2 G_F (1 - \Delta_{\hat{r}})}} \tag{A.12}$$

Details about the one-loop corrections δM_Z^2 are shown in Ref. [299] and the expression for $\Delta_{\hat{r}}$ is found in Ref. [433]. The running fermion masses in $\overline{\text{DR}}'$ ($q = d, u, s, c, b$) are calculated from

$$m_q^{\overline{\text{DR}}',\text{SM}} = m_q \left[1 - \frac{\alpha_s^{\overline{\text{DR}}'}}{3\pi} + \Delta m_q^{(2),\text{QCD}} + \Delta m_q^{(2),\text{EW}} \right], \tag{A.13a}$$

$$m_t^{\overline{\text{DR}}',\text{SM}} = m_t \left[1 - \frac{\alpha_s^{\overline{\text{DR}}'}}{3\pi} \left(5 + 3 \log \frac{M_Z^2}{m_t^2} \right) + \Delta m_t^{(2),\text{QCD}} + \Delta m_t^{(2),\text{EW}} \right]. \tag{A.13b}$$

The QCD and EW two-loop parts are not shown here for brevity and can be found in Ref. [299], or Refs. [434, 435]. As a next step, the one-loop corrected fermion mass matrix is calculated,

$$\mathcal{M}_f^{(1L)}(p^2) = \mathcal{M}_f^{(0)} - \tilde{\Sigma}_S(p^2) - \tilde{\Sigma}_R(p^2) \mathcal{M}_f^{(0)} - \mathcal{M}_f \tilde{\Sigma}_L(p^2), \tag{A.14}$$

using only reduced self-energies $\tilde{\Sigma}_S(p^2), \tilde{\Sigma}_{L,R}(p^2)$, without pure QCD and EW contributions (they are already considered in the matching conditions, eq. (A.13)). The eigenvalues of $\mathcal{M}_f^{(1L)}(p^2)$ are matched to the previously calculated $\overline{\text{DR}}'$ SM fermion masses,

$$\text{Eig} \left[\mathcal{M}_d^{(1L)}(p^2 = m_{d_i}^2) \right] = (m_d^{\overline{\text{DR}}',\text{SM}}, m_s^{\overline{\text{DR}}',\text{SM}}, m_b^{\overline{\text{DR}}',\text{SM}}), \tag{A.15a}$$

$$\text{Eig} \left[\mathcal{M}_u^{(1L)}(p^2 = m_{u_i}^2) \right] = (m_u^{\overline{\text{DR}}',\text{SM}}, m_c^{\overline{\text{DR}}',\text{SM}}, m_t^{\overline{\text{DR}}',\text{SM}}, m_{t'}^{\overline{\text{DR}}'}). \tag{A.15b}$$

The tree-level mass matrices are given by the Yukawas, $\mathcal{M}_f^{(0)} = v_f Y_f / \sqrt{2}$ for $f = d, u$ and $\mathcal{M}_e^{(0)} = v_d Y_e / \sqrt{2}$. The equations (A.15) can be solved for the Yukawa matrices, where the CKM matrix can be used to constrain the rotation matrices U_L^q, U_R^q. Because the tree-level mass matrix and the self-energies both depend on the Yukawa matrices $Y_d^{\overline{\text{DR}}'}, Y_u^{\overline{\text{DR}}'}$, the solving procedure has to be done iteratively.

Once the running gauge and Yukawa couplings are determined at M_Z in $\overline{\text{DR}}'$, they are run up to M_{SUSY}, because some input parameters are defined only at M_{SUSY}. Then, the complete set of parameters is again run down to M_Z with two-loop RGEs, where the calculation of all other observables takes place.

Loop calculations

This chapter gives the definitions of the relevant loop functions. The second part (B.2) shows the calculation of the prefactors that are needed to express the effective potential in the spinor convention used by `SARAH`. In the third part (B.3) the collection of tadpoles and self-energies for the diagrammatic approach is presented, as it was published in Ref. [188]. In addition, we give the complete expressions for the tadpoles including massive vector bosons.

B.1 Basic loop functions

The loop function defined by Passarino and Veltman [264, 436] use the $(-, +, +, +)$ metric signature with $s = -p^2$. This is also preferred by Martin [266] whose calculations and definitions we use. In the main body of this thesis, the Bjorken-Drell metric $(+, -, -, -)$ is used instead ($s = p^2$). However, this does not pose a problem because the loop functions are defined in Euclidean space (after Wick rotation) and the results do not depend on the metric. One can use the Mandelstam variable s instead of $\pm p^2$ in final results for a metric independent expression.

Dimensional regularisation in $d = 4 - 2\epsilon$ dimensions is performed by the substitution

$$\int \mathrm{d}^4 q \to (2\pi\mu)^{2\epsilon} \int \mathrm{d}^d q. \tag{B.1}$$

It is useful to introduce the constant factor

$$C = 16\pi^2 \frac{\mu^{2\epsilon}}{(2\pi)^d} = (2\pi\mu)^{2\epsilon} \frac{1}{\pi^2}. \tag{B.2}$$

The scale μ is the regularisation scale, related to the renormalisation scale used in the $\overline{\text{MS}}$, $\overline{\text{DR}}$ and $\overline{\text{DR}}'$ schemes by

$$\log Q^2 = \log \mu^2 + \log(4\pi) - \gamma, \tag{B.3}$$

with γ the Euler-Mascheroni constant ($\Gamma'(1) = -\gamma$). The definition of eq. (B.3) is equivalent to encapsulating the two constants into the divergence using $\Delta = 1/\epsilon - \gamma + \log 4\pi$. For convenience, logarithms of dimensionful quantities are given in terms of

$$\overline{\ln}\left(m^2\right) \equiv \ln\left(\frac{m^2}{Q^2}\right). \tag{B.4}$$

Integrals with an explicit regulator are written in bold face, while finite integrals are written in normal typeface.

B.1.1 One-loop functions

The basic function for vacuum diagrams and tadpoles is $\mathbf{A}_0(m^2)$. The factor of i from Wick rotation is usually factored out to obtain a real function.

$$
\begin{aligned}
\mathbf{A}_0(m^2) &\equiv -\frac{1}{i} C \int \mathrm{d}^d q \frac{1}{q^2 - m^2} \\
&\xrightarrow{\text{Wick}} C \int \mathrm{d}^d r \frac{1}{r^2 + m^2} \\
&= m^2 \left(4\pi \frac{\mu^2}{m^2} \right)^\epsilon \left(-\frac{1}{\epsilon} - 1 + \gamma + \mathcal{O}(\epsilon) \right) \\
&= m^2 \left(-\frac{1}{\epsilon} + \overline{\ln}\left(m^2\right) - 1 \right) \\
&= -\frac{m^2}{\epsilon} + m^2 \left(\overline{\ln}\left(m^2\right) - 1 \right)
\end{aligned} \tag{B.5a}
$$

$$
A_0(m^2) = \mathbf{A}_0(m^2) + \frac{m^2}{\epsilon} = m^2 \left(\overline{\ln}(m)^2 - 1 \right) \tag{B.5b}
$$

$$
J(x) = A_0(x) = x \left(\overline{\ln}(x) - 1 \right) \tag{B.5c}
$$

Alternatively, $\mathbf{A}_0$ can be regularised with a cut-off Λ and $d = 4$,

$$
\begin{aligned}
\mathbf{A}_0(m^2) &= C \int \mathrm{d}^d r \frac{1}{r^2 + m^2} = \frac{1}{\pi^2} \int \mathrm{d}^4 r \frac{1}{r^2 + m^2} \\
&= 2 \int_0^\Lambda \mathrm{d}r \frac{r^3}{r^2 + m^2} = -2 \left[\frac{r^2}{2} - \frac{m^2}{2} \ln\left(m^2 + r^2\right) \right]_0^\Lambda \\
&= \Lambda^2 - m^2 \ln\left(\frac{\Lambda^2}{m^2} \right) + \mathcal{O}\left(\Lambda^{-2}\right).
\end{aligned} \tag{B.6}
$$

$$
\begin{aligned}
\mathbf{B}_0(s, x, y) &= \frac{1}{i} C \int \mathrm{d}^d q \frac{1}{q^2 - x} \frac{1}{(q - p)^2 - y} \\
&= \frac{(2\pi\mu)^{2\epsilon}}{i\pi^2} \int_0^1 \mathrm{d}\alpha \int \mathrm{d}^d q \frac{1}{(q^2 + \Delta)^2} \qquad \Delta \equiv (1 - \alpha)x + \alpha y - \alpha(1 - \alpha)s \\
&= \int_0^1 \mathrm{d}\alpha \left(\frac{4\pi\mu^2}{\Delta} \right)^\epsilon \left(\frac{1}{\epsilon} - \gamma \right) \\
&= \frac{1}{\epsilon} - \int_0^1 \mathrm{d}\alpha \, \overline{\ln}(\Delta) = \frac{1}{\epsilon} + B_0(s, x, y)
\end{aligned} \tag{B.7}
$$

Depending on the roots α_i of the quadratic function $\Delta(\alpha)$, it can be factorised and integrated [264], giving

$$B_0(s, x, y) = \mathbf{B_0}(s, x, y) - \frac{1}{\epsilon} = -\overline{\ln}(-s - i\epsilon) - \sum_i \left(\ln(1 - \alpha_i) + f(\alpha_i) \right), \tag{B.8a}$$

with

$$f(x) = F(1, x) = -x \ln \frac{x-1}{x} - 1, \tag{B.9a}$$

$$F(n, x) = -x^n \ln \frac{x-1}{x} - x^{n-1} - \frac{1}{2} x^{n-2} - \frac{1}{3} x^{n-3} \cdots - \frac{1}{n}, \tag{B.9b}$$

$$\int_0^1 x^n \ln(x - x_1) = \frac{1}{n+1} \left(\ln(1 - x_1) + F(n+1, x_1) \right). \tag{B.9c}$$

Using cut-off regularisation, the result is

$$\mathbf{B_0}(s, x, y) = \frac{1}{\pi^2} \int_0^1 d\alpha \int d^4 r \frac{1}{(r^2 + \Delta)^2} = 2 \int_0^1 d\alpha \int_0^\Lambda \frac{r^3}{(r^2 + \Delta)^2}$$

$$= 1 + \int_0^1 d\alpha \ln \left(\frac{\Delta + \Lambda^2}{\Delta} \right) \tag{B.10a}$$

$$\mathbf{B_0}(0, m^2, m^2) = \ln \frac{\Lambda^2 + m^2}{m^2} + 1 \tag{B.10b}$$

For $p^2 = 0$ we have

$$B_0(x, y) \equiv B_0(0, x, y) = -\int_0^1 d\alpha \overline{\ln} \left((1 - \alpha)x + \alpha y \right) = -\frac{J(x) - J(y)}{x - y}$$

$$= 1 - \left(x \overline{\ln}(x) - y \overline{\ln}(y) \right) / (x - y), \tag{B.11}$$

$$B_0(x, x) = -\overline{\ln}(x). \tag{B.12}$$

From this we can define

$$C_0(x, y, z) \equiv -\frac{B_0(x, y) - B_0(x, z)}{y - z} \tag{B.13}$$

which is symmetric in all arguments. C_0 corresponds to a loop with three external lines and vanishing external momenta.

B.1.2 Two-loop functions

We now define the two-loop functions, using the definition of Refs. [265, 266]. The index 0 means that the external momentum is set to zero, which is all that is needed for our purposes.

$$\mathbf{S}_0(x,y,z) = C^2 \int \mathrm{d}^d k \int \mathrm{d}^d q \frac{1}{(k^2+x)(q^2+y)((k+q)^2+z)}, \tag{B.14}$$

$$\mathbf{T}_0(x,y,z) = -\frac{\partial}{\partial x} \mathbf{S}_0(x,y,z), \tag{B.15}$$

$$\mathbf{U}_0(x,y,z,u) = C^2 \int \mathrm{d}^d k \int \mathrm{d}^d q \frac{1}{(k^2+x)(k^2+y)(q^2+z)((k+q)^2+u)}, \tag{B.16}$$

$$\mathbf{M}_0(x,y,z,u,v) = C^2 \int \mathrm{d}^d k \int \mathrm{d}^d q \frac{1}{(k^2+x)(q^2+y)(k^2+z)(q^2+u)((k-q)^2+v)}. \tag{B.17}$$

The master integral is finite, $\mathbf{M}_0 = M_0$, even for non-vanishing p^2. All integrals have various symmetries,

- $S_0(x,y,z)$ is completely symmetric,

- $T_0(x,y,z)$ is symmetric under $y \leftrightarrow z$,

- $U_0(x,y,z,u)$ is symmetric under $z \leftrightarrow u$ and $x \leftrightarrow y$,

- $M_0(x,y,z,u,v)$ is symmetric under $(z,x) \leftrightarrow (y,u)$, $(x,y) \leftrightarrow (z,u)$ and $(x,u) \leftrightarrow (y,z)$.

The snowman vacuum diagram (fig. 3.3) is simply the product of two $\mathbf{J}$ functions and a coupling,

$$J(x,y) = xy\left(\overline{\ln}(x) - 1\right)\left(\overline{\ln}(y) - 1\right) = J(x)J(y). \tag{B.18}$$

The sunrise diagram represents the function

$$
\begin{aligned}
I(x,y,z) \equiv & S_0(x,y,z) \\
= & \frac{1}{2}(x-y-z)\overline{\ln}(y)\overline{\ln}(z) + \frac{1}{2}(y-x-z)\overline{\ln}(x)\overline{\ln}(z) + \frac{1}{2}(z-x-y)\overline{\ln}(x)\overline{\ln}(y) \\
& + 2x\overline{\ln}(x) + 2y\overline{\ln}(y) + 2z\overline{\ln}(z) - \frac{5}{2}(x+y+z) - \frac{1}{2}\xi(x,y,z),
\end{aligned} \tag{B.19a}
$$

$$
\begin{aligned}
\xi(x,y,z) = R\Bigg(& 2\ln\left(\frac{x+z-y-R}{2z}\right)\ln\left(\frac{z+y-x-R}{2z}\right) - \ln\left(\frac{x}{z}\right)\ln\left(\frac{y}{z}\right) \\
& - 2\mathrm{Li}_2\left(\frac{x+z-y-R}{2z}\right) - 2\mathrm{Li}_2\left(\frac{z+y-x-R}{2z}\right) + \frac{\pi^2}{3}\Bigg),
\end{aligned} \tag{B.19b}
$$

$$\Delta(x,y,z) = x^2 + y^2 + z^2 - 2(xy + xz + yz), \tag{B.19c}$$

$$R(x,y,z) = \sqrt{\Delta(x,y,z)}. \tag{B.19d}$$

The dilogarithm is defined as

$$\mathrm{Li}_2(z) = -\int_0^z \frac{\ln(1-t)}{t}\mathrm{d}t. \tag{B.20}$$

and complex logarithms are defined by

$$-\pi < \Im\left(\ln(z)\right) \le \pi, \qquad z \in \mathbb{C}. \tag{B.21}$$

The functions are continuous for any real argument, but for negative arguments there will be an imaginary part. Also the limits for vanishing masses are often needed.

$$I(0, x, y) = (x - y) \left(\text{Li}_2 \left(\frac{y}{x} \right) - \ln \left(\frac{x}{y} \right) \overline{\ln} (x - y) + \frac{1}{2} \left(\overline{\ln} (x) \right)^2 - \frac{\pi^2}{6} \right)$$
$$- \frac{5}{2} (x + y) + 2x \overline{\ln} (x) + 2y \overline{\ln} (y) - x \overline{\ln} (x) \overline{\ln} (y) , \tag{B.22a}$$

$$I(0, x, x) = 2J(x) - 2x - \frac{J(x, x)}{x} = -x \left(\overline{\ln} (x) \right)^2 + 4x \overline{\ln} (x) - 5x, \tag{B.22b}$$

$$I(0, 0, x) = -\frac{1}{2} \left(\overline{\ln} (x) \right)^2 + 2x \overline{\ln} (x) - \frac{5}{2} x - \frac{\pi^2}{6} x, \tag{B.22c}$$

$$B_0(x, x) = -\overline{\ln} (x) . \tag{B.22d}$$

Furthermore, some functions are related to each other by the difference quotient operation.

$$T_0(x, y, z) = -\frac{\partial}{\partial x} I(x, y, z) \tag{B.23}$$

$$U_0(x, y, z, u) = -\mathcal{D}_{x,y} I(x, z, u) = \frac{1}{y - x} (I(x, z, u) - I(y, z, u)) \tag{B.24}$$

$$V_0(x, y, z, u) = -\frac{\partial}{\partial y} U_0(x, y, z, u) \tag{B.25}$$

$$M_0(x, y, z, u, v) = -\mathcal{D}_{y,u} U_0(x, z, y, v) = \frac{1}{(u - y)} (U_0(x, z, y, v) - U_0(x, z, u, v)) \tag{B.26}$$

$$\overline{T}_0(x, y) = \lim_{\delta \to 0} [T_0(\delta, x, y) + B_0(x, y) \overline{\ln} \delta] \tag{B.27}$$

These functions suffice as a basis for the various loop diagrams.

B.2 The two-loop effective potential in the `SARAH` convention

The two-loop effective potential for a general renormalisable theory calculated by Martin [265] uses a convention with real bosons and two-component fermions only. This convention, which we call the R-convention, is the most economic when dealing with a general theory. However, in a specific model it is more useful to organise particles into groups, including both real and complex scalars and vectors, as well as Majorana and Dirac fermions. We will call this the C-convention (C for complex). This section shows the calculation of prefactors that are required to translate the effective potential from the R-convention into the C-convention.

Note, the calculations shown here are lengthy and repetitive (presented in Ref. [187]). The interesting result is found in the summary tables of each subsection.

Within `SARAH`, the model description is done in the superfield formalism which uses two-component spinors. In the end, all fermions are expressed as four-component spinors which is better suited to describe the SM fermions. The vertex factor for three fields ϕ_1, ϕ_2, ϕ_3 is understood as

$$\mathcal{C} [\phi_1, \phi_2, \phi_3] = i \frac{\delta \mathcal{L}}{\delta \phi_1 \delta \phi_2 \delta \phi_3} \equiv i \Gamma c. \tag{B.28}$$

The vertex factor is decomposed into a kinematic part Γ and a coefficient. For example, two

Dirac fermions and a vector boson have a vertex factor

$$\mathcal{C}\left[\overline{\Psi}, \Psi, A_\mu\right] = i(c_L P_L + c_R P_R)\gamma^\mu. \tag{B.29}$$

P_L and P_R are the polarisation operators $P_{L,R} = \frac{1}{2}\left(1 \mp \gamma_5\right)$. The vertex factors of eq. (B.28) for particles `p1,p2,p3,(p4)` can be obtained in `SARAH` by the command

```
1  Vertex [{ p1 , p2 , p3 }]
2  Vertex [{ p1 , p2 , p3 , p4 }].
```

This returns a list

```
   { {p1[{i1}], p2[{i2}], p3[{i3}]},
     { {cL, GammaL},
       {cR, GammaR} }}
```

where the `i1,i2,i3` are tuples of internal indices. The Vertex function works for Dirac spinors as well as for two-component spinors because both definitions coexist internally. If ξ and χ are 2-component spinors with the same quantum numbers, a Dirac spinor can be constructed using the chiral representation

$$\Psi = \begin{pmatrix} \xi \\ \chi^\dagger \end{pmatrix}, \qquad \overline{\Psi} = \Psi^\dagger \gamma^0 = (\chi, \xi^\dagger) \tag{B.30}$$

with the translation table

$$\overline{\Psi}_i \gamma^\mu P_L \Psi_j = \xi_i^\dagger \bar{\sigma}^\mu \xi_j, \tag{B.31a}$$

$$\overline{\Psi}_i \gamma^\mu P_R \Psi_j = \chi_i \sigma^\mu \chi_j^\dagger, \tag{B.31b}$$

$$\overline{\Psi}_i P_L \Psi_j = \chi_i \xi_j, \tag{B.31c}$$

$$\overline{\Psi}_i P_R \Psi_j = \xi_i^\dagger \chi_j^\dagger \tag{B.31d}$$

with $\sigma^\mu = (1, \sigma^i)$ and $\bar{\sigma}^\mu = (1, -\sigma^i)$ and the Pauli matrices σ^i. A complex scalar can be split up like $\Phi(x) = (R(x) + iI(x))/\sqrt{2}$ such that Φ, R, I all have the same mass.

In the following we will set up a Lagrangian term $\delta\mathcal{L}$ for each interaction term in eq. (3.18) such that the output of a `SARAH` `Vertex` command (eq. (B.28)) would give ic or $ic_{L/R}$ in the C-convention. The value of c or $c_{L/R}$ will later be stored in a Fortran variable in `SPheno`. The Lagrangian term $\delta\mathcal{L}$ is then re-expressed in terms of real bosons and two-component fermions, such that the couplings can be matched to the R-convention. For the latter we will use capital indices I, J, K to label Weyl spinors ($\psi_I = (\xi_1, \chi_1, \xi_2, \chi_2, \dots)$) and real degrees of freedom ($R_K = (\varphi_1, \sigma_1, \varphi_2, \sigma_2, \dots)$). Lowercase indices i, j, k are used to denote generation/flavour/colour. For Majorana fermions and real scalars, this differentiation is not needed and the indices can be used interchangeably.

B.2.1 FFV and $\overline{FF}V$

Given a set of Dirac fermions Ψ_i and a complex vector W_μ^a, the Lagrangian term is

$$
\begin{aligned}
\mathcal{L}_{FFV} &= \bar{\Psi}_i \gamma^\mu (c_L P_L + c_R P_R) \Psi_j W_\mu^a + \text{h.c.} \\
&= c_L \xi_i^\dagger \bar{\sigma}^\mu \xi_j W_\mu^a + c_R \chi_i \sigma^\mu \chi_j^\dagger W_\mu^a + \text{h.c.} \\
&= c_L \xi_i^\dagger \bar{\sigma}^\mu \xi_j W_\mu^a - c_R \chi_j^\dagger \bar{\sigma}^\mu \chi_i W_\mu^a + \text{h.c.}
\end{aligned}
\tag{B.32}
$$

There is **no** implicit sum over i, j, a here. The coefficients are $c_{L/R} = c_{L/R}(i, j, a)$. The Minus sign comes from the rearrangement $\chi \sigma^\mu \xi^\dagger = -\xi^\dagger \bar{\sigma}^\mu \chi$ (in signatures with mostly plus as well as mostly minus). We can arrange all 2-component spinors in a list: $(\psi_I) = (\xi_1, \chi_1, \xi_2, \chi_2, \dots)$. The interaction in the R-convention is given by

$$
\mathcal{L}_{FFV} = \sum_{IJa} g_I^{aJ} \psi^{I\dagger} \bar{\sigma}^\mu \psi_J A_\mu^a.
\tag{B.33}
$$

Since this term has to be real, $g_I^{aJ} = (g_J^{aI})^\star$ holds. Vectors only couple left to left and right to right, so a rewriting of appendix B.2.1 is useful:

$$
\mathcal{L} = g_{Li}^{aj} \xi^{i\dagger} \bar{\sigma}^\mu \xi_j W_\mu^a + g_{Ri}^{aj} \chi^{i\dagger} \bar{\sigma}^\mu \chi_j W_\mu^a + \text{h.c.}.
\tag{B.34}
$$

We can match the coefficients using $W_\mu^a = (A_\mu^a + iB_\mu^a)/\sqrt{2}$ and writing $(A_\mu^A) = (A_\mu^1, B_\mu^1, A_\mu^2, \dots)$

$$
g_{Li}^{Aj} = \left(\frac{c_L}{\sqrt{2}}, i\frac{c_L}{\sqrt{2}} \right), \, A = 1, 2
\tag{B.35a}
$$

$$
g_{Ri}^{Aj} = \left(-\frac{c_R^*}{\sqrt{2}}, \frac{ic_R^*}{\sqrt{2}} \right), \, A = 1, 2.
\tag{B.35b}
$$

The original expression for $\overline{FF}V$ is given by

$$
V_{\overline{FF}V}^{(2)} = \frac{1}{2} \sum_{II'JJ'A} g_I^{AJ} g_{I'}^{AJ'} M^{II'} M_{JJ'}^\star F_{\overline{FF}V}(I, J, A).
\tag{B.36}
$$

M_{IJ} denotes a mass insertion, which in case of a single Dirac fermion is assumed to have the form $\begin{pmatrix} 0 & m_D \\ m_D & 0 \end{pmatrix}$ in the basis of the mass eigenstates. The whole expression becomes

$$
\begin{aligned}
V_{\overline{FF}V, i\neq j}^{(2)} &= \frac{1}{2} \sum_{I,J,I',J'} g_I^{aJ} g_{I'}^{aJ'} M^{II'} M_{JJ'}^\star F_{\overline{FF}V}(I, J, A) \\
&= \sum_A (g_{Li}^{Aj} g_{Ri}^{Aj} + \text{c.c.}) m_{Di} m_{Dj} F_{\overline{FF}V}(m_{Di}^2, m_{Dj}^2, m_A^2) \\
&= \left(-\frac{c_L c_R^*}{2} \cdot 2 + \text{c.c.} \right) m_{Di} m_{Dj} F_{\overline{FF}V}(i, j, a) \\
&= -2\Re[c_L c_R^*] m_{Di} m_{Dj} F_{\overline{FF}V}(i, j, a)
\end{aligned}
\tag{B.37}
$$

If we fix the same particle $i = j$, the factor 2 disappears.

$$V^{(2)}_{\overline{FFV},i=j} = -\Re[c_L c_R^*] m_{Di}^2 F_{\overline{FFV}}(i,i,a) \tag{B.38}$$

Starting with a real vector instead of a complex W_μ^a, we have $g_{Li}^{aj} = c_L$ and $g_{Ri}^{aj} = -c_R^*$, leading to a missing factor of $1/2$, but on the other hand there is also a missing factor of 2 from the sum over I, J, I', J'. Hence, the result is equal to (B.41) for $i \neq j$. If one of the fermions is a Majorana fermion, e.g. $\Psi_{Mi} = \begin{pmatrix} \xi_i \\ \xi_i^\dagger \end{pmatrix}$, then $\chi_j = \xi_j$ has to be replaced, but nothing else changes compared to (B.41) except that $m_{Dj} \to m_{Mj}$ becomes a Majorana mass. If both fermions are Majorana, the interaction terms are

$$\begin{aligned}
\mathcal{L}_{FFV} &= \bar\Psi_i \gamma^\mu (c_L P_L + c_R P_R) \Psi_j W_\mu^a + \text{h.c.} \\
&= c_L \xi_i^\dagger \bar\sigma^\mu \xi_j W_\mu^a - c_R \xi_j^\dagger \bar\sigma^\mu \xi_i W_\mu^a + \text{h.c.} \\
&= \frac{c_L - c_R^*}{\sqrt{2}} \xi_i^\dagger \bar\sigma^\mu \xi_j A_\mu^a + \frac{ic_L + ic_R^*}{\sqrt{2}} \xi_i^\dagger \bar\sigma^\mu \xi_j B_\mu^a + \text{h.c.}.
\end{aligned} \tag{B.39}$$

This gives the relation

$$g_{IJ}^A = \left(\frac{c_L - c_R^*}{\sqrt{2}}, i\frac{c_L + c_R^*}{\sqrt{2}} \right), \; A = 1, 2 \tag{B.40}$$

and leads to

$$\begin{aligned}
V^{(2)}_{\overline{FFV},i\neq j} &= \frac{1}{2} \sum_{IJI'J'A} g_I^{AJ} g_{I'}^{AJ'} M^{II'} M_{JJ'}^\star F_{\overline{FFV}}(I,J,A) \\
&= \frac{1}{2} \sum_A ((g_j^{Aj})^2 + (g_j^{Ai})^2) m_{Mi} m_{Mj} F_{\overline{FFV}}(i,j,A) \\
&= -2\Re[c_L c_R^*] m_{Mi} m_{Mj} F_{\overline{FFV}}(i,j,a).
\end{aligned} \tag{B.41}$$

If $i = j$, the line eq. (B.39) becomes

$$\begin{aligned}
\mathcal{L}_{\overline{FFV}} &= \underbrace{(c_L - c_R)}_{\equiv c} \xi_i^\dagger \bar\sigma^\mu \xi_i W_\mu^a + \text{h.c.} \\
&= \left(\frac{2\Re[c_L - c_R]}{\sqrt{2}} A_\mu^a + \frac{-2\Im[c_L - c_R]}{\sqrt{2}} B_\mu^a \right) \xi_i^\dagger \bar\sigma^\mu \xi_i \\
&= \sqrt{2} \left(\Re[c] A_\mu^a - \Im[c] B_\mu^a \right) \xi_i^\dagger \bar\sigma^\mu \xi_i.
\end{aligned} \tag{B.42}$$

The number $c = c_L - c_R$ is the observable coupling, giving

$$\begin{aligned}
V^{(2)}_{\overline{FFV}} &= \frac{1}{2} \sum_A (g_I^{AI})^2 |M_{II}|^2 F_{\overline{FFV}}(I,I,A) \\
&= |c|^2 m_{Mi}^2 F_{\overline{FFV}}(i,i,a).
\end{aligned} \tag{B.43}$$

In we consider only a real vector A_μ^a and $i \neq j$ from the start, the +h.c. can be dropped, and $c_R = -c_L^*$ must hold for a real Lagrangian, giving

$$
\begin{aligned}
V_{\overline{FFV}}^{(2)} &= \frac{1}{2}(c_L^2 + c_R^2) m_{Mi} m_{Mj} F_{\overline{FFV}}(i, j, a) \\
&= \Re[c_L^2] m_{Mi} m_{Mj} F_{\overline{FFV}}(i, j, a).
\end{aligned}
\tag{B.44}
$$

In the case $i = j$ we have $\mathcal{L} = (c_L - c_R)\xi_i^\dagger \bar{\sigma}^\mu \xi_i A_\mu^a$, requiring to redefine $c \equiv c_L - c_R$ as the observable coupling where c is a real number. Then, the coupling term is $\frac{1}{2}(c_L - c_R)^2 = \frac{1}{2}c^2$. Once the couplings of the different cases have been matched for the $\overline{FFV}$ case, it is straightforward to evaluate FFV:

$$
V_{FFV}^{(2)} = \frac{1}{2} \sum_{I,J,A} \left| g_I^{AJ} \right|^2 F_{FFV}(I, J, A) = K \cdot F_{FFV}(i, j, a)
\tag{B.45}
$$

$$
K = \frac{1}{2} \cdot 2 \sum_A \cdot \left(\left| g_{Li}^{Aj} \right|^2 + \left| g_{Ri}^{Aj} \right|^2 \right) = \left(|c_L|^2 + |c_R|^2 \right) \quad (D_i D_j c, D_i D_j r)
\tag{B.46a}
$$

$$
K = \frac{1}{2} \sum_A \cdot \left(\left| g_{Li}^{Aj} \right|^2 + \left| g_{Ri}^{Ai} \right|^2 \right) = \frac{1}{2} \left(|c_L|^2 + |c_R|^2 \right) \quad (D_i D_i c, D_i D_i r)
\tag{B.46b}
$$

$$
K = \frac{1}{2} \cdot 2 \sum_A \left| g_i^{Aj} \right|^2 = \left(\left| \frac{c_L - c_R^*}{\sqrt{2}} \right|^2 + \left| \frac{c_L + c_R^*}{\sqrt{2}} \right|^2 \right) = \left(|c_L|^2 + |c_R|^2 \right) \quad (M_i M_j c)
\tag{B.46c}
$$

$$
K = \frac{1}{2} \sum_A \left| g_i^{Ai} \right|^2 = |c|^2 \quad (M_i M_i c)
\tag{B.46d}
$$

$$
K = \frac{1}{2} \left(\left| g_i^{aj} \right|^2 + \left| g_j^{ai} \right|^2 \right) = \frac{1}{2} \left(|c_L|^2 + |c_R|^2 \right) = |c_L|^2 \quad (M_i M_j r)
\tag{B.46e}
$$

$$
K = \frac{1}{2} \left| g_i^{ai} \right|^2 = \frac{1}{2} |c|^2 \quad (M_i M_i r)
\tag{B.46f}
$$

The different cases are summarised in tab. B.1.

Example: In the case of the gluinos and gluons, the gauge interaction term is

$$
\mathcal{L}_{\text{Gluino}} = i g_3 f^{abc} \lambda^{a\dagger} \bar{\sigma}^\mu A_\mu^b \lambda^c,
\tag{B.47}
$$

with $g_c^{ba} = i g_3 f^{abc}$ and f^{abc} the structure constants of $SU(3)$. The result should be summed freely over a, b, c, thus a factor of $1/2$ must be introduced to avoid double counting. Evaluating

	D_iD_jc	D_iD_jr	D_iM_j	M_iM_jc	M_iM_jr
$V^{(2)}_{FFV}, i \neq j$	$(|c_L|^2 + |c_R|^2)$	$(|c_L|^2 + |c_R|^2)$	$(|c_L|^2 + |c_R|^2)$	$|c_L|^2 + |c_R|^2$	$|c|^2$
$V^{(2)}_{FFV}, i = j$	$\frac{1}{2}(|c_L|^2 + |c_R|^2)$	$\frac{1}{2}(|c_L|^2 + |c_R|^2)$	$-$	$|c|^2$	$\frac{1}{2}|c|^2$
$V^{(2)}_{\overline{FF}V}, i \neq j$	$-2\Re(c_L c_R^*)$	$-2\Re(c_L c_R^*)$	$-2\Re(c_L c_R^*)$	$-2\Re(c_L c_R^*)$	$\Re(c^2)$
$V^{(2)}_{\overline{FF}V}, i = j$	$-\Re(c_L c_R^*)$	$-\Re(c_L c_R^*)$	$-$	$|c|^2$	$\frac{1}{2}\Re(c^2)$
$V^{(2)}_{FFS}, i \neq j$	$(|c_L|^2 + |c_R|^2)$	$(|c_L|^2 + |c_R|^2)$	$(|c_L|^2 + |c_R|^2)$	$|c_L|^2 + |c_R|^2$	$|c|^2$
$V^{(2)}_{FFS}, i = j$	$(|c_L|^2 + |c_R|^2)$	$\frac{1}{2}(|c_L|^2 + |c_R|^2)$	$-$	$\frac{1}{2}(|c_L|^2 + |c_R|^2)$	$\frac{1}{2}|c|^2$
$V^{(2)}_{\overline{FF}S}, i \neq j$	$2\Re(c_L c_R^*)$	$2\Re(c_L c_R^*)$	$2\Re(c_L c_R^*)$	$2\Re(c_L c_R^*)$	$\Re((c)^2)$
$V^{(2)}_{\overline{FF}S}, i = j$	$2\Re(c_L c_R^*)$	$\Re(c_L c_R^*)$	$-$	$\Re(c_L c_R^*)$	$\frac{1}{2}\Re(c^2)$

Table B.1: Summary of FFV, $\overline{FF}V$, FFS, $\overline{FF}S$ contributions. The contribution is given by the prefactor that is multiplied with the loop function (times $m_i m_j$ for the $\overline{FF}V$, $\overline{FF}S$). $D_iD_jc(r)$ stands for Dirac fermions with complex (real) scalars or vectors, $M_iM_jc(r)$ for Majorana fermions.

eq. (B.44) gives

$$V^{(2)}_{\overline{FF}V,\tilde{g}} = \frac{1}{2}(-g_3^2)\underbrace{\left(\sum_{a,b,c=1}^{8} (f^{abc})^2\right)}_{=24} |M_3|^2 \, F_{\overline{FF}V}(M_3^2, M_3^2, 0)$$

$$= -12g^2 \left|M_3^2\right| F_{\overline{FF}V}(M_3^2, M_3^2, 0). \tag{B.48}$$

$$V^{(2)}_{FFV,\tilde{g}} = \frac{1}{2} \sum_{a,b,c} |c_L|^2 \, F_{FFV}(M_3^2, M_3^2, 0)$$

$$= \frac{1}{2}g_3^2 \sum_{a,b,c} \left|f^{abc}\right|^2 f(M_3^2, M_3^2, 0) = 12g^2 F_{FFV}(M_3^2, M_3^2, 0) \tag{B.49}$$

$$\Rightarrow V^{(2)}_{\tilde{g}\tilde{g}g} = 12g_3^2 \left(F_{FFV}(M_3^2, M_3^2, 0) - |M_3|^2 \, F_{\overline{FF}V}(M_3^2, M_3^2, 0)\right) \tag{B.50}$$

The result matches that of Ref. [209], Eq. (3.74).

B.2.2 FFS and $\overline{FF}S$

These contributions are similar in structure to FFV, $\overline{FF}V$. Consider a set of 4-component fermions Ψ_i and scalars $\phi_k = (\varphi_k + iI_k)/\sqrt{2}$. Again, for simplicity, consider i, j, k fixed.

$$
\begin{aligned}
\mathcal{L}_{FFS} &= -\overline{\Psi}_i(c_L P_L + c_R P_R)\Psi_j \cdot \phi_k + \text{h.c.} \\
&= -(c_L \chi_i \xi_j + c_R \xi_i^\dagger \chi_j^\dagger)\phi_k + \text{h.c.} \\
&= -(c_L \chi_i \xi_j \phi_k + c_R^* \xi_i \chi_j \phi_k^*) + \text{h.c.} \\
&= -\left(\frac{c_L}{\sqrt{2}}\chi_i \xi_j R_k + \frac{ic_L}{\sqrt{2}}\chi_i \xi_j I_k + \frac{c_R^*}{\sqrt{2}}\chi_j \xi_i R_k + \frac{-ic_R^*}{\sqrt{2}}\chi_j \xi_i I_k\right) + \text{h.c.} \tag{B.51}
\end{aligned}
$$

Note that scalars couple left to right handed parts. In R-convention all scalars are real, labelled as $R_K = (\varphi_1, I_1, \varphi_2, I_2 \ldots)$. In this convention, the interaction is given by

$$
\begin{aligned}
\mathcal{L}_{FFS} &= -\frac{1}{2} \sum_{I,J,K} y^{IJK} \psi_I \psi_J R_K + \text{h.c.} \\
&= -\frac{1}{2} \sum_{I,K} y^{IIK} (\psi_I)^2 R_K - \sum_{I<J,\ K} y^{IJK} \psi_I \psi_J R_K + \text{h.c.},
\end{aligned}
\tag{B.52}
$$

thus the coefficient of every term in appendix B.2.2 corresponds to a different y^{IJK} with $I < J$. The two-loop contributions to FFS and $\overline{FFS}$ are

$$
V^{(2)}_{FFS} = \frac{1}{2} \sum_{I,J,K} \left| y^{IJK} \right|^2 F_{FFS}(I, J, K),
\tag{B.53}
$$

$$
V^{(2)}_{\overline{FFS}} = \frac{1}{4} \sum_{I,J,K} y^{IJK} y^{I'J'k} M^*_{II'} M^*_{JJ'} F_{\overline{FFS}}(I, J, K) + \text{h.c.}
\tag{B.54}
$$

The sum runs freely over I, J, K. When evaluating this sum, a symmetry factor of 2 appears in B.53 because for each pair $I \neq J$ there is an equal term with I, J interchanged. In the $\overline{FFS}$ case, I can take 4 different indices, each of which gives the same expression in the sum.

$$
\begin{aligned}
V^{(2)}_{FFS} &= \left(\left| \frac{c_L}{\sqrt{2}} \right|^2 + \left| \frac{ic_L}{\sqrt{2}} \right|^2 + \left| \frac{c^*_R}{\sqrt{2}} \right|^2 + \left| \frac{-ic^*_R}{\sqrt{2}} \right|^2 \right) F_{FFS}(i, j, k) \\
&= (|c_L|^2 + |c_R|^2) F_{FFS}(i, j, k)
\end{aligned}
\tag{B.55}
$$

$$
\begin{aligned}
V^{(2)}_{\overline{FFS}} &= \left(\frac{c_L}{\sqrt{2}} \frac{c^*_R}{\sqrt{2}} + \frac{ic_L}{\sqrt{2}} \frac{-ic^*_R}{\sqrt{2}} \right) m_{Di} m_{Dj} F_{\overline{FFS}}(i, j, k) + \text{hc} \\
&= 2\Re(c_L c^*_R) m_{Di} m_{Dj} F_{\overline{FFS}}(i, j, k)
\end{aligned}
\tag{B.56}
$$

If the scalar is real instead of complex, the $\sqrt{2}$ will disappear everywhere and I_k can be dropped. This leads to the exact same results as eqs. (B.55) and (B.56). If there is one Dirac and one Majorana fermion, we can set $\chi_j = \xi_j$ in appendix B.2.2. The result also stays the same, eqs. (B.55) and (B.56). Considering two Majorana fermions, i.e. setting $\chi_j = \xi_j$ and $\chi_i = \xi_i$, we get

$$
\mathcal{L}_{FFS} = -\left(\frac{c_L + c^*_R}{\sqrt{2}} \xi_i \xi_j R_k + i \frac{c_L - c^*_R}{\sqrt{2}} \xi_i \xi_j I_k \right) + \text{h.c.}
\tag{B.57}
$$

Evaluating the contribution to the potential gives

$$
\begin{aligned}
V_{FFS}^{(2)} &= \left(\left| \frac{c_L + c_R^*}{\sqrt{2}} \right|^2 + \left| i \frac{c_L - c_R^*}{\sqrt{2}} \right|^2 \right) F_{FFS}(i,j,k) \\
&= \left(|c_L|^2 + |c_R|^2 \right) F_{FFS}(i,j,k), \quad (B.58) \\
V_{\overline{FFS}}^{(2)} &= \frac{1}{2} \sum_{I<J} (y^{IJK})^2 m_{Mi} m_{Mj} f_{\overline{FFS}}(i,j,k) + \text{h.c.} \\
&= \frac{1}{2} \left(\left(\frac{c_L + c_R^*}{\sqrt{2}} \right)^2 + \left(i \frac{c_L - c_R^*}{\sqrt{2}} \right)^2 \right) m_{Mi} m_{Mj} f_{\overline{FFS}}(i,j,k) + \text{h.c.} \\
&= 2\Re(c_L c_R^*) m_{Mi} m_{Mj} f_{\overline{FFS}}(i,j,k). \quad (B.59)
\end{aligned}
$$

If there are two Majoranas and one real scalar, the interaction would be

$$
\begin{aligned}
\mathcal{L} &= -\overline{\Psi}_i (c_L P_L + c_R P_R) \Psi_j R_k \\
&= -c_L \xi_i \xi_j R_k + c_R \xi_i^\dagger \xi_j^\dagger R_k. \quad (B.60)
\end{aligned}
$$

The complex conjugate is not needed, because the right-handed part already describes the conjugate if $c_R = c_L^*$ is imposed. The contribution to $V^{(2)}$ is

$$
\begin{aligned}
V_{FFS}^{(2)} &= |c_L|^2 F_{FFS}(i,j,k), \quad (B.61) \\
V_{\overline{FFS}}^{(2)} &= \frac{1}{2} (c_L)^2 m_{Mi} m_{Mj} F_{\overline{FFS}}(i,j,k) + \text{h.c.} \\
&= \Re((c_L)^2) m_{Mi} m_{Mj} F_{\overline{FFS}}(i,j,k). \quad (B.62)
\end{aligned}
$$

In the case of equal Dirac fermions and a complex scalar, the interaction Lagrangian will be

$$
\begin{aligned}
\mathcal{L}_{FFS} &= -\overline{\Psi}_i (c_L P_L + c_R P_R) \Psi_i \cdot \phi_k + \text{h.c.} \\
&= -\left(\frac{c_L + c_R^*}{\sqrt{2}} \chi_i \xi_i R_k + \frac{i(c_L - c_R^*)}{\sqrt{2}} \chi_i \xi_i I_k \right) + \text{h.c.}, \quad (B.63)
\end{aligned}
$$

which gives

$$
\begin{aligned}
V_{FFS}^{(2)} &= (|c_L|^2 + |c_R|) F_{FFS}(i,i,k), \quad (B.64) \\
V_{\overline{FFS}}^{(2)} &= \frac{1}{2} \left(\left(\frac{c_L + c_R^*}{\sqrt{2}} \right)^2 + \left(\frac{i(c_L - c_R^*)}{\sqrt{2}} \right)^2 \right) m_{Di}^2 F_{\overline{FFS}}(i,i,k) + \text{h.c.} \\
&= 2\Re(c_L c_R^*) m_{Di}^2 F_{\overline{FFS}}(i,i,k). \quad (B.65)
\end{aligned}
$$

In the case of equal Dirac fermions and a real scalar, the interaction Lagrangian is

$$
\begin{aligned}
\mathcal{L}_{FFS} &= -\overline{\Psi}_i (c_L P_L + c_R P_R) \Psi_i \cdot R_k + \text{h.c.} \\
&= -\left(c_L \chi_i \xi_i + c_R \chi_i^\dagger \xi_i^\dagger \right) R_k, \quad (B.66)
\end{aligned}
$$

where again $c_R = c_L^*$ is required. This leads to

$$
\begin{aligned}
V_{FFS}^{(2)} &= |c_L|^2 \, F_{FFS}(i,i,k) = \frac{1}{2}\left(|c_L|^2 + |c_R|^2\right) F_{FFS}(i,i,k), && \text{(B.67)} \\
V_{\overline{FFS}}^{(2)} &= \frac{1}{2}\,(c_L)^2\, m_{Di}^2 F_{\overline{FFS}}(i,i,k) + \text{h.c.} && \\
&= \Re((c_L)^2) m_{Di}^2 F_{\overline{FFS}}(i,i,k) = \Re(c_L c_R^*) m_{Di}^2 F_{\overline{FFS}}(i,i,k). && \text{(B.68)}
\end{aligned}
$$

Finally, there is the case of equal Majorana fermions and a complex scalar, where we have to start with a factor of $\frac{1}{2}$ in $\mathcal{L}$,

$$
\begin{aligned}
\mathcal{L}_{FFS} &= -\frac{1}{2}\overline{\Psi}_i(c_L P_L + c_R P_R)\Psi_i \phi_k + \text{h.c.} \\
&= -\frac{1}{2}\left(c_L \xi_i^2 + c_R (\xi_i^\dagger)^2\right)\phi_k + \text{h.c.} \\
&= -\frac{1}{2}\left(\frac{c_L + c_R^*}{\sqrt{2}}\xi_i^2 R_k + i\frac{c_L - c_R^*}{\sqrt{2}}\xi_i^2 I_k\right) + \text{h.c.} && \text{(B.69)}
\end{aligned}
$$

This time there is no symmetry factor in the sum over I, J, so we end up with

$$
\begin{aligned}
V_{FFS}^{(2)} &= \frac{1}{2}(|c_L|^2 + |c_R|^2)F_{FFS}(i,j,k), && \text{(B.70)} \\
V_{\overline{FFS}}^{(2)} &= \frac{1}{4}\,(2c_L c_R^*)\, m_{Mi}^2 F_{\overline{FFS}}(i,i,k) + \text{h.c.} && \\
&= \Re((c_L c_R^*) m_{Mi}^2 F_{\overline{FFS}}(i,i,k). && \text{(B.71)}
\end{aligned}
$$

If the scalar is real, we have $c_L = c_R^*$ and

$$
\begin{aligned}
\mathcal{L}_{FFS} &= -\frac{1}{2}\overline{\Psi}_i(c_L P_L + c_R P_R)\Psi_i R_k \\
&= -\frac{1}{2}c_L \xi_i^2 R_k + \text{h.c.}, && \text{(B.72)} \\
\Rightarrow V_{FFS}^{(2)} &= \frac{1}{2}\,|c_L|^2\, F_{FFS}(i,i,k), && \text{(B.73)} \\
\Rightarrow V_{\overline{FFS}}^{(2)} &= \frac{1}{4}\left(c_L^2\right) m_{Mi}^2 F_{\overline{FFS}}(i,i,k) + \text{h.c.} \\
&= \frac{1}{2}\Re(c_L^2)F_{\overline{FFS}}(i,i,k). && \text{(B.74)}
\end{aligned}
$$

The results for the coefficients are summarised in table B.1.

B.2.3 SSS

In the R-convention this interaction is given by

$$
\begin{aligned}
\mathcal{L} &= -\frac{1}{6}\lambda_{ijk} R_i R_j R_k \\
&= \sum_i (-\frac{1}{6}\lambda_{iii})R_i^3 + \sum_{i \neq j}(-\frac{1}{2}\lambda_{ijj})R_i R_j^2 + \sum_{i<j<k}(-\lambda_{ijk})R_i R_j R_k && \text{(B.75)}
\end{aligned}
$$

with three real scalars and λ_{ijk} symmetric. The contribution to V can be split up in a similar way,

$$
\begin{aligned}
V_{SSS} &= \frac{1}{12}\sum_{ijk}(\lambda_{ijk})^2 F_{SSS}(i,j,k) \\
&= \sum_{i<j<k}\frac{1}{2}(\lambda_{ijk})^2 F_{SSS}(i,j,k) + \sum_{i\neq j}\frac{1}{4}(\lambda_{ijj})^2 F_{SSS}(i,j,j) \\
&+ \sum_{i}\frac{1}{12}(\lambda_{iii})^2 F_{SSS}(i,i,i).
\end{aligned}
\tag{B.76}
$$

Consider complex scalars $\phi_i = (R_i + iI_i)/\sqrt{2}$.

$$
\begin{aligned}
\mathcal{L} &= c\phi_1\phi_2\phi_3 + \text{c.c.} \\
&= \frac{c}{2\sqrt{2}}(R_1R_2R_3 - (I_1I_2R_3 + I_2I_3R_1 + I_3I_1R_2) - i(I_1I_2I_3 - (R_1R_2I_3 + R_2R_3I_1 + R_3R_1I_2))) + \text{c.c.} \\
&= \frac{c+c^*}{2\sqrt{2}}(R_1R_2R_3 - (I_1I_2R_3 + I_2I_3R_1 + I_3I_1R_2)) \\
&+ (-i)\frac{c-c^*}{2\sqrt{2}}(I_1I_2I_3 - (R_1R_2I_3 + R_2R_3I_1 + R_3R_1I_2)) \\
&= \frac{\Re c}{\sqrt{2}}(R_1R_2R_3 - (I_1I_2R_3 + I_2I_3R_1 + I_3I_1R_2)) \\
&+ \frac{\Im c}{\sqrt{2}}(I_1I_2I_3 - (R_1R_2I_3 + R_2R_3I_1 + R_3R_1I_2))
\end{aligned}
\tag{B.77}
$$

Identifying the particles $R_1, R_2, R_3, I_1, I_2, I_3$ with labels $1\ldots 6$, we get

$$
\frac{\Re(c)}{\sqrt{2}} = -\lambda_{123} = \lambda_{453} = \lambda_{561} = \lambda_{642},
\tag{B.78}
$$

$$
\frac{\Im(c)}{\sqrt{2}} = -\lambda_{456} = \lambda_{126} = \lambda_{234} = \lambda_{315}.
\tag{B.79}
$$

The effective potential contribution is

$$
\begin{aligned}
V_{SSS} &= \frac{1}{12}(\lambda_{ijk})^2 F_{SSS}(i,j,k) \\
&= \sum_{i<j<k}\frac{1}{2}(\lambda_{ijk})^2 F_{SSS}(i,j,k) = (\Re(c)^2 + \Im(c)^2)F_{SSS}(m_1^2, m_2^2, m_3^2) \\
&= |c|^2 F_{SSS}(m_1^2, m_2^2, m_3^2).
\end{aligned}
\tag{B.80}
$$

Now consider one real scalar, $\phi_3 = R_3 \in \mathbb{R}$,

$$
\begin{aligned}
\mathcal{L} &= c\phi_1\phi_2\phi_3 + \text{c.c.} = \frac{c}{2}(R_1R_2 - I_1I_2 + i(R_1I_2 + R_2I_1))R_3 + \text{c.c.} \\
&= \Re(c)(R_1R_2 - I_1I_2)R_3 - \Im(c)(R_1I_2 + R_2I_1)R_3.
\end{aligned}
\tag{B.81}
$$

The remaining five real scalars $(R_1, R_2, R_3, I_1, I_2)$ are labelled $1 \ldots 5$.

$$
\begin{align}
\Re(c) &= -\lambda_{123} = \lambda_{345} \tag{B.82} \\
\Im(c) &= \lambda_{134} = \lambda_{234} \tag{B.83}
\end{align}
$$

Plugging this into (B.76), we get

$$
\begin{align}
V_{SSS} &= \frac{1}{12}(\lambda_{ijk})^2 F_{SSS}(i,j,k) = \sum_{i<j<k} \frac{1}{2}(\lambda_{ijk})^2 F_{SSS}(i,j,k) \tag{B.84} \\
&= (\Re(c)^2 + \Im(c)^2) F_{SSS}(m_1^2, m_2^2, m_3^2) = |c|^2 \, F_{SSS}(m_1^2, m_2^2, m_3^2), \tag{B.85}
\end{align}
$$

which is the same result as (B.80). There is an additional factor of 2 in the coupling, but there are only half the number of independent λ's. Now, in the case of two real fields ϕ_2, ϕ_3 and one complex field ϕ_1,

$$
\begin{align}
\mathcal{L} &= c\phi_1\phi_2\phi_3 + \text{c.c.} = \frac{c}{\sqrt{2}}(R_1 + iI_1)R_2R_3 + \text{c.c.} \\
&= \sqrt{2}\Re(c)R_1R_2R_3 + \sqrt{2}\Im(c)I_1R_2R_3, \tag{B.86} \\
\Rightarrow \quad & \sqrt{2}\Re(c) = -\lambda_{123}, \tag{B.87} \\
& \sqrt{2}\Im(c) = \lambda_{234}, \tag{B.88}
\end{align}
$$

there is again a factor of 2 and half the number of real field combinations. The result is the same as in (B.80),

$$
V_{SSS} = |c|^2 \, F_{SSS}(m_1^2, m_2^2, m_3^2). \tag{B.89}
$$

In the case of three real fields, c is real from the start and +c.c. can be omitted. There is only one $\lambda_{123} = -c$,

$$
V_{SSS} = \frac{1}{2}(c)^2 F_{SSS}(m_1^2, m_2^2, m_3^2). \tag{B.90}
$$

Now consider two equal complex scalars, $\phi_2 = \phi_3$.

$$
\begin{align}
\mathcal{L} &= \frac{c}{2}\phi_1\phi_2^2 + \text{c.c.} \\
&= \frac{\Re(c)}{2\sqrt{2}}(R_1 R_2^2 - (2I_1 I_2 R_2 + I_2^2 R_1)) \\
&\quad + \frac{\Im(c)}{2\sqrt{2}}(I_1 I_2^2 - (2R_1 R_2 I_2 + R_2^2 I_1)) \tag{B.91} \\
\Rightarrow \quad & \frac{\Re(c)}{\sqrt{2}} = -\lambda_{122} = -\lambda_{155} = \lambda_{245} \tag{B.92} \\
& \frac{\Im(c)}{\sqrt{2}} = -\lambda_{455} = \lambda_{125} = \lambda_{224} \tag{B.93}
\end{align}
$$

Plugging this into (B.76), we obtain

$$
\begin{aligned}
V_{SSS} &= \sum_{i\neq j}\frac{1}{4}(\lambda_{ijj})^2 F_{SSS}(i,j,j) + \sum_{i<j<k}\frac{1}{2}(\lambda_{ijk})^2 F_{SSS}(i,j,k) \\
&= \frac{1}{2}|c|^2\, F_{SSS}(m_1^2,m_2^2,m_2^2)
\end{aligned}
\tag{B.94}
$$

with a factor of $\frac{1}{2}$ compared to (B.80). If $\phi_1 = R_1$ is real instead of complex, $\mathcal{L}$ reads

$$
\begin{aligned}
\mathcal{L} &= \frac{c}{2}R_1\phi_2^2 + \text{c.c.} \\
&= \frac{\Re(c)}{2}(R_1 R_2^2 - R_1 I_2^2) - \Im(c)R_1 R_2 I_2, \tag{B.95} \\
\Rightarrow\quad \Re(c) &= -\lambda_{133} = +\lambda_{144}, \tag{B.96} \\
\Im(c) &= -\lambda_{134}, \tag{B.97} \\
\Rightarrow V_{SSS} &= \sum_{i\neq j}\frac{1}{4}(\lambda_{ijj})^2 F_{SSS}(i,j,j) + \sum_{i<j<k}\frac{1}{2}(\lambda_{ijk})^2 F_{SSS}(i,j,k) \\
&= \frac{1}{2}|c|^2\, F_{SSS}(m_1^2,m_2^2,m_2^2). \tag{B.98}
\end{aligned}
$$

In the case of two equal real scalars $R_2 = R_3$ and one complex scalar ϕ_1, we get

$$
\begin{aligned}
\mathcal{L} &= \frac{c}{2}\phi_1 R_2^2 + \text{c.c.} \\
&= \frac{\Re(c)}{\sqrt{2}}(R_1 R_2^2) + \frac{\Im(c)}{\sqrt{2}}(I_1 I_2^2), \tag{B.99} \\
\Rightarrow\quad \frac{\Re(c)}{\sqrt{2}} &= -\frac{1}{2}\lambda_{122}, \qquad \frac{\Im(c)}{\sqrt{2}} = -\frac{1}{2}\lambda_{455} \tag{B.100}
\end{aligned}
$$

and

$$
\begin{aligned}
V_{SSS} &= \sum_{i\neq j}\frac{1}{4}(\lambda_{ijj})^2 F_{SSS}(i,j,j) \\
&= \frac{1}{2}|c|^2\, F_{SSS}(m_1^2,m_2^2,m_2^2). \tag{B.101}
\end{aligned}
$$

Turning ϕ_1 into a real scalar will produce only one term $(\frac{c}{2}R_1 R_2^2)$ with a real $c = -\lambda_{122}$. This gives

$$
\begin{aligned}
V_{SSS} &= \sum_{i\neq j}\frac{1}{4}(\lambda_{ijj})^2 F_{SSS}(i,j,j) \\
&= \frac{1}{4}|c|^2\, F_{SSS}(m_1^2,m_2^2,m_2^2). \tag{B.102}
\end{aligned}
$$

Consider three equal complex scalars $\phi_1 = \phi_2 = \phi_3$.

$$
\begin{aligned}
\mathcal{L} &= \frac{c}{6}\phi_1^3 + \text{c.c.} \\
&= \frac{\Re(c)}{6\sqrt{2}}(R_1^3 - 3R_1 I_1^2) - \frac{\Im(c)}{6\sqrt{2}}(3R_1 I_1^2 - I_1^3) \tag{B.103}
\end{aligned}
$$

$$
\Rightarrow \frac{\Re(c)}{\sqrt{2}} = -\lambda_{111} = \lambda_{122} \tag{B.104}
$$

$$
\frac{\Im(c)}{\sqrt{2}} = -\lambda_{222} = \lambda_{112} \tag{B.105}
$$

$$
\Rightarrow V_{SSS} = \left(\frac{1}{8} + \frac{1}{24}\right)|c|^2 F_{SSS}(m^2, m^2, m^2) = \frac{1}{6}|c|^2 F_{SSS}(m^2, m^2, m^2) \tag{B.106}
$$

At last, if there are three equal real scalars, we get

$$
\mathcal{L} = \frac{c}{6}R_1^3, \tag{B.107}
$$

$$
\Rightarrow c = -\lambda_{111}, \tag{B.108}
$$

$$
\Rightarrow V_{SSS} = \sum_i \frac{1}{12}(\lambda_{iii})^2 F_{SSS}(m^2, m^2, m^2). \tag{B.109}
$$

All these results are summarised in tab. B.2.

fields	all different	two equal	all equal ($\phi_1 = \phi_2 = \phi_3$)
$\phi_{1,2,3} \in \mathbb{C}$	1	$1/2$	$1/6$
$\phi_{1,2} \in \mathbb{C}, \phi_3 \in \mathbb{R}$	1	$1/2$	-
$\phi_1 \in \mathbb{C}, \phi_{2,3} \in \mathbb{R}$	1	$1/2$	-
$\phi_{1,2,3} \in \mathbb{R}$	$1/2$	$1/4$	$1/12$

Table B.2: Prefactors for SSS contributions. The contribution is given by $V_{SSS}^{(2)} = k \cdot |c|^2 F_{SSS}(m_1^2, m_2^2, m_3^2)$, where m_i is the mass of ϕ_i. The table shows k for various cases.

B.2.4 SS

The SS contribution is given by

$$
V_{SS}^{(2)} = \frac{1}{8}\sum_{ij}\lambda^{iijj}F_{SS}(m_i^2, m_j^2). \tag{B.110}
$$

In the R-convention this interaction is described by

$$
\mathcal{L} = -\frac{1}{24}\sum_{ijkl}\lambda^{ijkl}R_i R_j R_K R_l \tag{B.111}
$$

with a real and completely symmetric λ^{ijkl}. Picking out only terms where $i = j$ and $k = l$ (both fixed), the sum reads

$$
\mathcal{L} = -\frac{1}{4}\lambda^{iijj}R_i^2 R_j^2 \quad \textbf{(no sum, } i \neq j\textbf{).} \tag{B.112}
$$

If all four scalars are equal, the term is just

$$\mathcal{L} = -\frac{1}{24}\lambda^{iiii}R_i^4 \quad \textbf{(no sum).} \tag{B.113}$$

Because there are only two scalars in the loop, we only have to distinguish the cases of different scalars and equal scalars. In the C-convention with two complex scalars ϕ_1, ϕ_2 we have

$$\mathcal{L} = c\,|\phi_1|^2\,|\phi_2|^2\,, \tag{B.114}$$

$$\mathcal{L} = \frac{c}{4}\,|\phi_1|^4 \quad \text{(equal scalars)}, \tag{B.115}$$

where c is the vertex factor in both cases. Introducing $\phi_i = (R_i + iI_i)/\sqrt{2}$ gives

$$\mathcal{L} = \frac{c}{4}\left(R_1^2 + I_1^2\right)\left(R_2^2 + I_2^2\right), \tag{B.116}$$

$$\mathcal{L} = \frac{c}{16}\left(R_1^4 + I_1^4 + 2R_1^2 I_1^2\right) \quad \text{(equal scalars)}. \tag{B.117}$$

With this equation, the conventions can be matched. All real scalars (R_1, R_2, I_1, I_2) can be labelled with indices $1, 2, 3, 4$. The coefficients are

$$-c = \lambda^{1122} = \lambda^{1144} = \lambda^{3322} = \lambda^{3344} \quad \text{(different scalars)}, \tag{B.118}$$

$$-c = \frac{2}{3}\lambda^{1111} = \frac{2}{3}\lambda^{2222} = 2\lambda^{1122} \quad \text{(equal scalars)}. \tag{B.119}$$

Now simplify the contribution eq. (B.110) for complex different scalars. There is a factor of 2 because of the symmetry in i, j.

$$
\begin{aligned}
V_{SS}^{(2)} &= \frac{1}{8}\lambda^{iijj}F_{SS}(i,j) \\
&= 2\cdot\frac{1}{8}\left(\lambda^{1122} + \lambda^{1144} + \lambda^{3322} + \lambda^{3344}\right)F_{SS}(i,j) \\
&= -cF_{SS}(i,j)
\end{aligned} \tag{B.120}
$$

Now repeat the calculation for two equal complex scalars:

$$
\begin{aligned}
V_{SS}^{(2)} &= \frac{1}{8}\lambda^{iijj}F_{SS}(i,j) \\
&= \frac{1}{8}\left(\lambda^{RRRR} + \lambda^{IIII} + 2\lambda^{RRII}\right)F_{SS}(i,i) \\
&= -\frac{1}{8}\left(\frac{3}{2}c + \frac{3}{2}c + c\right)F_{SS}(i,i) \\
&= -\frac{1}{2}cF_{SS}(i,i).
\end{aligned} \tag{B.121}
$$

For one real (R_2) and one complex scalar, we get

$$
\begin{aligned}
\mathcal{L} &= \frac{c}{2}|\phi_1|^2 R_2^2 \\
&= \frac{c}{4}(R_1^2 + I_1^2)R_2^2, \tag{B.122}
\end{aligned}
$$

$$
\Rightarrow -c = \lambda^{1122} = \lambda^{2233}, \tag{B.123}
$$

$$
\Rightarrow V_{SS}^{(2)} = 2 \cdot \frac{1}{8}\left(\lambda^{1122} + \lambda^{2233}\right) F_{SS}(i,j) = -\frac{c}{2}F_{SS}(i,j). \tag{B.124}
$$

In the case of two real scalar R_1, R_2, we get

$$
\mathcal{L} = \frac{c}{4}R_1^2 R_2^2, \tag{B.125}
$$

$$
\Rightarrow -c = \lambda^{1122}, \tag{B.126}
$$

$$
\Rightarrow V_{SS}^{(2)} = 2 \cdot \frac{1}{8}\left(\lambda^{1122}\right) F_{SS}(i,j) = -\frac{c}{4}F_{SS}(i,j), \tag{B.127}
$$

and finally, for two equal real scalars $R_1 = R_2$,

$$
\mathcal{L} = \frac{c}{24}R_1^4, \tag{B.128}
$$

$$
\Rightarrow -c = \lambda^{1111}, \tag{B.129}
$$

$$
\Rightarrow V_{SS}^{(2)} = \frac{1}{8}\left(\lambda^{1111}\right) F_{SS}(i,i) = -\frac{c}{8}F_{SS}(i,i). \tag{B.130}
$$

The results for SS are summarised in tab. B.3.

fields	$\phi_{1,2}$ different	$\phi_1 = \phi_2$ equal
$\phi_{1,2} \in \mathbb{C}$	1	1/2
$\phi_1 \in \mathbb{C}, \phi_2 \in \mathbb{R}$	1/2	-
$\phi_{1,2} \in \mathbb{R}$	1/4	1/8

Table B.3: Prefactors for SS. The contribution is $V_{SS}^{(2)} = k \cdot (-c)F_{SS}(m_1^2, m_2^2)$. The table shows k for various cases.

B.2.5 VS

The VS contribution is given by

$$
V_{VS}^{(2)} = \frac{1}{4}\sum_{a,i}(g^{aaii})^2 F_{VS}(m_a^2, m_i^2). \tag{B.131}
$$

In the R-convention this interaction is described by

$$
\mathcal{L} = -\frac{1}{4}\sum_{a,i} g^{aaii}(A_\mu^a)^2 R_i^2. \tag{B.132}
$$

	k
V, S complex	1
one real, one complex	$1/2$
V, S real	$1/4$

Table B.4: Prefactor k for the $V_{VS}^{(2)}$ contribution.

Starting with a single complex vector W_a^μ and complex scalar ϕ_i, the interaction reads

$$\mathcal{L} = c\,|W_a^\mu|^2\,|\phi_i|^2 = \frac{c}{4}\left((A_a^\mu)^2 + (B_a^\mu)^2 + R_i^2 + I_i^2)\right), \tag{B.133}$$

which gives $g^{aaii} = c$. In this case, the sum in eq. (B.131) counts four identical terms, giving

$$V_{VS}^{(2)} = k \cdot \sum_{a,i} c^2 F_{VS}(m_a^2, m_i^2) \tag{B.134}$$

with $k = 1$. If one of the particles is real, one needs to start with a factor $\frac{1}{2}$ in the interaction to keep $g^{aaii} = c$. The sum in eq. (B.131) only counts two identical terms, resulting in $k = \frac{1}{2}$. If both particles are real, the prefactor in the interaction needs to be $\frac{1}{4}$ and the contribution has $k = \frac{1}{4}$. The cases are summarised in table B.4.

B.2.6 SSV

In C-convention, the interaction between two complex scalars ϕ_i, ϕ_j and a complex vector $W_\mu^a = (A_\mu^a + iB_\mu^a)/\sqrt{2}$ is described by

$$\mathcal{L}_{SSV} = c\phi_i \overleftrightarrow{\partial^\mu} \phi_j W_\mu^a + \text{h.c.} \tag{B.135}$$

with $c = c(a, i, j)$ (a, i, j fixed) and $f\overleftrightarrow{\partial^\mu}g = f\partial^\mu g - g\partial^\mu f$. The same interaction in the R-convention is given by

$$\mathcal{L}_{SSV} = -\sum_{A,I,J} g_{IJ}^A A_\mu^A R_I \partial^\mu R_J, \tag{B.136}$$

with $g_{IJ}^A = -g_{JI}^A$, real scalars R_I and real vectors A_μ^A. The potential in the R-convention is

$$V_{SSV}^{(2)} = \frac{1}{4}\sum_{A,I,J} (g_{IJ}^A)^2 F_{SSV}(I, J, A). \tag{B.137}$$

Now break down eq. (B.135) to real parts,

$$
\begin{aligned}
\mathcal{L}_{SSV} &= c\phi_i \overleftrightarrow{\partial^\mu} \phi_j W_\mu^a + \text{h.c.} \\
&= \frac{c}{2\sqrt{2}}(R_i + iI_i)\overleftrightarrow{\partial^\mu}(R_j + iI_j)(A_\mu^a + iB_\mu^a) + \text{h.c.} \\
&= \frac{\Re(c)}{\sqrt{2}}\left((R_i\overleftrightarrow{\partial^\mu}R_j - I_i\overleftrightarrow{\partial^\mu}I_j)A_\mu^a - (R_i\overleftrightarrow{\partial^\mu}I_j + I_i\overleftrightarrow{\partial^\mu}R_j)B_\mu^a\right) \\
&\quad - \frac{\Im(c)}{\sqrt{2}}\left((I_i\overleftrightarrow{\partial^\mu}R_j + R_i\overleftrightarrow{\partial^\mu}I_j)A_\mu^a + (R_i\overleftrightarrow{\partial^\mu}R_j - I_i\overleftrightarrow{\partial^\mu}I_j)B_\mu^a\right).
\end{aligned} \tag{B.138}
$$

There are four terms for each $\Re(c)$ and $\Im(c)$ which all involve different fields, thus evaluating eq. (B.137) gives

$$V_{SSV}^{(2)} \;=\; 2 \cdot \frac{1}{4} \left(4 \left(\frac{\Re(c)}{\sqrt{2}} \right)^2 + 4 \left(\frac{\Im(c)}{\sqrt{2}} \right)^2 \right) = |c|^2 \, F_{SSV}(i,j,a), \qquad (B.139)$$

with a symmetry factor of 2 because of $g_{IJ}^A = -g_{JI}^A$. If the two scalars are complex conjugates of each other, $\phi_j = \phi_i^*$, appendix B.2.6 reduces to

$$\rightarrow \quad \frac{\Re(c)}{\sqrt{2}} \left(-(R_i \overleftrightarrow{\partial^\mu}(-I_i) + I_i \overleftrightarrow{\partial^\mu} R_i) B_\mu^a \right) - \frac{\Im(c)}{\sqrt{2}} \left((I_i \overleftrightarrow{\partial^\mu} R_i + R_i \overleftrightarrow{\partial^\mu}(-I_i)) A_\mu^a \right) \quad (B.140)$$

$$= \quad \frac{2\Re(c)}{\sqrt{2}} \left(R_i \overleftrightarrow{\partial^\mu} I_i B_\mu^a \right) - \frac{2\Im(c)}{\sqrt{2}} \left(I_i \overleftrightarrow{\partial^\mu} R_i A_\mu^a \right), \qquad (B.141)$$

which gives

$$V_{SSV}^{(2)} \;=\; 2 \cdot \frac{1}{4} \left(2 \left(\Re(c) \right)^2 + 2 \left(\Im(c) \right)^2 \right) = |c|^2 \, F_{SSV}(i,j,a). \qquad (B.142)$$

However, if the vector is real and $\phi_i = \phi_j^*$, (B.138) becomes

$$\mathcal{L}_{SSV} \;=\; ic(I_i \overleftrightarrow{\partial^\mu} R_i) A_\mu^a + \text{h.c.}, \qquad (B.143)$$

where the Hermitean conjugate can be dropped if c is chosen purely imaginary from the start. If that is the case,

$$V_{SSV}^{(2)} = \frac{1}{2} |c|^2 \, F_{SSV}(i,j,a). \qquad (B.144)$$

If another field is considered real, a factor of $\sqrt{2}$ disappears in the denominator and we end up with half the terms in $\mathcal{L}$, which gives again $V_{SSV}^{(2)} = |c|^2 \, F_{SSV}(i,j,a)$. Note that for two real equal scalars, $\mathcal{L}_{SSV}$ vanishes. All the cases are collected in tab. B.5.

Example: $\tilde{q}_i^b, \tilde{q}_i^{c*}, g^a$ with $c = -\frac{g_3}{2}(\lambda^a)_{cb}$ and λ^a the Gell-Mann matrices.

$$\Rightarrow V_{\tilde{q}_i \tilde{q}_i^* g}^{(2)} \;=\; \frac{1}{2} \left| \frac{g_3}{2} \right|^2 \underbrace{\left(\sum_{a=1}^{8} \sum_{b,c=1}^{3} |\lambda_{bc}^a|^2 \right)}_{16} F_{SSV}(\tilde{q}_i, \tilde{q}_i, 0) \qquad (B.145)$$

$$= \quad 2g_3^2 F_{SSV}(\tilde{q}, \tilde{q}, 0) \quad \text{c.f. [209], (3.48).} \qquad (B.146)$$

fields	k
ϕ_i, ϕ_j, V	1
$\phi_i = \phi_j^*, V \in \mathbb{C}$	1
$\phi_i = \phi_j^*, V \in \mathbb{R}$	$1/2$
else	1

Table B.5: This table gives k for the SSV contribution, $V_{SSV}^{(2)} = k \cdot |c|^2 \, F_{SSV}(i,j,a)$.

B.3 Self-energies and tadpoles at two loops

In this section we list the results for the first and second derivatives of the effective potential. Although the expressions are largely identical to those calculated in Ref. [267] (with zero external momentum), we give the full set for completeness. Further, some expressions are considerably simplified compared to Ref. [267], but fully equivalent.

B.3.1 First derivatives of the effective potential (tadpoles)

The complete first derivative splits up in the following terms, each corresponding to a tadpole diagram,

$$\frac{\partial V^{(2)}}{\partial R_p^0} = N_{rp}^{(S)}[T_S + T_{SSFF} + T_{FFFS} + T_{SSV} + T_{VS} + T_{VVS} + T_{FFV} + T_{\overline{FF}V} + T_{\text{gauge}}]. \tag{B.147}$$

T_S contains purely scalar diagrams,

$$T_S = T_{SS} + T_{SSS} + T_{SSSS}, \tag{B.148}$$

$$T_{SS} = \frac{1}{4}\lambda^{ikjj}\lambda^{ikr}f_{SS}^{(1,0)}(m_i^2, m_k^2; m_j^2), \tag{B.149}$$

$$T_{SSS} = \frac{1}{6}\lambda^{rijk}\lambda^{ijk}f_{SSS}(m_i^2, m_j^2, m_k^2), \tag{B.150}$$

$$T_{SSSS} = \frac{1}{4}\lambda^{rii'}\lambda^{ijk}\lambda^{i'jk}f_{SSS}^{(1,0,0)}(m_i^2, m_{i'}^2; m_j^2, m_k^2). \tag{B.151}$$

The new loop functions are defined as

$$f_{SS}^{(1,0)}(x, y; z) \equiv -B_0(x, y)J(z), \tag{B.152}$$

$$f_{SSS}^{(1,0,0)}(x, y; u, v) \equiv U_0(x, y, u, v). \tag{B.153}$$

Next, the diagrams with only fermions and scalars are given by

$$T_{SSFF} = \frac{1}{2}y^{IJk}y_{IJl}f_{FFS}^{0,0,1}(m_I^2, m_J^2; m_k^2, m_l^2)\lambda^{klr}$$
$$- \left[\frac{1}{2}y^{IJk}y^{I'J'k}M_{II'}^*M_{JJ'}^*\lambda^{klr}U_0(m_l^2, m_k^2, m_I^2, m_J^2) + \text{c.c.}\right], \tag{B.154}$$

$$T_{FFFS} = 2\text{Re}[y^{IJr}y_{IKm}y^{KLm}M_{JL}^*]T_{F\overline{F}FS}(m_I^2, m_J^2, m_K^2, m_m^2)$$
$$+ 2\text{Re}[y_{IJr}y^{IKm}y^{JLm}M_{KL}^*]T_{FF\overline{F}S}(m_I^2, m_J^2, m_K^2, m_m^2)$$
$$- 2\text{Re}[y^{IJr}y^{KLm}y^{MNm}M_{IK}^*M_{JM}^*M_{LN}^*]T_{\overline{FFF}S}(m_I^2, m_J^2, m_L^2, m_m^2), \tag{B.155}$$

where the following definitions were used,

$$
\begin{aligned}
f_{FFS}^{(1,0,0)}(m_{I'}^2, m_I^2, m_J^2; m_k^2) \equiv &- B_0(m_{I'}^2, m_I^2)J(m_J^2) + B_0(m_{I'}^2, m_I^2)J(m_k^2) + I(m_{I'}^2, m_J^2, m_k^2) \\
&- (m_I^2 + m_J^2 - m_k^2)U_0(m_{I'}^2, m_I^2, m_J^2, m_k^2),
\end{aligned}
$$

$$
\begin{aligned}
f_{FFS}^{(0,0,1)}(m_I^2, m_J^2; m_k^2, m_l^2) \equiv & B_0(m_l^2, m_k^2)J(m_I^2) + B_0(m_l^2, m_k^2)J(m_J^2) - I(m_I^2, m_J^2, m_l^2) \\
&- (m_I^2 + m_J^2 - m_k^2)U_0(m_l^2, m_k^2, m_I^2, m_J^2),
\end{aligned}
$$

$$
T_{\overline{FFFS}}(m_I^2, m_J^2, m_L^2, m_m^2) \equiv U_0(m_I^2, m_J^2, m_L^2, m_m^2),
$$

$$
T_{F\overline{F}FS}(m_I^2, m_J^2, m_K^2, m_m^2) \equiv f_{FFS}^{(1,0,0)}(m_I^2, m_J^2, m_K^2; m_m^2),
$$

$$
T_{FF\overline{F}S}(m_I^2, m_J^2, m_K^2, m_m^2) \equiv I(m_I^2, m_K^2, m_m^2) - m_I^2 U_0(m_I^2, m_J^2, m_K^2, m_m^2). \tag{B.156}
$$

Lastly, the tadpoles with vector bosons are given. In the cause of unbroken gauge groups, T_{FFV} and $T_{\overline{FF}V}$ can be combined into T_{FV},

$$
\begin{aligned}
T_{SSV} =& \frac{g^2}{2}d(i)C(i)\lambda^{iir}\left(3I(0, m_i^2, m_i^2) - J(m_i^2) + 2m_i^2\right) \\
=& \frac{g^2}{2}d(i)C(i)\lambda^{iir}m_i^2\Big[-12 + 11\log m_i^2/Q^2 - 3\log^2 m_i^2/Q^2)\Big],
\end{aligned} \tag{B.157}
$$

$$
T_{FV} = g^2 d(I)C(I)\mathrm{Re}(M_{II'}y^{II'r})4\left(-3I(0, m_I^2, m_I^2) + 5J(m_I^2) - 4m_I^2 + \delta_{\overline{\mathrm{MS}}}[2J(m_I^2) + m_I^2]\right) \tag{B.158}
$$

$$
= g^2 d(I)C(I)\mathrm{Re}(M_{II'}y^{II'r})4m_I^2\Big[6 - 7\log m_I^2/Q^2 + 3\log^2 m_I^2/Q^2 + \delta_{\overline{\mathrm{MS}}}[2\log m_I^2/Q^2 - 1]\Big].
$$

B.3.2 Tadpoles with broken gauge groups

It is likely that the two-loop calculation of `SARAH/SPheno` will be extended to broken gauge groups in the near future. Therefore, it is necessary to calculate the first derivatives of the effective potential for the case of massive vector bosons. This work was partially done in Ref. [188], resulting in the following expressions,

$$
T_{SSV} = \frac{1}{2}g^{aij}g^{akj}\lambda^{ikr}f_{SSV}^{(1,0,0)}(m_i^2, m_k^2; m_j^2, m_a^2) + \frac{1}{4}g^{aij}g^{bij}g^{abr}f_{SSV}^{(0,0,1)}(m_i^2, m_j^2; m_a^2, m_b^2), \tag{B.159}
$$

$$
T_{VS} = \frac{1}{4}g^{abii}g^{abr}f_{VS}^{(1,0)}(m_a^2, m_b^2; m_i^2) + \frac{1}{4}g^{aaik}\lambda^{ikr}f_{VS}^{(0,1)}(m_a^2; m_i^2, m_k^2), \tag{B.160}
$$

$$
T_{VVS} = \frac{1}{2}g^{abi}g^{cbi}g^{acr}f_{VVS}^{(1,0,0)}(m_a^2, m_c^2; m_b^2, m_i^2) + \frac{1}{4}g^{abi}g^{abj}\lambda^{ijr}f_{VVS}^{(0,0,1)}(m_a^2, m_b^2; m_i^2, m_j^2), \tag{B.161}
$$

$$
\begin{aligned}
T_{FFV} =& 2g_I^{aJ}\overline{g}_{bJ}^K\mathrm{Re}(M_{KI'}y^{I'Ir})f_{FFV}^{(1,0,0)}(m_I^2, m_K^2; m_J^2, m_a^2) \\
&+ \frac{1}{2}g_I^{aJ}\overline{g}_{bJ}^I g^{abr}f_{FFV}^{(0,0,1)}(m_I^2, m_J^2; m_a^2, m_b^2),
\end{aligned} \tag{B.162}
$$

$$
\begin{aligned}
T_{FFV} =\,& 2g_I^{aJ}\bar{g}_{bJ}^{K}\mathrm{Re}(M_{KI'}y^{I'Ir})f_{FFV}^{(1,0,0)}(m_I^2,m_K^2;m_J^2,m_a^2)\\
&+\frac{1}{2}g_I^{aJ}\bar{g}_{bJ}^{I}g^{abr}f_{FFV}^{(0,0,1)}(m_I^2,m_J^2;m_a^2,m_b^2),
\end{aligned}
\tag{B.163}
$$

$$
\begin{aligned}
T_{\overline{FF}V} =\,& g_I^{aJ}g_{I'}^{aJ'}\mathrm{Re}(y^{II'r}M_{JJ'}^{*})\big[f_{\overline{FF}V}(m_I^2,m_J^2,m_a^2)+M_I^2 f_{\overline{FF}V}^{(1,0,0)}(m_I^2,m_{I'}^2;m_J^2,m_a^2)\big]\\
&+g_I^{aJ}g_{I'}^{aJ'}\mathrm{Re}(M^{IK'}M^{KI'}M_{JJ'}^{*}y_{KK'r})f_{\overline{FF}V}^{(1,0,0)}(m_I^2,m_{I'}^2;m_J^2,m_a^2)\\
&+\frac{1}{2}g_I^{aJ}g_{I'}^{bJ'}g^{abr}M^{II'}M_{JJ'}^{*}f_{\overline{FF}V}^{(0,0,1)}(m_I^2,m_J^2;m_a^2,m_b^2),
\end{aligned}
\tag{B.164}
$$

$$
T_{\mathrm{gauge}} =\frac{1}{4}g^{abc}g^{dbc}g^{adr}f_{\mathrm{gauge}}^{(1,0,0)}(m_a^2,m_d^2;m_b^2,m_c^2).
\tag{B.165}
$$

However, the emerging derivatives of the loop functions $f_{SSV}, f_{VS}, f_{FFV}, f_{\overline{FF}V}, f_{\mathrm{gauge}}$ were not calculated. This is done in this thesis for the first time. Note that the tadpole corrections are needed in this form even for a full momentum dependent calculation. In the $\overline{\mathrm{MS}}$ scheme the functions have extra terms

$$
f_{X,\overline{\mathrm{MS}}} = f_{X,\overline{\mathrm{DR}}'} + \Delta_{\overline{\mathrm{MS}}}f_X
$$

which are needed for non-supersymmetric models. First, we quote the loop functions from the effective potential as published in Ref. [265]. Here we include the $\overline{\mathrm{MS}}$ term with a $\delta_{\overline{\mathrm{MS}}}$ that can be 0 for $\overline{\mathrm{DR}}'$ and 1 for $\overline{\mathrm{MS}}$.

$$
\begin{aligned}
f_{SSV} =\,&\frac{1}{z}\Big[-\Delta(x,y,z)I(x,y,z)+(x-y)^2 I(0,x,y)\\
&+(y-x-z)J(x,z)+(x-y-z)J(y,z)+zJ(x,y)\Big]\\
&+2(x+y-z/3)J(z),
\end{aligned}
\tag{B.166}
$$

$$
f_{VS} =3J(x,y)+\delta_{\overline{\mathrm{MS}}}2xJ(y),
\tag{B.167}
$$

$$
\begin{aligned}
f_{VVS} =\,&\frac{1}{4xy}\big[(-\Delta(x,y,z)-12xy)I(x,y,z)\\
&+(x-z)^2 I(0,x,z)+(y-z)^2 I(0,y,z)-z^2 I(0,0,z)\\
&+(z-x-y)J(x,y)+yJ(x,z)+xJ(y,z)\big]\\
&+\frac{1}{2}J(x)+\frac{1}{2}J(y)+\delta_{\overline{\mathrm{MS}}}\left(2J(z)-x-y-z\right),
\end{aligned}
\tag{B.168}
$$

$$
\begin{aligned}
f_{FFV} =\,&\frac{1}{z}\big[(\Delta(x,y,z)-3z^2+3xz+3yz))I(x,y,z)-(x-y)^2 I(0,x,y)\\
&+(x-y-2z)J(x,z)+(y-x-2z)J(y,z)+2zJ(x,y)\big]\\
&+2(-x-y+z/3)J(z)+\delta_{\overline{\mathrm{MS}}}\left(-2xJ(x)-2yJ(y)+(x+y)^2-z^2\right),
\end{aligned}
\tag{B.169}
$$

$$
f_{\overline{FF}V} =6I(x,y,z)+\delta_{\overline{\mathrm{MS}}}\left(2(x+y+z)-4J(x)-4J(y)\right),
\tag{B.170}
$$

$$f_{\text{gauge}} = \frac{1}{4xyz}\Big\{(-x^4 - 8x^3y - 8x^3z + 32x^2yz + 18y^2z^2)I(x,y,z)$$
$$+ (y-z)^2(y^2 + 10yz + z^2)I(0,y,z) + x^2(2yz - x^2)I(0,0,x)$$
$$+ (x^2 - 9y^2 - 9z^2 + 9xy + 9xz + 14yz)xJ(y,z)$$
$$+ (22y + 22z - 40x/3)xyzJ(x)\Big\} + (x \leftrightarrow y) + (x \leftrightarrow z)$$
$$+ \delta_{\overline{\text{MS}}}\Big(x^2 + 12yz + 2xJ(x) + (x \leftrightarrow y) + (x \leftrightarrow z)\Big), \tag{B.171}$$

where $\Delta(x,y,z) \equiv x^2 + y^2 + z^2 - 2xy - 2xz - 2yz$. What we need is the result of applying the operators $\mathcal{D}_{x,u}$ and $\mathcal{D}_{z,u}$ (defined by eq. (3.53)) on all of these functions (for f_{gauge} only one derivative is needed). It is highly useful to make systematic use of the product rule (eq. (3.54)) and the following list of replacement rules,

$$\mathcal{D}_{x,u}J(x) = -B_0(x,u), \tag{B.172}$$
$$\mathcal{D}_{x,u}J(x,y) = -B_0(x,u)J(y), \tag{B.173}$$
$$\mathcal{D}_{x,u}I(x,y,z) = -U_0(x,u,y,z), \tag{B.174}$$
$$\Delta(x,y,z) = x^2 + y^2 + z^2 - 2(xy - yz - xz), \tag{B.175}$$
$$\Delta(x,y,0) = (x-y)^2, \tag{B.176}$$
$$\mathcal{D}_{x,u}\Delta(x,y,z) = x + u - 2(y+z), \tag{B.177}$$
$$\mathcal{D}_{z,u}\frac{1}{z} = \left(\frac{1}{z} - \frac{1}{u}\right)\frac{1}{z-u} = -\frac{1}{zu}, \tag{B.178}$$
$$\mathcal{D}_{z,u}\frac{\Delta(x,y,z)}{z} = 1 - \frac{\Delta(x,y,0)}{zu}. \tag{B.179}$$

The functions f_{VS} and $f_{\overline{FFV}}$ have the simplest structure and are easy to differentiate.

$$f_{VS}^{(1,0)}(x,u;y) = \mathcal{D}_{x,u}f_{VS}(x,y) = -3B_0(x,u)J(y) + \delta_{\overline{\text{MS}}}2J(y), \tag{B.180}$$
$$f_{VS}^{(0,1)}(x,y,u) = \mathcal{D}_{y,u}f_{VS}(x,y) = -3J(x)B_0(y,u) + \delta_{\overline{\text{MS}}}\left(-2xB_0(y,u)\right), \tag{B.181}$$
$$f_{\overline{FFV}}^{(1,0,0)}(x,u;y,z) = \mathcal{D}_{x,u}f_{\overline{FFV}}(x,y,z) = -6U_0(x,u,y,z) + \delta_{\overline{\text{MS}}}\left[2 + 4B_0(x,u)\right], \tag{B.182}$$
$$f_{\overline{FFV}}^{(0,0,1)}(x,y,z,u) = \mathcal{D}_{z,u}f_{\overline{FFV}}(x,y,z) = -6U_0(x,y,z,u) + 2\delta_{\overline{\text{MS}}}. \tag{B.183}$$

The other functions are more complicated combinations of polynomials and loop functions.

$$f_{SSV,\overline{\text{DR}}'}^{(1,0,0)}(x,u;y,z)$$
$$= \frac{1}{z}(-\mathcal{D}_{x,u}\Delta(x,y,z))I(x,y,z) - \frac{1}{z}\Delta(u,y,z)(\mathcal{D}_{x,u}I(x,y,z))$$
$$+ \frac{1}{z}(\mathcal{D}_{x,u}\Delta(x,y,0))I(x,y,0) + \frac{1}{z}(\mathcal{D}_{x,u}I(x,y,0))\Delta(u,y,0) - \frac{1}{z}J(x,z)$$
$$+ \frac{1}{z}(y-u-z)\mathcal{D}_{x,u}J(x,z) + \frac{1}{z}J(y,z) + \mathcal{D}_{x,u}J(x,y) + 2J(z)$$
$$= \frac{1}{z}\left[-(x+u-2(y+z))I(x,y,z) + \Delta(u,y,z)U_0(x,u,y,z) - J(x,z)\right.$$
$$\left. -(y-u-z)B_0(x,u)J(z) + J(y,z)\right] - B_0(x,u)J(y) + 2J(z) \tag{B.184}$$

$$f_{SSV,\overline{\mathrm{DR}}'}^{(0,0,1)}(x,y,z,u)$$

$$
\begin{aligned}
=& - \mathcal{D}_{z,u}\frac{\Delta(x,y,z)}{z}I(x,y,z) - \frac{\Delta(x,y,u)}{u}\mathcal{D}_{z,u}I(x,y,z) - \frac{(x-y)^2}{zu}I(x,y,0) \\
&+ \frac{y-x-u}{u}\mathcal{D}_{z,u}J(x,z) + \left(-\frac{y-x}{zu}\right)J(x,z) + \frac{x-y-u}{u}\mathcal{D}_{z,u}J(y,z) + \left(-\frac{x-y}{zu}\right)J(y,z) \\
&+ 2\left(x-y-\frac{u}{3}\right)\mathcal{D}_{z,u}J(z) - \frac{2}{3}J(z) \\
=& -\frac{1}{z}\left(z+u-2(x+y)-\frac{\Delta(x,y,u)}{u}\right)I(x,y,z) + \frac{\Delta(x,y,u)}{u}U_0(z,u,y,x) - \frac{(x-y)^2}{zu}I(x,y,0) \\
&- \frac{y-x-u}{u}J(x)B_0(z,u) - \frac{y-x}{zu}J(x,z) - \frac{x-y-u}{u}J(y)B_0(z,u) - \frac{x-y}{zu}J(y,z) \\
&- 2\left(x-y-\frac{u}{3}\right)B_0(z,u) - \frac{2}{3}J(z)
\end{aligned}
\tag{B.185}
$$

The function f_{SSV} is equal in the $\overline{\mathrm{MS}}$ and $\overline{\mathrm{DR}}'$ schemes, $\Delta_{\overline{\mathrm{MS}}}f_{SSV}=0$.

$$f_{FFV,\overline{\mathrm{DR}}'}^{(1,0,0)}(x,u;y,z)$$

$$
\begin{aligned}
=& \left(3 + \frac{1}{z}\mathcal{D}_{x,u}\Delta(x,y,z)\right)I(x,y,z) + \frac{\Delta(u,y,z)-3z^2+3uz+3yz}{z}\mathcal{D}_{x,u}I(x,y,z) \\
&- \frac{1}{z}(\mathcal{D}_{x,u}\Delta(x,y,0))I(x,y,0) \\
&- \frac{1}{z}(\mathcal{D}_{x,u}I(x,y,0))\Delta(u,y,0) + \frac{1}{z}J(x,z) + \frac{u-y-2z}{z}\mathcal{D}_{x,u}J(x,z) \\
&- \frac{1}{z}J(y,z) + 2\mathcal{D}_{x,u}J(x,y) - 2J(z) \\
=& \left(3 + \frac{x+u-2(y+z)}{z}\right)I(x,y,z) - \frac{\Delta(u,y,z)-3z^2+3uz+3yz}{z}U_0(x,u,y,z) \\
&- \frac{x+u-2y}{z}I(x,y,0) + \frac{(u-y)^2}{z}U_0(x,u,y,0) \\
&+ \frac{J(x,z)-J(y,z)}{z} - \frac{u-y-2z}{z}B_0(x,u)J(z) - 2B_0(x,u)J(y) - 2J(z)
\end{aligned}
\tag{B.186}
$$

$$f_{FFV,\overline{\mathrm{DR}}'}^{(0,0,1)}(x,y,z,u)$$

$$= \left[\mathcal{D}_{z,u} \frac{\Delta(x,y,z)}{z} - 3 \right] I(x,y,z) + \left[\frac{\Delta(x,y,u)}{u} - 3(u-x-y) \right] \mathcal{D}_{z,u} I(x,y,z) + \frac{(x-y)^2}{zu} I(x,y,0)$$

$$- \frac{x-y}{zu} J(x,z) + \frac{x-y-2u}{u} \mathcal{D}_{z,u} J(x,z) - \frac{y-x}{zu} J(y,z) + \frac{y-x-2u}{u} \mathcal{D}_{z,u} J(y,z)$$

$$+ \frac{2}{3} J(z) - 2(x+y-\frac{u}{3}) \mathcal{D}_{z,u} J(z)$$

$$= - \left[2 + \frac{\Delta(x,y,0)}{zu} \right] I(x,y,z) + \left[\frac{\Delta(x,y,u)}{u} - 3(u-x-y) \right] U_0(z,u,x,y)$$

$$+ \frac{(x-y)^2}{zu} I(x,y,0) - \frac{x-y}{zu} \left[J(x,z) - J(y,z) \right] - \frac{x-y}{u} B_0(z,u) \left[J(x) - J(y) \right]$$

$$+ 2B_0(z,u) \left[J(x) + J(y) \right] + \frac{2}{3} J(z) + 2(x+y-\frac{u}{3}) B_0(z,u) \qquad (B.187)$$

The function f_{FFV} has a non-vanishing $\overline{\mathrm{MS}}$ correction,

$$\Delta_{\overline{\mathrm{MS}}} f_{FFV} = - 2xJ(x) - 2yJ(y) + (x+y)^2 - z^2, \qquad (B.188)$$

$$\mathcal{D}_{x,u} \Delta_{\overline{\mathrm{MS}}} f_{FFV} = - 2J(x) + 2uB_0(x,u) + x + u + 2y, \qquad (B.189)$$

$$\mathcal{D}_{z,u} \Delta_{\overline{\mathrm{MS}}} f_{FFV} = - z - u. \qquad (B.190)$$

$$f_{VVS,\overline{\mathrm{DR}}'}^{(1,0,0)}(x,u;y,z)$$

$$= \left[-\frac{1}{4y} \left(1 - \frac{\Delta(y,z,0)}{xu} \right) \right] I(x,y,z) + \left[-\frac{\Delta(u,y,z)}{4uy} - 3 \right] \mathcal{D}_{x,u} I(x,y,z)$$

$$+ \frac{1}{4y} \left(1 - \frac{z^2}{xu} \right) I(0,x,z) + \frac{(u-z)^2}{4uy} \mathcal{D}_{x,u} I(0,x,z)$$

$$- \frac{(y-z)^2}{4xuy} I(0,y,z) + \frac{z^2}{4xuy} I(0,0,z) - \frac{z-y}{4xuy} J(x,y) + \frac{z-u-y}{4uy} \mathcal{D}_{x,u} J(x,y)$$

$$- \frac{1}{4xu} J(x,z) + \frac{1}{4u} \mathcal{D}_{x,u} J(x,z) + \frac{1}{2} \mathcal{D}_{x,u} J(x)$$

$$= - \frac{1}{4y} \left(1 - \frac{\Delta(y,z,0)}{xu} \right) I(x,y,z) + \left[3 + \frac{\Delta(u,y,z)}{4uy} \right] U_0(x,u,y,z)$$

$$+ \frac{1}{4y} \left(1 - \frac{z^2}{xu} \right) I(0,x,z) - \frac{(u-z)^2}{4uy} U_0(x,u,z,0)$$

$$- \frac{(y-z)^2}{4xuy} I(0,y,z) + \frac{z^2}{4xuy} I(0,0,z) - \frac{z-y}{4xuy} J(x,y) - \frac{z-u-y}{4uy} B_0(x,u) J(y)$$

$$- \frac{1}{4xu} J(x,z) - \frac{1}{4u} B_0(x,u) J(z) - \frac{1}{2} B_0(x,u). \qquad (B.191)$$

$$f_{VVS,\overline{\mathrm{DR}}'}^{(0,0,1)}(x,y,z,u)$$

$$= -\frac{z+u-2(y+x)}{4xy}I(x,y,z) + \left[-\frac{\Delta(x,y,u)}{4xy} - 3\right]\mathcal{D}_{z,u}I(x,y,z)$$

$$+ \frac{z+u-2x}{4xy}I(0,y,z) + \frac{(y-u)^2}{4xy}\mathcal{D}_{z,u}I(0,y,z) - \frac{z+u}{4xy}I(0,0,z) - \frac{u^2}{4xy}\mathcal{D}_{z,u}I(0,0,z)$$

$$+ \frac{1}{4xy}J(x,y) + \frac{1}{4x}\mathcal{D}_{z,u}J(x,z) + \frac{1}{4y}\mathcal{D}_{z,u}J(y,z)$$

$$= -\frac{z+u-2(y+x)}{4xy}I(x,y,z) + \left[\frac{\Delta(x,y,u)}{4xy} + 3\right]U_0(z,u,x,y)$$

$$+ \frac{z+u-2x}{4xy}I(0,y,z) - \frac{(y-u)^2}{4xy}U_0(z,u,y,0) - \frac{z+u}{4xy}I(0,0,z) + \frac{u^2}{4xy}U_0(z,u,0,0)$$

$$+ \frac{1}{4xy}J(x,y) - \frac{1}{4}B_0(z,u)\left[\frac{J(x)}{x} + \frac{J(y)}{y}\right] \tag{B.192}$$

The function f_{VVS} has a non-vanishing $\overline{\mathrm{MS}}$ correction,

$$\delta_{\overline{\mathrm{MS}}}f_{VVS} = -2J(z) - x - y - z, \tag{B.193}$$

$$\mathcal{D}_{x,u}\delta_{\overline{\mathrm{MS}}}f_{VVS} = -1, \tag{B.194}$$

$$\mathcal{D}_{z,u}\delta_{\overline{\mathrm{MS}}}f_{VVS} = -1 - 2B_0(z,u). \tag{B.195}$$

Finally, the pure gauge function f_{gauge} is by far the most complicated one and needs to be split up:

$$f_{\mathrm{gauge}}(x,y,z) = f_{\mathrm{part,gauge}}(x,y,z) + (x \leftrightarrow y) + (x \leftrightarrow z), \tag{B.196}$$

$$f_{\mathrm{part,gauge}}(x,y,z) = A(x,y,z)I(x,y,z) + B(x,y,z)I(0,y,z) + C(x,y,z)I(0,0,x)$$

$$+ D(x,y,z)J(y,z) + E(x,y,z)J(x), \tag{B.197}$$

$$A(x,y,z) = \left(-x^4 - 8x^3y - 8x^3z + 32x^2yz + 18y^2z^2\right)/(4xyz), \tag{B.198}$$

$$B(x,y,z) = (y-z)^2(y^2 + 10yz + z^2)/(4xyz), \tag{B.199}$$

$$C(x,y,z) = x^2(2yz - x^2)/(4xyz), \tag{B.200}$$

$$D(x,y,z) = (x^2 - 9y^2 - 9z^2 + 9xy + 9xz + 14yz)/(4yz), \tag{B.201}$$

$$E(x,y,z) = \frac{11}{2}(y+z) - \frac{10}{3}x. \tag{B.202}$$

Note how the derivative operator acts on a symmetry term with an arbitrary function g,

$$\mathcal{D}_{x,u}\left[g(x,y,z)\Big|_{x \leftrightarrow y}\right] = \mathcal{D}_{x,u}g(y,x,z) = [\mathcal{D}_{y,u}g(x,y,z)]_{x \leftrightarrow y}. \tag{B.203}$$

Using this, we can write

$$f_{\mathrm{gauge}}^{(1,0,0)}(x,u;y,z) = \mathcal{D}_{x,u}f_{\mathrm{gauge}}^{(1,0,0)}(x,y,z)$$

$$= \mathcal{D}_{x,u}f_{\mathrm{part,gauge}}(x,y,z) + [\mathcal{D}_{y,u}f_{\mathrm{part,gauge}}(x,y,z)]_{x \leftrightarrow y}$$

$$+ [\mathcal{D}_{z,u}f_{\mathrm{part,gauge}}(x,y,z)]_{x \leftrightarrow z}, \tag{B.204}$$

hence we need all three derivatives of $f_{\mathrm{part,gauge}}(x,y,z)$ with respect to x,y and z.

$$
\begin{aligned}
\mathcal{D}_{x,u}f_{\mathrm{part,gauge}}(x,y,z) =&(\mathcal{D}_{x,u}A(x,y,z))I(x,y,z) - A(u,y,z)U_0(x,u,y,z)\\
&+ (\mathcal{D}_{x,u}B(x,y,z))I(0,y,z)\\
&+ (\mathcal{D}_{x,u}C(x,y,z))I(0,0,x) - C(u,y,z)U_0(x,u,0,0)\\
&+ (\mathcal{D}_{x,u}D(x,y,z))J(y,z)\\
&(\mathcal{D}_{x,u}E(x,y,z))J(x) - E(u,y,z)B_0(x,u)
\end{aligned}
\tag{B.205}
$$

$$
\begin{aligned}
\mathcal{D}_{y,u}f_{\mathrm{part,gauge}}(x,y,z) =&(\mathcal{D}_{y,u}A(x,y,z))I(x,y,z) - A(x,u,z)U_0(y,u,x,z)\\
&+ (\mathcal{D}_{y,u}B(x,y,z))I(0,y,z) - B(x,u,z)U_0(y,u,z,0)\\
&+ (\mathcal{D}_{y,u}C(x,y,z))I(0,0,x)\\
&+ (\mathcal{D}_{y,u}D(x,y,z))J(y,z) - D(x,u,z))B_0(y,u)J(z)\\
&(\mathcal{D}_{y,u}E(x,y,z))J(x)
\end{aligned}
\tag{B.206}
$$

$$
\begin{aligned}
\mathcal{D}_{z,u}f_{\mathrm{part,gauge}}(x,y,z) =&(\mathcal{D}_{z,u}A(x,y,z))I(x,y,z) - A(x,y,u)U_0(z,u,x,y)\\
&+ (\mathcal{D}_{z,u}B(x,y,z))I(0,y,z) - B(x,y,u)U_0(z,u,y,0)\\
&+ (\mathcal{D}_{z,u}C(x,y,z))I(0,0,x)\\
&+ (\mathcal{D}_{z,u}D(x,y,z))J(y,z) - D(x,y,u))B_0(z,u)J(y)\\
&(\mathcal{D}_{z,u}E(x,y,z))J(x)
\end{aligned}
\tag{B.207}
$$

Up to now, we have merely used the product rule and the known replacements for derivatives of $J(x), J(x,y), I(x,y,z)$. Only the derivatives of the functions A, B, C, D, E are needed now to complete the calculation.

$$
\mathcal{D}_{x,u}A(x,y,z) = \left[-ux(u^2 + ux + x^2 + 8(u+x)y) + 8ux(u + x - 4y)z + 18y^2z^2\right]/(4uxyz)
\tag{B.208}
$$

$$
\mathcal{D}_{x,u}B(x,y,z) = -(y-z)^2(y^2 + 10yz + z^2)/(4uxyz)
\tag{B.209}
$$

$$
\mathcal{D}_{x,u}C(x,y,z) = -\left[u^2 + ux + x^2 - 2yz\right]/(4yz)
\tag{B.210}
$$

$$
\mathcal{D}_{x,u}D(x,y,z) = \left[u + x + 9(y+z)\right]/(4yz)
\tag{B.211}
$$

$$
\mathcal{D}_{x,u}E(x,y,z) = -\frac{10}{3}
\tag{B.212}
$$

$$\mathcal{D}_{y,u}A(x,y,z) = \frac{x^2(x+8z)}{4uyz} + \frac{9z}{2x} \tag{B.213}$$

$$\mathcal{D}_{y,u}B(x,y,z) = \left[uy(u^2 + uy + y^2) + 8uy(u+y)z - 18uyz^2 - z^4 \right]/(4uxyz) \tag{B.214}$$

$$\mathcal{D}_{y,u}C(x,y,z) = \frac{x^3}{4uyz} \tag{B.215}$$

$$\mathcal{D}_{y,u}D(x,y,z) = - \left[x^2 + 9uy + 9xz - 9z^2 \right]/(4uyz) \tag{B.216}$$

$$\mathcal{D}_{y,u}E(x,y,z) = \frac{11}{2} \tag{B.217}$$

The derivatives with respect to z are similar to the y derivatives,

$$\mathcal{D}_{z,u}F(x,y,z) = [\mathcal{D}_{y,u}F(x,y,z)]_{y \leftrightarrow z}, \qquad F = A, B, C, D, E \tag{B.218}$$

Including the $\overline{\text{MS}}$ remainder,

$$\Delta_{\overline{\text{MS}}} f_{\text{gauge}} = x^2 + 12yz + 2xJ(x) + (x \leftrightarrow y) + (x \leftrightarrow z), \tag{B.219}$$

$$\mathcal{D}_{x,u}\Delta_{\overline{\text{MS}}} f_{\text{gauge}} = x + u + 2J(x) - 2uB_0(x,u) + 12(z+y), \tag{B.220}$$

the calculation is complete.

B.3.3 Second derivatives of the effective potential (self-energies)

The two-loop self-energy of a scalar particle at zero external momentum is given by Π_{ij},

$$-\frac{\partial V^{(2)}}{\partial R_p^0 \partial R_q^0} = N_{ip}^{(S)} N_{jq}^{(S)} \Pi_{ij}, \tag{B.221}$$

$$-\Pi_{ij} = \Pi_{ij}^{S} + \Pi_{ij}^{S_2 F_2(W)} + \Pi_{ij}^{S_1 F_4(M)} + \Pi_{ij}^{S_2 F_3(M)} + \Pi_{ij}^{S_3 F_2(V)} + \Pi_{ij}^{S_1 F_4(V)} + \Pi_{ij}^{S_k V_1} + \Pi_{ij}^{F_4 V_1}, \tag{B.222}$$

where the minus is included to avoid having a minus in front of every Π_{ij}^{XY} component in the following.

Diagrams with only scalar propagators

The purely scalar contributions corresponding to the diagrams of fig. 3.5 are contained in Π_{ij}^{S} and identical to the expressions of Ref. [267].

$$\Pi_{ij}^{S} = \frac{1}{4}\lambda^{ijkl}\lambda^{kmn}\lambda^{lmn}\mathrm{W}_{SSSS}(m_k^2, m_l^2, m_m^2, m_n^2) + \frac{1}{4}\lambda^{ijkl}\lambda^{klmm}\mathrm{X}_{SSS}(m_k^2, m_l^2, m_m^2) \tag{B.223}$$

$$+ \frac{1}{2}\lambda^{ikl}\lambda^{jkm}\lambda^{lmnn}\mathrm{Y}_{SSSS}(m_k^2, m_l^2, m_m^2, m_n^2) + \frac{1}{4}\lambda^{ikl}\lambda^{jmn}\lambda^{klmn}\mathrm{Z}_{SSSS}(m_k^2, m_l^2, m_m^2, m_n^2)$$

$$+ \frac{1}{6}\lambda^{iklm}\lambda^{jklm}\mathrm{S}_{SSS}(m_k^2, m_l^2, m_m^2) + \frac{1}{2}\left(\lambda^{ikl}\lambda^{jkmn} + \lambda^{jkl}\lambda^{ikmn} \right)\lambda^{lmn}\mathrm{U}_{SSSS}(m_k^2, m_l^2, m_m^2, m_n^2)$$

$$+ \frac{1}{2}\lambda^{ikl}\lambda^{jkm}\lambda^{lnp}\lambda^{mnp}\mathrm{V}_{SSSSS}(m_k^2, m_l^2, m_m^2, m_n^2, m_p^2) \tag{B.224}$$

$$+ \frac{1}{2}\lambda^{ikm}\lambda^{jln}\lambda^{klp}\lambda^{mnp}\mathrm{M}_{SSSSS}(m_k^2, m_l^2, m_m^2, m_n^2, m_p^2)$$

The loop integral functions are given by:

$$
\begin{align}
\mathrm{W}_{SSSS}(x,y,z,u) &= U_0(x,y,z,u), \tag{B.225}\\
\mathrm{X}_{SSS}(x,y,z) &= -J(z)B_0(x,y), \tag{B.226}\\
\mathrm{Y}_{SSSS}(x,y,z,u) &= J(u)C_0(x,y,z), \tag{B.227}\\
\mathrm{Z}_{SSSS}(x,y,z,u) &= B_0(x,y)B_0(z,u), \tag{B.228}\\
\mathrm{S}_{SSS}(x,y,z) &= -I(x,y,z), \tag{B.229}\\
\mathrm{U}_{SSSS}(x,y,z,u) &= U_0(x,y,z,u), \tag{B.230}\\
\mathrm{V}_{SSSSS}(x,y,z,u,v) &= [U_0(x,y,u,v) - U_0(x,z,u,v)]/(y-z), \tag{B.231}\\
\mathrm{M}_{SSSSS}(x,y,z,u,v) &= -M_0(x,y,z,u,v). \tag{B.232}
\end{align}
$$

In the case that $y = z$, we have a simplification

$$
V_{SSSSS}(x,y,y,u,v) = = \frac{\partial}{\partial y} U(x,y,u,v) \equiv -V(x,y,u,v). \tag{B.233}
$$

Note that the expressions $\mathrm{X}_{SSS}, \mathrm{Y}_{SSS}, \mathrm{Z}_{SSS}$ follow from differentiating the tadpole T_{SS} (snowman topology), while the others follow from differentiating the tadpoles T_{SSS}, T_{SSSS} (sunrise topology).

Diagrams with scalar and fermion propagators

The contributions from diagrams with the topology W are

$$
\begin{align}
\Pi_{ij}^{S_2 F_2(W)} &= \frac{1}{2}\lambda^{ijkl}\mathrm{Re}[y^{MNk}y^{M'N'l}M_{MM'}M_{NN'}]\mathrm{W}_{SS\overline{FF}}(m_k^2, m_l^2, m_M^2, m_N^2) \\
&\quad + \frac{1}{2}\lambda^{ijkl}y^{MNk}y_{MNl}\mathrm{W}_{SSFF}(m_k^2, m_l^2, m_M^2, m_N^2), \tag{B.234}
\end{align}
$$

where the appearing loop functions are given by

$$
\mathrm{W}_{SS\overline{FF}}(x,y,z,u) = -2\mathrm{W}_{SSSS}(x,y,z,u), \tag{B.235}
$$
$$
\mathrm{W}_{SSFF}(x,y,z,u) = -(z+u-y)U_0(x,y,z,u) - I(x,z,u) + B_0(x,y)(J(z)+J(u)). \tag{B.236}
$$

The contributions from diagrams of the topology M with four fermions are

$$
\begin{align}
&\Pi_{ij}^{S_1 F_4(M)}\\
&=\mathrm{Re}[y^{KMi}y^{LNj}y^{K'L'p}y^{M'N'p}M_{KK'}M_{LL'}M_{MM'}M_{NN'}]\mathrm{M}_{\overline{FFFF}S}(m_K^2, m_L^2, m_M^2, m_N^2, m_p^2)\\
&\quad + 2\mathrm{Re}[y^{KMi}y_{LNj}y_{KL'p}y^{M'Np}M^{LL'}M_{MM'}]\mathrm{M}_{F\overline{FF}FS}(m_K^2, m_L^2, m_M^2, m_N^2, m_p^2)\\
&\quad + \mathrm{Re}\big[\big(y^{KMi}y_{LNj} + y^{KMj}y_{LNi}\big)y_{KL'p}y_{MN'p}M^{LL'}M^{NN'}\big]\mathrm{M}_{F\overline{FF}\overline{F}S}(m_K^2, m_L^2, m_M^2, m_N^2, m_p^2)\\
&\quad + 2\mathrm{Re}[y^{KMi}y^{LNj}y_{KLp}y^{M'N'p}M_{MM'}M_{NN'}]\mathrm{M}_{FF\overline{FF}S}(m_K^2, m_L^2, m_M^2, m_N^2, m_p^2)\\
&\quad + \mathrm{Re}[y^{KMi}y^{LNj}y_{KLp}y_{MNp}]\mathrm{M}_{FFFFS}(m_K^2, m_L^2, m_M^2, m_N^2, m_p^2), \tag{B.237}
\end{align}
$$

where

$$
\mathrm{M}_{\overline{FFFF}S}(x,y,z,u,v) = 2M_0(x,y,z,u,v), \tag{B.238}
$$

$$
\begin{aligned}
\mathrm{M}_{F\overline{FF}FS}(x,y,z,u,v) =& (y+z-v)M_0(x,y,z,u,v) - U_0(x,z,u,v) - U_0(u,y,x,v) \\
& + B_0(x,z)B_0(y,u), \tag{B.239}
\end{aligned}
$$

$$
\mathrm{M}_{F\overline{FF}\overline{F}S}(x,y,z,u,v) = (x+z)M_0(x,y,z,u,v) - U_0(y,u,z,v) - U_0(u,y,x,v), \tag{B.240}
$$

$$
\begin{aligned}
\mathrm{M}_{FF\overline{FF}S}(x,y,z,u,v) =& (x+y-v)M_0(x,y,z,u,v) - U_0(x,z,u,v) - U_0(y,u,z,v) \\
& + B_0(x,z)B_0(y,u), \tag{B.241}
\end{aligned}
$$

$$
\begin{aligned}
\mathrm{M}_{FFFFS}(x,y,z,u,v) =& (xu+yz)M_0(x,y,z,u,v) - xU_0(z,x,y,v) - zU_0(x,z,u,v) \\
& - uU_0(y,u,z,v) - yU_0(u,y,x,v) + I(x,u,v) + I(y,z,v). \tag{B.242}
\end{aligned}
$$

The diagrams with three fermion propagators and two scalar propagators (M topology) are

$$
\begin{aligned}
\Pi_{ij}^{S_2 F_3(M)} =& \lambda^{ikm}\Big(\mathrm{Re}\big[y^{LNj}y^{L'Pk}y^{N'P'm}M_{LL'}M_{NN'}M_{PP'}\big]\mathrm{M}_{S\overline{F}S\overline{FF}}(m_k^2,m_L^2,m_m^2,m_N^2,m_P^2) \\
& + 2\mathrm{Re}\big[y^{LNj}y_{LPk}y^{N'Pm}M_{NN'}\big]\mathrm{M}_{SFS\overline{FF}}(m_k^2,m_L^2,m_m^2,m_N^2,m_P^2) \\
& + \mathrm{Re}\big[y^{LNj}y_{LPk}y_{NP'm}M^{PP'}\big]\mathrm{M}_{SFSF\overline{F}}(m_k^2,m_L^2,m_m^2,m_N^2,m_P^2)\Big) + (i \leftrightarrow j), \tag{B.243}
\end{aligned}
$$

where

$$
\mathrm{M}_{S\overline{F}S\overline{FF}}(x,y,z,u,v) = 2M_0(x,y,z,u,v), \tag{B.244}
$$

$$
\begin{aligned}
\mathrm{M}_{SFS\overline{FF}}(x,y,z,u,v) =& (v-x+y)M_0(x,y,z,u,v) + U_0(y,u,z,v) - U_0(x,z,u,v) \\
& - B_0(x,z)B_0(y,u), \tag{B.245}
\end{aligned}
$$

$$
\mathrm{M}_{SFSF\overline{F}}(x,y,z,u,v) = (y+u)M_0(x,y,z,u,v) - U_0(x,z,u,v) - U_0(z,x,y,v). \tag{B.246}
$$

The diagrams with two fermion propagators and three scalar propagators of the topology V are

$$
\begin{aligned}
\Pi_{ij}^{S_3 F_2(V)} =& \lambda^{ikl}\lambda^{jkm}\Big(\mathrm{Re}\big[y^{NPl}y^{N'P'm}M_{NN'}M_{PP'}\big]\mathrm{V}_{SSS\overline{FF}}(m_k^2,m_l^2,m_m^2,m_N^2,m_P^2) \\
& + \mathrm{Re}\big[y^{NPl}y_{NPm}\big]\mathrm{V}_{SSSFF}(m_k^2,m_l^2,m_m^2,m_N^2,m_P^2)\Big), \tag{B.247}
\end{aligned}
$$

where

$$
\mathrm{V}_{SSS\overline{FF}}(x,y,z,u,v) = -2\mathrm{V}_{SSSSS}(x,y,z,u,v), \tag{B.248}
$$

$$
\begin{aligned}
\mathrm{V}_{SSSFF}(x,y,z,u,v) =& U_0(x,y,u,v) + (z-u-v)V_{SSSSS}(x,y,z,u,v) \\
& - (J(u) + J(v))C_0(x,y,z). \tag{B.249}
\end{aligned}
$$

The results from the V diagrams with four fermions are

$$\Pi_{ij}^{S_1 F_4(V)}$$
$$=2\text{Re}\big[y^{KLi}y^{K'Mj}y^{L'Np}y^{M'N'p}M_{KK'}M_{LL'}M_{MM'}M_{NN'}\big]\text{V}_{\overline{FFFF}S}(m_K^2,m_L^2,m_M^2,m_N^2,m_p^2)$$
$$+\,2\text{Re}\big[(y^{KLi}y^{K'Mj}+y^{KLj}y^{K'Mi})y_{LNp}y^{M'Np}M_{KK'}M_{MM'}\big]\text{V}_{\overline{FF}\overline{F}FS}(m_K^2,m_L^2,m_M^2,m_N^2,m_p^2)$$
$$+\,2\text{Re}\big[y^{KLi}y^{K'Mj}y_{LNp}y_{MN'p}M_{KK'}M^{NN'}\big]\text{V}_{\overline{FFF}\overline{F}S}(m_K^2,m_L^2,m_M^2,m_N^2,m_p^2)$$
$$+\,2\text{Re}\big[y^{KLi}y_{KMj}y^{L'Np}y_{M'Np}M_{LL'}M^{MM'}\big]\text{V}_{F\overline{FF}FS}(m_K^2,m_L^2,m_M^2,m_N^2,m_p^2)$$
$$+\,2\text{Re}\big[\big(y^{KLi}y_{KMj}+y^{KLj}y_{KMi}\big)y_{LNp}y_{M'N'p}M^{MM'}M^{NN'}\big]\text{V}_{FF\overline{FF}S}(m_K^2,m_L^2,m_M^2,m_N^2,m_p^2)$$
$$+\,2\text{Re}\big[y^{KLi}y_{KMj}y_{LNp}y^{MNp}\big]\text{V}_{FFFFS}(m_K^2,m_L^2,m_M^2,m_N^2,m_p^2), \tag{B.250}$$

where

$$\text{V}_{\overline{FFFF}S}(x,y,z,u,v) = -\,2\text{V}_{SSSSS}(x,y,z,u,v), \tag{B.251}$$
$$\text{V}_{\overline{FF}\overline{F}FS}(x,y,z,u,v) = -\,U_0(x,y,u,v)+(v-z-u)V_{SSSSS}(x,y,z,u,v)$$
$$-\,(J(v)-J(u))C_0(x,y,z), \tag{B.252}$$
$$\tag{B.253}$$
$$\text{V}_{\overline{FFF}\overline{F}S}(x,y,z,u,v) = -\,2U_0(x,y,u,v)-2zV_{SSSSS}(x,y,z,u,v), \tag{B.254}$$
$$\text{V}_{F\overline{FF}FS}(x,y,z,u,v) = f_{FFS}^{(2,0,0)}(x,y,z;u,v), \tag{B.255}$$
$$\text{V}_{FF\overline{FF}S}(x,y,z,u,v) = -\,U_0(x,y,u,v)-U_0(y,z,u,v)-(x+z)V_{SSSSS}(x,y,z,u,v), \tag{B.256}$$
$$\text{V}_{FFFFS}(x,y,z,u,v) = f_{FFS}^{(1,0,0)}(y,z,u;v)+xf_{FFS}^{(2,0,0)}(x,y,z,u;v). \tag{B.257}$$

The required derivatives of f_{FFS} are

$$f_{FFS}^{(1,0,0)}(x,y,u;v) \equiv B_0(x,y)(J(v)-J(u))+I(x,u,v)-(y+u-v)U_0(x,y,u,v),$$
$$f_{FFS}^{(2,0,0)}(x,y,z,u;v) \equiv C_0(x,y,z)(J(u)-J(v))-U_0(x,z,u,v)-(y+u-v)V_{SSSSS}(x,y,z,u,v),$$
$$\tag{B.258}$$

with $f_{FFS}^{(2,0,0)}$ symmetric in its first three indices. In this case there are some simplifications compared to the source Ref. [267], (4.33)–(4.39).

Diagrams with one vector propagator and scalars

If only unbroken gauge groups and massless vectors are considered, the expressions for diagrams including one vector propagator are greatly simplified. Diagrams involving only scalars and one vector are given by

$$\Pi_{ij}^{S_k V_1} = \frac{1}{2}g^2 d(i)C(i)\Big[\lambda^{ijkk}W_{SSSV}(m_k^2,m_k^2,m_k^2,0)+\lambda^{ikl}\lambda^{jkl}G_{SS}(m_k^2,m_l^2)\Big], \tag{B.259}$$

where G_{SS} combines several diagrams into one. The full expressions of Ref. [267] simplify to the following loop functions,

$$W_{SSSV}(x,x,x,0) \equiv 3I(x,x,0)-J(x)+2x, \tag{B.260}$$

$$
\begin{aligned}
G_{SS}(x,y) \equiv & 4yV(x,y,y,0) + 4xV(y,x,x,0) - 2U_0(x,y,y,0) - 2U_0(y,x,x,0) \\
& - 2J(y)B_0(x,y') - 2J(x)B_0(y,x') \\
& + 2(x+y)M(x,x,y,y,0) - 2U_0(x,y,y,0) - 2U_0(y,x,x,0) + B_0(x,y)^2. \quad \text{(B.261)}
\end{aligned}
$$

Equivalently, G_{SS} can also be obtained by differentiating eq. (B.158)), resulting in

$$
\begin{aligned}
G_{SS}(x,y) = & 2\left[-U_0(m_i^2, m_k^2, m_k^2, 0) - U_0(m_m^2, m_i^2, m_i^2, 0) + B_0(m_i^2, m_k^2) + 2) \right] \\
= & -12 + \frac{11(x\overline{\ln}x - y\overline{\ln}y) - 3(x\overline{\ln}^2 x - y\overline{\ln}^2 y)}{x-y} \ , \quad \text{(B.262)}
\end{aligned}
$$

$$
G_{SS}(x,x) = -1 + 5\overline{\ln}x - 3\overline{\ln}^2 x \ . \quad \text{(B.263)}
$$

Diagrams with one vector propagator and fermions

For the diagrams involving only fermions and one vector propagator we obtain

$$
\begin{aligned}
\Pi_{ij}^{F_k V_1} = & g^2 d(K)C(K)\big[\mathrm{Re}(y^{iKL}y_{jKL})G_{FF}(m_K^2, m_L^2) \\
& + \mathrm{Re}(y^{iKL}y^{jK'L'}M_{KK'}M_{LL'})G_{\overline{FF}}(m_K^2, m_L^2)\big], \quad \text{(B.264)}
\end{aligned}
$$

where again several diagrams are combined into $G_{FF}, G_{\overline{FF}}$,

$$
\begin{aligned}
G_{FF}(x,y) \equiv & 2(x+y)[3U_0(x,y,x,0) + 3U_0(x,y,y,0) - 5B_0(x,y)] \\
& - 6I(x,x,0) - 6I(y,y,0) + 10J(x) + 10J(y) - 16(x+y) \\
& + \delta_{\overline{\mathrm{MS}}}\, 4\big[J(x) + J(y) - (x+y)B_0(x,y)\big], \\
G_{\overline{FF}}(x,y) \equiv & 4\Big(3U_0(x,y,x,0) + 3U_0(x,y,y,0) - 5B_0(x,y) - 4\Big) \\
& - \delta_{\overline{\mathrm{MS}}}4\big[1 + 2B_0(x,y)\big]. \quad \text{(B.265)}
\end{aligned}
$$

Cross section limits for long-lived particles

C.1 Escape probability approximation

In the analysis presented in chapter 6, the probability $p(D)$ for an LL particle to leave the detector with the mean decay distance $D = c\beta\gamma\tau$ was calculated using the pseudorapidity η and energy E from Monte Carlo events and the detector dimensions. Defining the distance that an LL particle travelled when it decays as $r = c\beta\gamma t$, we have the probability $\exp(-r/D)$ of decaying *beyond* a certain distance r. One can make the simplifying assumption that the particles are produced isotropically and that their energies are not correlated (which is not necessarily accurate). In that case, the probability of a particle crossing a small area S at a boundary at a distance r from the origin is

$$p(D) = \int_S f(r, D)\mathrm{d}S \tag{C.1}$$

with

$$f(r, D) = \frac{1}{4\pi r^2} \exp\left(\frac{-r}{D}\right). \tag{C.2}$$

In our case we wish to find the probability of a particle reaching beyond the boundary of a cylindrical detector, $P_{\mathrm{c}}(D)$. Splitting the cylinder into a barrel and endcaps, we have

$$
\begin{aligned}
P_{\mathrm{c}}(D) &= \int_{\text{barrel}} f(r, D)\mathrm{d}S + 2\int_{\text{endcap}} f(r, D)\mathrm{d}S \\
&= 4\pi R \int_0^{L/2} f(\sqrt{z^2 + R^2}, D)\frac{R}{\sqrt{z^2 + R^2}}\mathrm{d}z \\
&+ 4\pi \int_0^R f(\sqrt{(L/2)^2 + \rho^2}, D)\frac{L/2}{\sqrt{(L/2)^2 + \rho^2}}\rho \, \mathrm{d}\rho.
\end{aligned}
\tag{C.3}
$$

The function $P_{\mathrm{c}}(D)$ is universal and is shown in fig. C.1. To obtain a probability as a function of $c\tau$, we need to integrate over the relativistic factors $\beta\gamma = \sqrt{\gamma^2 - 1}$, or substituting $\gamma = E/m$, equivalently integrate over the energy E. The integration has to be weighted with an energy distribution function, $g_m(E)$. The resulting function is $\bar{P}_{\mathrm{c}}(c\tau)$, which is also mass dependent

because of the substitution $\gamma = E/m$,

$$\bar{P}_{\mathrm{c}}(c\tau) = \int \mathrm{d}E \, g_m(E) \, P_{\mathrm{c}}(D). \tag{C.4}$$

Since $\bar{P}_{\mathrm{c}}(c\tau)$ describes the fraction of events that will contribute to the E_T^{miss} signature in case of unstable particles, we have the relation

$$\sigma_{c\tau}^{95\%} \times \bar{P}_{\mathrm{c}}(c\tau)^2 = \sigma_{\mathrm{stable}}^{95\%}, \tag{C.5}$$

which can be rearranged into

$$\sigma_{c\tau}^{95\%} = \sigma_{\mathrm{stable}}^{95\%} \times [\bar{P}_{\mathrm{c}}(c\tau)]^{-2}. \tag{C.6}$$

This equation (C.6) provides the needed relation between $\sigma_{c\tau}^{95\%}$ and $\sigma_{\mathrm{stable}}^{95\%}$.
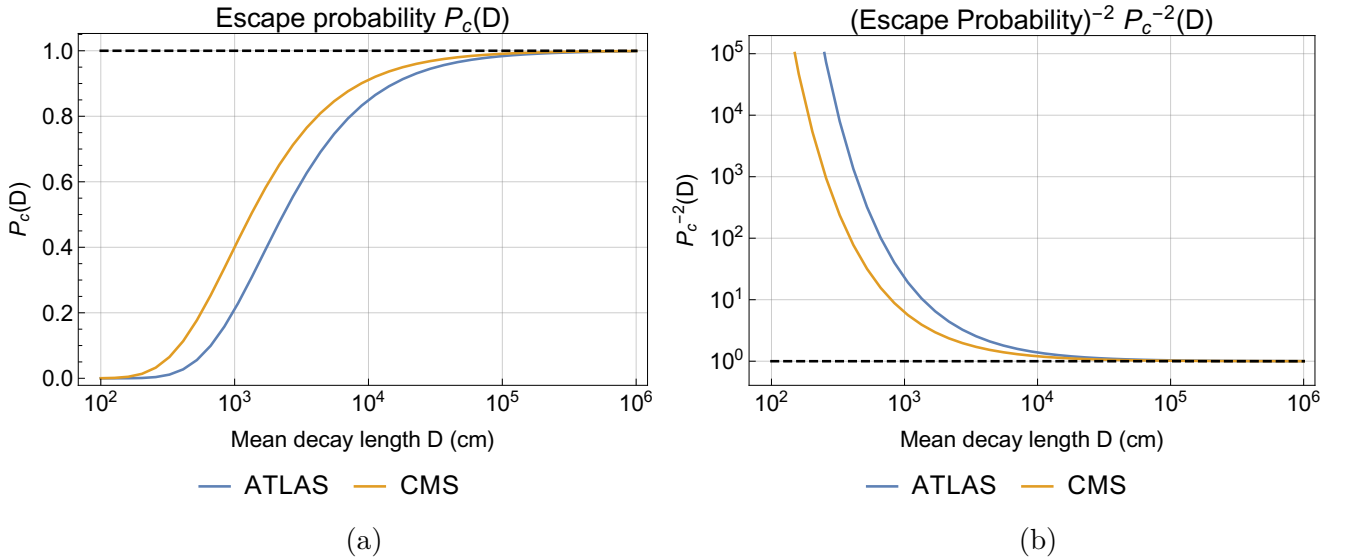
Figure C.1: Escape probability $P_{\mathrm{c}}(D)$ of LL particles within a detector (left). On the right side, $P_{\mathrm{c}}^{-2}(D)$ is shown.

We compare in fig. C.2 how well the approximation performs against the fully MC-based calculation. For the benchmark points considered here, the approximation is shifted by 10–30% towards smaller cross section limits for large values of $c\tau$, while for smaller $c\tau$ it is even shifted by a factor of 10. Since the exclusion plots cover several orders of magnitude, the approximation can still be useful.

C.2 Result tables

We give the results of the two grid scans performed in chapter 6 (published in Ref. [394]). Table C.1 shows the 95% upper cross section limits $\sigma_{\mathrm{stable}}^{95\%}$ for stable LL particles in the HXX model for different masses m_X and m_H. Also the analysis and signal region that give the best result are given. The same information for the SUSY model is given in table C.2 for masses $m_{\tilde{q}}$ and $m_{\tilde{\chi}}$.
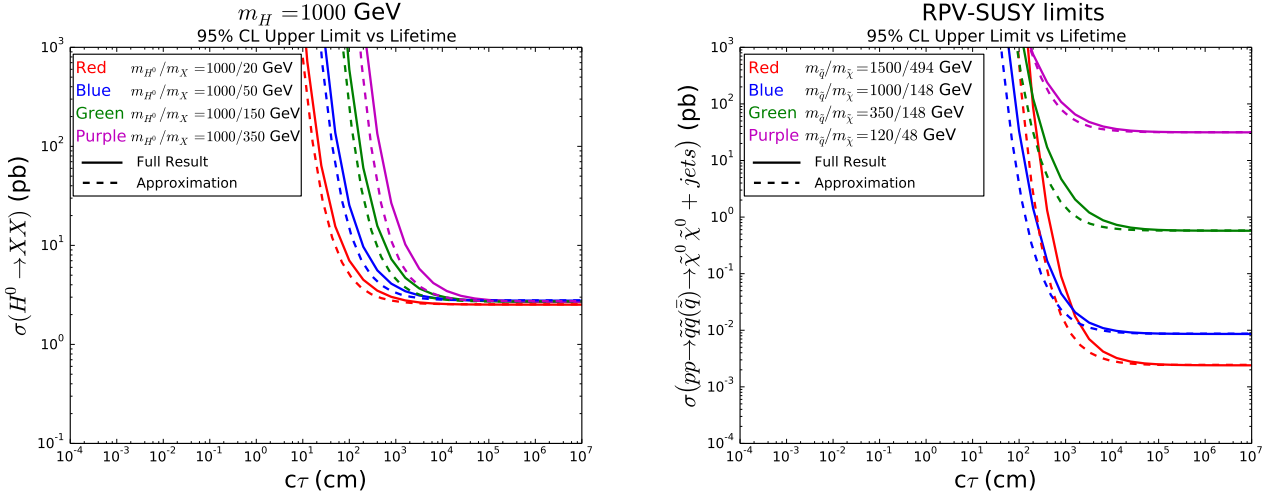
Figure C.2: A comparison of limits derived using the exact method (solid) as described in the main text versus the approximation (dashed) described in appendix C.1.

Table C.1: The complete grid scan result of the HXX model.

m_H (GeV)	m_X (GeV)	analysis	signal region	$\sigma^{95\%}_{\text{stable}}$ (pb)
100	10	ATLAS monojet [419]	SR4	5.77e+01
100	20	ATLAS monojet [419]	SR4	5.58e+01
100	50	ATLAS monojet [419]	SR4	5.38e+01
125	20	ATLAS monojet [419]	SR4	3.83e+01
125	50	ATLAS monojet [419]	SR4	3.99e+01
125	62	ATLAS monojet [419]	SR4	3.79e+01
200	10	ATLAS monojet [419]	SR4	1.67e+01
200	20	ATLAS monojet [419]	SR4	1.71e+01
200	50	ATLAS monojet [419]	SR4	1.75e+01
200	100	ATLAS monojet [419]	SR4	1.65e+01
400	10	ATLAS monojet [419]	SR6	3.26e+00
400	20	ATLAS monojet [419]	SR6	3.29e+00
400	50	ATLAS monojet [419]	SR6	3.17e+00
400	150	ATLAS monojet [419]	SR6	3.16e+00
400	200	ATLAS monojet [419]	SR6	3.12e+00
600	300	ATLAS monojet [419]	SR6	1.57e+00
750	10	ATLAS monojet [419]	SR7	1.48e+00
750	20	ATLAS monojet [419]	SR7	1.61e+00
750	50	ATLAS monojet [419]	SR7	1.51e+00
750	150	ATLAS monojet [419]	SR7	1.48e+00
750	250	ATLAS monojet [419]	SR7	1.57e+00
750	300	ATLAS monojet [419]	SR7	1.49e+00
750	350	ATLAS monojet [419]	SR7	1.46e+00
750	375	ATLAS monojet [419]	SR7	1.46e+00
850	300	ATLAS monojet [419]	SR7	1.19e+00

m_H (GeV)	m_X (GeV)	analysis	signal region	$\sigma^{95\%}_{\text{stable}}$ (pb)
850	400	ATLAS monojet [419]	SR7	1.22e+00
1000	10	ATLAS monojet [419]	SR7	9.31e-01
1000	20	ATLAS monojet [419]	SR7	9.39e-01
1000	50	ATLAS monojet [419]	SR7	9.55e-01
1000	150	ATLAS monojet [419]	SR7	9.41e-01
1000	250	ATLAS monojet [419]	SR7	9.64e-01
1000	350	ATLAS monojet [419]	SR7	9.67e-01
1000	500	ATLAS monojet [419]	SR7	9.69e-01
1200	150	ATLAS monojet [419]	SR8	8.00e-01
1200	250	ATLAS monojet [419]	SR8	8.32e-01
1200	300	ATLAS monojet [419]	SR8	8.11e-01
1200	350	ATLAS monojet [419]	SR8	7.85e-01
1200	400	ATLAS monojet [419]	SR8	8.30e-01
1200	450	ATLAS monojet [419]	SR8	7.93e-01
1200	600	ATLAS monojet [419]	SR8	8.11e-01
1500	10	ATLAS monojet [419]	SR8	6.17e-01
1500	20	ATLAS monojet [419]	SR8	6.33e-01
1500	50	ATLAS monojet [419]	SR8	6.10e-01
1500	150	ATLAS monojet [419]	SR8	6.27e-01
1500	250	ATLAS monojet [419]	SR8	6.32e-01
1500	350	ATLAS monojet [419]	SR8	6.41e-01
1500	500	ATLAS monojet [419]	SR8	6.32e-01
1500	750	ATLAS monojet [419]	SR8	6.47e-01
2000	10	ATLAS monojet [419]	SR8	4.90e-01
2000	20	ATLAS monojet [419]	SR8	4.93e-01
2000	50	ATLAS monojet [419]	SR8	5.11e-01
2000	150	ATLAS monojet [419]	SR8	5.10e-01
2000	250	ATLAS monojet [419]	SR8	4.90e-01
2000	350	ATLAS monojet [419]	SR8	4.99e-01
2000	500	ATLAS monojet [419]	SR8	4.72e-01
2000	750	ATLAS monojet [419]	SR8	5.00e-01
2000	1000	ATLAS monojet [419]	SR8	5.06e-01

Table C.2: The complete grid scan result of the RPV-SUSY model.

$m_{\tilde{q}}$ (GeV)	$m_{\tilde{\chi}}$ (GeV)	analysis	signal region	$\sigma^{95\%}_{\text{stable}}$ (pb)
120	10	CMS α_T [420]	23j_0b_275	2.96e+01
120	48	CMS α_T [420]	4j_0b_325	3.35e+01
120	100	CMS α_T [420]	23j_0b_375	3.36e+01
200	20	CMS α_T [420]	23j_0b_275	2.46e+00
200	100	CMS α_T [420]	4j_0b_325	5.00e+00
200	180	CMS α_T [420]	23j_0b_325	8.77e+00

$m_{\tilde{q}}$ (GeV)	$m_{\tilde{\chi}}$ (GeV)	analysis	signal region	$\sigma_{\text{stable}}^{95\%}$ (pb)
350	148	CMS α_T [420]	23j_0b_325	5.73e-01
350	150	CMS α_T [420]	23j_0b_325	5.33e-01
400	20	CMS α_T [420]	23j_0b_375	1.71e-01
400	200	CMS α_T [420]	23j_0b_375	4.27e-01
400	380	CMS α_T [420]	23j_0b_375	2.68e+00
600	20	CMS α_T [420]	23j_0b_675	7.33e-02
600	200	CMS α_T [420]	23j_0b_475	7.74e-02
600	400	CMS α_T [420]	23j_0b_375	2.75e-01
600	580	ATLAS multijet [418]	AM	1.56e+00
700	150	ATLAS multijet [418]	AM	4.14e-02
700	500	CMS α_T [420]	23j_0b_375	2.43e-01
800	20	ATLAS multijet [418]	AM	1.62e-02
800	200	ATLAS multijet [418]	AM	2.24e-02
800	400	CMS α_T [420]	23j_0b_675	6.69e-02
800	600	CMS α_T [420]	23j_0b_375	2.15e-01
800	780	ATLAS multijet [418]	AM	1.39e+00
1000	20	ATLAS multijet [418]	AM	7.80e-03
1000	148	ATLAS multijet [418]	AM	8.56e-03
1000	150	ATLAS multijet [418]	AM	8.38e-03
1000	200	ATLAS multijet [418]	AM	8.68e-03
1000	400	ATLAS multijet [418]	AM	1.40e-02
1000	500	ATLAS multijet [418]	AM	2.54e-02
1000	600	CMS α_T [420]	23j_0b_675	4.80e-02
1000	800	CMS α_T [420]	23j_0b_375	1.87e-01
1000	980	ATLAS multijet [418]	AM	1.55e+00
1200	20	ATLAS multijet [418]	CT	3.05e-03
1200	200	ATLAS multijet [418]	CT	3.49e-03
1200	400	ATLAS multijet [418]	AM	6.89e-03
1200	600	ATLAS multijet [418]	AM	1.14e-02
1200	800	CMS α_T [420]	23j_0b_675	3.90e-02
1200	1000	CMS α_T [420]	23j_0b_375	1.60e-01
1200	1180	ATLAS monojet [419]	SR7	1.57e+00
1400	20	ATLAS multijet [418]	CT	1.96e-03
1400	100	ATLAS multijet [418]	CT	2.02e-03
1400	200	ATLAS multijet [418]	CT	2.07e-03
1400	300	ATLAS multijet [418]	CT	2.25e-03
1400	600	ATLAS multijet [418]	AM	6.11e-03
1400	800	CMS α_T [420]	23j_0b_875	1.29e-02
1400	1000	CMS α_T [420]	23j_0b_675	3.44e-02
1400	1200	CMS α_T [420]	23j_0b_375	1.48e-01
1400	1380	ATLAS monojet [419]	SR8	1.94e+00
1500	150	ATLAS multijet [418]	CT	1.79e-03
1500	200	ATLAS multijet [418]	CT	1.76e-03
1500	400	ATLAS multijet [418]	CT	2.06e-03

$m_{\tilde{q}}$ (GeV)	$m_{\tilde{\chi}}$ (GeV)	analysis	signal region	$\sigma^{95\%}_{\text{stable}}$ (pb)
1500	494	ATLAS multijet [418]	CT	2.40e-03
1600	20	ATLAS multijet [418]	CT	1.51e-03
1600	200	ATLAS multijet [418]	CT	1.53e-03
1600	400	ATLAS multijet [418]	CT	1.73e-03
1600	600	ATLAS multijet [418]	CT	2.31e-03
1600	800	ATLAS multijet [418]	AM	5.68e-03
1600	1000	CMS α_T [420]	23j_0b_875	1.11e-02
1600	1200	CMS α_T [420]	23j_0b_675	3.06e-02
1600	1400	CMS α_T [420]	23j_0b_375	1.38e-01
1600	1580	ATLAS monojet [419]	SR8	2.34e+00
1700	100	ATLAS multijet [418]	CT	1.35e-03
1700	400	ATLAS multijet [418]	CT	1.54e-03
1800	20	ATLAS multijet [418]	CT	1.23e-03
1800	200	ATLAS multijet [418]	CT	1.27e-03
1800	400	ATLAS multijet [418]	CT	1.38e-03
1800	600	ATLAS multijet [418]	BT	2.43e-03
1800	800	ATLAS multijet [418]	BT	2.97e-03
1800	1000	ATLAS multijet [418]	AM	5.39e-03
1800	1200	CMS α_T [420]	23j_0b_875	9.88e-03
1800	1400	CMS α_T [420]	23j_0b_675	2.84e-02
1800	1600	CMS α_T [420]	23j_0b_375	1.26e-01
1800	1780	ATLAS monojet [419]	SR6	1.80e+00
1900	100	ATLAS multijet [418]	CT	1.17e-03
2000	20	ATLAS multijet [418]	CT	1.10e-03
2000	200	ATLAS multijet [418]	CT	1.13e-03
2000	400	ATLAS multijet [418]	CT	1.18e-03
2000	600	ATLAS multijet [418]	BT	1.99e-03
2000	800	ATLAS multijet [418]	BT	2.21e-03
2000	1000	ATLAS multijet [418]	BT	2.83e-03
2000	1200	ATLAS multijet [418]	BT	5.02e-03
2000	1400	CMS α_T [420]	23j_0b_875	9.19e-03
2000	1600	CMS α_T [420]	23j_0b_675	2.65e-02
2000	1800	CMS α_T [420]	23j_0b_375	1.21e-01
2000	1980	ATLAS monojet [419]	SR7	2.71e+00

Bibliography

[1] S. L. Glashow, *Partial Symmetries of Weak Interactions*, Nucl. Phys. **22** (1961) 579 (cit. on pp. 1, 14).

[2] S. Weinberg, *A Model of Leptons*, Phys. Rev. Lett. **19** (1967) 1264 (cit. on pp. 1, 14).

[3] S. L. Glashow, J. Iliopoulos and L. Maiani, *Weak Interactions with Lepton-Hadron Symmetry*, Phys. Rev. **D2** (1970) 1285 (cit. on pp. 1, 14).

[4] H. Fritzsch, M. Gell-Mann and H. Leutwyler, *Advantages of the Color Octet Gluon Picture*, Phys. Lett. **B47** (1973) 365 (cit. on p. 1).

[5] H. D. Politzer, *Reliable Perturbative Results for Strong Interactions?*, Phys. Rev. Lett. **30** (1973) 1346 (cit. on p. 1).

[6] D. J. Gross and F. Wilczek, *Ultraviolet Behavior of Nonabelian Gauge Theories*, Phys. Rev. Lett. **30** (1973) 1343 (cit. on p. 1).

[7] D. J. Gross and F. Wilczek, *Asymptotically Free Gauge Theories. 1*, Phys. Rev. **D8** (1973) 3633 (cit. on p. 1).

[8] D. J. Gross and F. Wilczek, *Asymptotically Free Gauge Theories. 2.*, Phys. Rev. **D9** (1974) 980 (cit. on p. 1).

[9] G. Arnison et al., *Experimental Observation of Isolated Large Transverse Energy Electrons with Associated Missing Energy at s**(1/2) = 540-GeV*, Phys. Lett. **B122** (1983) 103, [,611(1983)] (cit. on p. 1).

[10] M. Banner et al., *Observation of Single Isolated Electrons of High Transverse Momentum in Events with Missing Transverse Energy at the CERN anti-p p Collider*, Phys. Lett. **B122** (1983) 476 (cit. on p. 1).

[11] G. Arnison et al., *Experimental Observation of Lepton Pairs of Invariant Mass Around 95-GeV/c**2 at the CERN SPS Collider*, Phys. Lett. **B126** (1983) 398 (cit. on p. 1).

[12] P. Bagnaia et al., *Evidence for Z0 —> e+ e- at the CERN anti-p p Collider*, Phys. Lett. **B129** (1983) 130 (cit. on p. 1).

[13] F. Abe et al., *Observation of top quark production in $\bar{p}p$ collisions*, Phys. Rev. Lett. **74** (1995) 2626, arXiv: `hep-ex/9503002 [hep-ex]` (cit. on p. 1).

[14] S. Abachi et al., *Observation of the top quark*, Phys. Rev. Lett. **74** (1995) 2632, arXiv: `hep-ex/9503003 [hep-ex]` (cit. on p. 1).

[15] G. S. Guralnik, C. R. Hagen and T. W. B. Kibble, *Global Conservation Laws and Massless Particles*, Phys. Rev. Lett. **13** (1964) 585 (cit. on p. 2).

[16] P. W. Higgs, *Broken symmetries, massless particles and gauge fields*,
Phys. Lett. **12** (1964) 132 (cit. on p. 2).

[17] P. W. Higgs, *Broken Symmetries and the Masses of Gauge Bosons*,
Phys. Rev. Lett. **13** (1964) 508 (cit. on p. 2).

[18] P. W. Higgs, *Spontaneous Symmetry Breakdown without Massless Bosons*,
Phys. Rev. **145** (1966) 1156 (cit. on p. 2).

[19] F. Englert and R. Brout, *Broken Symmetry and the Mass of Gauge Vector Mesons*,
Phys. Rev. Lett. **13** (1964) 321 (cit. on p. 2).

[20] T. W. B. Kibble, *Symmetry breaking in nonAbelian gauge theories*,
Phys. Rev. **155** (1967) 1554 (cit. on p. 2).

[21] S. Chatrchyan et al.,
Observation of a new boson at a mass of 125 GeV with the CMS experiment at the LHC,
Phys.Lett. **B716** (2012) 30, arXiv: `1207.7235` `[hep-ex]` (cit. on pp. 2, 9, 123).

[22] G. Aad et al., *Observation of a new particle in the search for the Standard Model Higgs boson with the ATLAS detector at the LHC*, Phys.Lett. **B716** (2012) 1,
arXiv: `1207.7214` `[hep-ex]` (cit. on pp. 2, 9, 123).

[23] G. Aad et al., *Combined Measurement of the Higgs Boson Mass in pp Collisions at $\sqrt{s} = 7$ and 8 TeV with the ATLAS and CMS Experiments*,
Phys. Rev. Lett. **114** (2015) 191803, arXiv: `1503.07589` `[hep-ex]` (cit. on pp. 2, 9, 31).

[24] V. Khachatryan et al.,
Precise determination of the mass of the Higgs boson and tests of compatibility of its couplings with the standard model predictions using proton collisions at 7 and 8 TeV,
Eur. Phys. J. **C75**.5 (2015) 212, arXiv: `1412.8662` `[hep-ex]` (cit. on pp. 2, 9, 31).

[25] G. Aad et al., *Measurement of the Higgs boson mass from the $H \to \gamma\gamma$ and $H \to ZZ^* \to 4\ell$ channels with the ATLAS detector using 25 fb^{-1} of pp collision data*,
Phys. Rev. **D90**.5 (2014) 052004, arXiv: `1406.3827` `[hep-ex]` (cit. on pp. 2, 9, 31).

[26] V. Khachatryan et al., *Search for Lepton-Flavour-Violating Decays of the Higgs Boson*,
Phys. Lett. **B749** (2015) 337, arXiv: `1502.07400` `[hep-ex]` (cit. on p. 2).

[27] G. Aad et al., *Search for lepton-flavour-violating $H \to \mu\tau$ decays of the Higgs boson with the ATLAS detector*, JHEP **11** (2015) 211, arXiv: `1508.03372` `[hep-ex]` (cit. on p. 2).

[28] E. Gildener, *Gauge Symmetry Hierarchies*, Phys. Rev. **D14** (1976) 1667
(cit. on pp. 3, 11).

[29] H. P. Nilles, *Dynamically Broken Supergravity and the Hierarchy Problem*,
Phys. Lett. **B115** (1982) 193 (cit. on pp. 3, 11).

[30] E. Witten, *Dynamical Breaking of Supersymmetry*, Nucl. Phys. **B188** (1981) 513
(cit. on pp. 3, 11).

[31] M. J. G. Veltman, *The Infrared - Ultraviolet Connection*,
Acta Phys. Polon. **B12** (1981) 437 (cit. on pp. 3, 11).

[32] J. H. Oort, *The force exerted by the stellar system in the direction perpendicular to the galactic plane and some related problems*, Bull. Astr. Inst. Netherlands **4** (1932) 249
(cit. on pp. 3, 10).

[33] F. Zwicky, *Die Rotverschiebung von extragalaktischen Nebeln*,
Helv. Phys. Acta **6** (1933) 110 (cit. on pp. 3, 10).

[34] F. Zwicky, *On the Masses of Nebulae and of Clusters of Nebulae*,
Astrophys. J. **86** (1937) 217 (cit. on pp. 3, 10).

[35] V. C. Rubin and W. K. Ford Jr.,
Rotation of the Andromeda Nebula from a Spectroscopic Survey of Emission Regions,
Astrophys. J. **159** (1970) 379 (cit. on pp. 3, 10).

[36] H. Goldberg, *Constraint on the Photino Mass from Cosmology*,
Phys. Rev. Lett. **50** (1983) 1419, [Erratum: Phys. Rev. Lett.103,099905(2009)]
(cit. on p. 3).

[37] K. G. Begeman, *H I rotation curves of spiral galaxies. I - NGC 3198*,
Astron. Astrophys. **223** (1989) 47 (cit. on pp. 3, 10).

[38] K. G. Begeman, A. H. Broeils and R. H. Sanders,
Extended rotation curves of spiral galaxies: Dark haloes and modified dynamics,
Mon. Not. Roy. Astron. Soc. **249** (1991) 523 (cit. on pp. 3, 10).

[39] M. C. Gonzalez-Garcia and M. Maltoni, *Phenomenology with Massive Neutrinos*,
Phys. Rept. **460** (2008) 1, arXiv: `0704.1800` `[hep-ph]` (cit. on p. 3).

[40] A. de Gouvea et al., *Working Group Report: Neutrinos*, (2013),
arXiv: `1310.4340` `[hep-ex]`,
URL: `https://inspirehep.net/record/1260555/files/arXiv:1310.4340.pdf`
(cit. on p. 3).

[41] S. F. King, *Neutrino mass*, Contemp. Phys. **48** (2007) 195,
arXiv: `0712.1750` `[physics.pop-ph]` (cit. on p. 3).

[42] A. D. Sakharov,
Violation of CP Invariance, c Asymmetry, and Baryon Asymmetry of the Universe,
Pisma Zh. Eksp. Teor. Fiz. **5** (1967) 32, [Usp. Fiz. Nauk161,61(1991)] (cit. on pp. 3, 10).

[43] M. Trodden, *Electroweak baryogenesis*, Rev. Mod. Phys. **71** (1999) 1463,
arXiv: `hep-ph/9803479` `[hep-ph]` (cit. on pp. 3, 11).

[44] M. Dine and A. Kusenko, *The Origin of the matter - antimatter asymmetry*,
Rev. Mod. Phys. **76** (2003) 1, arXiv: `hep-ph/0303065` `[hep-ph]` (cit. on pp. 3, 11).

[45] J. M. Cline, *Baryogenesis*, (2006), arXiv: `hep-ph/0609145` `[hep-ph]` (cit. on pp. 3, 11).

[46] D. E. Morrissey and M. J. Ramsey-Musolf, *Electroweak baryogenesis*,
New J. Phys. **14** (2012) 125003, arXiv: `1206.2942` `[hep-ph]` (cit. on p. 3).

[47] Yu. A. Golfand and E. P. Likhtman,
Extension of the Algebra of Poincare Group Generators and Violation of p Invariance,
JETP Lett. **13** (1971) 323, [Pisma Zh. Eksp. Teor. Fiz.13,452(1971)] (cit. on p. 3).

[48] J.-L. Gervais and B. Sakita, *Field Theory Interpretation of Supergauges in Dual Models*,
Nucl. Phys. **B34** (1971) 632 (cit. on p. 3).

[49] D. V. Volkov and V. P. Akulov, Pisma Zh. Eksp. Teor. Fiz. **16** (1972) 621 (cit. on p. 3).

[50] H. Miyazawa, *Baryon Number Changing Currents*, Prog. Theor. Phys. **36**.6 (1966) 1266
(cit. on p. 3).

[51] J. Wess and B. Zumino, *Supergauge Transformations in Four-Dimensions*,
Nucl. Phys. **B70** (1974) 39 (cit. on pp. 3, 16).

[52] P. Fayet and S. Ferrara, *Supersymmetry*, Phys. Rept. **32** (1977) 249 (cit. on pp. 3, 16).

[53] S. Dimopoulos and H. Georgi, *Softly Broken Supersymmetry and SU(5)*,
Nucl. Phys. **B193** (1981) 150 (cit. on pp. 3, 16).

[54] H. P. Nilles, *Supersymmetry, Supergravity and Particle Physics*,
Phys. Rept. **110** (1984) 1 (cit. on pp. 3, 16, 76).

[55] H. Baer and X. Tata, *Weak scale supersymmetry: From superfields to scattering events*,
Cambridge University Press, 2006,
ISBN: 0521290317, 9780521290319, 9780511190117, 9780521290319, 9780521857864,
URL: `http://www.cambridge.org/9780521290319` (cit. on pp. 3, 16).

[56] J. Wess and J. Bagger, *Supersymmetry and supergravity*, 1992 (cit. on pp. 3, 16).

[57] H. E. Haber and G. L. Kane,
The Search for Supersymmetry: Probing Physics Beyond the Standard Model,
Phys. Rept. **117** (1985) 75 (cit. on pp. 3, 16).

[58] H. E. Haber, *Introductory low-energy supersymmetry*, (1993),
arXiv: `hep-ph/9306207 [hep-ph]` (cit. on pp. 3, 16).

[59] M. Drees, *An Introduction to supersymmetry*, (1996), arXiv: `hep-ph/9611409 [hep-ph]`
(cit. on pp. 3, 16).

[60] S. P. Martin, *A Supersymmetry primer*,
(1997), [Adv. Ser. Direct. High Energy Phys.18,1(1998)],
arXiv: `hep-ph/9709356 [hep-ph]` (cit. on pp. 3, 16, 19, 22).

[61] H. E. Haber, *The Status of the minimal supersymmetric standard model and beyond*,
Nucl. Phys. Proc. Suppl. **62** (1998) 469, arXiv: `hep-ph/9709450 [hep-ph]`
(cit. on pp. 3, 16).

[62] A. Djouadi, *The Anatomy of electro-weak symmetry breaking. II. The Higgs bosons in
the minimal supersymmetric model*, Phys. Rept. **459** (2008) 1,
arXiv: `hep-ph/0503173 [hep-ph]` (cit. on pp. 3, 16).

[63] P. Langacker and M.-x. Luo, *Implications of precision electroweak experiments for M_t,
ρ_0, $\sin^2 \theta_W$ and grand unification*, Phys. Rev. **D44** (1991) 817 (cit. on pp. 3, 16).

[64] U. Amaldi, W. de Boer and H. Furstenau, *Comparison of grand unified theories with
electroweak and strong coupling constants measured at LEP*,
Phys. Lett. **B260** (1991) 447 (cit. on pp. 3, 16).

[65] L. E. Ibanez and G. G. Ross,
Low-Energy Predictions in Supersymmetric Grand Unified Theories,
Phys. Lett. **B105** (1981) 439 (cit. on pp. 3, 16).

[66] S. Dimopoulos, S. Raby and F. Wilczek, *Supersymmetry and the Scale of Unification*,
Phys. Rev. **D24** (1981) 1681 (cit. on pp. 3, 14, 16).

[67] M. Drees, R. Godbole and P. Roy, *Theory and phenomenology of sparticles: An account
of four-dimensional N=1 supersymmetry in high energy physics*, 2004
(cit. on pp. 3, 13, 16).

[68]   F. Staub, *SARAH*, (2008), arXiv: `0806.0538` [`hep-ph`] (cit. on pp. 3, 48, 123).

[69]   F. Staub, *From Superpotential to Model Files for FeynArts and CalcHep/CompHep*, Comput. Phys. Commun. **181** (2010) 1077, arXiv: `0909.2863` [`hep-ph`] (cit. on pp. 3, 48, 123).

[70]   F. Staub, *Automatic Calculation of supersymmetric Renormalization Group Equations and Self Energies*, Comput. Phys. Commun. **182** (2011) 808, arXiv: `1002.0840` [`hep-ph`] (cit. on pp. 3, 8, 48, 123).

[71]   F. Staub et al., *A Tool Box for Implementing Supersymmetric Models*, Comput.Phys.Commun. **183** (2012) 2165, arXiv: `1109.5147` [`hep-ph`] (cit. on pp. 3, 48, 123).

[72]   F. Staub, *SARAH 3.2: Dirac Gauginos, UFO output, and more*, Comput. Phys. Commun. **184** (2013) 1792, [Comput. Phys. Commun.184,1792(2013)], arXiv: `1207.0906` [`hep-ph`] (cit. on pp. 3, 48, 123).

[73]   F. Staub, *SARAH 4 : A tool for (not only SUSY) model builders*, Comput. Phys. Commun. **185** (2014) 1773, arXiv: `1309.7223` [`hep-ph`] (cit. on pp. 3, 48, 123).

[74]   F. Staub, *Exploring new models in all detail with SARAH*, (2015), arXiv: `1503.04200` [`hep-ph`] (cit. on pp. 3, 48, 123).

[75]   G. Aarons et al., *International Linear Collider Reference Design Report Volume 2: Physics at the ILC*, (2007), arXiv: `0709.1893` [`hep-ph`] (cit. on p. 3).

[76]   J. Goldstone, *Field Theories with Superconductor Solutions*, Nuovo Cim. **19** (1961) 154 (cit. on p. 7).

[77]   J. Goldstone, A. Salam and S. Weinberg, *Broken Symmetries*, Phys. Rev. **127** (1962) 965 (cit. on p. 7).

[78]   P. Garcia-Abia and W. Lohmann, *Measurement of the Higgs cross-section and mass with linear colliders*, Eur. Phys. J.direct **C2** (2000) 2, [,1377(1999)], arXiv: `hep-ex/9908065` [`hep-ex`] (cit. on p. 9).

[79]   ATLAS CDF CMS D0, *First combination of Tevatron and LHC measurements of the top-quark mass*, (2014), arXiv: `1403.4427` [`hep-ex`] (cit. on p. 9).

[80]   N. Cabibbo, *Unitary Symmetry and Leptonic Decays*, Phys. Rev. Lett. **10** (1963) 531, [,648(1963)] (cit. on p. 9).

[81]   M. Kobayashi and T. Maskawa, *CP Violation in the Renormalizable Theory of Weak Interaction*, Prog. Theor. Phys. **49** (1973) 652 (cit. on pp. 9, 61).

[82]   M. E. Peskin and D. V. Schroeder, *An Introduction to quantum field theory*, 1995, ISBN: 9780201503975, 0201503972, URL: `http://www.slac.stanford.edu/spires/find/books/www?cl=QC174.45%3AP4` (cit. on p. 9).

[83] F. Halzen and A. D. Martin,
      Quarks and leptons: An introductory course in modern particle physics, 1984,
      ISBN: 0471887412, 9780471887416 (cit. on p. 9).

[84] D. Griffiths, *Introduction to elementary particles*, 2008 (cit. on p. 9).

[85] B. Pontecorvo,
      Neutrino Experiments and the Problem of Conservation of Leptonic Charge,
      Sov. Phys. JETP **26** (1968) 984, [Zh. Eksp. Teor. Fiz.53,1717(1967)] (cit. on p. 10).

[86] R. Davis, *A review of the Homestake solar neutrino experiment*,
      Prog. Part. Nucl. Phys. **32** (1994) 13 (cit. on p. 10).

[87] K. S. Hirata et al.,
      Results from one thousand days of real time directional solar neutrino data,
      Phys. Rev. Lett. **65** (1990) 1297 (cit. on p. 10).

[88] K. S. Hirata et al.,
      Real time, directional measurement of B-8 solar neutrinos in the Kamiokande-II detector,
      Phys. Rev. **D44** (1991) 2241, [Erratum: Phys. Rev.D45,2170(1992)] (cit. on p. 10).

[89] Y. Fukuda et al., *Solar neutrino data covering solar cycle 22*,
      Phys. Rev. Lett. **77** (1996) 1683 (cit. on p. 10).

[90] D. Abdurashitov et al., *Results from SAGE*, Phys. Lett. **B328** (1994) 234 (cit. on p. 10).

[91] P. Anselmann et al., *GALLEX results from the first 30 solar neutrino runs*,
      Phys. Lett. **B327** (1994) 377 (cit. on p. 10).

[92] P. A. R. Ade et al., *Planck 2015 results. XIII. Cosmological parameters*, (2015),
      arXiv: 1502.01589 [astro-ph.CO] (cit. on p. 10).

[93] A. Bandyopadhyay, *Physics at a future Neutrino Factory and super-beam facility*,
      Rept. Prog. Phys. **72** (2009) 106201, ed. by S. Choubey et al.,
      arXiv: 0710.4947 [hep-ph] (cit. on p. 10).

[94] P. Minkowski, $\mu \to e\gamma$ *at a Rate of One Out of* 10^9 *Muon Decays?*,
      Phys. Lett. **B67** (1977) 421; R. N. Mohapatra and G. Senjanovic,
      Neutrino Mass and Spontaneous Parity Violation, Phys.Rev.Lett. **44** (1980) 912;
      J. Schechter and J. Valle, *Neutrino Masses in SU(2) x U(1) Theories*,
      Phys.Rev. **D22** (1980) 2227; T. Yanagida,
      Horizontal Symmetry and Masses of Neutrinos, Prog.Theor.Phys. **64** (1980) 1103,
      cit. on p. 10.

[95] L. J. Hall and M. Suzuki, *Explicit R-Parity Breaking in Supersymmetric Models*,
      Nucl.Phys. **B231** (1984) 419; F. Borzumati et al.,
      Neutrino masses and mixing in supersymmetric models without R parity,
      Phys.Lett. **B384** (1996) 123, arXiv: hep-ph/9606251 [hep-ph];
      Y. Grossman and H. E. Haber, *Sneutrino mixing phenomena*,
      Phys.Rev.Lett. **78** (1997) 3438, arXiv: hep-ph/9702421 [hep-ph];
      Y. Grossman and H. E. Haber, *(S)neutrino properties in R-parity violating
      supersymmetry. 1. CP conserving phenomena*, Phys.Rev. **D59** (1999) 093008,
      arXiv: hep-ph/9810536 [hep-ph]; Y. Grossman and H. E. Haber,
      Neutrino masses and sneutrino mixing in R-parity violating supersymmetry, (1999),
      arXiv: hep-ph/9906310 [hep-ph]; S. Davidson and M. Losada,

Neutrino masses in the R(p) violating MSSM, JHEP **0005** (2000) 021,
arXiv: `hep-ph/0005080 [hep-ph]`; M. Hirsch et al.,
Neutrino masses and mixings from supersymmetry with bilinear R parity violation: A Theory for solar and atmospheric neutrino oscillations, Phys.Rev. **D62** (2000) 113008,
arXiv: `hep-ph/0004115 [hep-ph]`, cit. on pp. 10, 84.

[96] E. W. Kolb and M. S. Turner, *The Early Universe*, Front. Phys. **69** (1990) 1
(cit. on p. 10).

[97] D. Larson et al., *Seven-year Wilkinson Microwave Anisotropy Probe (WMAP) Observations: Power Spectra and WMAP-derived Parameters*, ApJS **192**, 16 (2011) 16,
arXiv: `1001.4635 [astro-ph.CO]` (cit. on p. 10).

[98] P. A. R. Ade et al., *Planck 2013 results. XVI. Cosmological parameters*,
Astron. Astrophys. **571** (2014) A16, arXiv: `1303.5076 [astro-ph.CO]` (cit. on p. 10).

[99] D. N. Schramm and G. Steigman, *Relic Neutrinos and the Density of the Universe*,
Astrophys. J. **243** (1981) 1; P. J. E. Peebles,
Primeval Adiabatic Perturbations: Effect of massive Neutrinos,
Astrophys. J. **258** (1982) 415; C. S. Frenk, S. D. M. White and M. Davis,
Nonlinear evolution of large-scale structure in the universe,
Astrophys. J. **271** (1983) 417, cit. on p. 10.

[100] S. D. M. White, C. S. Frenk and M. Davis,
Clustering in a Neutrino Dominated Universe, Astrophys. J. **274** (1983) L1
(cit. on p. 10).

[101] J. M. Cline et al., *Update on scalar singlet dark matter*,
Phys. Rev. **D88** (2013) 055025, [Erratum: Phys. Rev.D92,no.3,039906(2015)],
arXiv: `1306.4710 [hep-ph]` (cit. on p. 10).

[102] H.-C. Cheng, J. L. Feng and K. T. Matchev, *Kaluza-Klein dark matter*,
Phys.Rev.Lett. **89** (2002) 211301, arXiv: `hep-ph/0207125 [hep-ph]` (cit. on p. 10).

[103] G. Servant and T. M. Tait,
Is the lightest Kaluza-Klein particle a viable dark matter candidate?,
Nucl.Phys. **B650** (2003) 391, arXiv: `hep-ph/0206071 [hep-ph]` (cit. on p. 10).

[104] J. R. Ellis et al., *Supersymmetric Relics from the Big Bang*,
Nucl. Phys. **B238** (1984) 453 (cit. on p. 10).

[105] M. Drees and M. M. Nojiri, *The Neutralino relic density in minimal $N = 1$ supergravity*,
Phys. Rev. **D47** (1993) 376, arXiv: `hep-ph/9207234 [hep-ph]` (cit. on p. 10).

[106] L. Covi et al., *Axinos as dark matter*, JHEP **05** (2001) 033,
arXiv: `hep-ph/0101009 [hep-ph]` (cit. on p. 10).

[107] J. E. Kim and G. Carosi, *Axions and the Strong CP Problem*,
Rev. Mod. Phys. **82** (2010) 557, arXiv: `0807.3125 [hep-ph]` (cit. on p. 10).

[108] M. Bolz, A. Brandenburg and W. Buchmuller, *Thermal production of gravitinos*,
Nucl. Phys. **B606** (2001) 518, [Erratum: Nucl. Phys.B790,336(2008)],
arXiv: `hep-ph/0012052 [hep-ph]` (cit. on p. 10).

[109] A. G. Cohen, D. B. Kaplan and A. E. Nelson, *Weak scale baryogenesis*,
Phys. Lett. **B245** (1990) 561 (cit. on p. 11).

[110] A. G. Cohen, D. B. Kaplan and A. E. Nelson, *Baryogenesis at the weak phase transition*,
Nucl. Phys. **B349** (1991) 727 (cit. on p. 11).

[111] G. W. Anderson and L. J. Hall, *The Electroweak phase transition and baryogenesis*,
Phys. Rev. **D45** (1992) 2685 (cit. on p. 11).

[112] V. A. Rubakov and M. E. Shaposhnikov, *Electroweak baryon number nonconservation in
the early universe and in high-energy collisions*,
Usp. Fiz. Nauk **166** (1996) 493, [Phys. Usp.39,461(1996)],
arXiv: `hep-ph/9603208 [hep-ph]` (cit. on p. 11).

[113] W. Altmannshofer et al.,
Anatomy and Phenomenology of FCNC and CPV Effects in SUSY Theories,
Nucl.Phys. **B830** (2010) 17, arXiv: `0909.1333 [hep-ph]` (cit. on p. 11).

[114] G. Buchalla, G. Hiller and G. Isidori,
Phenomenology of nonstandard Z couplings in exclusive semileptonic $b \to s$ transitions,
Phys.Rev. **D63** (2000) 014015, arXiv: `hep-ph/0006136 [hep-ph]` (cit. on p. 11).

[115] M. Ciuchini et al., *$b \longrightarrow s$ transitions: A New frontier for indirect SUSY searches*,
Phys. Rev. **D67** (2003) 075016, [Erratum: Phys. Rev.D68,079901(2003)],
arXiv: `hep-ph/0212397 [hep-ph]` (cit. on p. 11).

[116] J. L. Hewett and J. D. Wells, *Searching for supersymmetry in rare B decays*,
Phys.Rev. **D55** (1997) 5549, arXiv: `hep-ph/9610323 [hep-ph]` (cit. on p. 11).

[117] K. Babu and C. F. Kolda, *Higgs mediated $B^0 \to \mu^+\mu^-$ in minimal supersymmetry*,
Phys.Rev.Lett. **84** (2000) 228, arXiv: `hep-ph/9909476 [hep-ph]` (cit. on p. 11).

[118] M. Baak et al., *The Electroweak Fit of the Standard Model after the Discovery of a New
Boson at the LHC*, Eur.Phys.J. **C72** (2012) 2205, Update (dated: Sept. 2013) available
at `http://gfitter.desy.de.`, arXiv: `1209.2716 [hep-ph]` (cit. on p. 11).

[119] S. Heinemeyer et al.,
Electroweak precision observables in the MSSM with nonminimal flavor violation,
Eur. Phys. J. **C37** (2004) 481, arXiv: `hep-ph/0403228 [hep-ph]` (cit. on pp. 11, 60).

[120] S. Heinemeyer, W. Hollik and G. Weiglein,
Electroweak precision observables in the minimal supersymmetric standard model,
Phys. Rept. **425** (2006) 265, arXiv: `hep-ph/0412214 [hep-ph]`
(cit. on pp. 11, 31, 60, 126).

[121] S. Heinemeyer et al.,
Implications of LHC search results on the W boson mass prediction in the MSSM,
JHEP **1312** (2013) 084, arXiv: `1311.1663 [hep-ph]` (cit. on p. 11).

[122] P. J. Mohr, B. N. Taylor and D. B. Newell,
CODATA Recommended Values of the Fundamental Physical Constants: 2010,
Rev. Mod. Phys. **84** (2012) 1527, arXiv: `1203.5425 [physics.atom-ph]`;
G. W. Bennett et al.,
Measurement of the positive muon anomalous magnetic moment to 0.7 ppm,
Phys. Rev. Lett. **89** (2002) 101804, [Erratum: Phys. Rev. Lett.89,129903(2002)],
arXiv: `hep-ex/0208001 [hep-ex]`; G. W. Bennett et al.,
Measurement of the negative muon anomalous magnetic moment to 0.7 ppm,
Phys. Rev. Lett. **92** (2004) 161802, arXiv: `hep-ex/0401008 [hep-ex]`;

G. W. Bennett et al.,
Final Report of the Muon E821 Anomalous Magnetic Moment Measurement at BNL,
Phys. Rev. **D73** (2006) 072003, arXiv: `hep-ex/0602035 [hep-ex]`, cit. on p. 11.

[123] A. Hoecker and W. J. Marciano, *The muon anomalous magnetic moment*, (2013), eprint:
`http://pdg.lbl.gov/2015/reviews/rpp2015-rev-g-2-muon-anom-mag-moment.pdf`
(cit. on p. 11).

[124] G. 't Hooft, *Renormalization of Massless Yang-Mills Fields*, Nucl.Phys. **B33** (1971) 173;
G. 't Hooft, *Renormalizable Lagrangians for Massive Yang-Mills Fields*,
Nucl.Phys. **B35** (1971) 167; G. 't Hooft and M. J. G. Veltman,
Regularization and Renormalization of Gauge Fields, Nucl. Phys. **B44** (1972) 189,
cit. on p. 12.

[125] G. F. Giudice, *Naturally Speaking: The Naturalness Criterion and Physics at the LHC*,
(2008), arXiv: `0801.2562 [hep-ph]` (cit. on p. 12).

[126] J. R. Ellis et al., *Observables in Low-Energy Superstring Models*,
Mod. Phys. Lett. **A1** (1986) 57 (cit. on pp. 13, 94).

[127] R. Barbieri and G. F. Giudice, *Upper Bounds on Supersymmetric Particle Masses*,
Nucl. Phys. **B306** (1988) 63 (cit. on pp. 13, 94).

[128] L. Girardello and M. T. Grisaru, *Soft Breaking of Supersymmetry*,
Nucl. Phys. **B194** (1982) 65 (cit. on pp. 14, 18).

[129] G. Aad et al., *ATLAS Run 1 searches for direct pair production of third-generation
squarks at the Large Hadron Collider*,
Eur. Phys. J. **C75**.10 (2015) 510, [Erratum: Eur. Phys. J.C76,no.3,153(2016)],
arXiv: `1506.08616 [hep-ex]` (cit. on p. 14).

[130] V. Khachatryan et al., *Search for Supersymmetry Using Razor Variables in Events with
b-Tagged Jets in pp Collisions at $\sqrt{s} = 8$ TeV*, Phys. Rev. **D91** (2015) 052018,
arXiv: `1502.00300 [hep-ex]` (cit. on p. 14).

[131] H. Georgi and S. Glashow, *Unity of All Elementary Particle Forces*,
Phys.Rev.Lett. **32** (1974) 438 (cit. on p. 14).

[132] H. Fritzsch and P. Minkowski, *Unified Interactions of Leptons and Hadrons*,
Annals Phys. **93** (1975) 193 (cit. on p. 14).

[133] P. Langacker, *Grand Unified Theories and Proton Decay*, Phys.Rept. **72** (1981) 185
(cit. on p. 14).

[134] L. P. Kadanoff, *Scaling laws for Ising models near T(c)*, Physics **2** (1966) 263
(cit. on p. 15).

[135] K. G. Wilson, *Renormalization group and critical phenomena. 1. Renormalization group
and the Kadanoff scaling picture*, Phys. Rev. **B4** (1971) 3174 (cit. on p. 15).

[136] J. Polchinski, *Renormalization and Effective Lagrangians*, Nucl. Phys. **B231** (1984) 269
(cit. on p. 15).

[137] E. C. G. Stueckelberg and A. Petermann, *The normalization group in quantum theory*,
Helv. Phys. Acta **24** (1951) 317 (cit. on p. 15).

[138] M. Gell-Mann and F. E. Low, *Quantum electrodynamics at small distances*,
Phys. Rev. **95** (1954) 1300 (cit. on p. 15).

[139] C. G. Callan Jr., *Broken scale invariance in scalar field theory*,
Phys. Rev. **D2** (1970) 1541 (cit. on p. 15).

[140] K. Symanzik, *Small distance behavior in field theory and power counting*,
Commun. Math. Phys. **18** (1970) 227 (cit. on p. 15).

[141] M. E. Machacek and M. T. Vaughn, *Two Loop Renormalization Group Equations in a General Quantum Field Theory. 1. Wave Function Renormalization*,
Nucl. Phys. **B222** (1983) 83 (cit. on p. 15).

[142] D. J. H. Chung et al.,
The Soft supersymmetry breaking Lagrangian: Theory and applications,
Phys. Rept. **407** (2005) 1, arXiv: `hep-ph/0312378` `[hep-ph]` (cit. on p. 15).

[143] S. R. Coleman and J. Mandula, *All Possible Symmetries of the S Matrix*,
Phys. Rev. **159** (1967) 1251 (cit. on p. 16).

[144] R. Haag, J. T. Lopuszanski and M. Sohnius,
All Possible Generators of Supersymmetries of the s Matrix, Nucl. Phys. **B88** (1975) 257
(cit. on p. 16).

[145] H. K. Dreiner, H. E. Haber and S. P. Martin, *Two-component spinor techniques and Feynman rules for quantum field theory and supersymmetry*,
Physics Reports **494**.1–2 (2010) 1, ISSN: 0370-1573,
URL: `http://www.sciencedirect.com/science/article/pii/S0370157310001171`
(cit. on p. 16).

[146] P. Nath and R. L. Arnowitt,
Generalized Supergauge Symmetry as a New Framework for Unified Gauge Theories,
Phys. Lett. **B56** (1975) 177 (cit. on p. 16).

[147] R. L. Arnowitt, P. Nath and B. Zumino,
Superfield Densities and Action Principle in Curved Superspace,
Phys. Lett. **B56** (1975) 81 (cit. on p. 16).

[148] M. Kuroda, *Complete Lagrangian of MSSM*, (1999), arXiv: `hep-ph/9902340` `[hep-ph]`
(cit. on p. 16).

[149] J. Rosiek, *Complete set of Feynman rules for the MSSM: Erratum*, (1995),
arXiv: `hep-ph/9511250` `[hep-ph]` (cit. on p. 16).

[150] H. K. Dreiner, H. E. Haber and S. P. Martin, *Two-component spinor techniques and Feynman rules for quantum field theory and supersymmetry*, Phys. Rept. **494** (2010) 1,
arXiv: `0812.1594` `[hep-ph]` (cit. on pp. 16, 36).

[151] J. E. Kim and H. P. Nilles, *The mu Problem and the Strong CP Problem*,
Phys. Lett. **B138** (1984) 150 (cit. on pp. 17, 71).

[152] I. J. R. Aitchison, *Supersymmetry and the MSSM: An Elementary introduction*, (2005),
arXiv: `hep-ph/0505105` `[hep-ph]` (cit. on pp. 21, 22).

[153] A. H. Chamseddine, R. L. Arnowitt and P. Nath,
Locally Supersymmetric Grand Unification, Phys. Rev. Lett. **49** (1982) 970
(cit. on pp. 22, 48).

[154] R. Barbieri, S. Ferrara and C. A. Savoy,
Gauge Models with Spontaneously Broken Local Supersymmetry,
Phys. Lett. **B119** (1982) 343 (cit. on pp. 22, 48).

[155] L. J. Hall, J. D. Lykken and S. Weinberg,
Supergravity as the Messenger of Supersymmetry Breaking, Phys. Rev. **D27** (1983) 2359
(cit. on pp. 22, 48).

[156] N. Ohta, *Grand Uunified Theories based on local supersymmetry*,
Prog. Theor. Phys. **70** (1983) 542 (cit. on pp. 22, 48).

[157] M. Dine and W. Fischler,
A Phenomenological Model of Particle Physics Based on Supersymmetry,
Phys. Lett. **B110** (1982) 227 (cit. on pp. 22, 48, 89).

[158] L. Alvarez-Gaume, M. Claudson and M. B. Wise, *Low-Energy Supersymmetry*,
Nucl. Phys. **B207** (1982) 96 (cit. on pp. 22, 48, 89).

[159] M. Dine and A. E. Nelson, *Dynamical supersymmetry breaking at low-energies*,
Phys. Rev. **D48** (1993) 1277, arXiv: `hep-ph/9303230` `[hep-ph]` (cit. on pp. 22, 48, 89).

[160] M. Dine, A. E. Nelson and Y. Shirman,
Low-energy dynamical supersymmetry breaking simplified, Phys. Rev. **D51** (1995) 1362,
arXiv: `hep-ph/9408384` `[hep-ph]` (cit. on pp. 22, 48, 89).

[161] G. F. Giudice and R. Rattazzi, *Theories with gauge mediated supersymmetry breaking*,
Phys. Rept. **322** (1999) 419, arXiv: `hep-ph/9801271` `[hep-ph]`
(cit. on pp. 22, 48, 89, 92, 93).

[162] G. Aad et al., *Summary of the searches for squarks and gluinos using $\sqrt{s} = 8$ TeV pp
collisions with the ATLAS experiment at the LHC*, JHEP **10** (2015) 054,
arXiv: `1507.05525` `[hep-ex]` (cit. on p. 22).

[163] S. R. Coleman and E. J. Weinberg,
Radiative Corrections as the Origin of Spontaneous Symmetry Breaking,
Phys. Rev. **D7** (1973) 1888 (cit. on pp. 23, 24).

[164] R. Jackiw, *Functional evaluation of the effective potential*, Phys. Rev. **D9** (1974) 1686
(cit. on p. 23).

[165] M. Sher, *Electroweak Higgs Potentials and Vacuum Stability*,
Phys. Rept. **179** (1989) 273 (cit. on p. 23).

[166] E. J. Weinberg and A.-q. Wu, *Understanding Complex Perturbative Effective Potentials*,
Phys. Rev. **D36** (1987) 2474 (cit. on pp. 23, 25).

[167] C. Ford et al., *The Effective potential and the renormalization group*,
Nucl. Phys. **B395** (1993) 17, arXiv: `hep-lat/9210033` `[hep-lat]` (cit. on p. 23).

[168] J. A. Casas, J. R. Espinosa and M. Quiros, *Improved Higgs mass stability bound in the
standard model and implications for supersymmetry*, Phys. Lett. **B342** (1995) 171,
arXiv: `hep-ph/9409458` `[hep-ph]` (cit. on p. 23).

[169] J. R. Espinosa and M. Quiros,
Improved metastability bounds on the standard model Higgs mass,
Phys. Lett. **B353** (1995) 257, arXiv: `hep-ph/9504241` `[hep-ph]` (cit. on p. 23).

[170] J. A. Casas, J. R. Espinosa and M. Quiros,
Standard model stability bounds for new physics within LHC reach,
Phys. Lett. **B382** (1996) 374, arXiv: `hep-ph/9603227` `[hep-ph]` (cit. on p. 23).

[171]   A. Andreassen, W. Frost and M. D. Schwartz, *Consistent Use of Effective Potentials*, Phys. Rev. **D91**.1 (2015) 016009, arXiv: `1408.0287` `[hep-ph]` (cit. on pp. 23–25).

[172]   G. Isidori, G. Ridolfi and A. Strumia, *On the metastability of the standard model vacuum*, Nucl. Phys. **B609** (2001) 387, arXiv: `hep-ph/0104016` `[hep-ph]` (cit. on p. 23).

[173]   M. B. Einhorn and D. R. T. Jones, *The Effective potential, the renormalisation group and vacuum stability*, JHEP **04** (2007) 051, arXiv: `hep-ph/0702295` `[HEP-PH]` (cit. on p. 23).

[174]   J. Ellis et al., *The Probable Fate of the Standard Model*, Phys. Lett. **B679** (2009) 369, arXiv: `0906.0954` `[hep-ph]` (cit. on p. 23).

[175]   J. Elias-Miro et al., *Higgs mass implications on the stability of the electroweak vacuum*, Phys. Lett. **B709** (2012) 222, arXiv: `1112.3022` `[hep-ph]` (cit. on p. 23).

[176]   G. Degrassi et al., *Higgs mass and vacuum stability in the Standard Model at NNLO*, JHEP **08** (2012) 098, arXiv: `1205.6497` `[hep-ph]` (cit. on p. 23).

[177]   C. Itzykson and J. B. Zuber, *Quantum Field Theory*, International Series In Pure and Applied Physics, New York: McGraw-Hill, 1980, ISBN: 9780486445687, 0486445682, URL: `http://dx.doi.org/10.1063/1.2916419` (cit. on p. 23).

[178]   R. H. Brandenberger, *Quantum Field Theory Methods and Inflationary Universe Models*, Rev. Mod. Phys. **57** (1985) 1 (cit. on pp. 23, 24).

[179]   S. P. Martin, *Three-loop Standard Model effective potential at leading order in strong and top Yukawa couplings*, Phys.Rev. **D89** (2014) 013003, arXiv: `1310.7553` `[hep-ph]` (cit. on pp. 24, 26).

[180]   S. P. Martin, *Four-loop Standard Model effective potential at leading order in QCD*, Phys. Rev. **D92**.5 (2015) 054029, arXiv: `1508.00912` `[hep-ph]` (cit. on p. 24).

[181]   N. K. Nielsen, *On the Gauge Dependence of Spontaneous Symmetry Breaking in Gauge Theories*, Nucl. Phys. **B101** (1975) 173 (cit. on p. 24).

[182]   D. Buttazzo et al., *Investigating the near-criticality of the Higgs boson*, JHEP **12** (2013) 089, arXiv: `1307.3536` `[hep-ph]` (cit. on p. 25).

[183]   S. P. Martin, *Complete two loop effective potential approximation to the lightest Higgs scalar boson mass in supersymmetry*, Phys.Rev. **D67** (2003) 095012, arXiv: `hep-ph/0211366` `[hep-ph]` (cit. on pp. 26, 27, 30, 52, 53, 124).

[184]   J. Elias-Miro, J. Espinosa and T. Konstandin, *Taming Infrared Divergences in the Effective Potential*, JHEP **1408** (2014) 034, arXiv: `1406.2652` `[hep-ph]` (cit. on p. 26).

[185]   S. P. Martin, *Taming the Goldstone contributions to the effective potential*, Phys.Rev. **D90** (2014) 016013, arXiv: `1406.2355` `[hep-ph]` (cit. on p. 26).

[186]   N. Kumar and S. P. Martin, *Resummation of Goldstone boson contributions to the MSSM effective potential*, (2016), arXiv: `1605.02059` `[hep-ph]` (cit. on pp. 26, 27).

[187] M. D. Goodsell, K. Nickel and F. Staub, *Two-Loop Higgs mass calculations in supersymmetric models beyond the MSSM with SARAH and SPheno*, Eur.Phys.J. **C75**.1 (2015) 32, arXiv: 1411.0675 [hep-ph] (cit. on pp. 29, 55, 57, 59, 60, 76, 108, 124, 125, 137).

[188] M. Goodsell, K. Nickel and F. Staub, *Generic two-loop Higgs mass calculation from a diagrammatic approach*, Eur. Phys. J. **C75**.6 (2015) 290, arXiv: 1503.03098 [hep-ph] (cit. on pp. 29, 40, 45, 53, 56, 108, 124, 125, 133, 155).

[189] H. E. Haber and R. Hempfling, *Can the mass of the lightest Higgs boson of the minimal supersymmetric model be larger than m(Z)?*, Phys. Rev. Lett. **66** (1991) 1815 (cit. on p. 29).

[190] J. R. Ellis, G. Ridolfi and F. Zwirner, *Radiative corrections to the masses of supersymmetric Higgs bosons*, Phys. Lett. **B257** (1991) 83 (cit. on p. 29).

[191] Y. Okada, M. Yamaguchi and T. Yanagida, *Upper bound of the lightest Higgs boson mass in the minimal supersymmetric standard model*, Prog. Theor. Phys. **85** (1991) 1 (cit. on p. 29).

[192] Y. Okada, M. Yamaguchi and T. Yanagida, *Renormalization group analysis on the Higgs mass in the softly broken supersymmetric standard model*, Phys. Lett. **B262** (1991) 54 (cit. on p. 29).

[193] J. R. Ellis, G. Ridolfi and F. Zwirner, *On radiative corrections to supersymmetric Higgs boson masses and their implications for LEP searches*, Phys. Lett. **B262** (1991) 477 (cit. on p. 29).

[194] M. Carena et al., *Reconciling the two loop diagrammatic and effective field theory computations of the mass of the lightest CP - even Higgs boson in the MSSM*, Nucl.Phys. **B580** (2000) 29, arXiv: hep-ph/0001002 [hep-ph] (cit. on pp. 29, 30).

[195] G. Degrassi et al., *Towards high precision predictions for the MSSM Higgs sector*, Eur. Phys. J. **C28** (2003) 133, arXiv: hep-ph/0212020 [hep-ph] (cit. on pp. 29–31, 60, 125).

[196] A. Brignole, *Radiative corrections to the supersymmetric neutral Higgs boson masses*, Phys. Lett. **B281** (1992) 284 (cit. on pp. 30, 123).

[197] P. H. Chankowski, S. Pokorski and J. Rosiek, *Charged and neutral supersymmetric Higgs boson masses: Complete one loop analysis*, Phys. Lett. **B274** (1992) 191 (cit. on pp. 30, 123).

[198] A. Dabelstein, *The One loop renormalization of the MSSM Higgs sector and its application to the neutral scalar Higgs masses*, Z. Phys. **C67** (1995) 495, arXiv: hep-ph/9409375 [hep-ph] (cit. on pp. 30, 123).

[199] D. M. Pierce et al., *Precision corrections in the minimal supersymmetric standard model*, Nucl.Phys. **B491** (1997) 3, arXiv: hep-ph/9606211 [hep-ph] (cit. on pp. 30, 85, 89, 95, 96, 123, 130).

[200] A. Brignole et al., *On the O(alpha(t)**2) two loop corrections to the neutral Higgs boson masses in the MSSM*, Nucl.Phys. **B631** (2002) 195, arXiv: `hep-ph/0112177` `[hep-ph]`; G. Degrassi, P. Slavich and F. Zwirner, *On the neutral Higgs boson masses in the MSSM for arbitrary stop mixing*, Nucl.Phys. **B611** (2001) 403, arXiv: `hep-ph/0105096` `[hep-ph]`; A. Brignole et al., *On the two loop sbottom corrections to the neutral Higgs boson masses in the MSSM*, Nucl.Phys. **B643** (2002) 79, arXiv: `hep-ph/0206101` `[hep-ph]`; A. Dedes and P. Slavich, *Two loop corrections to radiative electroweak symmetry breaking in the MSSM*, Nucl.Phys. **B657** (2003) 333, arXiv: `hep-ph/0212132` `[hep-ph]`; A. Dedes, G. Degrassi and P. Slavich, *On the two loop Yukawa corrections to the MSSM Higgs boson masses at large tan beta*, Nucl.Phys. **B672** (2003) 144, arXiv: `hep-ph/0305127` `[hep-ph]`, cit. on pp. 30, 54–57, 61, 68, 70, 76, 89, 123, 124.

[201] R. Hempfling and A. H. Hoang, *Two loop radiative corrections to the upper limit of the lightest Higgs boson mass in the minimal supersymmetric model*, Phys. Lett. **B331** (1994) 99, arXiv: `hep-ph/9401219` `[hep-ph]` (cit. on p. 30).

[202] M. Carena, M. Quiros and C. Wagner, *Effective potential methods and the Higgs mass spectrum in the MSSM*, Nucl.Phys. **B461** (1996) 407, arXiv: `hep-ph/9508343` `[hep-ph]` (cit. on p. 30).

[203] S. Heinemeyer, W. Hollik and G. Weiglein, *QCD corrections to the masses of the neutral CP - even Higgs bosons in the MSSM*, Phys.Rev. **D58** (1998) 091701, arXiv: `hep-ph/9803277` `[hep-ph]` (cit. on p. 30).

[204] R.-J. Zhang, *Two loop effective potential calculation of the lightest CP even Higgs boson mass in the MSSM*, Phys. Lett. **B447** (1999) 89, arXiv: `hep-ph/9808299` `[hep-ph]` (cit. on p. 30).

[205] S. Heinemeyer, W. Hollik and G. Weiglein, *The Masses of the neutral CP - even Higgs bosons in the MSSM: Accurate analysis at the two loop level*, Eur.Phys.J. **C9** (1999) 343, arXiv: `hep-ph/9812472` `[hep-ph]` (cit. on p. 30).

[206] S. Heinemeyer, W. Hollik and G. Weiglein, *The Mass of the lightest MSSM Higgs boson: A Compact analytical expression at the two loop level*, Phys.Lett. **B455** (1999) 179, arXiv: `hep-ph/9903404` `[hep-ph]` (cit. on p. 30).

[207] J. R. Espinosa and R.-J. Zhang, *MSSM lightest CP even Higgs boson mass to O(alpha(s) alpha(t)): The Effective potential approach*, JHEP **03** (2000) 026, arXiv: `hep-ph/9912236` `[hep-ph]` (cit. on p. 30).

[208] J. R. Espinosa and R.-J. Zhang, *Complete two loop dominant corrections to the mass of the lightest CP even Higgs boson in the minimal supersymmetric standard model*, Nucl. Phys. **B586** (2000) 3, arXiv: `hep-ph/0003246` `[hep-ph]` (cit. on p. 30).

[209] S. P. Martin, *Two loop effective potential for the minimal supersymmetric standard model*, Phys. Rev. **D66** (2002) 096001, arXiv: `hep-ph/0206136` `[hep-ph]` (cit. on pp. 30, 142, 153).

[210] S. Heinemeyer et al., *High-precision predictions for the MSSM Higgs sector at* $O(\alpha_b \alpha_s)$, Eur. Phys. J. **C39** (2005) 465, arXiv: `hep-ph/0411114` `[hep-ph]` (cit. on p. 30).

[211] K. Sasaki, M. Carena and C. Wagner, *Renormalization group analysis of the Higgs sector in the minimal supersymmetric standard model*, Nucl.Phys. **B381** (1992) 66 (cit. on p. 30).

[212] M. Carena et al., *Analytical expressions for radiatively corrected Higgs masses and couplings in the MSSM*, Phys.Lett. **B355** (1995) 209, arXiv: `hep-ph/9504316` [`hep-ph`] (cit. on p. 30).

[213] H. E. Haber, R. Hempfling and A. H. Hoang, *Approximating the radiatively corrected Higgs mass in the minimal supersymmetric model*, Z. Phys. **C75** (1997) 539, arXiv: `hep-ph/9609331` [`hep-ph`] (cit. on p. 30).

[214] M. Carena et al., *Renormalization group improved effective potential for the MSSM Higgs sector with explicit CP violation*, Nucl.Phys. **B586** (2000) 92, arXiv: `hep-ph/0003180` [`hep-ph`] (cit. on p. 30).

[215] M. Carena et al., *Higgs boson pole masses in the MSSM with explicit CP violation*, Nucl.Phys. **B625** (2002) 345, arXiv: `hep-ph/0111245` [`hep-ph`] (cit. on p. 30).

[216] J. R. Espinosa and I. Navarro, *Radiative corrections to the Higgs boson mass for a hierarchical stop spectrum*, Nucl. Phys. **B615** (2001) 82, arXiv: `hep-ph/0104047` [`hep-ph`] (cit. on p. 30).

[217] B. C. Allanach, *SOFTSUSY: a program for calculating supersymmetric spectra*, Comput. Phys. Commun. **143** (2002) 305, arXiv: `hep-ph/0104145` [`hep-ph`] (cit. on pp. 30, 71).

[218] B. Allanach and M. Bernhardt, *Including R-parity violation in the numerical computation of the spectrum of the minimal supersymmetric standard model: SOFTSUSY*, Comput.Phys.Commun. **181** (2010) 232, arXiv: `0903.1805` [`hep-ph`] (cit. on pp. 30, 71).

[219] B. Allanach et al., *Next-to-Minimal SOFTSUSY*, Comput.Phys.Commun. **185** (2014) 2322, arXiv: `1311.7659` [`hep-ph`] (cit. on pp. 30, 71).

[220] B. Allanach, A. Bednyakov and R. R. de Austri, *Higher Order Corrections and Unification in the Minimal Supersymmetric Standard Model: SOFTSUSY3.5.0*, (2014), arXiv: `1407.6130` [`hep-ph`] (cit. on pp. 30, 71).

[221] W. Porod, *SPheno, a program for calculating supersymmetric spectra, SUSY particle decays and SUSY particle production at e+ e- colliders*, Comput. Phys. Commun. **153** (2003) 275, arXiv: `hep-ph/0301101` [`hep-ph`] (cit. on pp. 30, 48, 123).

[222] W. Porod and F. Staub, *SPheno 3.1: Extensions including flavour, CP-phases and models beyond the MSSM*, Comput. Phys. Commun. **183** (2012) 2458, arXiv: `1104.1573` [`hep-ph`] (cit. on pp. 30, 48, 123).

[223] A. Djouadi, J.-L. Kneur and G. Moultaka, *SuSpect: A Fortran code for the supersymmetric and Higgs particle spectrum in the MSSM*, Comput.Phys.Commun. **176** (2007) 426, arXiv: `hep-ph/0211331` [`hep-ph`] (cit. on p. 30).

[224]   T. Hahn et al., *High-Precision Predictions for the Light CP -Even Higgs Boson Mass of the Minimal Supersymmetric Standard Model*, Phys. Rev. Lett. **112**.14 (2014) 141801, arXiv: `1312.4937` [`hep-ph`] (cit. on pp. 30, 60, 71, 123).

[225]   S. Heinemeyer et al., *The Higgs sector of the complex MSSM at two-loop order: QCD contributions*, Phys.Lett. **B652** (2007) 300, arXiv: `0705.0746` [`hep-ph`] (cit. on pp. 30, 71).

[226]   T. Hahn et al., *Precision Higgs masses with FeynHiggs 2.2*, eConf **C050318** (2005) 0106, arXiv: `hep-ph/0507009` [`hep-ph`] (cit. on pp. 30, 71).

[227]   S. Heinemeyer, W. Hollik and G. Weiglein, *FeynHiggs: A Program for the calculation of the masses of the neutral CP even Higgs bosons in the MSSM*, Comput.Phys.Commun. **124** (2000) 76, arXiv: `hep-ph/9812320` [`hep-ph`] (cit. on pp. 30, 71, 123).

[228]   S. P. Martin, *Three-loop corrections to the lightest Higgs scalar boson mass in supersymmetry*, Phys.Rev. **D75** (2007) 055005, arXiv: `hep-ph/0701051` [`hep-ph`] (cit. on pp. 30, 123).

[229]   P. Kant et al., *Light MSSM Higgs boson mass to three-loop accuracy*, JHEP **08** (2010) 104, arXiv: `1005.5709` [`hep-ph`] (cit. on pp. 30, 123).

[230]   R. Harlander et al., *Higgs boson mass in supersymmetry to three loops*, Phys.Rev.Lett. **100** (2008) 191602, arXiv: `0803.0672` [`hep-ph`] (cit. on pp. 30, 123).

[231]   S. P. Martin, *Strong and Yukawa two-loop contributions to Higgs scalar boson self-energies and pole masses in supersymmetry*, Phys.Rev. **D71** (2005) 016012, arXiv: `hep-ph/0405022` [`hep-ph`] (cit. on pp. 30, 36).

[232]   S. Borowka et al., *Momentum-dependent two-loop QCD corrections to the neutral Higgs-boson masses in the MSSM*, (2014), arXiv: `1404.7074` [`hep-ph`] (cit. on pp. 30, 36).

[233]   W. Hollik and S. Paßehr, *Higgs boson masses and mixings in the complex MSSM with two-loop top-Yukawa-coupling corrections*, (2014), arXiv: `1409.1687` [`hep-ph`] (cit. on p. 30).

[234]   G. Degrassi, S. Di Vita and P. Slavich, *Two-loop QCD corrections to the MSSM Higgs masses beyond the effective-potential approximation*, Eur. Phys. J. **C75**.2 (2015) 61, arXiv: `1410.3432` [`hep-ph`] (cit. on pp. 30, 36).

[235]   P. Draper, G. Lee and C. E. M. Wagner, *Precise Estimates of the Higgs Mass in Heavy SUSY*, Phys.Rev. **D89** (2014) 055023, arXiv: `1312.5743` [`hep-ph`] (cit. on p. 30).

[236]   E. Bagnaschi et al., *Higgs Mass and Unnatural Supersymmetry*, JHEP **09** (2014) 092, arXiv: `1407.4081` [`hep-ph`] (cit. on p. 30).

[237]   P. Draper and H. Rzehak, *A Review of Higgs Mass Calculations in Supersymmetric Models*, Phys. Rept. **619** (2016) 1, arXiv: `1601.01890` [`hep-ph`] (cit. on p. 30).

[238]   U. Ellwanger, C. Hugonie and A. M. Teixeira, *The Next-to-Minimal Supersymmetric Standard Model*, Phys.Rept. **496** (2010) 1, arXiv: `0910.1785` [`hep-ph`] (cit. on pp. 30, 71, 73).

[239] U. Ellwanger and C. Hugonie,
The Upper bound on the lightest Higgs mass in the NMSSM revisited,
Mod.Phys.Lett. **A22** (2007) 1581, arXiv: `hep-ph/0612133 [hep-ph]`
(cit. on pp. 30, 71).

[240] G. G. Ross and K. Schmidt-Hoberg, *The Fine-Tuning of the Generalised NMSSM*,
Nucl.Phys. **B862** (2012) 710, arXiv: `1108.1284 [hep-ph]` (cit. on pp. 30, 71).

[241] G. G. Ross, K. Schmidt-Hoberg and F. Staub,
The Generalised NMSSM at One Loop: Fine Tuning and Phenomenology,
JHEP **1208** (2012) 074, arXiv: `1205.1509 [hep-ph]` (cit. on pp. 30, 71, 83).

[242] A. Kaminska, G. G. Ross and K. Schmidt-Hoberg, *Non-universal gaugino masses and
fine tuning implications for SUSY searches in the MSSM and the GNMSSM*,
JHEP **1311** (2013) 209, arXiv: `1308.4168 [hep-ph]` (cit. on p. 30).

[243] X. Lu et al., *A Natural Higgs Mass in Supersymmetry from NonDecoupling Effects*,
Phys.Rev.Lett. **112** (2014) 191803, arXiv: `1308.0792 [hep-ph]` (cit. on p. 30).

[244] A. Kaminska et al., *A precision study of the fine tuning in the DiracNMSSM*,
JHEP **1406** (2014) 153, arXiv: `1401.1816 [hep-ph]` (cit. on pp. 30, 71).

[245] R. Ding et al., *The Supersymmetric Standard Models with a Pseudo-Dirac Gluino from
Hybrid F− and D−Term Supersymmetry Breakings*, (2015),
arXiv: `1502.03614 [hep-ph]` (cit. on p. 30).

[246] K. Benakli, M. D. Goodsell and F. Staub, *Dirac Gauginos and the 125 GeV Higgs*,
JHEP **1306** (2013) 073, arXiv: `1211.0552 [hep-ph]` (cit. on p. 30).

[247] H. E. Haber and M. Sher, *Higgs Mass Bound in E(6) Based Supersymmetric Theories*,
Phys.Rev. **D35** (1987) 2206 (cit. on p. 30).

[248] M. Drees,
Comment on 'Higgs Boson Mass Bound in E(6) Based Supersymmetric Theories.',
Phys.Rev. **D35** (1987) 2910 (cit. on p. 30).

[249] M. Cvetic et al.,
Electroweak breaking and the mu problem in supergravity models with an additional U(1),
Phys.Rev. **D56** (1997) 2861, arXiv: `hep-ph/9703317 [hep-ph]` (cit. on p. 30).

[250] E. Ma,
Exceeding the MSSM Higgs Mass Bound in a Special Class of U(1) Gauge Models,
Phys.Lett. **B705** (2011) 320, arXiv: `1108.4029 [hep-ph]` (cit. on p. 30).

[251] Y. Zhang et al., *Light Higgs Mass Bound in SUSY Left-Right Models*,
Phys.Rev. **D78** (2008) 011302, arXiv: `0804.0268 [hep-ph]` (cit. on p. 30).

[252] M. Hirsch et al., *Hefty MSSM-like light Higgs in extended gauge models*,
JHEP **1202** (2012) 084, arXiv: `1110.3037 [hep-ph]` (cit. on p. 30).

[253] M. E. Krauss, W. Porod and F. Staub,
SO(10) inspired gauge-mediated supersymmetry breaking,
Phys.Rev. **D88**.1 (2013) 015014, arXiv: `1304.0769 [hep-ph]` (cit. on p. 30).

[254] M. Bastero-Gil et al., *Does LEP prefer the NMSSM?*, Phys.Lett. **B489** (2000) 359,
arXiv: `hep-ph/0006198 [hep-ph]` (cit. on pp. 30, 71).

[255] R. Dermisek and J. F. Gunion, *Consistency of LEP event excesses with an h -> aa decay scenario and low-fine-tuning NMSSM models*, Phys.Rev. **D73** (2006) 111701, arXiv: `hep-ph/0510322 [hep-ph]` (cit. on pp. 30, 71).

[256] U. Ellwanger, G. Espitalier-Noel and C. Hugonie, *Naturalness and Fine Tuning in the NMSSM: Implications of Early LHC Results*, JHEP **1109** (2011) 105, arXiv: `1107.2472 [hep-ph]` (cit. on pp. 30, 71).

[257] F. Staub, *Beyond-MSSM Higgs sectors*, (2014), arXiv: `1409.7182 [hep-ph]` (cit. on p. 30).

[258] H. K. Dreiner, M. Kramer and J. Tattersall, *How low can SUSY go? Matching, monojets and compressed spectra*, Europhys.Lett. **99** (2012) 61001, arXiv: `1207.1613 [hep-ph]` (cit. on p. 30).

[259] B. Bhattacherjee et al., *Natural supersymmetry's last hope: R-parity violation via UDD operators*, Phys.Rev. **D87**.11 (2013) 115002, arXiv: `1301.2336 [hep-ph]` (cit. on p. 30).

[260] U. Ellwanger and A. M. Teixeira, *NMSSM with a singlino LSP: possible challenges for searches for supersymmetry at the LHC*, (2014), arXiv: `1406.7221 [hep-ph]` (cit. on pp. 30, 71).

[261] J. S. Kim et al., *'Stop' that ambulance! New physics at the LHC?*, (2014), arXiv: `1406.0858 [hep-ph]` (cit. on p. 30).

[262] H. Baer et al., *The International Linear Collider Technical Design Report - Volume 2: Physics*, (2013), arXiv: `1306.6352 [hep-ph]` (cit. on p. 31).

[263] J. P. Vega and G. Villadoro, *SusyHD: Higgs mass Determination in Supersymmetry*, JHEP **07** (2015) 159, arXiv: `1504.05200 [hep-ph]` (cit. on p. 31).

[264] G. Passarino and M. J. G. Veltman, *One Loop Corrections for e+ e- Annihilation Into mu+ mu- in the Weinberg Model*, Nucl. Phys. **B160** (1979) 151 (cit. on pp. 33, 133, 135).

[265] S. P. Martin, *Two loop effective potential for a general renormalizable theory and softly broken supersymmetry*, Phys.Rev. **D65** (2002) 116003, arXiv: `hep-ph/0111209 [hep-ph]` (cit. on pp. 34, 36, 37, 124, 136, 137, 156).

[266] S. P. Martin, *Evaluation of two loop selfenergy basis integrals using differential equations*, Phys. Rev. **D68** (2003) 075002, arXiv: `hep-ph/0307101 [hep-ph]` (cit. on pp. 36, 40, 133, 136).

[267] S. P. Martin, *Two loop scalar self energies in a general renormalizable theory at leading order in gauge couplings*, Phys. Rev. **D70** (2004) 016005, arXiv: `hep-ph/0312092 [hep-ph]` (cit. on pp. 36, 40, 45, 124, 154, 162, 165).

[268] C. Ford, I. Jack and D. R. T. Jones, *The Standard model effective potential at two loops*, Nucl. Phys. **B387** (1992) 373, [Erratum: Nucl. Phys.B504,551(1997)], arXiv: `hep-ph/0111190 [hep-ph]` (cit. on p. 36).

[269] O. V. Tarasov, *Generalized recurrence relations for two loop propagator integrals with arbitrary masses*, Nucl. Phys. **B502** (1997) 455, arXiv: `hep-ph/9703319 [hep-ph]` (cit. on p. 40).

[270] S. P. Martin, *Two-loop scalar self-energies and pole masses in a general renormalizable theory with massless gauge bosons*, Phys. Rev. **D71** (2005) 116004, arXiv: `hep-ph/0502168` [`hep-ph`] (cit. on p. 40).

[271] S. P. Martin, *Z-boson pole mass at two-loop order in the pure $\overline{MS}$ scheme*, Phys. Rev. **D92**.1 (2015) 014026, arXiv: `1505.04833` [`hep-ph`] (cit. on p. 40).

[272] P. Z. Skands et al., *SUSY Les Houches accord: Interfacing SUSY spectrum calculators, decay packages, and event generators*, JHEP **07** (2004) 036, arXiv: `hep-ph/0311123` [`hep-ph`] (cit. on p. 47).

[273] B. C. Allanach et al., *SUSY Les Houches Accord 2*, Comput. Phys. Commun. **180** (2009) 8, arXiv: `0801.0045` [`hep-ph`] (cit. on p. 47).

[274] F. Mahmoudi et al., *Flavour Les Houches Accord: Interfacing Flavour related Codes*, Comput. Phys. Commun. **183** (2012) 285, arXiv: `1008.0762` [`hep-ph`] (cit. on p. 47).

[275] L. Randall and R. Sundrum, *Out of this world supersymmetry breaking*, Nucl. Phys. **B557** (1999) 79, arXiv: `hep-th/9810155` [`hep-th`] (cit. on p. 48).

[276] G. F. Giudice et al., *Gaugino mass without singlets*, JHEP **12** (1998) 027, arXiv: `hep-ph/9810442` [`hep-ph`] (cit. on p. 48).

[277] J. A. Bagger, T. Moroi and E. Poppitz, *Anomaly mediation in supergravity theories*, JHEP **04** (2000) 009, arXiv: `hep-th/9911029` [`hep-th`] (cit. on p. 48).

[278] S. P. Martin and M. T. Vaughn, *Two loop renormalization group equations for soft supersymmetry breaking couplings*, Phys.Rev. **D50** (1994) 2282, arXiv: `hep-ph/9311340` [`hep-ph`] (cit. on pp. 48, 91).

[279] Y. Yamada, *Two loop renormalization of gaugino masses in general supersymmetric gauge models*, Phys. Rev. Lett. **72** (1994) 25, arXiv: `hep-ph/9308304` [`hep-ph`] (cit. on p. 48).

[280] Y. Yamada, *Two loop renormalization of gaugino mass in supersymmetric gauge model*, Phys. Lett. **B316** (1993) 109, arXiv: `hep-ph/9307217` [`hep-ph`] (cit. on p. 48).

[281] Y. Yamada, *Two loop renormalization group equations for soft SUSY breaking scalar interactions: Supergraph method*, Phys.Rev. **D50** (1994) 3537, arXiv: `hep-ph/9401241` [`hep-ph`] (cit. on p. 48).

[282] T. Hahn, *Generating Feynman diagrams and amplitudes with FeynArts 3*, Comput. Phys. Commun. **140** (2001) 418, arXiv: `hep-ph/0012260` [`hep-ph`] (cit. on p. 48).

[283] A. Belyaev, N. D. Christensen and A. Pukhov, *CalcHEP 3.4 for collider physics within and beyond the Standard Model*, Comput. Phys. Commun. **184** (2013) 1729, arXiv: `1207.6082` [`hep-ph`] (cit. on p. 48).

[284] W. Kilian, T. Ohl and J. Reuter, *WHIZARD: Simulating Multi-Particle Processes at LHC and ILC*, Eur. Phys. J. **C71** (2011) 1742, arXiv: `0708.4233` [`hep-ph`], cit. on p. 48.

[285] J. Alwall et al., *The automated computation of tree-level and next-to-leading order differential cross sections, and their matching to parton shower simulations*, JHEP **07** (2014) 079, arXiv: `1405.0301` [`hep-ph`] (cit. on pp. 48, 111).

[286] P. Bechtle et al., *HiggsBounds: Confronting Arbitrary Higgs Sectors with Exclusion Bounds from LEP and the Tevatron*, Comput. Phys. Commun. **181** (2010) 138, arXiv: `0811.4169` `[hep-ph]` (cit. on p. 48).

[287] P. Bechtle et al., *HiggsBounds 2.0.0: Confronting Neutral and Charged Higgs Sector Predictions with Exclusion Bounds from LEP and the Tevatron*, Comput. Phys. Commun. **182** (2011) 2605, arXiv: `1102.1898` `[hep-ph]` (cit. on p. 48).

[288] P. Bechtle et al., *HiggsSignals: Confronting arbitrary Higgs sectors with measurements at the Tevatron and the LHC*, Eur. Phys. J. **C74**.2 (2014) 2711, arXiv: `1305.1933` `[hep-ph]` (cit. on p. 48).

[289] J. E. Camargo-Molina et al., **Vevacious**: *A Tool For Finding The Global Minima Of One-Loop Effective Potentials With Many Scalars*, Eur. Phys. J. **C73**.10 (2013) 2588, arXiv: `1307.1477` `[hep-ph]` (cit. on pp. 48, 66, 86).

[290] P. Athron et al., *FlexibleSUSY – A spectrum generator generator for supersymmetric models*, (2014), arXiv: `1406.2319` `[hep-ph]` (cit. on pp. 48, 123).

[291] P. Athron et al., *FlexibleSUSY - a meta spectrum generator for supersymmetric models*, (2014), arXiv: `1410.7385` `[hep-ph]`, URL: `https://inspirehep.net/record/1324800/files/arXiv:1410.7385.pdf` (cit. on pp. 48, 123).

[292] C. Ridders, *A new algorithm for computing a single root of a real continuous function*, Circuits and Systems, IEEE Transactions on **26**.11 (1979) 979, ISSN: 0098-4094, URL: `http://dx.doi.org/10.1109/TCS.1979.1084580` (cit. on p. 52).

[293] S. P. Martin and D. G. Robertson, *TSIL: A Program for the calculation of two-loop self-energy integrals*, Comput. Phys. Commun. **174** (2006) 133, arXiv: `hep-ph/0501132` `[hep-ph]` (cit. on pp. 53, 126).

[294] G. Degrassi and P. Slavich, *On the radiative corrections to the neutral Higgs boson masses in the NMSSM*, Nucl.Phys. **B825** (2010) 119, arXiv: `0907.4682` `[hep-ph]` (cit. on pp. 55, 71, 75, 83).

[295] N. Bernal, A. Djouadi and P. Slavich, *The MSSM with heavy scalars*, JHEP **0707** (2007) 016, arXiv: `0705.1496` `[hep-ph]` (cit. on p. 56).

[296] M. D. Goodsell, K. Nickel and F. Staub, *The Higgs Mass in the MSSM at two-loop order beyond minimal flavour violation*, Phys. Lett. **B758** (2016) 18, arXiv: `1511.01904` `[hep-ph]` (cit. on p. 59).

[297] M. D. Goodsell, K. Nickel and F. Staub, *Two-loop corrections to the Higgs masses in the NMSSM*, Phys. Rev. **D91** (2015) 035021, arXiv: `1411.4665` `[hep-ph]` (cit. on pp. 59, 71).

[298] H. K. Dreiner, K. Nickel and F. Staub, *On the two-loop corrections to the Higgs mass in trilinear R-parity violation*, Phys.Lett. **B742** (2015) 261, arXiv: `1411.3731` `[hep-ph]` (cit. on pp. 59, 84).

[299] K. Nickel and F. Staub, *Precise determination of the Higgs mass in supersymmetric models with vectorlike tops and the impact on naturalness in minimal GMSB*, JHEP **07** (2015) 139, arXiv: `1505.06077` `[hep-ph]` (cit. on pp. 59, 89, 131).

[300]   O. Buchmueller et al.,
        Implications of Improved Higgs Mass Calculations for Supersymmetric Models,
        Eur. Phys. J. **C74**.3 (2014) 2809, arXiv: `1312.5233` [`hep-ph`] (cit. on pp. 60, 123).

[301]   L. J. Hall, V. A. Kostelecky and S. Raby, *New Flavor Violations in Supergravity Models*,
        Nucl. Phys. **B267** (1986) 415 (cit. on p. 60).

[302]   G. D'Ambrosio et al., *Minimal flavor violation: An Effective field theory approach*,
        Nucl. Phys. **B645** (2002) 155, arXiv: `hep-ph/0207036` [`hep-ph`] (cit. on p. 60).

[303]   V. Cirigliano et al., *Minimal flavor violation in the lepton sector*,
        Nucl. Phys. **B728** (2005) 121, arXiv: `hep-ph/0507001` [`hep-ph`] (cit. on p. 60).

[304]   R. Kallosh et al., *Gravity and global symmetries*, Phys. Rev. **D52** (1995) 912,
        arXiv: `hep-th/9502069` [`hep-th`] (cit. on p. 60).

[305]   G. D. Kribs, T. Okui and T. S. Roy, *Viable Gravity-Mediated Supersymmetry Breaking*,
        Phys. Rev. **D82** (2010) 115010, arXiv: `1008.1798` [`hep-ph`] (cit. on p. 60).

[306]   Y. Shadmi and P. Z. Szabo, *Flavored Gauge-Mediation*, JHEP **1206** (2012) 124,
        arXiv: `1103.0292` [`hep-ph`] (cit. on p. 60).

[307]   L. Calibbi, P. Paradisi and R. Ziegler,
        Gauge Mediation beyond Minimal Flavor Violation, JHEP **06** (2013) 052,
        arXiv: `1304.1453` [`hep-ph`] (cit. on p. 60).

[308]   I. Galon, G. Perez and Y. Shadmi,
        Non-Degenerate Squarks from Flavored Gauge Mediation, JHEP **09** (2013) 117,
        arXiv: `1306.6631` [`hep-ph`] (cit. on p. 60).

[309]   F. Brümmer, M. McGarrie and A. Weiler,
        Light third-generation squarks from flavour gauge messengers, JHEP **04** (2014) 078,
        arXiv: `1312.0935` [`hep-ph`] (cit. on p. 60).

[310]   S. Abel and M. McGarrie,
        Natural supersymmetry and dynamical flavour with meta-stable vacua,
        JHEP **07** (2014) 145, arXiv: `1404.1318` [`hep-ph`] (cit. on p. 60).

[311]   A. Delgado, M. Garcia-Pepin and M. Quiros, *GMSB with Light Stops*,
        JHEP **08** (2015) 159, arXiv: `1505.07469` [`hep-ph`] (cit. on p. 60).

[312]   F. del Aguila et al., *Collider aspects of flavour physics at high Q*,
        Eur. Phys. J. **C57** (2008) 183, arXiv: `0801.1800` [`hep-ph`]; A. Bartl et al., *Impact of
        squark generation mixing on the search for squarks decaying into fermions at LHC*,
        Phys. Lett. **B698** (2011) 380, [Erratum: Phys. Lett.B700,390(2011)],
        arXiv: `1007.5483` [`hep-ph`]; A. Bartl et al.,
        Flavor violating bosonic squark decays at LHC,
        Int. J. Mod. Phys. **A29**.07 (2014) 1450035, arXiv: `1212.4688` [`hep-ph`];
        M. Blanke et al., *Flavoured Naturalness*, JHEP **06** (2013) 022,
        arXiv: `1302.7232` [`hep-ph`]; M. Backović, A. Mariotti and M. Spannowsky,
        Signs of Tops from Highly Mixed Stops, JHEP **06** (2015) 122,
        arXiv: `1504.00927` [`hep-ph`]; K. De Causmaecker et al.,
        General squark flavour mixing: constraints, phenomenology and benchmarks, (2015),
        arXiv: `1509.05414` [`hep-ph`], cit. on p. 60.

[313] M. Artuso et al., *B, D and K decays*, Eur. Phys. J. **C57** (2008) 309,
arXiv: 0801.1833 [hep-ph] (cit. on p. 60).

[314] J. J. Cao et al., *SUSY-induced FCNC top-quark processes at the large hadron collider*,
Phys. Rev. **D75** (2007) 075021, arXiv: hep-ph/0702264 [hep-ph] (cit. on p. 60).

[315] K. Kowalska, *Phenomenology of SUSY with General Flavour Violation*,
JHEP **09** (2014) 139, arXiv: 1406.0710 [hep-ph] (cit. on p. 60).

[316] A. Brignole, *The supersymmetric Higgs boson with flavoured A-terms*,
Nucl. Phys. **B898** (2015) 644, arXiv: 1504.03273 [hep-ph] (cit. on p. 60).

[317] M. Arana-Catania et al., *Higgs Boson masses and B-Physics Constraints in
Non-Minimal Flavor Violating SUSY scenarios*, JHEP **05** (2012) 015,
arXiv: 1109.6232 [hep-ph] (cit. on p. 60).

[318] M. Arana-Catania, S. Heinemeyer and M. J. Herrero,
Updated Constraints on General Squark Flavor Mixing, Phys. Rev. **D90**.7 (2014) 075003,
arXiv: 1405.6960 [hep-ph] (cit. on p. 60).

[319] M. Dugan, B. Grinstein and L. J. Hall,
CP Violation in the Minimal N=1 Supergravity Theory, Nucl. Phys. **B255** (1985) 413
(cit. on p. 60).

[320] G. Aad et al., *Search for pair-produced third-generation squarks decaying via charm
quarks or in compressed supersymmetric scenarios in pp collisions at $\sqrt{s} = 8$ TeV with
the ATLAS detector*, Phys. Rev. **D90**.5 (2014) 052008, arXiv: 1407.0608 [hep-ex]
(cit. on p. 62).

[321] W. Porod, F. Staub and A. Vicente, *A Flavor Kit for BSM models*,
Eur.Phys.J. **C74**.8 (2014) 2992, arXiv: 1405.1434 [hep-ph] (cit. on pp. 63, 98).

[322] J. Camargo-Molina et al., *Stability of the CMSSM against sfermion VEVs*,
JHEP **1312** (2013) 103, arXiv: 1309.7212 [hep-ph] (cit. on pp. 65, 86).

[323] N. Blinov and D. E. Morrissey, *Vacuum Stability and the MSSM Higgs Mass*,
JHEP **1403** (2014) 106, arXiv: 1310.4174 [hep-ph] (cit. on p. 65).

[324] D. Chowdhury et al.,
Charge and Color Breaking Constraints in MSSM after the Higgs Discovery at LHC,
JHEP **1402** (2014) 110, arXiv: 1310.1932 [hep-ph] (cit. on p. 65).

[325] J. Camargo-Molina et al., *Constraining the Natural MSSM through tunneling to
color-breaking vacua at zero and non-zero temperature*, Phys.Lett. **B737** (2014) 156,
arXiv: 1405.7376 [hep-ph] (cit. on pp. 65, 86).

[326] U. Chattopadhyay and A. Dey, *Exploring MSSM for Charge and Color Breaking and
Other Constraints in the Context of Higgs@125 GeV*, JHEP **1411** (2014) 161,
arXiv: 1409.0611 [hep-ph] (cit. on p. 65).

[327] C. L. Wainwright, *CosmoTransitions: Computing Cosmological Phase Transition
Temperatures and Bubble Profiles with Multiple Fields*,
Comput. Phys. Commun. **183** (2012) 2006, arXiv: 1109.4189 [hep-ph] (cit. on p. 66).

[328] J. Braathen, M. D. Goodsell and P. Slavich, *Leading two-loop corrections to the Higgs
boson masses in SUSY models with Dirac gauginos*, (2016),
arXiv: 1606.09213 [hep-ph] (cit. on p. 70).

[329] H. Dreiner, F. Staub and A. Vicente, *General NMSSM signatures at the LHC*,
       Phys.Rev. **D87**.3 (2013) 035009, arXiv: `1211.6987 [hep-ph]` (cit. on p. 71).

[330] F. Staub, W. Porod and B. Herrmann,
       The Electroweak sector of the NMSSM at the one-loop level, JHEP **1010** (2010) 040,
       arXiv: `1007.4049 [hep-ph]` (cit. on p. 71).

[331] K. Ender et al., *Analysis of the NMSSM Higgs Boson Masses at One-Loop Level*,
       Phys.Rev. **D85** (2012) 075024, arXiv: `1111.4952 [hep-ph]` (cit. on p. 71).

[332] T. Graf et al., *Higgs Boson Masses in the Complex NMSSM at One-Loop Level*,
       JHEP **1210** (2012) 122, arXiv: `1206.6806 [hep-ph]` (cit. on p. 71).

[333] U. Ellwanger and C. Hugonie, *NMSPEC: A Fortran code for the sparticle and Higgs
       masses in the NMSSM with GUT scale boundary conditions*,
       Comput.Phys.Commun. **177** (2007) 399, arXiv: `hep-ph/0612134 [hep-ph]`
       (cit. on p. 71).

[334] J. Baglio et al., *NMSSMCALC: A Program Package for the Calculation of
       Loop-Corrected Higgs Boson Masses and Decay Widths in the (Complex) NMSSM*,
       Comput. Phys. Commun. **185**.12 (2014) 3372, arXiv: `1312.4788 [hep-ph]`
       (cit. on p. 71).

[335] Ya. B. Zeldovich, I. Yu. Kobzarev and L. B. Okun,
       Cosmological Consequences of the Spontaneous Breakdown of Discrete Symmetry,
       Zh. Eksp. Teor. Fiz. **67** (1974) 3, [Sov. Phys. JETP40,1(1974)] (cit. on p. 71).

[336] A. Mazumdar et al., *Possible resolution of the domain wall problem in the NMSSM*,
       Phys. Rev. **D93**.2 (2016) 025002, arXiv: `1511.01905 [hep-ph]` (cit. on p. 71).

[337] S. A. Abel and P. L. White,
       Baryogenesis from domain walls in the next-to-minimal supersymmetric standard model,
       Phys. Rev. **D52** (1995) 4371, arXiv: `hep-ph/9505241 [hep-ph]` (cit. on p. 71).

[338] L. J. Hall, D. Pinner and J. T. Ruderman, *A Natural SUSY Higgs Near 126 GeV*,
       JHEP **1204** (2012) 131, arXiv: `1112.2703 [hep-ph]` (cit. on p. 77).

[339] K. Schmidt-Hoberg and F. Staub, *Enhanced $h \to \gamma\gamma$ rate in MSSM singlet extensions*,
       JHEP **1210** (2012) 195, arXiv: `1208.1683 [hep-ph]` (cit. on p. 77).

[340] K. Schmidt-Hoberg, F. Staub and M. W. Winkler,
       Enhanced diphoton rates at Fermi and the LHC, JHEP **1301** (2013) 124,
       arXiv: `1211.2835 [hep-ph]` (cit. on p. 77).

[341] D. Das, L. Mitzka and W. Porod, *Discovery of Charged Higgs through $\gamma\gamma$ final states*,
       (2014), arXiv: `1408.1704 [hep-ph]` (cit. on p. 80).

[342] H. K. Dreiner, *An Introduction to explicit R-parity violation*,
       (1997), [Adv. Ser. Direct. High Energy Phys.21,565(2010)],
       arXiv: `hep-ph/9707435 [hep-ph]` (cit. on p. 84).

[343] G. R. Farrar and P. Fayet, *Phenomenology of the Production, Decay, and Detection of
       New Hadronic States Associated with Supersymmetry*, Phys.Lett. **B76** (1978) 575
       (cit. on p. 84).

[344] R. Barbier et al., *R-parity violating supersymmetry*, Phys. Rept. **420** (2005) 1,
       arXiv: `hep-ph/0406039 [hep-ph]` (cit. on pp. 84, 109, 110).

[345] B. C. Allanach, A. Dedes and H. K. Dreiner,
R parity violating minimal supergravity model,
Phys. Rev. **D69** (2004) 115002, [Erratum: Phys. Rev.D72,079902(2005)],
arXiv: `hep-ph/0309196 [hep-ph]` (cit. on pp. 84, 85).

[346] H. K. Dreiner and M. Thormeier,
Supersymmetric Froggatt-Nielsen models with baryon and lepton number violation,
Phys. Rev. **D69** (2004) 053002, arXiv: `hep-ph/0305270 [hep-ph]` (cit. on p. 84).

[347] H. K. Dreiner, C. Luhn and M. Thormeier,
What is the discrete gauge symmetry of the MSSM?, Phys. Rev. **D73** (2006) 075007,
arXiv: `hep-ph/0512163 [hep-ph]` (cit. on p. 84).

[348] H. K. Dreiner et al.,
Baryon triality and neutrino masses from an anomalous flavor U(1),
Nucl. Phys. **B774** (2007) 127, arXiv: `hep-ph/0610026 [hep-ph]` (cit. on p. 84).

[349] H.-S. Lee, *Minimal gauge origin of baryon triality and flavorful signatures at the LHC*,
Phys. Lett. **B704** (2011) 316, arXiv: `1007.1040 [hep-ph]` (cit. on p. 84).

[350] H. K. Dreiner, M. Hanussek and C. Luhn,
What is the discrete gauge symmetry of the R-parity violating MSSM?,
Phys. Rev. **D86** (2012) 055012, arXiv: `1206.6305 [hep-ph]` (cit. on p. 84).

[351] G. Bhattacharyya, *A Brief review of R-parity violating couplings*, (1997),
arXiv: `hep-ph/9709395 [hep-ph]`,
URL: `http://alice.cern.ch/format/showfull?sysnb=0257845` (cit. on p. 84).

[352] H. K. Dreiner and G. G. Ross, *R-parity violation at hadron colliders*,
Nucl.Phys. **B365** (1991) 597 (cit. on p. 84).

[353] B. C. Allanach et al.,
Mass Spectrum in R-Parity Violating mSUGRA and Benchmark Points,
Phys. Rev. **D75** (2007) 035002, arXiv: `hep-ph/0609263 [hep-ph]` (cit. on p. 84).

[354] H. Dreiner, S. Grab and T. Stefaniak, *Discovery Potential of Selectron or Smuon as the Lightest Supersymmetric Particle at the LHC*, Phys.Rev. **D84** (2011) 035023,
arXiv: `1102.3189 [hep-ph]` (cit. on p. 84).

[355] H. K. Dreiner and T. Stefaniak,
Bounds on R-parity Violation from Resonant Slepton Production at the LHC,
Phys. Rev. **D86** (2012) 055010, arXiv: `1201.5014 [hep-ph]` (cit. on p. 84).

[356] H. K. Dreiner et al., *General MSSM signatures at the LHC with and without R-parity*,
Phys. Rev. **D86** (2012) 035021, arXiv: `1205.0557 [hep-ph]` (cit. on p. 84).

[357] B. C. Allanach and B. Gripaios,
Hide and Seek With Natural Supersymmetry at the LHC, JHEP **05** (2012) 062,
arXiv: `1202.6616 [hep-ph]` (cit. on p. 84).

[358] M. Asano, K. Rolbiecki and K. Sakurai,
Can R-parity violation hide vanilla supersymmetry at the LHC?, JHEP **01** (2013) 128,
arXiv: `1209.5778 [hep-ph]` (cit. on p. 84).

[359] R. Franceschini and R. Torre, *RPV stops bump off the background*,
Eur. Phys. J. **C73** (2013) 2422, arXiv: `1212.3622 [hep-ph]` (cit. on p. 84).

[360] J. A. Evans and Y. Kats, *LHC Coverage of RPV MSSM with Light Stops*,
JHEP **04** (2013) 028, arXiv: `1209.0764` `[hep-ph]` (cit. on p. 84).

[361] B. C. Allanach, A. Dedes and H. K. Dreiner, *Two loop supersymmetric renormalization group equations including R-parity violation and aspects of unification*,
Phys. Rev. **D60** (1999) 056002, [Erratum: Phys. Rev.D86,039906(2012)],
arXiv: `hep-ph/9902251` `[hep-ph]` (cit. on p. 84).

[362] V. D. Barger, G. F. Giudice and T. Han,
Some New Aspects of Supersymmetry R-Parity Violating Interactions,
Phys. Rev. **D40** (1989) 2987 (cit. on p. 84).

[363] K. Agashe and M. Graesser,
R-parity violation in flavor changing neutral current processes and top quark decays,
Phys. Rev. **D54** (1996) 4445, arXiv: `hep-ph/9510439` `[hep-ph]` (cit. on p. 84).

[364] N. Chamoun et al.,
Resurrecting light stops after the 125 GeV Higgs in the baryon number violating CMSSM,
JHEP **08** (2014) 142, arXiv: `1407.2248` `[hep-ph]` (cit. on p. 86).

[365] B. Brahmachari and P. Roy,
Constraints on baryon nonconserving Yukawa couplings in a supersymmetric theory,
Phys. Rev. **D50** (1994) 39, [Erratum: Phys. Rev.D51,3974(1995)],
arXiv: `hep-ph/9403350` `[hep-ph]` (cit. on p. 86).

[366] B. Allanach, A. Dedes and H. K. Dreiner,
Bounds on R-parity violating couplings at the weak scale and at the GUT scale,
Phys.Rev. **D60** (1999) 075014, arXiv: `hep-ph/9906209` `[hep-ph]` (cit. on p. 86).

[367] H. K. Dreiner, K. Nickel and F. Staub,
$B^0_{s,d} \to \mu\overline{\mu}$ and $B \to X_s\gamma$ in the R-parity violating MSSM,
Phys. Rev. **D88**.11 (2013) 115001, arXiv: `1309.1735` `[hep-ph]` (cit. on p. 87).

[368] G. Aad et al., *Search for production of vector-like quark pairs and of four top quarks in the lepton-plus-jets final state in pp collisions at $\sqrt{s} = 8$ TeV with the ATLAS detector*,
JHEP **08** (2015) 105, arXiv: `1505.04306` `[hep-ex]` (cit. on p. 89).

[369] C.-Y. Chen, S. Dawson and Y. Zhang, *Higgs CP Violation from Vectorlike Quarks*,
Phys. Rev. **D92**.7 (2015) 075026, arXiv: `1507.07020` `[hep-ph]` (cit. on p. 89).

[370] S. Dawson and E. Furlan, *A Higgs Conundrum with Vector Fermions*,
Phys. Rev. **D86** (2012) 015021, arXiv: `1205.4733` `[hep-ph]` (cit. on p. 89).

[371] J. A. Aguilar-Saavedra et al.,
Handbook of vectorlike quarks: Mixing and single production,
Phys. Rev. **D88**.9 (2013) 094010, arXiv: `1306.0572` `[hep-ph]` (cit. on p. 89).

[372] S. Fajfer et al., *Light Higgs and Vector-like Quarks without Prejudice*,
JHEP **07** (2013) 155, arXiv: `1304.4219` `[hep-ph]` (cit. on p. 89).

[373] A. Efrati, A. Falkowski and Y. Soreq,
Electroweak constraints on flavorful effective theories, JHEP **07** (2015) 018,
arXiv: `1503.07872` `[hep-ph]` (cit. on p. 89).

[374] A. Arbey et al., *Implications of a 125 GeV Higgs for supersymmetric models*,
Phys.Lett. **B708** (2012) 162, arXiv: `1112.3028` `[hep-ph]` (cit. on p. 89).

[375] J. A. Casas et al., *Reducing the Fine-Tuning of Gauge-Mediated SUSY Breaking*, (2016), arXiv: `1602.06892 [hep-ph]` (cit. on pp. 89, 104, 125).

[376] S. P. Martin, *Extra vector-like matter and the lightest Higgs scalar boson mass in low-energy supersymmetry*, Phys.Rev. **D81** (2010) 035004, arXiv: `0910.2732 [hep-ph]` (cit. on p. 89).

[377] Z.-z. Xing, H. Zhang and S. Zhou, *Updated Values of Running Quark and Lepton Masses*, Phys. Rev. **D77** (2008) 113016, arXiv: `0712.1419 [hep-ph]` (cit. on pp. 89, 96).

[378] M. Endo et al., *Higgs Mass and Muon Anomalous Magnetic Moment in Supersymmetric Models with Vector-Like Matters*, Phys.Rev. **D84** (2011) 075017, arXiv: `1108.3071 [hep-ph]` (cit. on p. 90).

[379] M. Endo et al., *Higgs mass, muon g-2, and LHC prospects in gauge mediation models with vector-like matters*, Phys.Rev. **D85** (2012) 095012, arXiv: `1112.5653 [hep-ph]` (cit. on p. 90).

[380] M. Endo et al., *Vacuum Stability Bound on Extended GMSB Models*, JHEP **1206** (2012) 060, arXiv: `1202.2751 [hep-ph]` (cit. on p. 90).

[381] S. Dimopoulos, G. F. Giudice and A. Pomarol, *Dark matter in theories of gauge mediated supersymmetry breaking*, Phys. Lett. **B389** (1996) 37, arXiv: `hep-ph/9607225 [hep-ph]` (cit. on pp. 93, 94).

[382] S. P. Martin, *Generalized messengers of supersymmetry breaking and the sparticle mass spectrum*, Phys. Rev. **D55** (1997) 3177, arXiv: `hep-ph/9608224 [hep-ph]` (cit. on p. 93).

[383] T. Han and R. Hempfling, *Messenger sneutrinos as cold dark matter*, Phys.Lett. **B415** (1997) 161, arXiv: `hep-ph/9708264 [hep-ph]` (cit. on p. 94).

[384] E. A. Baltz and H. Murayama, *Gravitino warm dark matter with entropy production*, JHEP **0305** (2003) 067, arXiv: `astro-ph/0108172 [astro-ph]` (cit. on p. 94).

[385] M. Fujii and T. Yanagida, *Natural gravitino dark matter and thermal leptogenesis in gauge mediated supersymmetry breaking models*, Phys.Lett. **B549** (2002) 273, arXiv: `hep-ph/0208191 [hep-ph]` (cit. on p. 94).

[386] M. Fujii and T. Yanagida, *Baryogenesis and gravitino dark matter in gauge mediated supersymmetry breaking models*, Phys.Rev. **D66** (2002) 123515, arXiv: `hep-ph/0207339 [hep-ph]` (cit. on p. 94).

[387] K. Jedamzik, M. Lemoine and G. Moultaka, *Gravitino dark matter in gauge mediated supersymmetry breaking*, Phys.Rev. **D73** (2006) 043514, arXiv: `hep-ph/0506129 [hep-ph]` (cit. on p. 94).

[388] F. Staub, W. Porod and J. Niemeyer, *Strong dark matter constraints on GMSB models*, JHEP **1001** (2010) 058, arXiv: `0907.0530 [hep-ph]` (cit. on p. 94).

[389] A. K. Alok et al., *New-physics signals of a model with a vector-singlet up-type quark*, (2015), arXiv: `1504.00517 [hep-ph]` (cit. on p. 95).

[390] S. Chatrchyan et al., *Inclusive search for a vector-like T quark with charge $\frac{2}{3}$ in pp collisions at $\sqrt{s} = 8$ TeV*, Phys.Lett. **B729** (2014) 149, arXiv: `1311.7667 [hep-ex]` (cit. on p. 98).

[391] S. Bhattacharya et al., *Prospects for a Heavy Vector-Like Charge* 2/3 *Quark T search at the LHC with* $\sqrt{s} = 14 TeV$ *and* 33 *TeV. "A Snowmass 2013 Whitepaper"*, (2013), arXiv: `1309.0026 [hep-ex]`, URL: `https://inspirehep.net/record/1252064/files/arXiv:1309.0026.pdf` (cit. on p. 98).

[392] J. A. Casas et al., *What is a Natural SUSY scenario?*, JHEP **06** (2015) 070, arXiv: `1407.6966 [hep-ph]` (cit. on pp. 104, 125).

[393] D. M. Ghilencea, H. M. Lee and M. Park, *Tuning supersymmetric models at the LHC: A comparative analysis at two-loop level*, JHEP **07** (2012) 046, arXiv: `1203.0569 [hep-ph]` (cit. on pp. 104, 125).

[394] A. Belyaev et al., *Hunting for neutral, long-lived exotica at the LHC using a missing transverse energy signature*, JHEP **03** (2016) 018, arXiv: `1512.02229 [hep-ph]` (cit. on pp. 109, 121, 168).

[395] J. L. Hewett et al., *Signatures of long-lived gluinos in split supersymmetry*, JHEP **09** (2004) 070, arXiv: `hep-ph/0408248 [hep-ph]` (cit. on p. 109).

[396] T. Han et al., *Phenomenology of hidden valleys at hadron colliders*, JHEP **07** (2008) 008, arXiv: `0712.2041 [hep-ph]` (cit. on p. 109).

[397] L. Basso et al., *Phenomenology of the minimal B-L extension of the Standard model: Z' and neutrinos*, Phys. Rev. **D80** (2009) 055030, arXiv: `0812.4313 [hep-ph]` (cit. on p. 109).

[398] V. Khachatryan et al., *Search for Displaced Supersymmetry in events with an electron and a muon with large impact parameters*, Phys. Rev. Lett. **114**.6 (2015) 061801, arXiv: `1409.4789 [hep-ex]` (cit. on p. 109).

[399] V. Khachatryan et al., *Search for long-lived particles that decay into final states containing two electrons or two muons in proton-proton collisions at* $\sqrt{s} = 8$ *TeV*, Phys. Rev. **D91**.5 (2015) 052012, arXiv: `1411.6977 [hep-ex]` (cit. on pp. 109, 110, 114–118, 121, 122).

[400] V. Khachatryan et al., *Search for Long-Lived Neutral Particles Decaying to Quark-Antiquark Pairs in Proton-Proton Collisions at* $\sqrt{s} = 8$ *TeV*, Phys. Rev. **D91**.1 (2015) 012007, arXiv: `1411.6530 [hep-ex]` (cit. on pp. 109, 110, 114–118, 121, 122).

[401] G. Aad et al., *Search for massive, long-lived particles using multitrack displaced vertices or displaced lepton pairs in pp collisions at* $\sqrt{s} = 8$ *TeV with the ATLAS detector*, Phys. Rev. **D92**.7 (2015) 072004, arXiv: `1504.05162 [hep-ex]` (cit. on p. 109).

[402] G. Aad et al., *Search for pair-produced long-lived neutral particles decaying in the ATLAS hadronic calorimeter in pp collisions at* $\sqrt{s} = 8$ *TeV*, Phys. Lett. **B743** (2015) 15, arXiv: `1501.04020 [hep-ex]` (cit. on p. 109).

[403] A. V. Semenov, *LanHEP: A Package for automatic generation of Feynman rules in gauge models*, (1996), arXiv: `hep-ph/9608488 [hep-ph]` (cit. on p. 111).

[404] A. V. Semenov, *LanHEP: A Package for automatic generation of Feynman rules in field theory. Version 2.0*, (2002), arXiv: `hep-ph/0208011 [hep-ph]` (cit. on p. 111).

[405] A. Semenov, *LanHEP - a package for automatic generation of Feynman rules from the Lagrangian. Updated version 3.1*, (2010), arXiv: `1005.1909` `[hep-ph]` (cit. on p. 111).

[406] T. Sjostrand, S. Mrenna and P. Z. Skands, *PYTHIA 6.4 Physics and Manual*, JHEP **05** (2006) 026, arXiv: `hep-ph/0603175` `[hep-ph]` (cit. on p. 111).

[407] P. Torrielli and S. Frixione, *Matching NLO QCD computations with PYTHIA using MC@NLO*, JHEP **04** (2010) 110, arXiv: `1002.4293` `[hep-ph]` (cit. on p. 111).

[408] M. Drees et al., *CheckMATE: Confronting your Favourite New Physics Model with LHC Data*, Comput. Phys. Commun. **187** (2014) 227, arXiv: `1312.2591` `[hep-ph]` (cit. on pp. 112, 126).

[409] J. de Favereau et al., *DELPHES 3, A modular framework for fast simulation of a generic collider experiment*, JHEP **1402** (2014) 057, arXiv: `1307.6346` `[hep-ex]` (cit. on p. 112).

[410] M. Cacciari, G. P. Salam and G. Soyez, *FastJet User Manual*, Eur. Phys. J. **C72** (2012) 1896, arXiv: `1111.6097` `[hep-ph]` (cit. on p. 112).

[411] M. Cacciari and G. P. Salam, *Dispelling the N^3 myth for the k_t jet-finder*, Phys. Lett. **B641** (2006) 57, arXiv: `hep-ph/0512210` `[hep-ph]` (cit. on p. 112).

[412] M. Cacciari, G. P. Salam and G. Soyez, *The Anti-k(t) jet clustering algorithm*, JHEP **04** (2008) 063, arXiv: `0802.1189` `[hep-ph]` (cit. on p. 112).

[413] A. L. Read, *Presentation of search results: The CL(s) technique*, J. Phys. **G28** (2002) 2693, [,11(2002)] (cit. on p. 112).

[414] C. G. Lester and D. J. Summers, *Measuring masses of semiinvisibly decaying particles pair produced at hadron colliders*, Phys. Lett. **B463** (1999) 99, arXiv: `hep-ph/9906349` `[hep-ph]` (cit. on p. 112).

[415] A. Barr, C. Lester and P. Stephens, *m(T2): The Truth behind the glamour*, J. Phys. **G29** (2003) 2343, arXiv: `hep-ph/0304226` `[hep-ph]` (cit. on p. 112).

[416] H.-C. Cheng and Z. Han, *Minimal Kinematic Constraints and m(T2)*, JHEP **12** (2008) 063, arXiv: `0810.5178` `[hep-ph]` (cit. on p. 112).

[417] V. Khachatryan et al., *Search for dark matter, extra dimensions, and unparticles in monojet events in proton–proton collisions at $\sqrt{s} = 8$ TeV*, Eur. Phys. J. **C75**.5 (2015) 235, arXiv: `1408.3583` `[hep-ex]` (cit. on p. 112).

[418] The ATLAS Collaboration, *Search for squarks and gluinos with the ATLAS detector in final states with jets and missing transverse momentum and 20.3 fb^{-1} of $\sqrt{s} = 8$ TeV proton-proton collision data*, (2013) (cit. on pp. 112, 114, 116, 120, 171, 172).

[419] G. Aad et al., *Search for new phenomena in final states with an energetic jet and large missing transverse momentum in pp collisions at $\sqrt{s} = 8$ TeV with the ATLAS detector*, Eur. Phys. J. **C75**.7 (2015) 299, arXiv: `1502.01518` `[hep-ex]` (cit. on pp. 112, 114, 116, 120, 169–172).

[420] S. Chatrchyan et al.,
Search for supersymmetry in hadronic final states with missing transverse energy using the variables α_T and b-quark multiplicity in pp collisions at $\sqrt{s} = 8$ TeV,
Eur. Phys. J. **C73**.9 (2013) 2568, arXiv: `1303.2985` `[hep-ex]`
(cit. on pp. 112, 114, 116, 120, 170–172).

[421] L. Randall and D. Tucker-Smith, *Dijet Searches for Supersymmetry at the LHC*,
Phys. Rev. Lett. **101** (2008) 221803, arXiv: `0806.1049` `[hep-ph]` (cit. on p. 112).

[422] V. Khachatryan et al., *Search for Supersymmetry in pp Collisions at 7 TeV in Events with Jets and Missing Transverse Energy*, Phys. Lett. **B698** (2011) 196,
arXiv: `1101.1628` `[hep-ex]` (cit. on p. 112).

[423] T. Hahn et al., *FeynHiggs: A program for the calculation of MSSM Higgs-boson observables - Version 2.6.5*, Comput.Phys.Commun. **180** (2009) 1426 (cit. on p. 123).

[424] F. Staub et al., *Higgs mass predictions of public NMSSM spectrum generators*,
Comput. Phys. Commun. **202** (2016) 113, arXiv: `1507.05093` `[hep-ph]` (cit. on p. 123).

[425] ATLAS Collaboration, *Search for resonances decaying to photon pairs in 3.2 fb^{-1} of pp collisions at $\sqrt{s} = 13$ TeV with the ATLAS detector*, (2015) (cit. on p. 126).

[426] CMS Collaboration, *Search for new physics in high mass diphoton events in proton-proton collisions at 13TeV*, (2015) (cit. on p. 126).

[427] F. Staub et al.,
Precision tools and models to narrow in on the 750 GeV diphoton resonance, (2016),
arXiv: `1602.05581` `[hep-ph]` (cit. on p. 127).

[428] W. A. Bardeen et al., *Deep Inelastic Scattering Beyond the Leading Order in Asymptotically Free Gauge Theories*, Phys. Rev. **D18** (1978) 3998, cit. on p. 129.

[429] W. Siegel, *Supersymmetric Dimensional Regularization via Dimensional Reduction*,
Phys. Lett. **B84** (1979) 193 (cit. on p. 129).

[430] D. M. Capper, D. R. T. Jones and P. van Nieuwenhuizen, *Regularization by Dimensional Reduction of Supersymmetric and Nonsupersymmetric Gauge Theories*,
Nucl. Phys. **B167** (1980) 479 (cit. on p. 129).

[431] I. Jack et al., *Decoupling of the epsilon scalar mass in softly broken supersymmetry*,
Phys.Rev. **D50** (1994) 5481, arXiv: `hep-ph/9407291` `[hep-ph]` (cit. on p. 129).

[432] J. C. Romao and J. P. Silva,
A resource for signs and Feynman diagrams of the Standard Model,
Int. J. Mod. Phys. **A27** (2012) 1230025, arXiv: `1209.6213` `[hep-ph]` (cit. on p. 129).

[433] P. H. Chankowski et al., *Delta R in the MSSM*, Nucl.Phys. **B417** (1994) 101
(cit. on p. 131).

[434] L. Avdeev and M. Y. Kalmykov, *Pole masses of quarks in dimensional reduction*,
Nucl.Phys. **B502** (1997) 419, arXiv: `hep-ph/9701308` `[hep-ph]` (cit. on p. 131).

[435] A. Bednyakov et al.,
*Two loop O(alpha-s**2) MSSM corrections to the pole masses of heavy quarks*,
Eur.Phys.J. **C29** (2003) 87, arXiv: `hep-ph/0210258` `[hep-ph]` (cit. on p. 131).

[436] G. 't Hooft and M. J. G. Veltman, *Scalar One Loop Integrals*,
Nucl. Phys. **B153** (1979) 365 (cit. on p. 133).